Role of cytoplasmic linker proteins (CLIPs) in microtubule dynamics and membrane traffic

ISBN 90 77017 07 0
Printed by Optima Grafische Communicatie, Rotterdam

The front cover shows a cultured COS-1 cell that has been triple-stained. The microtubule network (red) is visualized with anti-β-tubulin antibodies, CLIP-170 (green/yellow) is labeled with anti-CLIP-170 antibodies (#2360) and DNA in nucleus (blue) is stained with DAPI.

Role of cytoplasmic linker proteins (CLIPs) in microtubule dynamics and membrane traffic

De rol van cytoplasmatische linker eiwitten (CLIPs) bij microtubuli dynamiek en membraan transport

Proefschrift

ter verkrijging van de graad van doctor
aan de Erasmus Universiteit Rotterdam
op gezag van de Rector Magnificus
Prof.dr.ir. J. van Bemmel
en volgens besluit van het College voor Promoties

De openbare verdediging zal plaats vinden op
woensdag 12 september 2001 om 13.45 uur

door

Casper Cassander Hoogenraad

geboren te Delft

Promotiecommisie

Promotoren:	Prof.dr. F.G. Grosveld
	Prof.dr. C.I. de Zeeuw
Overige leden:	Prof.dr. B.A. Oostra
	Dr. J.G.G. Borst
	Dr.ir. D.N. Meijer
Co-promotor:	Dr.ir. N. Galjart

Dit proefschrift kwam tot stand binnen de vakgroepen Celbiologie en Genetica, en Anatomie, van de faculteit der Geneeskunde en Gezondheidswetenschappen van de Erasmus Universiteit Rotterdam. De vakgroepen maken deel uit van het Medisch Genetisch Centrum Zuid-West Nederland. Het onderzoek en publikatie van dit proefschrift zijn gedeeltelijk financieel ondersteund door de Nederlandse vereniging voor Wetenschappelijk Onderzoek (NWO-MW-903-47-067), BIOzymTC BV en BaseClear.

Voor Patricia en Tim

SCOPE OF THE THESIS

Microtubules play essential roles in cell division, cytoplasmic organization, generation and maintenance of cell polarity and many types of cell movement. The polymerization dynamics of microtubules are important for their biological functions. Microtubule dynamics allow a cell to adopt spatial arrangements that change rapidly in response to positional cues. Microtubule plus ends are among the primary sites for regulating microtubule dynamic behavior. These microtubule distal ends may also define local sites on microtubules for the interaction with cytoplasmic organelles and the plasma membrane, to mediate motility and morphogenesis. Various plus end binding proteins have been implicated in these phenomena. The aim of this thesis is to study the role of microtubule plus end binding proteins, especially cytoplasmic linker proteins (CLIPs), in microtubule dynamics and membrane traffic in order to better understand the molecular mechanisms that underly these essential cellular processes.

Chapter 1 reviews the current knowledge on the structure and function of the three cytoskeleton systems: actin filaments, intermediate filaments and microtubules. The attention is mainly focused on microtubules and their dynamic behavior in the cell. **Chapter 2** gives a broad introduction on microtubule associated proteins (MAPs), including classical MAPs, motor proteins and proteins that influence microtubule dynamics. A detailed description of microtubule plus end binding proteins, especially the cytoplasmic linker protein family, will be presented. These two chapters together give an overview of microtubule based processes in different organisms and cell types and serve as a framework for the next chapters.

The experimental work of this thesis is summarized in chapters 3-11. **Chapter 3** reports the isolation and characterization of a new cytoplasmic linker protein, CLIP-115, which is predominantly present in the brain. **Chapter 4** shows the binding of CLIP-115 to microtubule plus ends and defines the domains of CLIP-115 which are involved in efficient microtubule binding. **Chapter 5** describes the localization of CLIP-115 and CLIP-170 in the brain. Additional data suggest that CLIP-170 interacts with the dynactin complex and LIS1 protein. Dynactin is the accessory factor of the minus-end-directed microtubule motor protein dynein and mutated LIS1 is responsible for the brain abnormalities in type 1 lissencephaly. **Chapter 6** describes the isolation and characterization of CLASPs, CLIP associated proteins, which bind to both CLIP-115 and CLIP-170. CLASP2 is asymmetrically distributed in motile fibroblasts and has a microtubule stabilizing effect. In contrast to CLIPs, CLASP2 localizes specifically to the leading edge of fibroblasts that have been induced to polarize. The distribution of CLASP2 is dependent on the kinase activity of GSK3β. **Chapter 7** introduces the mammalian homologue of *Dropsophila* Bicaudal-D, BICD2. We demonstrate that BICD2 associates with the Golgi apparatus and cytoplasmic vesicles. BICD2 also binds directly to the p50 subunit of the dynactin complex and may have a role in the dynactin-dynein pathway. **Chapter 8** demonstrates the interaction between CLIP-115 and both BICD1 and BICD2. CLIP-170 is not able to bind to BICD. These

data suggest that CLIP-115 may act a linker protein involved in the binding of BICD2 coated vesicles to microtubules. **Chapter 9** describes the genomic organization and chromosome localization of the murine *CYLN2* gene, which encodes the CLIP-115 protein. The human *CYLN2* gene is located at chromosome 7q11.23 and is hemizygously deleted in Williams Syndrome patients. **Chapter 10** describes the generation of CLIP-115 knock-out mice. The inheritance of the mutated CLIP-115 allele is Mendelian and homozygous CLIP-115 knock-out mice are apparently healthy without any gross abnormalies. However, both heterozygous and homozygous CLIP-115 knock-out mice show a growth deficiency and neurological deficits. These phenotypes are comparable to some of the symptoms observed in Williams Syndrome patients. In **chapter 11** the implications of the results presented in this thesis and some future prospects will be discussed.

Chapter 1

STRUCTURE, FUNCTION AND DYNAMICS OF THE CYTOSKELETON

1.1 General introduction

Cells in the human body come in more than two hundred different types and varieties. They differ in shapes and sizes, from the almost spherical lymphocyte, to flattened spindle-shaped fibroblasts, from mature male germ cells or polygonal epithelial cells, to wrapped Schwann cells, or neuronal cells, with many branching dendrites and a single long axon. Such a cellular architecture is constructed and maintained by a complex network of intracellular protein filaments, the cytoskeleton. The cytoskeleton is involved in cell morphology in almost all eukaryotic cells and provides mechanical strength to cells and tissues. This is especially important for animal cells which, compared to plant cells, have no rigid cell wall. On the other hand, it is the cytoskeleton which is very dynamic and helps a cell to change its shape and move in response to the environment. For example, the cytoskeleton is directly responsible for swimming of a single-celled amoeba, cell migration within the embryo during development, movement of macrophages as a response to a local infection in the body and contraction of muscle cells to produce mechanical force. The cytoskeleton also provides the machinery for movements within the cell, such as the segregation of chromosomes during mitosis and the transport of organelles or other cargo from one part of the cell to another. For example, intestinal epithelial cells require a polarized vesicle trafficking system to absorb nutrients from the gut and release them into the bloodstream. During embryonic patterning in worms and flies, which begins with the polarization of the body axis, the cytoskeleton is responsible for the polarity of the single cell zygote.

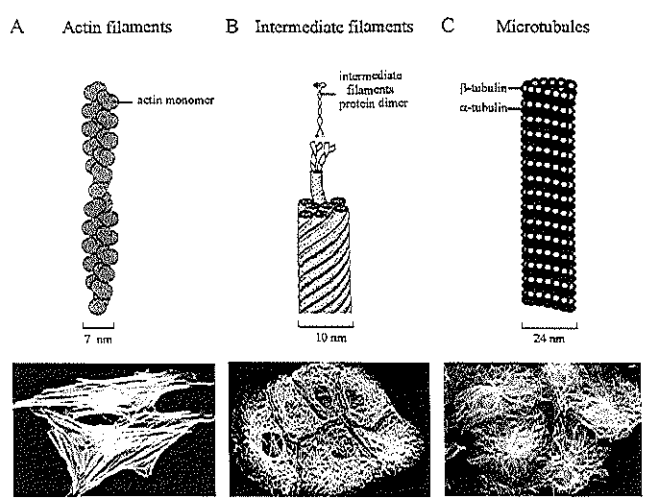

Figure 1: The three types of filaments that form the cytoskeleton
A Actin filaments are made of actin proteins that form two stranded helical structures of about 7 nm in diameter. **B** Intermediate filaments are made of intermediate filament protein dimers that form ropelike fibers of about 10 nm in diameter. **C** Microtubules are made of α/β-tubulin heterodimers that form a 25 nm wide hollow microtubule cylinder. Microscope images of actin filaments (A), intermediate filaments (B) and microtubule structures (C) in cultured cells are shown.

The diverse activities of the cytoskeleton depend on the three major types of protein filaments, which have been originally identified on the basis of their diameter; intermediate filaments (about 10 nm in diameter), actin filaments (about 7 nm in

diameter) and microtubules (about 24 nm in diameter) [1] (Fig. 1). Each filament type of the cytoskeleton is composed of linear polymers of protein subunits, which are assembled and disassembled by the cell in a carefully regulated fashion, sometimes at astonishing rates. During mitosis, for example, the microtubule network radiating throughout the cell changes within minutes to a compact, bipolar, mitotic spindle. Traditional genetic methods, together with a comparative genomic approach using the sequence of different organisms, have identified the genes encoding structural cytoskeleton or associated proteins. In the human genome six different actin genes are used to form actin filaments; six α-tubulin and six β-tubulin genes encode microtubule components and approximately 30 genes code for intermediate filament proteins [2,3]. A lot more genes in the genome code for cytoskeletal associated proteins. The human genome contains seventy families of actin-binding proteins; about a dozen families of microtubule binding proteins and 5 families of intermediate filament binding proteins. Each family consists again of multiple proteins. For example, the kinesin motor protein family, one type of microtubule binding protein, consists of more then forty different kinesin genes [4]. In *Drosophila* approximately 230 genes (2% of the total number of predicted genes) encode structural cytoskeleton or associated proteins [5,6]. The fraction of the *C. elegans* genome devoted to cytoskeletal function appears to be somewhat higher (approximately 5%) [7]. An extended overview of each class of cytoskeletal and associated proteins is given by Kreis and Vale, (1999) [8].

In humans, problems with the cytoskeleton can cause disorders of the muscles, the skin and the nervous system [9-14]. Changes in the cytoskeleton are important, and thus diagnostic, in the pathology of many diseases, including cancer [15-17]. Understanding the basic cell biology of the cytoskeleton has contributed to our understanding of the pathology of some of these disorders and will continue to affect approaches to diagnosis. Knowledge of the cytoskeleton may also reveal useful targets for the development of new therapies [18]. In this chapter the main characteristics of microtubules will be summarized, including microtubule structure, assembly and dynamics. Since microtubules are not independent identities and are part of an integrated cytoskeleton system, the actin filaments and intermediate filaments will be briefly addressed first.

1.2 Actin filaments

Actin filaments or microfilaments (F-actin) are rod-like structures about 7 nm in diameter (Fig. 2). They are built from small globular actin protein (G-actin), that is present at high concentrations in nearly all eukaryotic cells. The actin proteins are linked into chains and two of these chains twist about each other to form the actin filament [19] (Fig. 2). Actin filaments are polar structures with two structurally different ends, a slow growing minus (pointed) end and a fast growing plus (barbed) end [1,8,20-22]. The assembly of actin into filaments and the dynamic behavior of these actin filaments depend on ATP hydrolysis. This is similar to the role of GTP

hydrolysis in microtubule polymerization (see section 1.4.3). Although actin filaments are present in all eukaryotic cells, actin was first discovered in muscle cells, where it assembles into unusually stable filaments. In muscle, actin filaments are arranged in parallel to one another, with filaments containing the actin motor protein myosin placed between them. Sliding of myosin filaments along actin filaments creates the force responsible for muscle contraction [23,24].

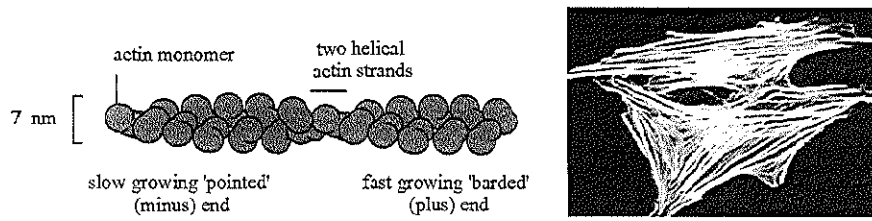

Figure 2: Structure of actin filaments
Actin filaments (microfilaments) are two stranded helical structures of the about 7 nm in diameter. Actin filaments are made of actin proteins and contain a slow growing 'pointed' end and a fast growing 'barbed' end. Although actin filaments are dispersed throughout the cell, they are found concentrated in lamellipodia and filopodia as parallel actin bundles and as anti-parallel actin bundles in stress fibers. Immunofluorescence of stress fibers in fibroblasts labeled with an anti-actin antibody is shown.

1.2.1 Actin and binding proteins

In yeast, actin is encoded by a single essential gene, named ACT1 [25]. Mammals express six different actin isoforms; four muscle actins and two non-muscle actins. In addition to the conventional actin genes, there are at least sixteen actin-related proteins (Arps) found in humans [3,26]. In budding yeast, *S. cerevisiae*, ten Arps are present, which are classified according to their similarity to actin. In yeast, the amino acid similarity between actin and Arps ranges from 50 to 70 percent [27]. Arps are thought to share the basic actin structure and to form filaments. For example, the highly conserved Arp1 protein can polymerize into long filaments and associates with spectrin, an actin binding protein [28]. Arp1 has also been described as one of the subunits in the dynactin complex [29] (see section 2.4.2)

There are approximately seventy distinct classes of proteins which bind to actin [8]. Much of the actin binding proteins modulate the dynamic properties of the actin filaments in the cell. They facilitate actin sequestration, actin filament severing, capping and crosslinking [30-32]. For example, the actin sequestering protein, profilin, forms a complex with ATP-bound actin and promotes actin polymerization at the plus end. Cofilin, on the other hand, associates with ADP-actin and increases the dissociation of actin from the minus end [33]. Another class of actin binding proteins are the myosin motor proteins. Myosins use ATP hydrolysis to move along actin filaments, either carrying membrane bound organelles or moving adjacent actin filaments against each other [34-36]. Interestingly, a growing number of myosin motors have been shown to be essential for the function of particular groups of neurons

[37]. For example, mutations in myosin-VI, VIIa and XV genes affect sensory cells in the inner ear and are responsible for deafness in mouse and human [10,14].

1.2.2 Function of actin in cellular processes

As stated above, in muscle cells actin filaments form a very stable structure. However, in non-muscle cells actin forms highly dynamic filaments which are responsible for a variety of functions, such as cell migration, macrophage phagocytosis and the propulsion of bacteria inside the host cell [38-42]. Cell migration starts with the protrusion or extension of the plasma membrane at the front of the cell. The protrusion structures, such as filopodia, or microspikes and lamellipodia, have been mostly studied in neuronal growth cones and motile fibroblasts, but are present on many other motile cell types. Filopodia are small plasma membrane extensions that contain bundles of long actin filaments [1,43]. Lamellipodia are sheet-like membrane structures which are comprised of a meshwork of unipolar actin filaments and show the characteristic ruffling appearance on motile fibroblasts. In both membrane protrusions the actin filaments are oriented with their fast growing ends pointing toward the plasma membrane [39]. Actin polymerization itself acts as a small machine for the force production at the leading edge of the cell and is sufficient to drive the formation of membrane protrusions in migrating cells [39,42,44]. It has been shown that members of the Rho GTPase family, such as Rac and Cdc42, regulate the assembly of the actin network in motile cells via the activation of actin binding proteins [45,46]. For example, proteins of the Wiskott-Aldrich syndrome (WASP) family are activated by GTPases and bring together an actin monomer and the Arp2/3 complex. The Arp2/3 complex initiates the growth of a new actin filament as a branch on the side of an older actin filament. The branch grows at its barbed end by addition of actin, which is bound by profilin and pushes the plasma membrane forward [33,42].

In addition to the uniparallel actin bundles in lamellipodia and filopodia, a second type of array is described, which has actin filaments arranged in opposite polarities. This contractile actin filament array is found in stress fibers in fibroblasts (Fig. 2), where it is associated with the actin motor myosin in a miniature version of the arrangement found in muscle cells. In migrating cells, the actomyosin filaments are responsible for the stabilization of adhesion complexes at the newly formed plasma membrane at the leading edge [41,44]. In this way the focal adhesion complexes serve as point of tracts over which the body of the cell moves.

The actin cytoskeleton is not only important for muscle contraction and cell motility, it is also involved in cytokinesis, transport and maintenance of subcellular material, such as organelles and mRNA and cell polarity [36,47]. A powerful example of how actin dynamics can be coupled to specific cell polarity comes from work on neuronal polarization [48,49]. Immature cultured hippocampal neurons initially project a number of short extensions called neurites. After several hours in culture, a single neurite elongates and differentiates into an axon. Actin depolymerizing drugs and the inhibition of Rho GTPases induce multiple primary neurites to elongate into axons.

These data clearly show that the process of actin assembly and disassembly is a major regulator of cell polarity and function.

1.3 Intermediate filaments

Intermediate filaments are tough ropelike polymers of about 10 nm in diameter (Fig. 3) that mainly provide mechanical strength to cells and tissues. Intermediate filaments are not restricted to the cytoplasm but are also found within the nuclear envelope. In contrast to actin filaments and microtubules, whose components are highly conserved during evolution and are very similar within cells, intermediate filaments display much diversity in gene number, sequence homology and expression pattern among metazoa [8,50,51]. Despite their diversity, members of the intermediate filament family share a common structure. Intermediate filament protein monomers are elongated fibrous molecules with a 300-330 amino-acid central α-helical rod domain separating N- and C-terminal domains of variable structure and chemical character [1,8,50,52]. The α-helical rod domain of intermediate filaments promotes formation of coiled-coil dimers between two parallel intermediate filament protein monomers (Fig. 3). Two polar dimers associate in an antiparallel, half staggered manner to form a protofilament. Eight protofilaments form the 10 nm intermediate filament, which yields a coiled-coil lattice of approximately 32 polypeptides in cross section (Fig. 3).

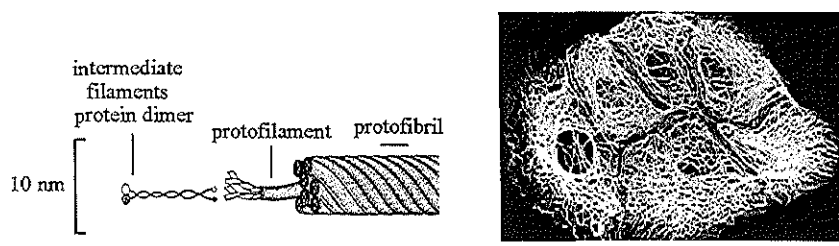

Figure 3. Structure of intermediate filaments
Intermediate filaments are ropelike fibers of about 10 nm in diameter. They are made of intermediate filament protein dimers which associate into protofilaments. Two protofilaments form a protofibril. Four protofibrils form the 10 nm intermediate filament. Immunofluorescence staining of the keratin network in epithelial cells is shown.

In contrast to actin filaments or microtubules, intermediate filaments subunits do not bind nucleotides and filament assembly does not require GTP or ATP hydrolysis. However, a detailed understanding of intermediate filament assembly is not yet available. In addition, intermediate filaments are not, like actin filaments and microtubules, dynamic structures. In most terminally differentiated cells, almost all intermediate filaments are in a fully polarized state, with very little free dimers. Even after extraction with solutions containing detergents and high concentrations of salt, most intermediate filaments remain polymerized while actin filaments and

microtubules are solubilized. These specialized properties of intermediate filaments make them excellent structures to provide mechanical strength to cells and tissue.

1.3.1 Intermediate filaments and binding proteins

On the basis of sequence homology the protein members of the intermediate filament family in humans are classified in six different types [8]; type I and II (keratins), type III (vimentin, desmin, glial fibrillary acidic protein (GFAP), peripherin), type IV (α-internexin, three neurofilament subunits; NF-L(ight), NF-M(edium) and NF-H(igh)), type V (nuclear lamins) and type VI (nestin). Interestingly, *Drosophila* lacks intermediate filaments other than nuclear lamins, while other invertebrates have multiple intermediate filament proteins. For example the nematode *C. elegans* appears to have eight genes encoding different intermediate filament proteins [6]. In *S. cerevisiae* only the MDM1 (mitochondria defect mutant) gene product may be related to intermediate filament proteins [54]. Sequence comparisons in several multicellular animals suggest that intermediate filament proteins arose from a mutated lamin gene [53].

The variable N- and C-terminal domains of intermediate filament proteins allow each type of filament to associate with other components in the cell. The interaction between intermediate filaments and other subcellular structures is also mediated by proteins that bind to specific intermediate filaments, such as desmoplakin, plectin and bulbous pemphigoid antigen 1 (BPAG1) [55]. Alternative splicing of BPAG1 and plectin mRNAs in turn produces functionally diverse proteins that can cross-bridge intermediate filaments with microtubules or intermediate filaments with actin filaments, to form an integrated cytoskeletal network [56,57]. Three types of cytoskeletal connections are implicated, for example, in cell substratum contacts and cell migration [58].

1.3.2 Function of keratins

Keratins are the main type of intermediate filaments and account for three-quarters of all known intermediate filament proteins [8,50]. Keratins are mainly expressed in epithelial cells. In contrast to other intermediate filament classes, keratins form heterodimers of type I (acidic) and type II (basic) keratin, while either type alone cannot assemble into filaments [8,53,59]. Keratin filaments are attached to desmosomes which link neighboring cells together and form a continuous network throughout the tissue. In this way the filaments are responsible for resisting externally applied stress to the epithelial cells of the skin, lung, esophagus, intestine and kidney [8,50,60]. Mutations in the keratin genes, which are expressed in keratinocytes in the epidermis, for example K14, cause different human skin defects, such as epidermolysis bullosa simplex (EBS) [9,60]. Transgenic mice expressing different mutated keratin genes show blistering of the skin, which resembles the phenotype observed in the human disorders [61]. So when keratin proteins are mutated, the structural framework for the cell becomes disorganized and the cells become fragile and prone to rupture

when stressed. Interestingly, in keratin K14 knock-out mice the blistering is somewhat milder than seen with the K14 mutations [62]. This suggests that mutated keratin protein forms aggregates that exacerbate the situation more than when the keratin network is missing.

1.3.3 Function of neurofilaments

Neurofilaments are the major intermediate filaments in mature neurons and are most abundant in large myelinated axons [8,50,63]. Neurofilaments are composed of three different proteins, NF-L (68 kDa), NF-M (150 kDa) and NF-H (200 kDa), with large variable carboxyl-terminal domains. NF-L is known to polymerize on its own, whereas NF-M and NF-H cannot. However, both NF-M and NF-H can co-assemble with NF-L both *in vitro* and *in vivo* [64]. They are thought to bind laterally to the NF-L backbone and protrude their carboxy-terminal tails out to the side of the filament. These projections extend from the filament backbone to form lateral cross-bridges between neurofilaments, which organizes them into parallel arrays in the axon. Additional cytoskeletal linker proteins can connect neurofilaments to actin filaments and microtubules [58]. The close correlation between the number of neurofilaments in axons and the axonal diameter and studies on neurofilament deficient mice have demonstrated that neurofilaments serve as cytoskeletal spacers and determine the axonal diameter [65]. This axonal diameter directly affects the conduction velocity of nerve impulses along the axon. The axonal caliber is modulated not only by the number of filaments but also by changing the stoichiometry of the three neurofilament subunits and their phosphorylation pattern [63,66]. In myelin-deficient *trembler* mice, neurofilaments are less phosphorylated and more closely spaced in axons, which results in a smaller axonal diameter compared to wild type mice [69], suggesting that the expression of neurofilaments subunits and the phosphorylation status of neurofilaments may be regulated by myelination [67,68].

Neurofilaments frequently appear altered in neurodegenerative diseases, including motor neuron diseases such as amyothrophic lateral sclerosis (ALS) and spinal muscular atrophy (SMA) [70,71]. The common clinical symptom of motor neuron disease is progressive failure of motor neurons. This causes atrophy of the skeletal muscles synapsed to the dying neurons, which eventually leads to paralysis and death. In human ALS, the large motor neurons, which contain most neurofilament, are most affected. Of the neuronal abnormalities, massive neurofilament accumulation in the cell body and proximal axons is the most prominent pathological feature, suggesting that neurofilament dysfunction may play a key role in the disease. In transgenic mice, overproduction of neurofilament subunits in motor neurons showed dysfunction of motor neurons and, later on, degeneration of motor axons [72,73]. However, only one mutation in the NF-H gene has been identified in a small percentage of patients with sporadic ALS [74]. No other mutation in the three neurofilament genes have been linked to disease. In contrast, about 20% of patients with familial ALS have a mutation in the ubiquitously expressed gene Zn, Cu

superoxide dismutase 1 (SOD1) [75,76]. Although many mechanisms have been proposed to account for the properties of the mutated SOD protein, it remains unknown how SOD is related to defective neurofilament accumulation [9]. One possible hypothesis is that motor neuron degeneration of patients with ALS may arise from disorganized neurofilaments which block transport of vesicles or other components into the axon [77]. To summarize; the data described in this section indicate that neurofilament proteins determine axonal diameter and are involved in some neurodegenerative diseases. Whether changes in neurofilament proteins, as for keratins, are a major cause of disease remains an open question.

1.4 Microtubules

Microtubules are dynamic polymers of α/β-tubulin heterodimers of about 24 nm in diameter (Fig. 4). Microtubules themselves have an intrinsic polarity with a slow growing minus end and fast growing plus end [78,79]. In all eukaryotic cells, microtubules are essential for a correct cell division. In interphase cells, microtubules usually originate at the centrosome and form a dynamic network of fibers. Here they play a major role in intracellular movement and positioning of organelles. Microtubules were originally identified as a prominent component of flagella and cilia [1,8,80]. Flagella provide the means for locomotion of single eukaryotic cells, like flagellated protozoa. In mammals, many epithelial cells are ciliated in order to move material along the tissue surface. Microtubules are also involved in the migration of cells which do not have flagella or cilia, like fibroblasts and macrophages.

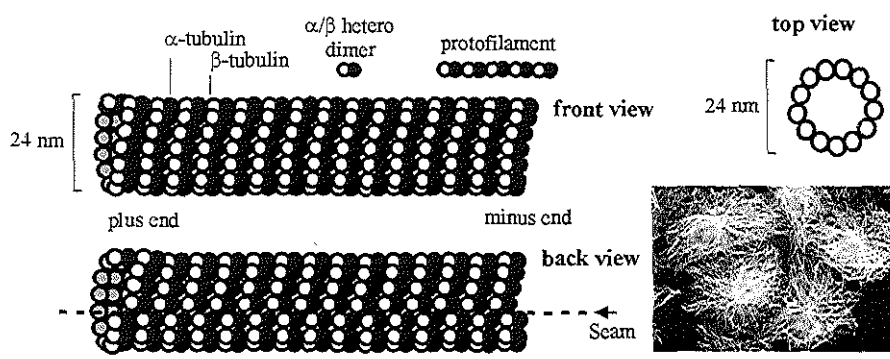

Figure 4: Structure of microtubules
Microtubule polymers are polar structures, with a plus end and a minus end and are made of α/β-tubulin heterodimers. Tubulin heterodimers interact head-to-tail to form linear protofilaments, which associate laterally to form the 25 nm wide hollow microtubule cylinder. The protofilaments are arranged slightly staggered and form spiraling rows of tubulin proteins. Microtubules, which contain 13 protofilaments (top view), have a packing discontinuity and a seam along their length (back view). Immunofluorescence of the microtubule network in COS-1 cells labeled with an anti-β-tubulin antibody is shown.

1.4.1 Tubulin family, properties and structure

Tubulin superfamily

Microtubule polymers are made of α– and β-tubulin proteins (Fig. 4). The tubulin superfamily consists of seven members, named α-, β-, γ-, δ-, ε-, ζ- and η-tubulin and a distantly related bacterial filamentous temperature sensitive protein (ftsZ) [81,82]. Genes for α-, β- and γ- tubulin are found in all eukaryotic organisms and are essential for microtubule polymerization. Five tubulins (α-, β-, γ-, δ-, ε-tubulin) are known to exist in vertebrates, while ζ- and η-tubulin are found in flagellated or ciliated protozoa [83]. FtsZ is only present in prokaryotes, is essential for cell division and shows remarkable similarity in sequence, structure and polymer arrangement to tubulin [79,84]. The vertebrate tubulin proteins have different but highly conserved functions; α- and β-tubulin assemble to form heterodimers and are the structural subunits of microtubules [79], γ-tubulin is localized in the centrosome and has been established as a key factor in nucleating microtubule assembly [85] and, δ- and ε-tubulin have recently been identified as new centrosomal components [86].

It has been established that lower eucaryotes have small multigene families encoding both α- and β-tubulin. For example, yeast cells contain two α-tubulin genes, whose protein products are 80% identical and only a single β-tubulin gene [25]. In humans and other vertebrates six functional α-tubulin and a corresponding number of β-tubulin genes have persisted during evolution [2]. Although sequence diversity often indicates that a protein has become specialized in a function, genetic evidence in yeast has clearly shown functional redundancy between the isotypes. If one of the two α-tubulin genes is disrupted, the yeast cell is still able to grow and divide normally [87]. In contrast, during spermatogenesis in *Drosophila*, one β-tubulin isoform can not be substituted for another, since mutant sperm cells lack microtubular structures in their flagella [88]. This indicates that at least some tubulin isotypes arose during evolution to carry out particular functions.

Tubulin stability and folding

The proper folding of α-, β- and γ-tubulins, and likely the other tubulin family members, cannot occur spontaneously and requires an ATP-dependent interaction with cytosolic chaperonins (c-cpn) [89-91]. Although newly synthesized γ-tubulin is folded properly by c-cpn, folding reactions for α- and β-tubulin molecules are far more complex. Since α- and β-tubulin are only partially folded by chaperonin and are highly unstable in the monomeric state, a special set of additional tubulin-specific chaperones, termed tubulin folding cofactors A-E, are needed to finish the folding and join α- and β-tubulin into functional dimers [89,90,92,93]. Cofactor D and E bind to partially folded β and α monomers, respectively. Subsequent binding of cofactor C combines the monomers and releases the stable dimer. Cofactor A and B each appear to act as reservoirs for the capture of chaperonin folded β and α monomers, respectively, and

probably regulate the balance of the α- and β-subunits. Experiments show that a higher expression of β-tubulin is lethal. Overexpressing cofactor A rescues this defect, suggesting that cofactor A sequesters the excess β monomer [94]. Homologues of cofactor A (Rbl2), B (Alf1), D (Cin1) and E (Pac2) exist in *S. cerevisiae* [25,94,95]. There is no cofactor C homologue in yeast, however, this factor exists in plants and nematodes. Although mutations in cofactor genes in *S. cerevisiae* result in cytoskeletal defects, none of the cofactors are essential for cell viability [96-98]. This contradicts with the expectations based on findings in mammalian systems, in which the cofactors are absolutely required for tubulin folding *in vitro* [91]. In fission yeast *S. pombe*, the cofactors, A (Cfa), B ($Alp11^B$), D ($Alp11^D$) and E ($Alp21^E$) were shown to be essential for life [99,100]. Interestingly, both mammalian cofactor B and E and their homologues in other organisms (except for $Alp21^E$ in fission yeast) contain a microtubule binding CAP-Gly motif, which is present in CLIP-115 and CLIP-170 (see section 2.5.1).

Tubulin structure

Microtubule polymers are formed by the self-assembly of α- and β-tubulin heterodimers (Fig. 4). The α- and β-tubulin monomers have a molecular mass of 50 kDa each and share 40 percent amino-acid sequence identity [79]. Both tubulins exist in several isotypes and undergo a variety of post-translational modifications [81,101]. Both α- and β-tubulin proteins and all other tubulin homologues have a seven amino acid region that is involved in GDP/GTP binding. This guanine nucleotide binding domain is structurally different from that of classical GTPases [102]. There is an important difference in GTP hydrolysis for α- and β-tubulin proteins. GTP is nonexchangeable when it is bound in the α subunit and exchangeable when bound in the β subunit. The GTP bound β-tubulin is hydrolyzed to GDP soon after the heterodimer is incorporated in the microtubule polymer [78] (see section 1.4.3). The structures of α- and β-tubulin are basically identical and can be divided into three functional domains: the amino-terminal domain containing the nucleotide-binding region, an intermediate domain containing the taxol-binding site (in the β subunit) and a carboxy-terminal domain, which forms the outside surface of the microtubule, where the microtubule-associated proteins are likely to bind [103]. The last 15 residues of the tubulin monomers are the most variable parts of the molecules and the main determinants of isotype variety. From the structural data of α- and β-tubulin, an molecular model for α/β-tubulin heterodimers has been presented [89,104]. Within a dimer, the GTP in the amino-terminal domain of the α-tubulin subunit interacts with the intermediate domain of the β-tubulin subunit. In this way, the nucleotide of α-tubulin is buried within the dimer, and thus, nonexchangeable, while the GTP in β-tubulin is exposed and exchangeable.

Tubulins are a major target for antitumor drug molecules [18]. The antiproliferative action of all microtubule drug agents appears to result from

modulation of the polymerization dynamics of spindle microtubules. Several synthetic inhibitors have been developed that are related to the natural products taxol, colchicine and vinblastine. Taxol, a drug from the bark of Pacific yew tree is effective in the treatment of a wide range of human malignancies [17,105]. Taxol has a specific binding site on the β-tubulin molecule and is able to stabilize microtubules [106]. The ability of taxol to block cells in mitosis, by preventing them to form a normal mitotic apparatus, in the absence of cofactors like GTP and microtubule-associated proteins, makes it unique among chemotherapeutic agents. In contrast to taxol, colchicine, colcemid, and nocadazole inhibit polymerization by preventing the addition of tubulin to the plus ends. At high concentrations vinblastine aggregates tubulin and also leads to microtubule depolymerization. New microtubule (de)polymerization inhibitors, developed on the basis of the α- and β-tubulin protein structure, will attract great attention in the future.

1.4.2 Microtubule structure, assembly and nucleation

Microtubule structure

Within a microtubule, α/β-tubulin heterodimers interact head-to-tail to form linear protofilaments, which associate laterally to form 25 nm wide hollow cylindrical polymers (Fig. 4). *In vitro*, the protofilament number of microtubules varies from 10 to 15. Microtubules *in vivo* and microtubules nucleated *in vitro* from centrosomes have predominantly 13 protofilaments [107]. Protofilament number can also be controlled by specific isoforms of β-tubulin [108]. A high-resolution map of microtubule structure has recently been obtained using electron crystallography [109]. This shows that, in contrast to earlier hypotheses, the lateral interaction between tubulin monomers of adjacent protofilaments are made between subunits of the same type, that is, α-α and β-β. This results in a slightly staggered protofilament arrangement, forming spiraling rows of α- and β-tubulin that travel up the microtubule lattice (Fig. 4). In this arrangement, microtubules with 13 protofilaments have a seam along their length, which results in a packing discontinuity and loss of helical symmetry (Fig. 4). At the seam the lateral monomer contacts are reversed (β-α and α-β) [110]. Although the relevance of this seam is still being debated, it is likely to be related to the microtubule polymerization process, which shows that microtubules grow by elongation of open sheets that later close into a cylinder (see section 1.4.3)

As a consequence of the head-to-tail interaction of α/β-tubulin heterodimers within the microtubule lattice, the microtubule itself forms a polar structure, with a plus end and a minus end (Fig. 4). After considerable controversy, it is now clear that within each protofilament, the α/β-tubulin heterodimers are oriented with their β-tubulin monomer pointing towards the plus end of the microtubule. Therefore β-tubulin is exposed at the distal end and α-tubulin is exposed at the minus end of the microtubule, which in turn is usually embedded in the centrosome [79,110]. The

polarity of the microtubule is of central importance for the function of microtubules in a variety of cellular processes (see section 1.4.4).

Microtubule assembly

Microtubule nucleation and assembly is quite different in a test tube compared to the living cell. *In vitro*, high concentrations of free tubulin cause microtubules to self-nucleate and grow from both ends, with their plus end growing more quickly. In most animal cells microtubules are nucleated within the centrosome, also called the microtubule organizing center (MTOC) or, in yeast, the spindle pole body (SPB) (Fig. 5a) [79,111-113]. The centrosome is about 1 μm in diameter, is composed of a pair of centrioles surrounded by pericentriolar material and is located normally in the center of the cell, next to the nucleus. The microtubule plus-ends, nucleated from the centrosome, are free to add tubulin molecules and extend distally to the periphery of the cell at approximately 0.2 μm per second (Fig. 5a). Thus, centrosomes have a dual function in interphase cells: they focus the microtubule array, which helps to organize the cytoplasm, both in positioning the organelles as well as in providing routes for vesicular transport [114] and they stabilize the microtubule minus ends, which might otherwise be subject to depolymerization. In addition, the centrosomes are duplicated during mitosis and help the formation of the mitotic spindle.

In vivo, microtubule nucleation requires a third tubulin, γ-tubulin, which does not polymerize with α/β-tubulin and is limited in its distribution to the centrosome. γ-Tubulin shares approximately 30 percent identity with α/β-tubulin. Disruption of γ-tubulin genes in fungi and yeast causes lethality and results in perturbations of the mitotic spindle structure [115,116]. In the pericentriolar material, γ-tubulin forms a complex with at least five other proteins, which is called the γ-tubulin ring complex (γ-TuRC) [85,112]. This γ-TuRC is of roughly the same diameter as a microtubule. Two models have been proposed to explain how γ-tubulin binds to the microtubule minus end and how γ-tubulin nucleates microtubule assembly [117]. The difference between the two models is the orientation of the γ-TuRC with respect to the microtubule lattice.

Non-centrosomal microtubules

As discussed above, in dividing cells, interphase microtubules are typically organized into a radial array with their minus end anchored at the centrosome and their plus ends, extending towards the cell periphery (Fig. 5a). However, in many terminally differentiated cells, microtubules are not only focused at the centrosome [118,119]. In polarized epithelial cells, for example, microtubules are parallel to the long axis of the cell, with their minus end located at the apical surface and their plus end at the basal surface. In addition, randomly oriented microtubules are located below the apical membrane (Fig. 5b). This arrangement is important for the proper sorting of membrane components and directing vesicle traffic to the apical or basal sites [120]. In migrating epithelial newt lung cells 80-90% of the microtubules are not bound to the centrosome [121]. In neurons, only a few microtubules are attached to the centrosome, which is

present in the cell body. The vast majority of the microtubules are free, they coalesce into bundles that reside in the axons and dendrites (Fig. 5c). In axonal processes, microtubules are uniformly polarized, with their plus ends orientated towards the growth cone whereas in dendrites the microtubules have mixed polarity, with about half the microtubule minus ends proximal and half distal to the cell body [122]. It has been widely speculated that the difference in microtubule polarity in dendrites and axons is the basis for selected protein sorting into the dendritic or axonal compartments [123-125].

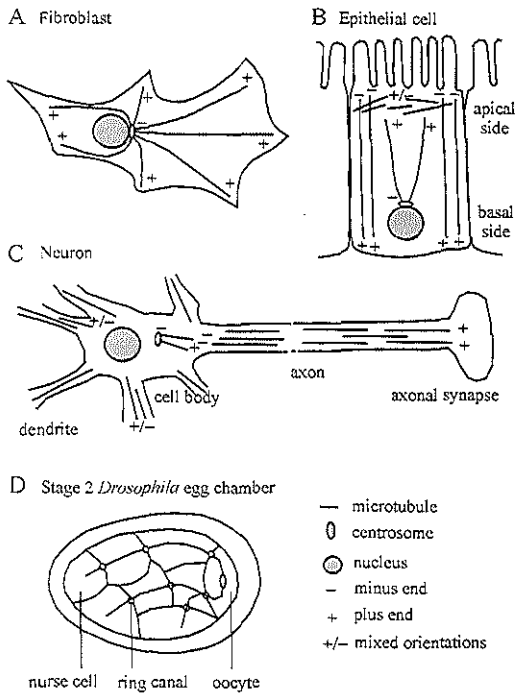

Figure 5: Microtubule organization in different cell types.
Schematic view of the microtubule network in **A** fibroblast, **B** epithelial cell, **C** neuronal cell and **D** *Drospohila* egg chamber. **A** In fibroblasts microtubules are nucleated within the centrosome or MTOC, which is located in the center of the cell, next to the nucleus. The centrosome binds the microtubules at their minus end and initiates microtubule assembly at the plus ends. The microtubule plus ends extend distally to the periphery of the cell, while the minus ends stay captured at the centrosome. **B** In epithelial cells, microtubules are initially nucleated within the centrosome. Some of the centrosome microtubules are broken and released from the centrosome. The free microtubules localize parallel to the long axis of the cell, with their minus end located at the apical surface and their plus end at the basal surface or randomly below the apical membrane. **C** In neurons, almost all microtubules are free and not attached to the centrosomal. Non-centrosomal microtubules are generated by self-assembly of microtubules in the cytoplasm or by severing of centrosomal microtubules. The free microtubules form bundles in axons and dendrites. The microtubule array of axons differs from that of dendrites. In axons, microtubules are uniformly polarized, with their plus ends orientated distally towards the synapse and their minus end towards the cell body. In contrast, in dendrites the microtubules are mixed in polarity orientation, with approximately equal numbers having a plus-end-distal or minus-end-distal orientation. **D** In the developing *Drosophila* egg chamber, after the fourth cystoblast division, a MTOC becomes active in one of the 16 interconnected cells. The cell containing the MTOC differentiates into the future oocyte, while the other form the nurse cells. The microtubules extend from this MTOC, through intercellular ring canals into the nurse cells.

Different types of mechanisms can generate non-centrosomal microtubules: self-assembly of microtubules in the cytoplasm, nucleation of microtubules at non-centrosomal sites, or breakage or severing of centrosomal microtubules along their length and release of microtubules from the centrosome. All mechanisms are observed in cultured cells or extract systems [111,118]. In vitro, free microtubule nucleation

only occurs at relatively high concentrations of pure tubulin. The tubulin concentration in cells is generally below that required for spontaneous nucleation, suggesting that non-centrosomal nucleation must be driven by cellular factors. Microtubules may grow from nucleation sites that are free in the cytoplasm or attached to the cell membrane or cytoplasmic vesicles. To date it is unknown which factors are involved in this process. Candidate proteins with possible nucleating activity are free cytoplasmic γ-TuRC and microtubule stabilizing proteins [126,127]. Another mechanism that can produce free microtubules is breaking or severing. A break in a microtubule, random or near the centrosome, can be caused by mechanical stress [121,128] or by specific mechanochemical enzymes, such as katanin [129]. Katanin consists of a heterodimer of an ATPase subunit, that possess an enzymatic activity and a WD40 domain containing subunit, which targets katanin to the centrosome. Katanin uses ATP hydrolysis to disassemble microtubules at internal sites, resulting in an ATP-dependent severing activity [130].

It has been shown in epithelial cell lines that microtubules released from the centrosome are generally prevented from disassembly. This suggests that free microtubule minus ends in these cells are specifically capped [131,132]. If the microtubules lose their cap, the microtubules are rapidly shortened from their minus end. Axonal and dendritic microtubules in neuronal cells show similar behavior, in that they are released from the centrosome and grow with their plus ends only [119,133,134]. One interesting candidate as a minus end cap protein is the γ-TuRC. The release of the microtubules from the centrosome may occur between the centrosomal material and the γ-TuRC , thereby producing a stable γ-tubulin capped microtubule [127]. Additional, unidentified minus end associated proteins might also serve this function.

1.4.3 Microtubule dynamics

Dynamic instability

The ability of microtubules to grow and shorten rapidly allows a cell to quickly re-arrange the microtubule network. Individual microtubules switch between phases of slow growth and fast shrinkage, so that within a single cell microtubules exhibit different polymerization dynamics. This process is called microtubule dynamic instability [135,136]. The 'dynamic instability' model provides a good mechanistic description of the dynamic behavior of microtubules [78].

Microtubule dynamic instability is defined by four parameters: the rate of growth (polymerization), the rate of shrinkage (depolymerization), and the transition frequencies between growing and shrinking (catastrophe) and shrinking and growing (rescue) (Fig. 6a). One other term used in the description of microtubule dynamics is pausing. Pauses are periods in which the microtubule length stays constant. This reflects either a non dynamic state or a dynamic state such as treadmilling (see below). It is generally accepted that the transition between growth and shrinkage most likely

depends on the biochemical nature and structure of the microtubule plus ends and the presence of a terminal stabilizing cap of unhydrolyzed GTP, the "GTP cap" (Fig. 6a) [78]. When a microtubule grows, α/β-tubulin heterodimers with bound GTP assemble at the microtubule plus end and protect the microtubule from shrinking. Soon after incorporation of tubulin subunits in the polymer, the GTP bound to the β-tubulin subunit is hydrolyzed to GDP. In this way the end of the microtubule consists of GTP-containing subunits, while the rest of the microtubule contains GDP in the exchangeable site on β-tubulin (Fig. 6a). However, it is not clear how long the lag is between incorporation into the lattice and GTP hydrolysis and how many GTP subunits need to be bound to the microtubule to stabilize it. Some experiments suggest that a stabilizing GTP cap can be as small as one layer of subunits [137]. The loss of the "GTP cap" results in exposure of an unstable GDP-tubulin core and causes destabilization and rapid disassembly of the microtubule. Experiments with nonhydrolysable GTP analogues have shown that polymerization does not require GTP hydrolysis and that the microtubule lattice is more stable with GTP bound to β-tubulin than with GDP [138]. This suggests that the primary role of GTP hydrolysis is to destabilize the microtubule lattice by creating GDP-bound subunits, that make weaker intersubunit contacts. Thus, tubulin dimers have a built-in lattice destabilization mechanism driven by GTP hydrolysis on β-tubulin.

The polymerization rate of tubulin in vivo is approximately tenfold higher than that of similar concentrations of pure tubulin. In addition, microtubules in vivo exhibit a high frequency of catastrophe [139]. Therefore, it is very likely that in a cell distinct mechanisms exist to promote polymerization and to induce catastrophe. Much effort has been directed toward identifying proteins that regulate microtubule dynamics (see section 2.3).

Structural basis for dynamic instability

Approaches using cryoelectron microscopy have shown that the structure of the protofilament lattice at the microtubule end is different during growing and shrinking phases [140]. During growth, the microtubule tip is not blunt but rather consists of a two-dimensional sheet of slightly curved protofilaments closing into tubes further down the lattice (Fig. 6b). The length of the sheet increases with increasing growth rate [141]. Thus, the length of the sheet appears to correlate with the stability of the microtubule. During shrinkage, the microtubules display curved protofilaments, peeling out from the plus end and dissolving almost immediately into subunits (Fig. 6b) [111]. The molecular structure of tubulin and measurements between GTP- and GDP-bound tubulin subunits have shown that tubulin can have two conformations; a straight, relaxed conformation of GTP-tubulin and a curved, stressed conformation of GDP-tubulin (split ends) [89,104,111,141]. This suggests that the sheets are composed of GTP-tubulin protofilaments, that the curled protofilaments contain GDP-tubulin and that GTP hydrolysis changes the protofilament conformation from straight to curled.

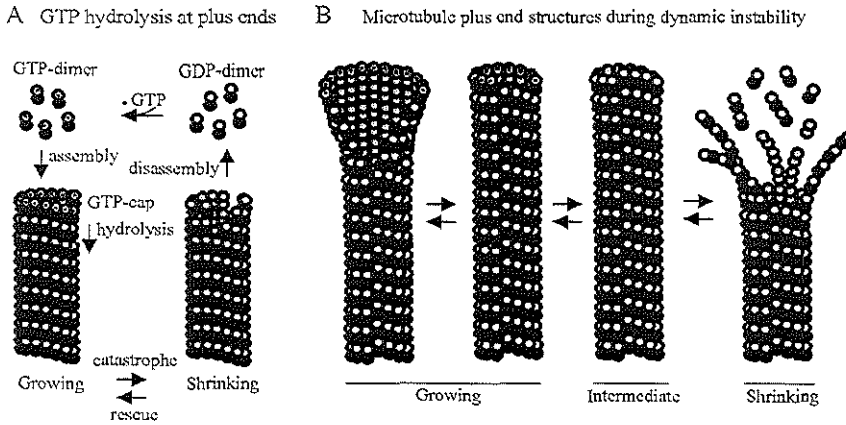

Figure 6: Dynamic instability
A GTP hydrolysis at microtubule plus ends. With the expectation of the microtubule plus end, all tubulin subunits in the microtubule polymer are bound to GDP. The microtubule plus end consists of GTP containing tubulins, also called the GTP-cap. Tubulin dimers that are assembled into the microtubule carry GTP. Soon after incorporation in the polymer, the GTP-tubulin is hydrolyzed to GDP. When a GTP-tubulin is added faster then the GTP is hydrolyzed, the GTP cap is created. The GTP cap forms a stable structure at the plus end of the microtubule and promotes tubulin assembly. Loss of the GTP cap results in destabilization and rapid disassembly of the microtubule. Microtubule disassembly results in the release of GDP-tubulin dimers. These tubulin dimers exchange their GDP for GTP and can be assembled into a newly growing microtubules. Microtubules utilize this mechanism of polymerization-induced GTP hydrolysis to generate dynamic instability B Microtubule plus end structures during dynamic instability. The microtubule plus ends have distinct conformations in the growing and shrinking phases. During microtubule growth, the plus end of the microtubule consists of a open flat sheet of protofilaments, which folds into a tube further down the lattice. At the tip of the sheet a stable GTP cap is present. When a microtubule stops the assembly of tubulin heterodimers, the sheet becomes shorter. This allows the microtubule tube to close all the way to the plus end, which will generate a microtubule blunt end without a GTP-cap (intermediate phase). At that stage, the protofilaments on plus ends will immediately peel back around the microtubules tube and break up into tubulin heterodimers. This will cause a rapid disassembly of the microtubule (shrinking).

How do these data correlate with the dynamic instability model? The most likely explanation is that the GDP-tubulin protofilaments in the lattice of the microtubule, which prefer a curved conformation, must be constrained within the straight wall of the microtubule. This puts mechanical strain on the lattice and results in an inherently unstable conformation of the microtubule. The GTP-tubulin protofilaments in sheets at the microtubule ends are relaxed and can easily interact with each other. This makes sheets at microtubules plus end extremely stable and prevents the GDP-tubulin protofilaments in the rest of the microtubule to relax into the preferred curved conformation [142]. For dynamic microtubules it means that when a microtubule polymerizes at a slower rate or stops the assembly of α/β-tubulin heterodimers, the stable sheet becomes shorter and the microtubule tube closes all the way to the tip, generating a blunt end (Fig. 6b). As the microtubule closes a GDP subunit will contact a GTP subunit at the seam, which may result in GTP hydrolysis

which propagates around the helix. Now, the mechanical stress in the GDP lattice is no longer constrained by the GTP cap and the GDP subunits can relax into the preferred curved conformation. GDP containing protofilaments release the strain by curling out, which causes rapid catastrophic depolymerization [111].

In summary; experimental data point to a microtubule (de)polymerization mechanism in which a sheet conformation prevents microtubule depolymerization and closure of the microtubule tube to the end of the polymer triggers catastrophy. It seems likely that factors influencing microtubule dynamics exert their function by interacting with protofilaments of the sheet structure, by enhancing or preventing tube closure.

Treadmilling

In many cells, the cytoplasmic microtubules are nucleated and anchored by their minus ends at the centrosome. The predominant dynamic behavior of such microtubules is dynamic instability at their plus ends. In contrast, in polarized cells, many free, non-centrosomal microtubules are present. These microtubules are stabilized at their minus ends and display dynamic instability at their plus ends or have both ends free and show a rapid treadmilling behavior in the absence of detectable dynamic instability [132]. Treadmilling involves the addition of α/β heterodimer tubulin to the plus end of a microtubule and loss of α/β tubulin subunits from the other end under conditions where the polymer maintains its length. As a consequence, there is a continuous tubulin subunit flux from one end of the polymer to the other [143].

Observations from fish melanophores revealed that some of the microtubule movement in the cytoplasm is achieved by treadmilling. Here, microtubules are detached from their nucleation site and depolymerize from their minus ends. However the rate of depolymerization at the minus end equals the rate of microtubule polymerization at the plus end. This results in microtubules of constant length that move in a steady manner away from the centrosome to the periphery with their plus ends leading. The rate of treadmilling was measured to be as high as 10 μm/min [132]. The functional implications for microtubule treadmilling are substantial, including a function during the construction of the mitotic spindle and the permission of passive transport of microtubule associated organelles [143].

Microtubule stabilization

In interphase cells, two populations of microtubules have been distinguished; short-lived or dynamic microtubules, with a half live of 5-10 minutes and long-lived or stable microtubules with a half live of more than 1 hour [144]. Dynamic microtubules have been described above and predominate in proliferating and undifferentiated cells, whereas stable microtubules may be the more abundant type in differentiated cells. Stable microtubules are enriched in post-translationally modified forms of α-tubulin, known as detyrosinated tubulin and acetylated tubulin, whereas dynamic microtubules contain predominantly tyrosinated tubulin [101,145]. Detyrosination involves the removal of a carboxy-terminal tyrosine from α-tubulin. Removal of the tyrosine by a

tubulin-specific carboxypeptidase leaves a terminal glutamic acid on the carboxy-terminus of α-tubulin which results in detyrosinated tubulin (also called glutamylated tubulin, or Glu-tubulin). Subsequently, tubulin tyrosine-ligase reattaches tyrosine to detyrosinated tubulin (or Tyr-tubulin) [101,146]. Removal of both tyrosine and glutamic acid residues yields non-tyrosinatable tubulin, which is the major α-tubulin in mammalian brain [147]. In addition to detyrosinated tubulin, subpopulations of stable microtubules also contain acetylated tubulin, where an acetyl group is attached to lysine at position 40. The different tubulin forms in a cell can be detected with antibodies that specifically recognize these modifications [148]. Despite the correlation between high levels of Glu-tubulin or acetylated tubulin and microtubule stability, neither modification directly cause microtubule stabilization nor distabilization. Instead, it is now clear that the modification is a consequence of microtubule stability [149,150].

1.4.4 Role of microtubules in cellular processes

Microtubules and transport

Several lines of evidence suggest that microtubules play an essential role in maintaining the distribution of cellular material [114]. Studies using video-enhanced light microscopy have demonstrated that membranous vesicles are transported bidirectionally along microtubules in living cells or in extruded axoplasm [151-153]. In addition, disruption of the microtubule cytoskeleton by microtubule depolarizing agents, such as nocodazole, results in an abnormal distribution of various organelles, such as mitochondria, endosomes and the Golgi apparatus [154-156]. Electron microscopy has shown the presence of various cross-bridge structures between transport organelles and microtubules [157,158]. These findings suggested the existence of an array of motor proteins that mediate the microtubule transport system. The identification of molecular motors such as kinesin and dynein, which are capable of movement to the microtubule plus end and the minus end, respectively, provided the first glimpse of the mechanisms involved in intracellular trafficking [158,159]. Over the last several years, multiple kinesin-related motors proteins (KIFs) have been identified (see section 2.4). Characterization of kinesin properties has revealed that the stable microtubules are the preferred tracks used for the translocation of membranous vesicles [160].

The microtubule network is not the only transport system in the cell. In plants, algae and budding yeast, for example, organelles are mainly transported along the actin filaments and depend on the actions of myosin motor proteins. In addition, treatment of animal cells with microtubule depolymerizing drugs shows that the actin transport system can take over from the microtubule system. Thus, some organelle translocations may be facilitated by both the microtubule and actin-based transport systems [161]. There is further evidence that the actin-based vesicle transport motor,

myosin Va, interacts directly with the microtubule-based kinesin motor, which provides a direct link between actin and microtubule trafficking systems [162].

Most experiments to determine the role of microtubules in intracellular transport have been done in neuronal cells. In neurons, microtubule dependent transport is the primary mechanism for the distribution of materials necessary for axonal and dendritic functions [125,163]. The microtubule cytoskeleton is very important in axonal transport because, due to the lack of protein synthesis in the synapse, most of the materials have to be transported down the axon after synthesis in the cell body. Two types of axonal transport occur in neurons: fast and slow. Fast transport is responsible for the movement of membranous organelles at 50-200 mm per day towards the synapse or back to the cell body. Synaptic vesicles, ion channels, neurotransmitters and neuropeptides are transported anterogradely towards the synaptic terminal by fast transport [164]. Slow axonal transport moves cytoskeletal proteins at 0.5-4 mm per day. The transport of tubulin itself is microtubule dependent. Two opposing models have been proposed to explain how tubulins are transported by slow axonal transport. The first, the polymer sliding theory, hypothesises that microtubule structures grow, as normal, in the nerve cell body, break away and then travel into the axon [165]. The second hypothesis is called the subunit transport theory and proposes that tubulin proteins are transported in an unassembled form in the axon and added where necessary to the exposed ends of the protein polymer [159]. Recent data have shown that a single labeled microtubule does not move as a polymer in cultured *Xenopus* neurons [166]. Fluorescence correlation spectroscopy revealed that labeled tubulin is actively transported by kinesins [167]. These data suggest that the subunit transport theory remains the most plausible model for tubulin protein transport.

One other example of the role of the microtubule cytoskeleton in intracellular transport comes from studies in the developing *Drosophila* oocyte [168,169]. Oocyte determination involves a complex process by which a single cell within an interconnected cyst of 16 germline cells differentiates into an oocyte. This process requires a proper organization of the microtubule cytoskeleton. A single cystocyte develops a microtubule organizing center (MTOC) and forms a polarized microtubule network that extends into all 16 cells. The single cell of the cyst that contains the MTOC develops into the oocyte (Fig. 5d). In this way, the microtubule cytoskeleton differentiates the pro-oocyte from the remaining nurse cells in the cyst and is involved in the establishment of cytoplasmic asymmetries. This polarized microtubule organization is responsible for the asymmetric accumulation of both specific mRNAs and proteins within the future oocyte, which are synthesized in the nurse cells and transported to the oocyte. Microtubule assembly inhibitors disrupt the accumulation of mRNA in the oocyte [170,171]. Once the oocyte is determined, it forms an anterior-posterior asymmetry. At this stage the MTOC becomes localized at the anterior cortex and microtubules are involved in the organization of the anterior-posterior axis [169]. The polarized microtubules position the main oocyte determinants, such as *bicoid* mRNA at the anterior pole and *oskar* and *nanos* mRNA at the posterior site. These

factors control axis formation in the oocyte and are essential for a proper spatial development of the embryo. Microtubule depolymerizing agents disrupt the localization of *bicoid*, *oskar* and *nanos* mRNAs in the oocyte [171,172]. Microtubule depolymerization also inhibits the dorsal-ventral asymmetry by mislocalization of specific mRNAs [169]. Together, these data reveal an important role for microtubules in the axis specification at each stage of oogenesis. However, how the microtubule cytoskeleton is precisely organized and how mRNAs are transported along microtubules remains unclear. Microtubule dependent motors and additional proteins, such as Bicaudal-D are likely to be involved [173-175].

The biological function of dynamic instability: search and capture mechanism

Modulation of dynamic microtubule instability allows a cell to generate a specific spatial organization of the microtubule network [78]. The cell can remodel the microtubules in such a way that an asymmetric network is generated. The asymmetric organization of microtubules towards specific membrane sites is crucial for a variety cellular processes, such as the navigation of the neuronal growth cone, the polarisation of T cells towards antigens, the movement of fibroblasts, the migration of the nucleus and the positioning of the mitotic spindle in dividing cells. Several mechanisms have been proposed to target microtubules to specific locations within the cell [79].

The search-and-capture model is the most prominent mechanism for microtubule asymmetry [78,176]. In this model, microtubules rapidly explore the three-dimensional cytoplasmic space and 'search' for specific targets or are captured by sites within the cell (Fig. 7a). Interactions between microtubules and binding sites on the cell cortex or the chromosomes (kinetochores) are thought to arise by this mechanism. In the model, dynamic instability of the microtubule plus end allows random growth of labile microtubules, which simply by a matter of chance contact the target site(s). As a result the microtubules get selectively stabilized and induce asymmetry in the microtubule cytoskeleton [78]. The captured microtubules may be stabilized by microtubule associated proteins and subsequently post-translationally modified (see section 1.4.3). The local microtubule contact sites may be formed in response to environmental cues [78,145].

However, not only a random search mechanism targets microtubules to specific locations within a cell, also a microtubule guidance mechanism exist. It has been shown that microtubules are directly guided towards target contact sites [177,178]. For example, microtubules in fission yeast can change their direction depending on the cortical membrane (Fig. 7b) (see also section 2.5.1) and microtubules in budding yeast may track along actin cables [179]. In motile fibroblasts, microtubules can repetitively target a single contact, side step to target a new contact, or even make an excursion from one contact to the other [178]. The successful connection between the microtubules and the specialised capture sites is likely to be enhanced by stabilised interactions between microtubule ends and capture sites as well as increasing local microtubule dynamics. The molecular basis for microtubule capture at the cortex and

other sites has remained elusive. However, it has been suggested that microtubule plus end binding proteins are involved in the interaction of microtubules and the cortex and may act as capture devices [180-182]. The last part of this chapter describes examples of cellular processes in which microtubule dynamics and the search and capture mechanism play an important role.

Microtubules and mitosis

Mitosis is the last step of the cell cycle and separates the replicated chromosomes into the two newly forming cells. The framework for the segregation of the chromosomes is provided by the mitotic spindle [183-185]. The mitotic spindle is composed of microtubules, two centrosomes (also called spindle poles) and their associated proteins (Fig. 7d) [111,185]. The kinetochores are the mechanical link between the chromosomes and the microtubules. The interaction between microtubules and the kinetochores is the best example of a search-and-capture mechanism [111]. In the early stages of mitosis, dynamic microtubules grow out in random directions from the two centrosomes. Their minus ends are anchored in the centrosomes, while their plus ends grow or shrink, while 'searching' for contact sites. Sometimes, individual microtubules are captured by the kinetochore, which prevents the microtubule from (de)polymerization. At anaphase, the microtubules depolymerize at the kinetochores and the attached chromatide is thereby carried to the spindle pole. This mechanism of chromosome segregation is highly regulated by microtubule motor proteins and microtubule stabilizing and destabilizing proteins [184,186,187]. However, the initial interactions between the microtubules and kinetchores are most likely regulated by growing microtubule search devices, such as microtubule plus end binding proteins [188].

The mitotic spindle also determines the plane of cleavage during cytokinesis. The position of the cleavage plane is between the two spindle pole asters. To orient the division plane, the astral microtubules of the mitotic spindle attach via the search and capture mechanism to specialised local regions of the cell cortex (Fig. 7d), resulting in a rotation of the mitotic spindle [189]. Whereas most cells divide symmetrically, sometimes the mitotic spindle is not positioned in the centre of the cell. This results in an asymmetric division and creates daughter cells of different sizes. During embryonic development, asymmetric divisions are crucial for the generation of cell diversity. Different 'microtubule capture' factors on the cortex have been described that influence the position of the spindle, these include actin, adherens junctions and PDZ-domain containing proteins [190,191].

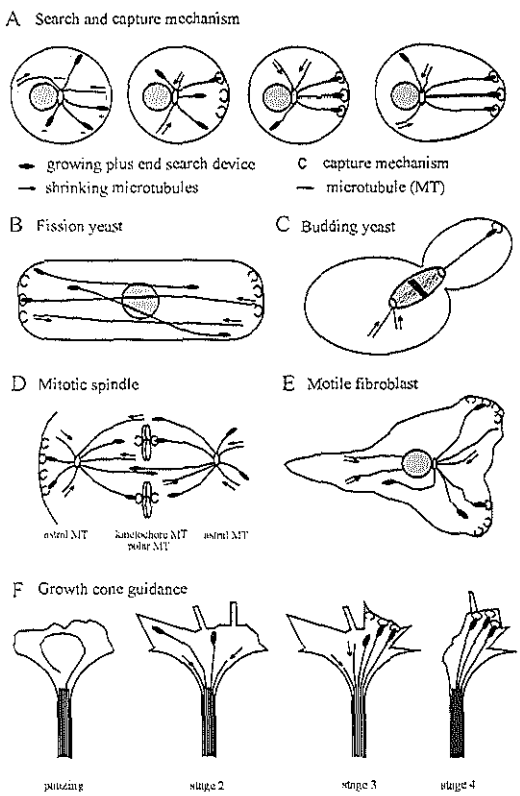

Figure 7: The search and capture mechanism

A Schematic representation of the search and capture mechanism. In a non polarized cell, the microtubules randomly grow and explore the three-dimensional cytoplasmic space. The growing microtubule plus ends act as search devices to contact potential target or capture sites. In response to positional cues, a specific region of the cell cortex sets up these capture sites that can cap the plus ends of the microtubules. The capped microtubules get selectively stabilized and induce asymmetry in the microtubule network. Asymmetry in the microtubule array converts a cell to a polarized form. **B** Microtubule network in fission yeast. Microtubules are nucleated near the nucleus and grow parallel to the long axis of the cell. Only when a microtubule reaches the capture sites at cortical membrane of the cell poles, it gets stabilized. If a microtubule contacts the cell cortex in a other region of the cell, were no capture sites are present, the microtubule is not disassembled but changes its direction to the cell poles. **C** Nuclear positioning in budding yeast. Chromosome segregation requires migration of the nucleus to the bud neck and the alignment of the spindle along the mother-bud axis. Astral microtubules probe the cell cortex with their plus end search devices. At the cortical tip of the bud the microtubules are captured. Subsequently the capped microtubules shorten and move the nucleus to the bud neck. **D** The mitotic spindle. Three types of microtubules are nucleated by the two centrosomes; kinetochore attached, pole-to-pole and astral microtubules. The kinetochores attach the chromosomes to the microtubules. A microtubule randomly grows out and can be captured by a kinetochore or at specific cortical regions. Kinetochore attached microtubules are involved in the chromosome segregation, while astral microtubules have a role in spindle positioning. Polar microtubules exert forces capable of moving opposite spindle poles. **E** Microtubule array in motile fibroblasts. When a cell migrates, microtubules that are orientated towards the leading edge of the cell are stabilized, while microtubules at the trealing edge depolymerize. The main pool of microtubules are randomly searching for a capture site at the cortex, though some microtubules are directly guided to contact sides, for example by actin filaments. **F** Microtubules within a pausing growth cone acquire a loop conformation. In stage 1 (the exploration stage) the filopodia and lamellipodia are highly dynamic and are mainly organized by actin filaments (see section 1.2.2). In stage 2, single microtubules invade randomly the peripheral domain and continuously extend into and retract from the actin rich areas. These microtubule rearrangements are most likely caused by dynamic instability. In stage 3, upon the interaction between the growth cone and its substrate or target, the microtubules change their orientation and begin to form stable bundles. Stage 4, the plasma membrane around the growth cone collapses around the microtubule bundle to generate a new axon tube. The stable microtubules in the growth cone most likely promote the formation of local membrane insertions and modulate the actin organization.

Microtubules and nuclear migration

In contrast to most cells, the mitotic spindle in budding yeast is inside the nucleus and the nuclear membrane remains intact during mitosis. In addition, the spindle position does not determine the cleavage plane but instead the division plane is predetermined by the position of the bud. The mitotic nucleus migrates through the narrow neck between the mother and daughter cell, breaks up in two and segregates to each cell [192-194]. Cytoplasmic microtubules are essential in this nuclear migration process. Cytoplasmic microtubules are attached to the nuclear membrane with their minus ends and probe the cell cortex of the bud by the search and capture mechanism (Fig. 7c). Once the microtubules are captured by the cortex of the bud, the nucleus is brought in position by pulling the astral microtubules. The motor proteins dynein and kinesin Kip3p play a critical role in the nuclear movement and positioning of the spindle [193]. Recently, the budding yeast homologue of EB1, Bim1p, has been shown to anchor astral microtubules to the cortical protein Kar9p and to be involved in positioning the nucleus by this cortical microtubule capture mechanism [195,196]. Since, Bim1p is present at the microtubule tip it is suggested that this microtubule plus end protein is involved in promoting microtubule search and capture (see section 2.5.2).

Nuclear migration is not only restricted to yeast cells, it is required for the proper growth and development of all eukaryotes [197]. For example, an important process in the developing mammalian brain is the movement of the nucleus in differentiating neurons and microtubules also play a key role in this process. Microtubules provide length dependent forces on the nuclei or transport nuclei, along microtubules analogous to motor driven motility of organelles [198]. Indentification of proteins involved microtubule based nuclear migration processes have come from nuclear migration mutants in filamentous fungi, *A. nidulans* and *N. crassa*. Many of the nud (nuclear distribution) or ro (ropy) mutant genes encode subunits of the cytoplasmic dynein motor complex and dynactin complex [197]. Of particular interest is the nudF gene of *A. nidulans*, which encodes a protein similar to mammalian microtubule associated LIS1. Mutations in a single LIS1 allele causes type I lissencephaly, a brain developmental disease with a gross disorganisation of cortical regions of the brain, caused by defects in neuronal migration [199]. Analysis of LIS1 knockout mice support the notion that a reduced gene dosage gives rise to the lissencephalic phenotypes [200]. Recent studies suggest that LIS1 may be part of the microtubule capture machinery present at the cell cortex [201].

Microtubules and cell motility

Migrating cells rely primarily on the dynamic reorganisation of their actin cytoskeleton to move (see section 1.2) [39]. However, other factors are also involved in the regulation of cell migration, such as G proteins, focal adhesions and microtubules [44]. The microtubule array is remodelled constantly as microtubules populate protrusive regions and vacate retracting regions of the cell. The importance of

the microtubule system is dependent on the cell type. In the presence of microtubular inhibitors, fibroblasts lose their polarity and motility, while lymphocytes still move, but undergo random migration in a chemotactic experiment [44,202]. In general, microtubules grow randomly from the centrosome but become captured and stabilized only at the leading edge of the cell. Thus, an asymmetric microtubule network is generated, which is oriented in the direction of migration (Fig. 7e) [203]. In this way, stabilized microtubules may serve as tracks for the directed delivery of membrane vesicles to the lamellipodium (see section 1.2.2) were the membrane vesicles are inserted into the plasma membrane at the leading edge to drive lamellipodium protrusion.

This phenomenon of microtubule asymmetry during cell migration is best described in *in vitro* wound healing experiments [203]. Here, fibroblasts are grown to confluency and a narrow strip of cells is scraped off. The cells at the wound edge are initially unpolarized, but in response to wounding, they become polarised with their leading edge facing the cell free area. As a result they are able to move into the wound. In response to wounding, a subset of microtubules, that are oriented towards the wound, gets stabilized [203]. Local microtubule stabilization is dependent on serum factors, in particular mitogenic lipid lysophosphatidic acid (LPA) [150,204]. This suggests the presence of a signalling pathway that mediates the LPA-induced stabilization of microtubules. Several factors have been proposed to play a role, such as the GTPase Rho [150]. Active Rho induces long episodes of pausing in a subset of microtubules and subsequently stimulates the formation of stable detyrosinated microtubules at the leading edge of the cell. At the same time, local microtubule pausing or stabilization must also be regulated by microtubule binding proteins. Such candidate proteins for these functions are the CLIP associated binding proteins (CLASPs) (Chapter 5) [205].

Another example of microtubule involvement in cell motility comes from studies on the neuronal growth cone at the tip of the axon. Neuronal growth cones are highly motile and navigate along specific pathways to find their correct target. This process, named axonal pathfinding, is essential for the formation of the highly specific pattern of connections in the nervous system [206]. The neuronal growth cone has two distinct domains created by the differential localization of actin filaments and microtubules; the neurite shaft and central domain have a high density of microtubules, while the pheripheral domain, which consists of filopodia and lamellipodia, is rich in actin filaments [40,207]. When a growth cone is stable or pauzes, some individual microtubule in the peripheral domain aquire a loop conformation [208] (Fig. 7f). When the growth cone migrates in response to attractive extracellular guidance cues, the microtubule loops disappear and a rapid rearrangement of the microtubule structure takes place [209,210]. During axonal guidance microtubules are able to cause asymmetry in the shape of the growth cone, possibly by local capture and stabilization of the microtubules [211] (Fig. 7f). Similar reorganizations of the microtubule cytoskeleton occur at the sites of axon branch formation [210,212].

References

1. Alberts, B. (1994) Molecular biology of the cell, 3rd Ed., Garland Pub., New York
2. Venter, J. C., Adams, M. D., Myers, E. W., Li, P. W., Mural, R. J., Sutton, G. G., Smith, H. O., Yandell, M., and et al. (2001) The sequence of the human genome. *Science* **291**(5507): 1304-51.
3. Pollard, T. D. (2001) Genomics, the cytoskeleton and motility. *Nature* **409**(6822): 842-3.
4. Miki, H., Setou, M., Kaneshiro, K., and Hirokawa, N. (2001) All kinesin superfamily protein, KIF, genes in mouse and human. *Proc Natl Acad Sci U S A* **98**(13): 7004-11.
5. Adams, M. D., Celniker, S. E., Holt, R. A., Evans, C. A., Gocayne, J. D., Amanatides, P. G., Scherer, S. E., Li, P. W., and et al. (2000) The genome sequence of Drosophila melanogaster. *Science* **287**(5461): 2185-95.
6. Rubin, G. M., Yandell, M. D., Wortman, J. R., Gabor Miklos, G. L., Nelson, C. R., Hariharan, I. K., Fortini, M. E., Li, P. W., and et al. (2000) Comparative genomics of the eukaryotes. *Science* **287**(5461): 2204-15.
7. Consortium, T. C. e. S. (1998) Genome sequence of the nematode C. elegans: a platform for investigating biology. The C. elegans Sequencing Consortium. *Science* **282**(5396): 2012-8.
8. Kreis, T., and Vale, R. (1999) Guidebook to the cytoskeletal and motor proteins, 2nd Ed., Oxford University Press, Oxford ; New York
9. Fuchs, E., and Cleveland, D. W. (1998) A structural scaffolding of intermediate filaments in health and disease. *Science* **279**(5350): 514-9.
10. Hasson, T. (1997) Unconventional myosins, the basis for deafness in mouse and man. *Am J Hum Genet* **61**(4): 801-5.
11. Mandelkow, E. M., and Mandelkow, E. (1998) Tau in Alzheimer's disease. *Trends Cell Biol* **8**(11): 425-7.
12. Garcia, M. L., and Cleveland, D. W. (2001) Going new places using an old MAP: tau, microtubules and human neurodegenerative disease. *Curr Opin Cell Biol* **13**(1): 41-8.
13. Swynghedauw, B., and Baillard, C. (2000) Biology of hypertensive cardiopathy. *Curr Opin Cardiol* **15**(4): 247-53.
14. Cremers, F. P. (1998) Genetic causes of hearing loss. *Curr Opin Neurol* **11**(1): 11-6.
15. Altmannsberger, M., Dirk, T., Osborn, M., and Weber, K. (1986) Immunohistochemistry of cytoskeletal filaments in the diagnosis of soft tissue tumors. *Semin Diagn Pathol* **3**(4): 306-16.
16. Winston, J. S., Asch, H. L., Zhang, P. J., Edge, S. B., Hyland, A., and Asch, B. B. (2001) Downregulation of gelsolin correlates with the progression to breast carcinoma. *Breast Cancer Res Treat* **65**(1): 11-21.
17. Parekh, H., and Simpkins, H. (1997) The transport and binding of taxol. *Gen Pharmacol* **29**(2): 167-72.
18. Jordan, M. A., and Wilson, L. (1998) Microtubules and actin filaments: dynamic targets for cancer chemotherapy. *Curr Opin Cell Biol* **10**(1): 123-30.
19. Holmes, K. C., Popp, D., Gebhard, W., and Kabsch, W. (1990) Atomic model of the actin filament. *Nature* **347**(6288): 44-9.
20. Bremer, A., and Aebi, U. (1992) The structure of the F-actin filament and the actin molecule. *Curr Opin Cell Biol* **4**(1): 20-6.
21. Egelman, E. H. (1994) Actin filament structure. The ghost of ribbons past. *Curr Biol* **4**(1): 79-81.
22. Reisler, E. (1993) Actin molecular structure and function. *Curr Opin Cell Biol* **5**(1): 41-7.
23. Rayment, I., Holden, H. M., Whittaker, M., Yohn, C. B., Lorenz, M., Holmes, K. C., and Milligan, R. A. (1993) Structure of the actin-myosin complex and its implications for muscle contraction. *Science* **261**(5117): 58-65.
24. Pollard, T. D., Blanchoin, L., and Mullins, R. D. (2001) Actin dynamics. *J Cell Sci* **114**(Pt 1): 3-4.
25. Goffeau, A., Barrell, B. G., Bussey, H., Davis, R. W., Dujon, B., Feldmann, H., Galibert, F., Hoheisel, J. D., Jacq, C., Johnston, M., Louis, E. J., Mewes, H. W., Murakami, Y., Philippsen, P., Tettelin, H., and Oliver, S. G. (1996) Life with 6000 genes. *Science* **274**(5287): 546, 563-7.
26. Frankel, S., and Mooseker, M. S. (1996) The actin-related proteins. *Curr Opin Cell Biol* **8**(1): 30-7.
27. Poch, O., and Winsor, B. (1997) Who's who among the Saccharomyces cerevisiae actin-related proteins? A classification and nomenclature proposal for a large family. *Yeast* **13**(11): 1053-8.
28. Holleran, E. A., Tokito, M. K., Karki, S., and Holzbaur, E. L. (1996) Centractin (ARP1) associates with spectrin revealing a potential mechanism to link dynactin to intracellular organelles. *J Cell Biol* **135**(6 Pt 2): 1815-29.
29. Schafer, D. A., Gill, S. R., Cooper, J. A., Heuser, J. E., and Schroer, T. A. (1994) Ultrastructural analysis of the dynactin complex: an actin-related protein is a component of a filament that resembles F-actin. *J Cell Biol* **126**(2): 403-12.

30. Pollard, T. D., Blanchoin, L., and Mullins, R. D. (2000) Molecular mechanisms controlling actin filament dynamics in nonmuscle cells. *Annu Rev Biophys Biomol Struct* **29**: 545-76
31. Cooper, J. A., and Schafer, D. A. (2000) Control of actin assembly and disassembly at filament ends. *Curr Opin Cell Biol* **12**(1): 97-103.
32. Mullins, R. D. (2000) How WASP-family proteins and the Arp2/3 complex convert intracellular signals into cytoskeletal structures. *Curr Opin Cell Biol* **12**(1): 91-6.
33. Holt, M. R., and Koffer, A. (2001) Cell motility: proline-rich proteins promote protrusions. *Trends Cell Biol* **11**(1): 38-46.
34. Howard, J. (1997) Molecular motors: structural adaptations to cellular functions. *Nature* **389**(6651): 561-7.
35. Baker, J. P., and Titus, M. A. (1998) Myosins: matching functions with motors. *Curr Opin Cell Biol* **10**(1): 80-6.
36. Mermall, V., Post, P. L., and Mooseker, M. S. (1998) Unconventional myosins in cell movement, membrane traffic, and signal transduction. *Science* **279**(5350): 527-33.
37. Hasson, T., and Mooseker, M. S. (1997) The growing family of myosin motors and their role in neurons and sensory cells. *Curr Opin Neurobiol* **7**(5): 615-23.
38. Mitchison, T., and Kirschner, M. (1988) Cytoskeletal dynamics and nerve growth. *Neuron* **1**(9): 761-72.
39. Mitchison, T. J., and Cramer, L. P. (1996) Actin-based cell motility and cell locomotion. *Cell* **84**(3): 371-9.
40. Lin, C. H., Thompson, C. A., and Forscher, P. (1994) Cytoskeletal reorganization underlying growth cone motility. *Curr Opin Neurobiol* **4**(5): 640-7.
41. Small, J. V., Rottner, K., and Kaverina, I. (1999) Functional design in the actin cytoskeleton. *Curr Opin Cell Biol* **11**(1): 54-60.
42. Borisy, G. G., and Svitkina, T. M. (2000) Actin machinery: pushing the envelope. *Curr Opin Cell Biol* **12**(1): 104-12.
43. Luo, Y., and Raper, J. A. (1994) Inhibitory factors controlling growth cone motility and guidance. *Curr Opin Neurobiol* **4**(5): 648-54.
44. Lauffenburger, D. A., and Horwitz, A. F. (1996) Cell migration: a physically integrated molecular process. *Cell* **84**(3): 359-69.
45. Hall, A. (1998) Rho GTPases and the actin cytoskeleton. *Science* **279**(5350): 509-14.
46. Machesky, L. M., and Insall, R. H. (1999) Signaling to actin dynamics. *J Cell Biol* **146**(2): 267-72.
47. Drubin, D. G., and Nelson, W. J. (1996) Origins of cell polarity. *Cell* **84**(3): 335-44.
48. Bradke, F., and Dotti, C. G. (2000) Establishment of neuronal polarity: lessons from cultured hippocampal neurons. *Curr Opin Neurobiol* **10**(5): 574-81.
49. Bradke, F., and Dotti, C. G. (1999) The role of local actin instability in axon formation. *Science* **283**(5409): 1931-4.
50. Fuchs, E., and Weber, K. (1994) Intermediate filaments: structure, dynamics, function, and disease. *Annu Rev Biochem* **63**: 345-82
51. Herrmann, H., and Aebi, U. (2000) Intermediate filaments and their associates: multi-talented structural elements specifying cytoarchitecture and cytodynamics. *Curr Opin Cell Biol* **12**(1): 79-90.
52. Parry, D. A., and Steinert, P. M. (1992) Intermediate filament structure. *Curr Opin Cell Biol* **4**(1): 94-8.
53. Weber, K., Plessmann, U., and Ulrich, W. (1989) Cytoplasmic intermediate filament proteins of invertebrates are closer to nuclear lamins than are vertebrate intermediate filament proteins; sequence characterization of two muscle proteins of a nematode. *Embo J* **8**(11): 3221-7.
54. McConnell, S. J., and Yaffe, M. P. (1993) Intermediate filament formation by a yeast protein essential for organelle inheritance. *Science* **260**(5108): 687-9.
55. Bousquet, O., and Coulombe, P. A. (1996) Cytoskeleton: missing links found? *Curr Biol* **6**(12): 1563-6.
56. Yang, Y., Bauer, C., Strasser, G., Wollman, R., Julien, J. P., and Fuchs, E. (1999) Integrators of the cytoskeleton that stabilize microtubules. *Cell* **98**(2): 229-38.
57. Steinbock, F. A., and Wiche, G. (1999) Plectin: a cytolinker by design. *Biol Chem* **380**(2): 151-8.
58. Fuchs, E., and Yang, Y. (1999) Crossroads on cytoskeletal highways. *Cell* **98**(5): 547-50.
59. Hatzfeld, M., and Weber, K. (1990) The coiled coil of in vitro assembled keratin filaments is a heterodimer of type I and II keratins: use of site-specific mutagenesis and recombinant protein expression. *J Cell Biol* **110**(4): 1199-210.
60. Fuchs, E., Coulombe, P., Cheng, J., Chan, Y. M., Hutton, E., Syder, A., Degenstein, L., Yu, Q. C., Letai, A., and Vassar, R. (1994) Genetic bases of epidermolysis bullosa simplex and epidermolytic hyperkeratosis. *J Invest Dermatol* **103**(5 Suppl): 25S-30S.
61. Vassar, R., Coulombe, P. A., Degenstein, L., Albers, K., and Fuchs, E. (1991) Mutant keratin expression in transgenic mice causes marked abnormalities resembling a human genetic skin disease. *Cell* **64**(2): 365-80.

62. Chan, Y., Anton-Lamprecht, I., Yu, Q. C., Jackel, A., Zabel, B., Ernst, J. P., and Fuchs, E. (1994) A human keratin 14 "knockout": the absence of K14 leads to severe epidermolysis bullosa simplex and a function for an intermediate filament protein. *Genes Dev* **8**(21): 2574-87.
63. Lee, M. K., and Cleveland, D. W. (1996) Neuronal intermediate filaments. *Annu Rev Neurosci* **19**: 187-217
64. Lee, M. K., Xu, Z., Wong, P. C., and Cleveland, D. W. (1993) Neurofilaments are obligate heteropolymers in vivo. *J Cell Biol* **122**(6): 1337-50.
65. Lee, M. K., and Cleveland, D. W. (1994) Neurofilament function and dysfunction: involvement in axonal growth and neuronal disease. *Curr Opin Cell Biol* **6**(1): 34-40.
66. Xu, Z., Marszalek, J. R., Lee, M. K., Wong, P. C., Folmer, J., Crawford, T. O., Hsieh, S. T., Griffin, J. W., and Cleveland, D. W. (1996) Subunit composition of neurofilaments specifies axonal diameter. *J Cell Biol* **133**(5): 1061-9.
67. de Waegh, S. M., Lee, V. M., and Brady, S. T. (1992) Local modulation of neurofilament phosphorylation, axonal caliber, and slow axonal transport by myelinating Schwann cells. *Cell* **68**(3): 451-63.
68. Starr, R., Attema, B., DeVries, G. H., and Monteiro, M. J. (1996) Neurofilament phosphorylation is modulated by myelination. *J Neurosci Res* **44**(4): 328-37.
69. Hsieh, S. T., Kidd, G. J., Crawford, T. O., Xu, Z., Lin, W. M., Trapp, B. D., Cleveland, D. W., and Griffin, J. W. (1994) Regional modulation of neurofilament organization by myelination in normal axons. *J Neurosci* **14**(11 Pt 1): 6392-401.
70. Perrone Capano, C., Pernas-Alonso, R., and di Porzio, U. (2001) Neurofilament homeostasis and motoneurone degeneration. *Bioessays* **23**(1): 24-33.
71. Julien, J. P. (1999) Neurofilament functions in health and disease. *Curr Opin Neurobiol* **9**(5): 554-60.
72. Xu, Z., Cork, L. C., Griffin, J. W., and Cleveland, D. W. (1993) Increased expression of neurofilament subunit NF-L produces morphological alterations that resemble the pathology of human motor neuron disease. *Cell* **73**(1): 23-33.
73. Cote, F., Collard, J. F., and Julien, J. P. (1993) Progressive neuronopathy in transgenic mice expressing the human neurofilament heavy gene: a mouse model of amyotrophic lateral sclerosis. *Cell* **73**(1): 35-46.
74. Al-Chalabi, A., Andersen, P. M., Nilsson, P., Chioza, B., Andersson, J. L., Russ, C., Shaw, C. E., Powell, J. F., and Leigh, P. N. (1999) Deletions of the heavy neurofilament subunit tail in amyotrophic lateral sclerosis. *Hum Mol Genet* **8**(2): 157-64.
75. Rosen, D. R., Siddique, T., Patterson, D., Figlewicz, D. A., Sapp, P., Hentati, A., Donaldson, D., Goto, J., O'Regan, J. P., Deng, H. X., and et al. (1993) Mutations in Cu/Zn superoxide dismutase gene are associated with familial amyotrophic lateral sclerosis. *Nature* **362**(6415): 59-62.
76. Deng, H. X., Hentati, A., Tainer, J. A., Iqbal, Z., Cayabyab, A., Hung, W. Y., Getzoff, E. D., Hu, P., Herzfeldt, B., Roos, R. P., and et al. (1993) Amyotrophic lateral sclerosis and structural defects in Cu,Zn superoxide dismutase. *Science* **261**(5124): 1047-51.
77. Williamson, T. L., and Cleveland, D. W. (1999) Slowing of axonal transport is a very early event in the toxicity of ALS-linked SOD1 mutants to motor neurons. *Nat Neurosci* **2**(1): 50-6.
78. Kirschner, M., and Mitchison, T. (1986) Beyond self-assembly: from microtubules to morphogenesis. *Cell* **45**(3): 329-42.
79. Desai, A., and Mitchison, T. J. (1997) Microtubule polymerization dynamics. *Annu Rev Cell Dev Biol* **13**: 83-117
80. Gibbons, I. R. (1981) Cilia and flagella of eukaryotes. *J Cell Biol* **91**(3 Pt 2): 107s-124s.
81. Luduena, R. F. (1998) Multiple forms of tubulin: different gene products and covalent modifications. *Int Rev Cytol* **178**: 207-75
82. Schiebel, E. (2000) Two new tubulins differ in a split decision. *Nat Cell Biol* **2**(1): E3-4.
83. Dutcher, S. K. (2001) The tubulin fraternity: alpha to eta. *Curr Opin Cell Biol* **13**(1): 49-54.
84. Erickson, H. P. (1995) FtsZ, a prokaryotic homolog of tubulin? *Cell* **80**(3): 367-70.
85. Jeng, R., and Stearns, T. (1999) Gamma-tubulin complexes: size does matter. *Trends Cell Biol* **9**(9): 339-42.
86. Chang, P., and Stearns, T. (2000) Delta-tubulin and epsilon-tubulin: two new human centrosomal tubulins reveal new aspects of centrosome structure and function. *Nat Cell Biol* **2**(1): 30-5.
87. Schatz, P. J., Solomon, F., and Botstein, D. (1986) Genetically essential and nonessential alpha-tubulin genes specify functionally interchangeable proteins. *Mol Cell Biol* **6**(11): 3722-33.
88. Hoyle, H. D., and Raff, E. C. (1990) Two Drosophila beta tubulin isoforms are not functionally equivalent. *J Cell Biol* **111**(3): 1009-26.
89. Downing, K. H., and Nogales, E. (1998) Tubulin structure: insights into microtubule properties and functions. *Curr Opin Struct Biol* **8**(6): 785-91.

90. Melki, R., Rommelaere, H., Leguy, R., Vandekerckhove, J., and Ampe, C. (1996) Cofactor A is a molecular chaperone required for beta-tubulin folding: functional and structural characterization. *Biochemistry* **35**(32): 10422-35.
91. Lewis, S. A., Tian, G., Vainberg, I. E., and Cowan, N. J. (1996) Chaperonin-mediated folding of actin and tubulin. *J Cell Biol* **132**(1-2): 1-4.
92. Tian, G., Huang, Y., Rommelaere, H., Vandekerckhove, J., Ampe, C., and Cowan, N. J. (1996) Pathway leading to correctly folded beta-tubulin. *Cell* **86**(2): 287-96.
93. Tian, G., Lewis, S. A., Feierbach, B., Stearns, T., Rommelaere, H., Ampe, C., and Cowan, N. J. (1997) Tubulin subunits exist in an activated conformational state generated and maintained by protein cofactors. *J Cell Biol* **138**(4): 821-32.
94. Archer, J. E., Vega, L. R., and Solomon, F. (1995) Rbl2p, a yeast protein that binds to beta-tubulin and participates in microtubule function in vivo. *Cell* **82**(3): 425-34.
95. Feierbach, B., Nogales, E., Downing, K. H., and Stearns, T. (1999) Alf1p, a CLIP-170 domain-containing protein, is functionally and physically associated with alpha-tubulin. *J Cell Biol* **144**(1): 113-24.
96. Hoyt, M. A., Stearns, T., and Botstein, D. (1990) Chromosome instability mutants of Saccharomyces cerevisiae that are defective in microtubule-mediated processes. *Mol Cell Biol* **10**(1): 223-34.
97. Hoyt, M. A., Macke, J. P., Roberts, B. T., and Geiser, J. R. (1997) Saccharomyces cerevisiae PAC2 functions with CIN1, 2 and 4 in a pathway leading to normal microtubule stability. *Genetics* **146**(3): 849-57.
98. Stearns, T., Hoyt, M. A., and Botstein, D. (1990) Yeast mutants sensitive to antimicrotubule drugs define three genes that affect microtubule function. *Genetics* **124**(2): 251-62.
99. Radcliffe, P. A., Hirata, D., Vardy, L., and Toda, T. (1999) Functional dissection and hierarchy of tubulin-folding cofactor homologues in fission yeast. *Mol Biol Cell* **10**(9): 2987-3001.
100. Hirata, D., Masuda, H., Eddison, M., and Toda, T. (1998) Essential role of tubulin-folding cofactor D in microtubule assembly and its association with microtubules in fission yeast. *Embo J* **17**(3): 658-66.
101. MacRae, T. H. (1997) Tubulin post-translational modifications--enzymes and their mechanisms of action. *Eur J Biochem* **244**(2): 265-78.
102. Nogales, E., Downing, K. H., Amos, L. A., and Lowe, J. (1998) Tubulin and FtsZ form a distinct family of GTPases. *Nat Struct Biol* **5**(6): 451-8.
103. Nogales, E., Wolf, S. G., and Downing, K. H. (1998) Structure of the alpha beta tubulin dimer by electron crystallography. *Nature* **391**(6663): 199-203.
104. Downing, K. H., and Nogales, E. (1998) Tubulin and microtubule structure. *Curr Opin Cell Biol* **10**(1): 16-22.
105. Horwitz, S. B. (1994) Taxol (paclitaxel): mechanisms of action. *Ann Oncol* **5**(Suppl 6): S3-6.
106. Jordan, M. A., Toso, R. J., Thrower, D., and Wilson, L. (1993) Mechanism of mitotic block and inhibition of cell proliferation by taxol at low concentrations. *Proc Natl Acad Sci U S A* **90**(20): 9552-6.
107. Evans, L., Mitchison, T., and Kirschner, M. (1985) Influence of the centrosome on the structure of nucleated microtubules. *J Cell Biol* **100**(4): 1185-91.
108. Raff, E. C., Fackenthal, J. D., Hutchens, J. A., Hoyle, H. D., and Turner, F. R. (1997) Microtubule architecture specified by a beta-tubulin isoform. *Science* **275**(5296): 70-3.
109. Nogales, E., Whittaker, M., Milligan, R. A., and Downing, K. H. (1999) High-resolution model of the microtubule. *Cell* **96**(1): 79-88.
110. Wade, R. H., and Hyman, A. A. (1997) Microtubule structure and dynamics. *Curr Opin Cell Biol* **9**(1): 12-7.
111. Hyman, A. A., and Karsenti, E. (1996) Morphogenetic properties of microtubules and mitotic spindle assembly. *Cell* **84**(3): 401-10.
112. Schiebel, E. (2000) gamma-tubulin complexes: binding to the centrosome, regulation and microtubule nucleation. *Curr Opin Cell Biol* **12**(1): 113-8.
113. Saunders, W. S. (1999) Action at the ends of microtubules. *Curr Opin Cell Biol* **11**(1): 129-33.
114. Cole, N. B., and Lippincott-Schwartz, J. (1995) Organization of organelles and membrane traffic by microtubules. *Curr Opin Cell Biol* **7**(1): 55-64.
115. Stearns, T., Evans, L., and Kirschner, M. (1991) Gamma-tubulin is a highly conserved component of the centrosome. *Cell* **65**(5): 825-36.
116. Oakley, B. R., Oakley, C. E., Yoon, Y., and Jung, M. K. (1990) Gamma-tubulin is a component of the spindle pole body that is essential for microtubule function in Aspergillus nidulans. *Cell* **61**(7): 1289-301.
117. Erickson, H. P. (2000) Gamma-tubulin nucleation: template or protofilament? *Nat Cell Biol* **2**(6): E93-6.

118. Keating, T. J., and Borisy, G. G. (1999) Centrosomal and non-centrosomal microtubules. *Biol Cell* **91**(4-5): 321-9.
119. Baas, P. W. (1999) Microtubules and neuronal polarity: lessons from mitosis. *Neuron* **22**(1): 23-31.
120. Mays, R. W., Beck, K. A., and Nelson, W. J. (1994) Organization and function of the cytoskeleton in polarized epithelial cells: a component of the protein sorting machinery. *Curr Opin Cell Biol* **6**(1): 16-24.
121. Waterman-Storer, C. M., and Salmon, E. D. (1997) Microtubule dynamics: treadmilling comes around again. *Curr Biol* **7**(6): R369-72.
122. Baas, P. W., Deitch, J. S., Black, M. M., and Banker, G. A. (1988) Polarity orientation of microtubules in hippocampal neurons: uniformity in the axon and nonuniformity in the dendrite. *Proc Natl Acad Sci U S A* **85**(21): 8335-9.
123. Schnapp, B. J. (1997) Retroactive motors. *Neuron* **18**(4): 523-6.
124. Black, M. M., and Baas, P. W. (1989) The basis of polarity in neurons. *Trends Neurosci* **12**(6): 211-4.
125. Foletti, D. L., Prekeris, R., and Scheller, R. H. (1999) Generation and maintenance of neuronal polarity: mechanisms of transport and targeting. *Neuron* **23**(4): 641-4.
126. Vorobjev, I. A., Svitkina, T. M., and Borisy, G. G. (1997) Cytoplasmic assembly of microtubules in cultured cells. *J Cell Sci* **110**(Pt 21): 2635-45.
127. Wiese, C., and Zheng, Y. (2000) A new function for the gamma-tubulin ring complex as a microtubule minus-end cap. *Nat Cell Biol* **2**(6): 358-64.
128. Odde, D. J., Ma, L., Briggs, A. H., DeMarco, A., and Kirschner, M. W. (1999) Microtubule bending and breaking in living fibroblast cells. *J Cell Sci* **112**(Pt 19): 3283-8.
129. Hartman, J. J., Mahr, J., McNally, K., Okawa, K., Iwamatsu, A., Thomas, S., Cheesman, S., Heuser, J., Vale, R. D., and McNally, F. J. (1998) Katanin, a microtubule-severing protein, is a novel AAA ATPase that targets to the centrosome using a WD40-containing subunit. *Cell* **93**(2): 277-87.
130. Hartman, J. J., and Vale, R. D. (1999) Microtubule disassembly by ATP-dependent oligomerization of the AAA enzyme katanin. *Science* **286**(5440): 782-5.
131. Keating, T. J., Peloquin, J. G., Rodionov, V. I., Momcilovic, D., and Borisy, G. G. (1997) Microtubule release from the centrosome. *Proc Natl Acad Sci U S A* **94**(10): 5078-83.
132. Rodionov, V., Nadezhdina, E., and Borisy, G. (1999) Centrosomal control of microtubule dynamics. *Proc Natl Acad Sci U S A* **96**(1): 115-20.
133. Yu, W., Centonze, V. E., Ahmad, F. J., and Baas, P. W. (1993) Microtubule nucleation and release from the neuronal centrosome. *J Cell Biol* **122**(2): 349-59.
134. Baas, P. W., and Ahmad, F. J. (1992) The plus ends of stable microtubules are the exclusive nucleating structures for microtubules in the axon. *J Cell Biol* **116**(5): 1231-41.
135. Sammak, P. J., and Borisy, G. G. (1988) Direct observation of microtubule dynamics in living cells. *Nature* **332**(6166): 724-6.
136. Walker, R. A., O'Brien, E. T., Pryer, N. K., Soboeiro, M. F., Voter, W. A., Erickson, H. P., and Salmon, E. D. (1988) Dynamic instability of individual microtubules analyzed by video light microscopy: rate constants and transition frequencies. *J Cell Biol* **107**(4): 1437-48.
137. Caplow, M., and Shanks, J. (1996) Evidence that a single monolayer tubulin-GTP cap is both necessary and sufficient to stabilize microtubules. *Mol Biol Cell* **7**(4): 663-75.
138. Hyman, A. A., Salser, S., Drechsel, D. N., Unwin, N., and Mitchison, T. J. (1992) Role of GTP hydrolysis in microtubule dynamics: information from a slowly hydrolyzable analogue, GMPCPP. *Mol Biol Cell* **3**(10): 1155-67.
139. Cassimeris, L. (1993) Regulation of microtubule dynamic instability. *Cell Motil Cytoskeleton* **26**(4): 275-81
140. Mandelkow, E. M., Mandelkow, E., and Milligan, R. A. (1991) Microtubule dynamics and microtubule caps: a time-resolved cryo- electron microscopy study. *J Cell Biol* **114**(5): 977-91.
141. Chretien, D., Fuller, S. D., and Karsenti, E. (1995) Structure of growing microtubule ends: two-dimensional sheets close into tubes at variable rates. *J Cell Biol* **129**(5): 1311-28.
142. Arnal, I., Karsenti, E., and Hyman, A. A. (2000) Structural transitions at microtubule ends correlate with their dynamic properties in Xenopus egg extracts. *J Cell Biol* **149**(4): 767-74.
143. Margolis, R. L., and Wilson, L. (1998) Microtubule treadmilling: what goes around comes around. *Bioessays* **20**(10): 830-6.
144. Schulze, E., and Kirschner, M. (1987) Dynamic and stable populations of microtubules in cells. *J Cell Biol* **104**(2): 277-88.
145. Bulinski, J. C., and Gundersen, G. G. (1991) Stabilization of post-translational modification of microtubules during cellular morphogenesis. *Bioessays* **13**(6): 285-93.
146. Ersfeld, K., Wehland, J., Plessmann, U., Dodemont, H., Gerke, V., and Weber, K. (1993) Characterization of the tubulin-tyrosine ligase. *J Cell Biol* **120**(3): 725-32.

147. Paturle-Lafanechere, L., Manier, M., Trigault, N., Pirollet, F., Mazarguil, H., and Job, D. (1994) Accumulation of delta 2-tubulin, a major tubulin variant that cannot be tyrosinated, in neuronal tissues and in stable microtubule assemblies. *J Cell Sci* **107**(Pt 6): 1529-43.
148. Gundersen, G. G., Kalnoski, M. H., and Bulinski, J. C. (1984) Distinct populations of microtubules: tyrosinated and nontyrosinated alpha tubulin are distributed differently in vivo. *Cell* **38**(3): 779-89.
149. Khawaja, S., Gundersen, G. G., and Bulinski, J. C. (1988) Enhanced stability of microtubules enriched in detyrosinated tubulin is not a direct function of detyrosination level. *J Cell Biol* **106**(1): 141-9.
150. Cook, T. A., Nagasaki, T., and Gundersen, G. G. (1998) Rho guanosine triphosphatase mediates the selective stabilization of microtubules induced by lysophosphatidic acid. *J Cell Biol* **141**(1): 175-85.
151. Vale, R. D., Schnapp, B. J., Mitchison, T., Steuer, E., Reese, T. S., and Sheetz, M. P. (1985) Different axoplasmic proteins generate movement in opposite directions along microtubules in vitro. *Cell* **43**(3 Pt 2): 623-32.
152. Schnapp, B. J., Vale, R. D., Sheetz, M. P., and Reese, T. S. (1985) Single microtubules from squid axoplasm support bidirectional movement of organelles. *Cell* **40**(2): 455-62.
153. Brady, S. T., Lasek, R. J., and Allen, R. D. (1982) Fast axonal transport in extruded axoplasm from squid giant axon. *Science* **218**(4577): 1129-31.
154. Ball, E. H., and Singer, S. J. (1982) Mitochondria are associated with microtubules and not with intermediate filaments in cultured fibroblasts. *Proc Natl Acad Sci U S A* **79**(1): 123-6.
155. Matteoni, R., and Kreis, T. E. (1987) Translocation and clustering of endosomes and lysosomes depends on microtubules. *J Cell Biol* **105**(3): 1253-65.
156. Thyberg, J., and Moskalewski, S. (1999) Role of microtubules in the organization of the Golgi complex. *Exp Cell Res* **246**(2): 263-79.
157. Hirokawa, N. (1982) Cross-linker system between neurofilaments, microtubules, and membranous organelles in frog axons revealed by the quick-freeze, deep- etching method. *J Cell Biol* **94**(1): 129-42.
158. Hirokawa, N. (1998) Kinesin and dynein superfamily proteins and the mechanism of organelle transport. *Science* **279**(5350): 519-26.
159. Hirokawa, N. (1997) The mechanisms of fast and slow transport in neurons: identification and characterization of the new kinesin superfamily motors. *Curr Opin Neurobiol* **7**(5): 605-14.
160. Liao, G., and Gundersen, G. G. (1998) Kinesin is a candidate for cross-bridging microtubules and intermediate filaments. Selective binding of kinesin to detyrosinated tubulin and vimentin. *J Biol Chem* **273**(16): 9797-803.
161. Allan, V. J., and Schroer, T. A. (1999) Membrane motors. *Curr Opin Cell Biol* **11**(4): 476-82.
162. Huang, J. D., Brady, S. T., Richards, B. W., Stenolen, D., Resau, J. H., Copeland, N. G., and Jenkins, N. A. (1999) Direct interaction of microtubule- and actin-based transport motors. *Nature* **397**(6716): 267-70.
163. Winckler, B., and Mellman, I. (1999) Neuronal polarity: controlling the sorting and diffusion of membrane components. *Neuron* **23**(4): 637-40.
164. Coy, D. L., and Howard, J. (1994) Organelle transport and sorting in axons. *Curr Opin Neurobiol* **4**(5): 662-7.
165. Baas, P. W. (1997) Microtubules and axonal growth. *Curr Opin Cell Biol* **9**(1): 29-36.
166. Chang, S., Svitkina, T. M., Borisy, G. G., and Popov, S. V. (1999) Speckle microscopic evaluation of microtubule transport in growing nerve processes. *Nat Cell Biol* **1**(7): 399-403.
167. Terada, S., Kinjo, M., and Hirokawa, N. (2000) Oligomeric tubulin in large transporting complex is transported via kinesin in squid giant axons. *Cell* **103**(1): 141-55.
168. Grunert, S., and St Johnston, D. (1996) RNA localization and the development of asymmetry during Drosophila oogenesis. *Curr Opin Genet Dev* **6**(4): 395-402.
169. Cooley, L., and Theurkauf, W. E. (1994) Cytoskeletal functions during Drosophila oogenesis. *Science* **266**(5185): 590-6.
170. Theurkauf, W. E., Alberts, B. M., Jan, Y. N., and Jongens, T. A. (1993) A central role for microtubules in the differentiation of Drosophila oocytes. *Development* **118**(4): 1169-80.
171. Pokrywka, N. J., and Stephenson, E. C. (1995) Microtubules are a general component of mRNA localization systems in Drosophila oocytes. *Dev Biol* **167**(1): 363-70.
172. Clark, I., Giniger, E., Ruohola-Baker, H., Jan, L. Y., and Jan, Y. N. (1994) Transient posterior localization of a kinesin fusion protein reflects anteroposterior polarity of the Drosophila oocyte. *Curr Biol* **4**(4): 289-300.
173. Swan, A., Nguyen, T., and Suter, B. (1999) Drosophila Lissencephaly-1 functions with Bic-D and dynein in oocyte determination and nuclear positioning. *Nat Cell Biol* **1**(7): 444-9.
174. Mach, J. M., and Lehmann, R. (1997) An Egalitarian-BicaudalD complex is essential for oocyte specification and axis determination in Drosophila. *Genes Dev* **11**(4): 423-35.

175. Suter, B., and Steward, R. (1991) Requirement for phosphorylation and localization of the Bicaudal-D protein in Drosophila oocyte differentiation. *Cell* **67**(5): 917-26.
176. Holy, T. E., and Leibler, S. (1994) Dynamic instability of microtubules as an efficient way to search in space. *Proc Natl Acad Sci U S A* **91**(12): 5682-5.
177. Brunner, D., and Nurse, P. (2000) CLIP170-like tip1p spatially organizes microtubular dynamics in fission yeast. *Cell* **102**(5): 695-704.
178. Kaverina, I., Rottner, K., and Small, J. V. (1998) Targeting, capture, and stabilization of microtubules at early focal adhesions. *J Cell Biol* **142**(1): 181-90.
179. Goode, B. L., Drubin, D. G., and Barnes, G. (2000) Functional cooperation between the microtubule and actin cytoskeletons. *Curr Opin Cell Biol* **12**(1): 63-71.
180. Perez, F., Diamantopoulos, G. S., Stalder, R., and Kreis, T. E. (1999) CLIP-170 highlights growing microtubule ends in vivo. *Cell* **96**(4): 517-27.
181. Tirnauer, J. S., and Bierer, B. E. (2000) EB1 proteins regulate microtubule dynamics, cell polarity, and chromosome stability. *J Cell Biol* **149**(4): 761-6.
182. Schroer, T. A. (2000) Motors, clutches and brakes for membrane traffic: a commemorative review in honor of Thomas Kreis. *Traffic* **1**(1): 3-10.
183. Sharp, D. J., Rogers, G. C., and Scholey, J. M. (2000) Cytoplasmic dynein is required for poleward chromosome movement during mitosis in Drosophila embryos. *Nat Cell Biol* **2**(12): 922-30.
184. Wittmann, T., Hyman, A., and Desai, A. (2001) The spindle: a dynamic assembly of microtubules and motors. *Nat Cell Biol* **3**(1): E28-34.
185. Koshland, D. (1994) Mitosis: back to the basics. *Cell* **77**(7): 951-4.
186. Cassimeris, L. (1999) Accessory protein regulation of microtubule dynamics throughout the cell cycle. *Curr Opin Cell Biol* **11**(1): 134-41.
187. Andersen, S. S. (2000) Spindle assembly and the art of regulating microtubule dynamics by MAPs and Stathmin/Op18. *Trends Cell Biol* **10**(7): 261-7.
188. Dujardin, D., Wacker, U. I., Moreau, A., Schroer, T. A., Rickard, J. E., and De Mey, J. R. (1998) Evidence for a role of CLIP-170 in the establishment of metaphase chromosome alignment. *J Cell Biol* **141**(4): 849-62.
189. Hyman, A. A. (1989) Centrosome movement in the early divisions of Caenorhabditis elegans: a cortical site determining centrosome position. *J Cell Biol* **109**(3): 1185-93.
190. Kuchinke, U., Grawe, F., and Knust, E. (1998) Control of spindle orientation in Drosophila by the Par-3-related PDZ- domain protein Bazooka. *Curr Biol* **8**(25): 1357-65.
191. Lu, B., Jan, L. Y., and Jan, Y. N. (1998) Asymmetric cell division: lessons from flies and worms. *Curr Opin Genet Dev* **8**(4): 392-9.
192. Segal, M., and Bloom, K. (2001) Control of spindle polarity and orientation in Saccharomyces cerevisiae. *Trends Cell Biol* **11**(4): 160-6.
193. Stearns, T. (1997) Motoring to the finish: kinesin and dynein work together to orient the yeast mitotic spindle. *J Cell Biol* **138**(5): 957-60.
194. Shaw, S. L., Yeh, E., Maddox, P., Salmon, E. D., and Bloom, K. (1997) Astral microtubule dynamics in yeast: a microtubule-based searching mechanism for spindle orientation and nuclear migration into the bud. *J Cell Biol* **139**(4): 985-94.
195. Korinek, W. S., Copeland, M. J., Chaudhuri, A., and Chant, J. (2000) Molecular linkage underlying microtubule orientation toward cortical sites in yeast. *Science* **287**(5461): 2257-9.
196. Lee, L., Tirnauer, J. S., Li, J., Schuyler, S. C., Liu, J. Y., and Pellman, D. (2000) Positioning of the mitotic spindle by a cortical-microtubule capture mechanism. *Science* **287**(5461): 2260-2.
197. Morris, N. R. (2000) Nuclear migration. From fungi to the mammalian brain. *J Cell Biol* **148**(6): 1097-101.
198. Reinsch, S., and Gonczy, P. (1998) Mechanisms of nuclear positioning. *J Cell Sci* **111**(Pt 16): 2283-95.
199. Reiner, O., Carrozzo, R., Shen, Y., Wehnert, M., Faustinella, F., Dobyns, W. B., Caskey, C. T., and Ledbetter, D. H. (1993) Isolation of a Miller-Dieker lissencephaly gene containing G protein beta-subunit-like repeats. *Nature* **364**(6439): 717-21.
200. Hirotsune, S., Fleck, M. W., Gambello, M. J., Bix, G. J., Chen, A., Clark, G. D., Ledbetter, D. H., McBain, C. J., and Wynshaw-Boris, A. (1998) Graded reduction of Pafah1b1 (Lis1) activity results in neuronal migration defects and early embryonic lethality. *Nat Genet* **19**(4): 333-9.
201. Vallee, R. B., Tai, C., and Faulkner, N. E. (2001) LIS1: cellular function of a disease-causing gene. *Trends Cell Biol* **11**(4): 155-60.
202. Vasiliev, J. M. (1991) Polarization of pseudopodial activities: cytoskeletal mechanisms. *J Cell Sci* **98**(Pt 1): 1-4.
203. Gundersen, G. G., and Bulinski, J. C. (1988) Selective stabilization of microtubules oriented toward the direction of cell migration. *Proc Natl Acad Sci U S A* **85**(16): 5946-50.

204. Nagasaki, T., and Gundersen, G. G. (1996) Depletion of lysophosphatidic acid triggers a loss of oriented detyrosinated microtubules in motile fibroblasts. *J Cell Sci* **109**(Pt 10): 2461-9.
205. Akhmanova, A., Hoogenraad, C. C., Drabek, K., Stepanova, T., Dortland, B., Verkerk, T., Vermeulen, W., Burgering, B. M., De Zeeuw, C. I., Grosveld, F., and Galjart, N. (2001) Clasps are CLIP-115 and -170 associating proteins involved in the regional regulation of microtubule dynamics in motile fibroblasts. *Cell* **104**(6): 923-35.
206. Tessier-Lavigne, M., and Goodman, C. S. (1996) The molecular biology of axon guidance. *Science* **274**(5290): 1123-33.
207. Suter, D. M., and Forscher, P. (1998) An emerging link between cytoskeletal dynamics and cell adhesion molecules in growth cone guidance. *Curr Opin Neurobiol* **8**(1): 106-16.
208. Tsui, H. T., Lankford, K. L., Ris, H., and Klein, W. L. (1984) Novel organization of microtubules in cultured central nervous system neurons: formation of hairpin loops at ends of maturing neurites. *J Neurosci* **4**(12): 3002-13.
209. Tanaka, E., and Sabry, J. (1995) Making the connection: cytoskeletal rearrangements during growth cone guidance. *Cell* **83**(2): 171-6.
210. Dent, E. W., Callaway, J. L., Szebenyi, G., Baas, P. W., and Kalil, K. (1999) Reorganization and movement of microtubules in axonal growth cones and developing interstitial branches. *J Neurosci* **19**(20): 8894-908.
211. Tanaka, E., and Kirschner, M. W. (1995) The role of microtubules in growth cone turning at substrate boundaries. *J Cell Biol* **128**(1-2): 127-37.
212. Acebes, A., and Ferrus, A. (2000) Cellular and molecular features of axon collaterals and dendrites. *Trends Neurosci* **23**(11): 557-65.

Chapter 2

MICROTUBULE ASSOCIATED PROTEINS

2.1 General introduction

Microtubules were originally isolated from brain extracts by multiple cycles of polymerization and depolymerization and differential centrifugation. About 80 percent of the microtubule preparation is α- and β-tubulin, while the remaining 20 percent contains a variety of microtubule associated proteins (MAPs). A protein was named a MAP if it copurified with tubulin during repeated cycles of assembly and disassembly and if it was able to stabilize microtubules. However, this definition of MAPs on the basis of their *in vitro* stabilizing behavior is unsatisfactory, since MAPs have been characterized that are unable to stabilize microtubules. Therefore, nowadays MAPs are defined as proteins that are attached to microtubules in vivo [1]. Most of the proteins that interact with microtubules are covered by this definition. Further classification of the MAPs on the basis of sequence homology, biochemical properties, or function has turned out to be difficult. It has been shown that some MAPs have a conserved structure but have a totally different function in vivo and vice versa [2]. Moreover, intermediate filament binding proteins can function as microtubule binding proteins by alternative splicing of a microtubule binding containing exon [3] and some general enzymes inside the cell, like formiminotransferase cyclodeaminase and glutamate dehydrogenase, possess affinity for microtubules [4-6]. In spite of this reservation, we have classified the MAPs into four major families. The first MAP family contains the classical or structural MAPs, like tau and MAP1 [7,8]. The second MAP family includes the microtubule motors, such as kinesin and the cytoplasmic dynein motor complex [9,10]. The third MAP family includes microtubule binding proteins that affect microtubule dynamics, like Op18/Stathmin and XMAP-215 [11,12]. The last MAP family contains microtubule plus end binding proteins, like CLIPs and EB1 family members [13-15]. In this chapter the first three MAP families will be briefly described. The microtubule plus end binding proteins will be addressed in more detail at the end of this chapter.

2.2 Classical or structural microtubule associated proteins

The structural or classical MAPs are also called the assembly MAPs or microtubule stabilizers. These proteins bind to microtubules reversibly with affinities in the low-micromolar range, lack enzymatic activity, promote tubulin polymerization and stabilize microtubules [8,16,17]. Generally, members of this MAP family are responsible for cross-linking microtubules. In this way, MAPs modulate microtubule organization during the development of cell processes, establishment of cell polarity and intracellular transport [7]. However some can also link microtubules to other subcellular structures, like membranes, membrane receptors, intermediate filaments or actin filaments. Classic MAPs are all composed of a microtubule binding domain and a projection domain, which protrudes from the microtubule surface. The length of the projection domain controls how far apart microtubules are spaced [18]. Based on their

sequence, classical MAPs can be grouped into two types. Type I MAP family members include the proteins MAP1A and MAP1B/MAP5 while type II MAPs include MAP2, MAP4 and tau proteins.

2.2.1 Type I MAPs

Type I MAPs are multimeric protein complexes that comprise a heavy chain (~250 kDa) and two or three light chains (~25 kDa) [16,17]. The heavy and light chains are proteolytic cleavage products of a common protein precursor [19]. MAP1A and MAP1B have been shown by rotary shadowing electron microscopy to be a long, thin rods of 150-200 nm in length. The heavy chain contains several repeats of the amino acid sequence KKEX which has been implicated in the microtubule binding. However, light chain 3 of MAP1A also has been shown to bind microtubules directly. MAP1A and MAP1B are predominantly expressed in brain. They are both distributed along the length of microtubules in neurons and form long cross-bridges between the microtubules [16]. It has shown that MAP1B, in addition to its function in linking and stabilizing microtubules, has a role in microtubule-membrane and microtubule-actin filament interactions [20]. Antisense oligonucleotide treatment and knock out mice revealed that MAP1B is required for the development and function of large myelinated axons and is involved in axon guidance of a subset of neurons [21]. The MAP1B homologue Futsch/22C10 in *Drosophila* is required for dendrite and axonal development and controls synaptic growth and branching [22,23].

2.2.2 Type II MAPs

Type II MAPs are composed of an N-terminal projection domain and a C-terminal microtubule binding domain which contains a proline-rich sequence and three or four repeats of 18 amino acids, with the consensus $GSX_2NX_2HXPG_3$ [17,24,25]. The main difference between MAP2, MAP4 and tau is the length of their projection domain, for example tau is about 50 nm in length while MAP2 is 100 nm. Type II MAPs reveal a characteristic distribution pattern in nerve cells; tau is predominantly localized in axons whereas MAP2 is abundant in dendrites. Overexpression of MAPs in cells induces bundles of microtubules and arranges the microtubules into patterns that reflect the neuronal phenotype [16,18,26]. For example, in cells expressing MAP2, the distance between microtubules is similar to that found in dendrites. Isolated MAPs show varying degrees of phosphorylation on several motifs flanking the microtubule binding domain. Phosphorylation of MAPs influences their microtubule stabilizing capacity. MAP/microtubule affinity regulated kinase (MARK) phosphorylates tau, MAP2 and MAP4 at the KXGS sequence and causes their dissociation from microtubules, which subsequently increases microtubule dynamics [7]. Studies form *C. elegans* suggest that the MARK homologue, PAR1 is important in the establishment of cell polarity.

Recently, it became clear that tau and MAP1B, which are both prominent in axons function synergistically. Tau deficient mice are essentially normal and only

show subtle differences in microtubule organization in small caliber axons [27]. Mating these mice with the MAP1B null animals show that deficiency of both MAPs is lethal by four weeks of age [28]. Moreover, tau/MAP1B double knock out mice show defects in axon tract formation, growth cone morphology and neuronal migration.

The tau protein is probably the best known and most studied microtubule binding protein. Tau is the major component of cytoplasmic filamentous aggregates, termed neurofibrillary tangles, observed in brains of patients with neurodegenerative disorders such as Alzheimer's disease, Pick's disease, frontotemporal dementia and cortico-basal degeneration [29-31]. These and other diseases with abundant tau positive filamentous lesions are called tauopathies. Although no Alzheimer's disease causing mutations have been detected thus far in the tau gene, the tau protein changes in several ways during the progression of disease [32]. The first sign in affected neurons is a hyperphosphorylation of the tau protein. Subsequently tau is released from the microtubule, redistributed to a somatodendritic compartment and forms aggregates. Since there is a good correlation between tau pathology and loss of synapses, it has been proposed that neuronal transport is impaired by blocking motor protein function [33]. This is consistent with the observation that overexpression of tau inhibits kinesin-dependent trafficking of vesicles [34]. However, overexpressing tau isoforms in transgenic mice does not result in an Alzheimer-like pathology [35,36]. These data indicate that abnormal tau may not be involved in the onset but more in the progression of the disease. Other proteins, such as presenilin or β-amyloid, may be involved in the initiation of Alzheimer's disease.

Recent studies have shown that mutations in coding and non-coding regions of the tau gene are directly associated with the development of frontotemporal dementia and parkinsonism linked to chromosome 17 (FTDP-17) [29-31]. Patients with these mutations show pronounced tau deposits. Mice expressing the FTDP-17-linked, missense tau mutant protein (P310L) show neurofibrillary tangles and other phenotypes comparable with FTDP-17 pathology [37]. However, transgenic mice expressing tau protein which mimics other FTDP-17 mutations have revealed that too much mutant tau protein displays neuronal dysfunction, but no filamentous tau lesions have been observed [29,38,39]. These data suggest that tau aggregates are themselves not responsible for the neurological deficits and that both different FTDP-17 mutations and expression levels in transgenic mice can influence the formation of tau lesions.

To summarize, different tauopathies can either be caused by mutations in the tau gene (FTDP-17) or are a consequence of the abnormal behavior of other neuronal factors that influence tau proteins (Alzheimer's disease). In both cases the molecular mechanisms underlying these phenomena remain unclear.

2.3 Proteins regulating microtubule dynamics

One of the key properties of microtubules is their polymerization dynamics (see section 1.4.3). The rapid switching of microtubules between growth and shrinkage allows them to search and explore the three dimensional space of the cell. Proteins that regulate microtubule dynamics have been identified and fall into two main classes [11,12,17,40,41]. Stabilizing factors, such as the classical MAPs and XMAPs promote microtubule growth by reducing the catastrophe frequency and destabilizing factors, such as Op18/Stathmin family proteins and Kin I kinesins destabilize microtubules by increasing the catastrophe rate.

2.3.1 Stabilizing MAPs

The stabilizing MAPs were originally isolated based on the promotion of microtubule assembly *in vitro* and in *Xenopus* egg extracts. The classical MAPs, such as tau and MAP2 stabilize microtubules but cause only a modest increase in growth rate of approximately 2 fold [42,43]. In contrast, the XMAP-215 protein, which was initially isolated from Xenopus extracts, speeds up the microtubule growth rate by 7-10 fold [42,44]. Little sequence homology exists between XMAP-215 and the classical MAPs. In contrast, XMAP-215 possesses a N-terminal domain with a HEAT repeat, which was originally identified in Huntingtin and the regulatory subunit of phosphatase 2A [45]. XMAP-215 homologues are found from yeast to human. For example, *S. cerevisiae* and *pombe* express the XMAP-215 related proteins Stu2p and p93dis1, respectively [46,47], while other homologues have been identified in *C. elegans* (ZYG-9), *Drosophila* (Msps) and human (TOGp) [48-50]. All XMAP-215 related proteins are associated with the microtubule network and centrosomes or spindle pole bodies in some stage of the cell cycle. In yeast, *Drosophila* and *C. elegans*, mutations in the XMAP-215 homologues result in mitotic defects resembling defects in microtubule dynamics [48-50]. Immunofluorescence observations showed that all family members label microtubules along their length [45,50]. However, recent data suggest that human XMAP-215 homologue preferentially binds to microtubule ends and has affinity for protofilaments and tubulin dimers [51].

2.3.2 Destabilizing MAPs

Microtubule destabilizing proteins are defined as factors which promote microtubule disassembly when added to the polymer. Proteins of the Kin I kinesin family include XKCM1 and XKIF2, and Op18/Stathmin-related proteins and are responsible for microtubule plus end catastrophes [2,17,52]. The Kar3 protein is a minus end directed motor identified in *S. cerevisiae* that destabilizes microtubules at their minus ends *in vitro*. Deletion of kar3 results in more and longer microtubules in the cytoplasm [53,54]. In addition, severing proteins, such as katanin, which cuts microtubules at internal sites, may also be involved in microtubule destabilization [55]. The best studied factor from the microtubule destabilizing subfamily is the oncoprotein

18 (Op18), also named Stathmin, prosolin or metablastin [52]. Op18/Stathmin is part of a small family of proteins, which includes the nervous system associated proteins SCG10, SCLIP and RB3 [56]. Op18/Stathmin is a small phosphoprotein which is highly upregulated in some tumors, but no evidence for mutations in the gene has been found [57]. Moreover, it has been reported that suppression of Op18/Stathmin abrogates the transformed phenotype [58]. Consistent with a function for Op18/Stathmin in microtubule destabilization, tubulin polymerization increases upon immunodepletion of Op18/Stathmin. Antisense treatment and overexpression of Op18/Stathmin in cells causes a dramatic increase or decrease, respectively, in polymerized tubulin [52,59,60]. However, mice lacking both Op18/Stathmin genes show normal development and behavior. Op18/Stathmin can destabilize microtubules via two different mechanisms, depending on the intracellular environment. At pH 7.5, Op18/Stathmin interacts with the microtubule polymer and induces catastrophes at the plus ends, while at pH 6.8, Op18/Stathmin sequesters tubulin dimers and induces catastrophes by lowering the amount of free tubulin. Interestingly, addition of Op18/Stathmin to microtubules decreases both the length and frequency of sheet structures at the plus ends and increases the number of split ends [61]. These data indicate that an increasing catastrophe frequency, induced by Op18/Stathmin, correlates with the structural state of the microtubule. Like for the XMAPs several models have been proposed for the role of Op18/Stathmin in microtubule dynamics [12,41]. It remains unclear whether regulation of microtubule dynamics by Op18/Stathmin is directly responsible for the progression of tumors.

2.4 Microtubule motor proteins

Microtubules act as railroad tracts on which the microtubule motor proteins, such as kinesin and dynein, transport cargo in a polarized manner through the cell (Fig. 1a). An array of motor proteins exists that mediates the transport of vesicles, mRNA and other material inside the cell. Another important function of motor proteins is their role in the movement of chromosomes during meiosis and mitosis [62,63]. Motor proteins produce opposing inward and outward forces on the microtubule [2,62,64]. In general, motor proteins of the kinesin superfamily (KIF) move to the microtubule plus end and cytoplasmic dynein motor proteins are able to move to the minus end [9,10]. For example, in neuronal axons the movement of membranes anterogradely from the cell body toward the synapse uses the kinesin motors, while membranes returning from the synapse via retrograde transport use cytoplasmic dynein [65,66]. (Fig. 1b). Some family members of the kinesin family, the C-terminal motor domain type (KIFC), show microtubule minus end motility, indicating that kinesin motors can also be involved in retrograde transport [9,67]. Motor proteins can be viewed as nanoscale macromolecular machines. They convert energy from ATP into protein motion [68,69]. If an appropriate cargo is attached to the motor protein, the cargo will be moved with the motor along the microtubule.

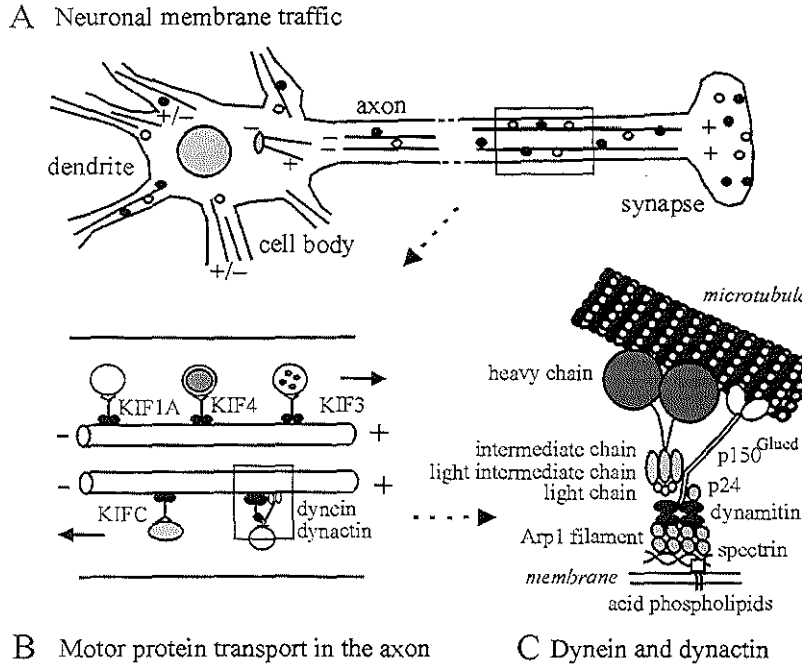

Figure 1: Dynein and dynactin in neurons.
A Scheme of membrane traffic in nerve cells. In the axon, the various types of membranous organelles are transported bidirectionally at 50-200 mm per day. Membranous organelles that move in an anterograde direction include mitochondria, axonal plasma membrane precursors, synaptic vesicles and synaptic plasma membrane. These membranous organelles can contain neuropeptides, neurotransmitters and associated proteins. In contrast, membranous organelles that move in a retrograde direction include endosomes, lysosomes, multivesicular bodies and mitochondria. Neurotrophic factors are transported retrogradely. Microtubules serve as rails for the transport of organelles. Within the axon, the microtubules point with their plus end to the synapse. **B** Motor protein transport in the axon. Microtubule motor proteins are responsible for in intracellular trafficking. Different types of motor proteins are involved in plus-end (anterograde) and minus-end (retrograde) directed transport. Plus-end directed motor proteins are members of the kinesin family. They are defined by the presence of a conserved N-terminal or middle motor domain, with ATP and putative microtubule bindings sites. Cytoplasmic dynein and C-terminal type kinesins are thought to move to the microtubule minus ends. **C** Schematic representation of the possible organization of cytoplasmic dynein and dynactin on microtubules and organelle membranes. Proteins present in both complexes are indicated in the text. The interaction between dynein and dynactin is mediated by the dynein intermediate chain and $p150^{Glued}$. Both dynein and dynactin can bind to microtubules. In this model, dynactin is proposed to mediate the association with membranes. The actin-like filament of dynactin binds to spectrin, which is present on the organelle surface. Dynein can also bind membranes by itself (not shown).

2.4.1 Kinesin superfamily

Three major types of kinesin motor proteins (KIFs) have been identified, according to the position of the motor domain; the N-terminal, middle and C-terminal motor domain type [70]. Different classes of kinesin motor proteins are identified per KIF type; eight classes of the N type, one class of the M type and four classes of the C type [9]. Until now approximately 150 KIFs have been identified from yeast to mammals carrying out a wide variety of functions [10,70]. KIF proteins transport

different types of vesicles, proteins and/or mRNAs [71]. KIFs also move chromosomes, crosslink and organize microtubules and sequester molecules involved in signal transduction on microtubules [72]. Of great interest is the role of KIFs in the left-right asymmetry in developing mouse embryos [73]. In patients, kinesin proteins have been shown to be autoantigens, upregulated in a variety of diseases and to be associated with disease causing mutations [74,75]. Defects in kinesin-encoding genes may cause neurological disorders or syndromes of clinical importance. For example, defective meiotic and mitotic kinesins may cause infertility, spontaneous abortion, neonatal chromosome disorders, somatic abnormalities or cellular transformation, including neoplasia. Recently, a mutation in the motor domain of KIF1B has been found to cause Charcot-Marie-Tooth disease, a peripheral neuropathy in humans [76]. However no other mutations in KIF genes have yet been found linked to a disease.

Conventional kinesin, also called KIF5, is the founder member of the kinesin superfamily and consists of 2 identical heavy chains and 2 light chains. The heavy chain contains 3 domains: a globular N-terminal motor domain, a central alpha-helical rod domain, which enables the 2 heavy chains to dimerize, and a globular C-terminal domain, which interacts with light chains. The light chains are thought to be responsible for the binding of cargo and the regulation of motor activity [72,77]. Analysis of conventional kinesin function in *C. elegans* and *Drosophila* revealed that mutations in the gene lead to neuronal defects of varying severity [78,79]. Disruption of one of the heavy chain genes, KIF5B, leads to embryonic lethality in knock-out mice, with a severe growth retardation at E10.5 [80]. KIF5B null mutant cells have a normal Golgi apparatus but are impaired in lysosome and mitochondria distribution, suggesting that other KIFs are involved in the transport of Golgi membranes. Consistent with this observation it has been shown that different KIFs are involved the transport of distinct types of organelles [71]. In neurons, specific KIF proteins exist that are responsible for the movement of only one type of organelle. For example, KIF1A transports synaptic vesicle precursors, KIF4 is associated with vesicles containing cell adhesion molecule (CAM) L1, KIF17 is able to transport vesicles containing NMDA receptor 2B and KIFC2 transports multivesicular endosomes. Furthermore, KIFs are likely to play a role in conveying synaptic plasma membrane proteins essential for vesicle docking, such as SNAP25 and syntaxin 1. An important question nowadays is how the different motors identify their cargo. One possibility is that there is a membrane receptor or a binding protein on the vesicle which is specific for each motor protein and vesicle [72,81]. For example, mammalian kinectin is an integral membrane protein which binds to conventional kinesin and is essential for organelle motility in vitro [82]. Amyloid precursor protein (APP), on the other hand, is a membrane receptor for the light chain of conventional kinesin. Transport of APP is greatly decreased in kinesin light chain mutant mice [83]. Some other likely candidates involved in membrane-kinesin interactions are, spectrin (fodrin), a complex of JIP scaffolding proteins and the Reelin membrane receptor, ApoER2 [71,72,84,85].

2.4.2 Cytoplasmic dynein and dynactin

In contrast to the functional specification of the many members of the kinesin superfamily, only one form of dynein appears to function in many different cellular roles, including mitotic chromosome movement, mitotic spindle migration during cell division, nuclear positioning, localization of the Golgi complex , retrograde axonal vesicle transport and mRNA tranport [17,66,81,86,87]. The functional diversity of cytoplasmic dynein is achieved through the use of alternative dynein subunits [87]. Cytoplasmic dynein is a large multisubunit complex of 1.2 MDa, composed of four classes of subunits. Each cytoplasmic dynein complex contains two heavy chains, three intermediate chains, and several light intermediate and light chains [88-90] (Fig, 1c). The dynein heavy chains are polypeptides of 530 kDa which contain four ATPase domains and are responsible for microtubule binding and force production. The intermediate chains are a diverse set of subunits, derived from alternative splicing of different genes, and have been proposed to bind to the dynactin complex, the accessory protein of dynein [91]. Both light intermediate chains and light chains are speculated to have a targeting function, by anchoring the appropriate cargo to cytoplasmic dynein. In different organisms, multiple genes are found for each subunit. This further supports the idea that distinct dynein subunit isoforms allow binding to different cargoes and indicates that the cytoplasmic dynein pool is heterogeneous in the cell. Mice lacking the dynein heavy chain, which normally is associated with vesicles, are embryonic lethal at day 8.5. Null mutant blastocyst cells showed Golgi vesiculation and endosome/lysosome dispersion, suggesting that dynein is involved in all major trafficking routes [92]. Interestingly, in mutant cells the Golgi apparatus, endosomes and lysosomes are still attached to the microtubules.

Cytoplasmic dynein is thought to bind cargo via its accessory protein, dynactin [81]. In addition to acting as an adapter for cargo binding, dynactin has been shown to improve dynein processivity along the microtubules, possibly by stabilizing the microtubule-dynein interaction [91,93,94]. Like dynein, dynactin is also a large multisubunit complex of about 1.1 MDa, which consists of 10-11 distinct polypeptides, including $p150^{Glued}$, dynamitin (p50) and the filament forming actin related protein, Arp1 [93,95,96] (Fig. 1c). Dynactin can be divided into two structural domains, an actin-like backbone, including Arp1, CapZ, p62, Arp11, p27 and p25 and a projecting shoulder/sidearm, including $p150^{Glued}$, dynamitin and p24 [97]. The actin-like backbone is thought to be responsible for the cargo attachment via the interaction with spectrin and acidic phospholipids (Holleran and Holzbaur, 1998; Muresan, et al., 2001), whereas the shoulder/sidearm interacts with dynein and microtubules [87,91,97] (Fig 1c). Overexpression of the dynamitin subunit in cells divides dynactin into the two structural domains [98,99]. It is believed that in these cells dynein can still bind to the shoulder/sidearm, but now lacks the mechanism for cargo attachment. Indeed, membrane transport is largely abolished in dynamitin overexpressing cells [98].

The *Drosophila* $p150^{Glued}$ gene, Glued, has been extensively characterized by traditional genetic approaches. Mutations in the Glued locus result in a variety of

neuronal phenotypes; disrupted sensory axon path finding, abnormal synaptogenesis and eye formation defects [100-102]. By genetic analysis in flies, dynein and dynactin have been deduced to function in the same pathway. Certain mutations in the *Drosophila* dynein heavy chain gene suppress or enhance the phenotype of the Glued mutation [103]. Further studies in yeast suggest that dynein and dynactin act in a common cellular process [87]. Despite the abundant evidence in support for a role of dynactin in the minus end directed dynein pathway, cytoplasmic dynein has been shown to bind cargo via a number of other interactions. For example, the dynein complex can bind directly to membrane lipids [104] and the dynein light chain Tctex1 is able to interact with the transmembrane protein rhodopsin [105]. This suggests that dynactin is not essential for all dynein-cargo interaction.

2.5 Microtubule plus end binding proteins

Dynamic instability, is also regulated at the plus ends of microtubules. It is likely that microtubule dynamics at plus ends depends on specific regulatory factors, such as Op18/Stathmin and XMAP215. However these proteins are localized along the microtubules and are not limited to the microtubule ends. EB1, APC, cytoplasmic linker proteins (CLIPs) and the dynactin complex have recently emerged as microtubule binding proteins that have been observed to be present on the microtubule plus ends. Such a localization is ideally suited for regulating microtubule dynamics. Microtubule plus end binding proteins, also called plus end-tracking proteins (+Tips), can also link the microtubule cytoskeleton to other structures within the cell [14,106,107]. Plus end binding proteins may promote, for example, microtubule interactions with the plasma membrane and could be involved in the microtubule search and capture mechanism. In this way microtubule plus end proteins may help to set up the general spatial organization of microtubules within a cell and contribute to overall cell morphology. On the other hand microtubule plus end binding proteins may prepare local sites on microtubules for establishing an initial contact between a membranous organelle or chromosomes. While the mechanism remains unknown, proteins that bind to the plus end could do this by using dynamic or structural cues. In this section, the main functions of microtubule plus end proteins will be highlighted. A historical overview of CLIP-170 is given, together with a classification of the different CLIPs and CLIP-like proteins. In addition, the EB1 and APC family proteins are discussed.

2.5.1 Cytoplasmic linker proteins (CLIPs)

The first member of the CLIP family, CLIP-170

It was the Thomas Kreis lab who described CLIP-170, the first member of the cytoplasmic linker protein (CLIP) family of 170 kDa. In search for linker proteins that bind microtubules and organelles, CLIP-170 was identified [108], by using a standard

microtubule motor preparation from HeLa cells, which was previously applied for the isolation of kinesin and cytoplasmic dynein [109]. Proteins within HeLa cell extracts were allowed to bind to polymerized microtubules and subsequently eluted with ATP. CLIP-170 was found to be one of the ATP-sensitive microtubule binding proteins [110]. CLIP-170 colocalized with microtubules by immunofluorescence but was characteristically different from kinesin and cytoplasmic dynein, as determined by sucrose gradients and nucleotide sensitive microtubule binding. The ATP-sensitive microtubule interaction suggested that CLIP-170 belongs to a novel class of microtubule-based mechanochemical enzymes. Further studies showed that the interaction of CLIP-170 with microtubules is regulated by phosphorylation on serine residues and is not directly sensitive to ATP. Inhibition of microtubule binding by phosphorylation of CLIP-170 accounts for the observed elution of CLIP-170 from microtubules by ATP [111]. Furthermore, the in vivo phosphorylation state of CLIP-170 is dependent on microtubules since nocodazole, a microtubule depolymerizing agent, induces a rapid dephosphorylation of CLIP-170. This suggests that a microtubule-associated kinase is responsible for the phosphorylation of CLIP-170. Thus, although CLIP-170 turned out not to be a motor protein, its binding to microtubules in an ATP dependent manner is relevant for its function.

Next, by using an *in vitro* assay to test for the binding of cytoplasmic vesicles to microtubules, CLIP-170 was found to be essential for the binding of endocytotic carrier vesicles to microtubules [108,112]. Immunodepletion of CLIP-170 from the cytosol abolished the binding of endocytotic vesicles to microtubules, whereas adding affinity purified CLIP-170 to cytosolic extracts depleted of CLIP-170 restored the ability to support binding in the assay. Furthermore, immunofluorescence in HeLa cells showed that CLIP-170 partially colocalized with transferrin receptor positive endocytic structures. In cells treated with BFA, which induces the tubulation of the endosome system, a more extensive colocalization was observed [108]. These data suggested that CLIP-170 links endocytotic vesicles to microtubules.

The cDNA for CLIP-170 was cloned from a HeLa cell expression library using CLIP-170 monoclonal antibodies [108]. The sequence predicted a protein that consists of three domains. A basic N-terminal domain of 350 amino acids, containing two microtubule binding motifs is separated by a long coiled coil of 900 amino acids, with numerous heptad repeats involved in dimerization, from a short C-terminal domain, with two putative metal binding motifs. The sequence however does not contain any consensus nucleotide binding motif, again indicating that CLIP-170 is not a motor protein. Physical characterization and rotary shadowing electron microscopy revealed that CLIP-170 is an elongated homodimer with the N-terminal and C-terminal domain separated by the 135 nm long rod domain [113].

Around the same time that the CLIP-170 sequence was published, another group identified a protein, named restin, which was highly expressed in Reed-Sternberg cells of Hodgkin's disease and in anaplastic large-cell lymphoma [114, 116-117]. This suggested that Restin overexpression may be a contributing factor to the

progression of Hodgkin's disease. Restin is identical to CLIP-170, except for a 35 amino acid insert in the coil-coiled region, but was proposed to be an intermediate filament-associated protein [118]. Although Restin shows some weak homology with intermediate filament proteins, such as keratin, GFAP, neurofilament protein and lamin and transfection studies indicated that restin forms filamentous structures, the evidence for restin as a intermediate filament-associated protein is not very strong. Later it was clearly demonstrated that overexpression of CLIP-170 has no effect on the organization of intermediate filaments in different cell types and that a complete collapse of the intermediate filament network does not relocalize endogenous CLIP-170 [119]. Thus, in contrast to the initial report by Bilbe et al. (1993) [114], restin is not an intermediate filament associated protein. However, the observation that restin/CLIP-170 is abundantly present in Reed-Sternberg cells of Hodgkin disease and other lymphomas remains valid and interesting.

Microtubule binding (CAP-Gly) domain in CLIPs

The N-terminal head domain of CLIP-170 contains two microtubule binding (CAP-Gly) domains surrounded by basic serine-rich regions [108]. Characterization of the microtubule binding sites was done by mutagenizing CLIP-170, either by truncation, internal deletions or point mutations. Binding of mutant CLIP-170 to microtubules was assayed by cosedimentation with polymerized tubulin or by transient expression in mammalian cells [108,119]. These experiments showed that both microtubule binding motifs are competent to bind to microtubules, although their contribution is not equivalent. The microtubule binding domains contain highly conserved glycine residues and a core sequence of PXGKND. Because of the highly conserved glycine residues, the microtubule binding domains of CLIPs are named cytoskeletal associated protein glycine conserved domain (CAP-Gly) [120]. These microtubule binding domains are different from microtubule binding motifs found in other MAPs.

Metal binding domain in CLIP-170

CLIP-170 has two putative metal binding motifs at the C-terminus of the protein. The second motif matches exactly the CCHC zinc finger-like consensus sequence $CX_2CX_4HX_4C$ [120]. CCHC modules are also found in the nucleocapsid p7 (NCp7) proteins of human immunodeficiency virus type 1 (HIV-1). The spacing pattern between the cysteine and histidine residues of these nucleocapside CCHC zinc fingers is highly conserved among retroviruses. In addition, single or multiple copies of the CCHC boxes are found in nucleic-acid binding proteins and have been shown to be responsible for binding to RNA and DNA [121,122]. The CCHC module also binds Zn^{2+}, as determined by UV/VIS spectrophotometric methods and NMR experiments [123,124]. However, whether CLIP-170 is able to bind zinc and/or nucleotides remains to be determined.

The first putative metal binding domain of CLIP-170 differs from the CCHC zinc finger-like module because of an additional cysteine residue, resulting in the sequence $CX_2CXCX_3HX_4C$. Although this motif is highly conserved between *Drosophila* CLIP-190 and chicken, rat and human CLIP-170, database searches have failed to find this motif in other proteins. However, CCHC domains with different spacing between conserved residues were found. For example, in the *Drosophila* Nanos protein, the CCHC module binds to RNA and is essential for the regulation of translation [122]. The differences between the two metal binding sites in CLIP-170 raise the possibility that both modules function independently of each other or that together both domains form a new specialized motif. Truncation of the complete C-terminal tail domain of CLIP-170 suggests a role for the metal binding motifs in cargo recognition. Interestingly, the forming of CLIP-170 induced patches in overexpressing cells and the targeting of CLIP-170 to prometaphase kinetochores depends on an intact C-terminal domain [119,125].

CLIP superfamily

Originally, the term cytoplasmic linker proteins (CLIPs) was used to identify non-motor proteins that link specific organelles to microtubules. With the identification of CLIP-170 and its specific endosome-microtubule interaction, it was suggested that there must be specific CLIPs for each organelle [126]. Indeed, additional CLIP proteins have been characterized in *in vitro* organelle-microtubule binding assays. For example, specific CLIPs have been found to link microtubules to the endoplasmatic reticulum, Golgi apparatus, lysosome and peroxisomes [4,5,127,128]. Thus, identification of these proteins supported the theory that other CLIPs exist that mediate the interaction of specific organelles with microtubules. However, these CLIP proteins have totally different structures and microtubule binding domains and are not homologues to CLIP-170. Nowadays, the nomenclature describes CLIPs as proteins which are homologous to CLIP-170.

The CLIP superfamily consists of proteins which share the highly conserved microtubule binding CAP-Gly motifs of CLIP-170. CLIP-like proteins have been identified from yeast to mammals. Based on their protein domains and putative functions, the family of CLIPs can be grouped into five classes (Fig. 2). Class I CLIPs include the CLIP-170-like proteins, which can be further subdivided in three subclasses; CLIP-170 (Class Ia), CLIP-115 (Class Ib) and $p150^{Glued}$ (Class Ic). Class II CLIPs include two tubulin folding factors protein; tubulin folding factor B (Class IIa) and tubulin folding factor E (Class IIb). Class III CLIPs include the kinesin-73-like proteins. Class IV CLIPs include proteins named CLIP-related proteins and class V CLIPs include CYLD. Members of class I and II are present in mammals, fly, worm and both budding and fission yeast. This suggests that the genes of these CLIP-like proteins are the oldest in evolutionary terms and that the other CLIP-related genes have appeared later in evolution.

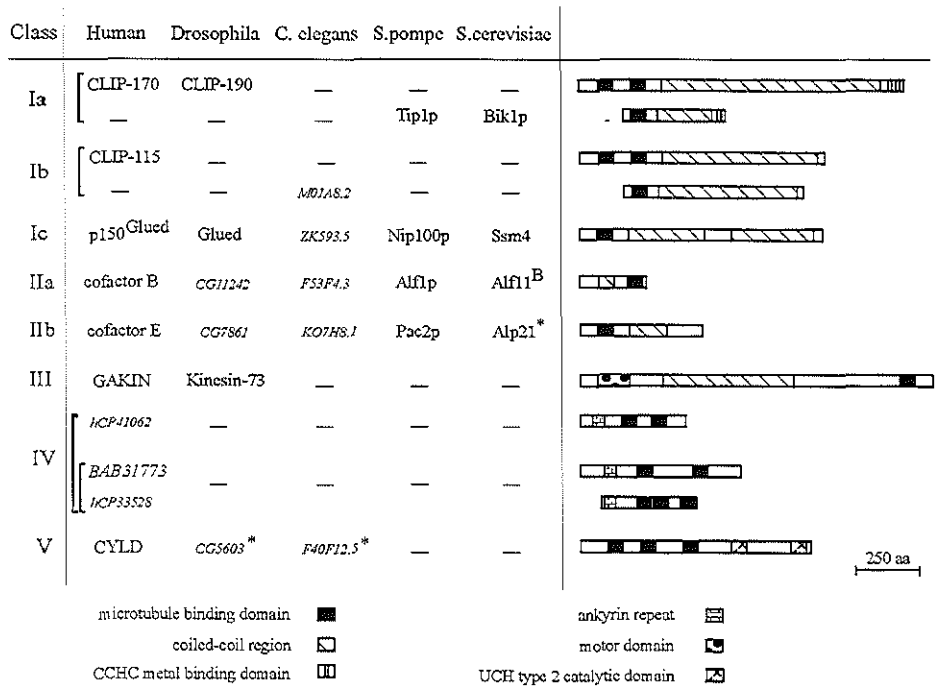

Figure 2: The CLIP superfamily.
CLIP family proteins are divided into five classes: CLIP-170-like proteins (I), tubulin folding factors (II), kinesin-73-like proteins (III), CLIP-related proteins (VI) and CYLD (V). Class I can be subdivided in CLIP-170 (Ia), CLIP-115 (Ib) and p150^{Glued} (Ic) en class II can be subdivided in tubulin folding factor B (IIa) and tubulin folding factor E (IIb) proteins. Asterisks indicate proteins that are homologous to members of the same class except they do not contain a conserved CAP-Gly microtubule binding domain. The schematic protein structure is indicated at the right. The different motifs found in CLIP family proteins are shown below the figure.

Class Ia proteins have one or two conserved microtubule CAP-Gly motifs, a long coiled-coil domain and a putative metal-binding motif at their C-terminus, that is similar to the domain in CLIP-170. Class Ia members include mammalian CLIP-170 [108], *Drosophila* CLIP-190 [129], S. *cerevisiae* Bik1p [130] and S. *pombe* Tip1p [131], also named Noc1p [132]. Bik1p and Tip1p contain one CCHC zinc finger module while CLIP-170 and CLIP-190 have two of these motifs. The metal binding motifs from Bik1p and Tip1p match with the second motif of CLIP-170 and CLIP-190 (see above). This suggests that the second zinc finger may have an evolutionary conserved function. Since most of the functional studies on CLIP proteins have been done on the class Ia members, the role of these CLIP-170-related proteins in microtubule dynamics and organelle transport will be summarized in the next paragraph.

Class Ib proteins have one or two microtubule binding motifs and a long coiled-coil domain. A metal binding motif is not present in class Ib proteins. Class Ib

members include mammalian CLIP-115 [133] and a hypothetical protein in *C. elegans* (M01A8.2) [134]. CLIP-115 bears a striking homology to CLIP-170, the overall similarity between CLIP-115 and CLIP-170 being 67% (chapter 3) [133]. In addition, both CLIPs have a highly similar secondary structure. Like CLIP-170, CLIP-115 has a basic amino-terminal domain, with two microtubule binding domains and surrounding serine-rich regions, and a long coiled coil structure which is involved in homodimerization (chapter 4) [135]. However, in contrast to CLIP-170, CLIP-115 lacks a C-terminal cysteine-rich structure and its tail is rather inconspicuous. The similarity between these CLIP-115 and CLIP-170 and the presence of only CLIP-170 homologue in lower eucaryotes, suggests that the CLIP-115 gene was formed from a duplication of the CLIP-170 gene late in evolution. Interestingly, mammalian CLIP-115 and CLIP-170 and *Drosophila* CLIP-190 are the only CLIP proteins with two microtubule binding (MTB) motifs and a coiled-coil region. Within their dimeric protein configuration, these CLIPs therefore have four microtubule binding domains, suggesting that CLIP-115, -170 and -190 may have a higher affinity for microtubules, than the other CLIP family members. On the other hand, site-specific phosphorylation of each microtubule binding domain, may regulate the interaction with microtubules or tubulin protofilaments (chapter 4) [135].

Class Ic proteins have one microtubule binding motif and two coiled-coil domains. Class Ic members include mammalian $p150^{Glued}$ [93], fission yeast Ssm4 [136], budding yeast Nip100p [137], a hypothetical protein in *C. elegans* (ZK593.5) [134], and Glued in *Drosophila* [100]. $p150^{Glued}$ is the biggest subunit of the dynactin complex (see section 2.4.2). $p150^{Glued}$ is reported to mediate the interaction between cytoplasmic dynein and dynactin [91]. Genetic analysis in flies and yeast reveals a important function for $p150^{Glued}$-like proteins in basic cellular processes (see section 2.4.2) [101,102,137].

Class II proteins are tubulin folding factors, which are tubulin specific chaperones and needed for the folding and joining of newly synthesized α- and β-tubulin into functional dimers (see 1.4.1). Class II include two tubulin folding factor B (Class IIa) and tubulin folding factor E (Class IIb). The protein structure of tubulin folding factor B and E are completely different. Tubulin folding factor B has a coiled-coil domain and a C-terminal microtubule binding CAP-Gly motif, while tubulin folding factor E has a N-terminal CAP-Gly motif and a coiled-coil domain containing ten times a leucine-rich repeating motif [138-140]. Homologues of human cofactor B and E, exist in *S. cerevisiae* (Alf1p and Pac2p) [141], *S. pombe* ($Alp11^{B}$ and $Alp21^{E}$) [138], *C. elegans* (hypothetical proteins F53F4.3 and K07H8.1) [134] and *Drosophila* (hypothetical protein CG11242 and CG7861) [142]. Interestingly, $Alp21^{E}$ in fission yeast has no conserved microtubule binding domain [138]. Feierbach et al. (1999) [141], showed that the microtubule binding CAP-Gly motif of Alf1p (cofactor B) interacts with α-tubulin monomers. These results raise the possibility that other members of the CLIP family may also interact with α-tubulin via their conserved microtubule binding motif.

Class III proteins are defined by a N-terminal motor domain of the KIF1A/unc-104 subfamily of the kinesin superfamily, in addition to a C-terminal microtubule binding domain and a coiled-coil structure. Class III members include *Drosophila* kinesin-73 [143] and human GAKIN [144]. In *Drosophila*, kinesin-73 is widely distributed in the syncytial embryo but becomes restricted to the central and peripheral nervous system upon development. The presence of a CAP-Gly domain and motor domain suggests that kinesin-73 may be a motor protein for the anterograde axonal transport of tubulin oligomers, or polymers, along microtubule tracks [143]. GAKIN, Guanylate kinase Associated KINesin, is identified as a binding protein of the human homologue of the *Drosophila* Disc Large tumor suppressor protein (Dlg) [144]. Dlg acts as a scaffold lattice for the assembly and organization of protein complexes, such as receptors, at specialized membrane sites. In neurons, Dlg has been shown to be required for the development of synaptic structures [145]. It is proposed that the GAKIN-Dlg interaction is involved in the reorganization of cytoskeleton and membrane receptors at synaptic sites in neuronal cells [146]. Interestingly, GAKIN is a candidate gene for schizophrenia on chromosome 6p23 [147].

Class IV proteins have an ankyrin (ANK) repeats in addition to their microtubule binding domain. Class IV members are only found in mammals and include proteins named CLIP-related proteins (CLIP-Rs) [148]. While most CLIP-like proteins carry their microtubule binding motif at the N-terminus, the CLIP-R proteins have microtubule binding motifs at the C-terminus, while at the N-terminus of these CLIPs, the ankyrin repeats are positioned. Ankyrin repeats have been identified in hundreds of proteins in viruses, prokaryotes and eucaryotes and are involved in specific protein-protein interaction. Two CLIP-R genes are found in the human genome with this composition; hCG23458 (protein code hCP41062) is located at chromosome 19 and hCG16535 (protein code hCP33528) is present on chromosome 2 [148]. The transcripts of both genes can be found as short ESTs and long cDNA isolated from several human, mice and rat libraries. Alignments of these sequences suggests the presents of alternatively spliced transcripts, containing one, two or three microtubule binding domains (AK005167, BAB31773 and data not shown). The different cDNAs are most likely the result of alternative splicing of the genes. Although this suggests a complex pattern of protein isoforms, nothing is reported about the characteristics and possible function of the CLIP-R proteins.

Class V proteins have a CAP-Gly microtubule binding domain together with an ubiquitin carboxy-terminal hydrolase (UCH2) motif. The only member of the class IV is the CYLD protein, which contains three CAP-Gly domains and two UCH2 motifs [149]. Likely orthologues are found in *Drosophila* and *C. elegans* (hypothetical proteins CG5603 and F40F12.5 respectively), however, sequence similarity is predominantly restricted to the C-terminal part of the protein, which contains the UCH2 motifs. The UCH2 motif can catalyze the hydrolysis of ubiquitin, which results in deubiquitination and a reduced degradation of proteins by the proteasome. Since mutations in CYLD are associated with the development of skin tumours

(cylindromas) it is thought that inactivation of CYLD may enhance the degradation of ubiquitinated proteins that are important in apoptosis [149].

To summarize, the CLIP superfamily is divided in five classes and consists of proteins which share the microtubule binding CAP-Gly motifs of CLIP-170. In addition, a number of CLIPs have a domain which forms a coiled-coil structure. Each class has a variety of characteristic domains, such as CCHC (class Ia), microtubule motor (class III), ANK (class IV), UCH2 (class V) domains. The precise function of these domains in concert with their microtubule binding domain has to determined.

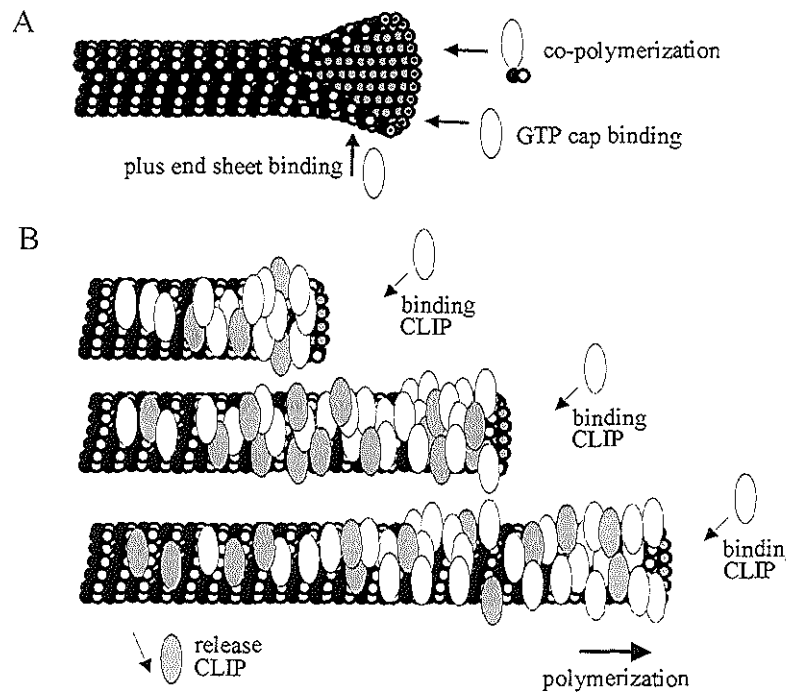

Figure 3: CLIPs treadmill on growing microtubule plus ends in a comet-like pattern.
A CLIPs bind to the microtubule plus ends either by recognizing a specific structural feature of the growing microtubule plus ends (GTP-cap or sheet structure) or by copolymerization with tubulin dimers or oligomers. **B** CLIP-170 is freely present in the cytosol. CLIP-170 binds the polymerizing plus end of the microtubule (white) and remains bound until it falls off (gray) behind the region of growth. The release of CLIP-170 creates a nonuniform comet-like pattern. This comet-like pattern is caused by the dissociation of individual CLIP-170 proteins from the microtubule. Phosphorylation of CLIP-170 is thought to be important for detachment from the microtubule plus ends.

CLIP-170 treadmills on growing microtubule plus ends

Already in the first CLIP-170 paper it was described that CLIP-170 localizes in stretches along a subset of microtubule plus ends [110]. Visualization of GFP-CLIP-170 in cells by time-lapse fluorescence microscopy subsequently revealed that these stretches move with the plus end of growing microtubules, while no GFP-CLIP-170 is found at the tips of retracting microtubules [150]. The fluorescent stretches move in a

comet like pattern (Fig. 3) at 0.15-0.4 μm/s, which is comparable to microtubule growth in vivo [151]. Using speckle microscopy, it is shown that CLIP-170 treadmills on the growing microtubules, instead of being continuously transported to the growing tip by motor proteins [150]. The scheme which is depicted in Figure 3 explains CLIP-170 treadmilling behavior in cells.

First, CLIP-170 derived from a diffusable cytoplasmic pool, associates with the peripheral segment of a newly synthesized tubulin polymer. CLIP-170 may recognize a specific structure at the microtubule plus end, such as the GTP-cap, or a tubulin sheet (see section 1.4.3) or, alternatively, CLIP-170 may associate with growing microtubules by copolymerization with tubulin [152] (Fig. 3a). While the microtubule tip grows further and acquires new cytoplasmic CLIP-170, the microtubule bound CLIP-170 distal to the plus end is released (Fig. 3b). This may occur by phosphorylation of CLIP-170, via an as yet unknown microtubule-associated kinase [111]. Alternatively, the departure of CLIP-170 from the microtubule could be due to conformational changes at the microtubule plus end (e.g. GTP-hydrolysis or tube closure) (see section 1.4.3) in concert with phosphorylation. In this way, CLIP-170 cruises on dynamic microtubules throughout the cytoplasm and continuously explores the cytoplasmic space. The class Ic protein, CLIP-115 also localizes at growing microtubule plus ends when expressed in fibroblasts (see chapter 4) [135]. The treadmilling behavior of CLIPs has important implications for the role of these proteins in regulating microtubule growth and membrane traffic.

Role of CLIPs in microtubule dynamics

There is compelling evidence that the CLIP-170 homologue from yeast, tip1p, is involved in the regulation of microtubule dynamics. In *S. pombe*, microtubules nucleate in the vicinity of the nuclear envelope in the center of the cell and grow parallel to the long axis until they reach the cell ends. The microtubule ends are oriented towards the cell tips at the sites where cell growth occurs [153]. The position of cell growth is also called the growth zone. *S. pombe* cells have two growth zones at both poles (chapter 1 Fig. 7b). It has been shown that microtubules transport the protein tea1p to the cell poles, were it acts as a marker for positioning of the growth zone [154]. Disruption of microtubules and deletion of tea1p inhibits the process by which the growth zone is positioned, leading to bent and branched cells [155]. If a microtubule initiates growth at an oblique angle to the longitudinal axis, the tubulin polymer will first contact the cell cortex in the central region of the cell and change the direction, by a combination of bending and rotation, while continuing growing underneath the cortical membrane. Only when it has reached the cortical membrane of the cell poles does a microtubule tend to pause and deliver components, such as tea1p, to the cell tip and subsequently undergo catastrophe. In any other region of the cell microtubule catastrophe is almost completely suppressed. In cells were Tip1 is deleted catastrophe occurs in any cortical region of the cell and is not restricted to the cell ends [106,131]. In addition, tea1p no longer accumulates at the cell poles but is distributed along the microtubules, which leads to bent and branched cells. This has lead to the conclusion that Tip1p, which is localized at the distal tips of microtubules, acts as a

suppressor of microtubule catastrophes. Tip1p delays microtubular catastrophe until microtubules have grown into the cortical regions of the cellular poles. There are several possibilities to explain how Tip1p affects catastrophe. The microtubule could be kept in a sheet conformation by Tip1p, which is thought to prevent catastrophe (section 1.4.3) or Tip1p could inhibit the binding of a catastrophe-inducing factor or recruit a catastrophe-inhibiting factor (section 2.3). Furthermore, Tip1p can distinguish different cortical regions of the cell. In this view, Tip1p is required for "sensing" the position of the cortical membrane within the cell. It might be that Tip1p is scanning the cortex for differences and regulates microtubule dynamics according to the specific membrane regions in the cell. The high degree of similarity between Tip1p and CLIP-170 suggests that the latter (and other CLIP-like proteins) also might function as anti-catastrophe factors. This notion is underscored by the phenotype caused by the deletion of the BIK1 gene in budding yeast [130]. In cells without Bik1p the cytoplasmic and spindle microtubules are absent or abnormally short. As a result of the defects in microtubule growth, BIK1 null mutant cells exhibit defects in chromosome segregation and nuclear migration. On the other hand, cells overexpressing Bik1p have abnormally long microtubule structures. Based on these results it has been proposed that Bik1p is required for formation or stabilization of microtubules. Other evidence for a role of CLIP proteins in microtubule dynamics, comes from studies on CLIP-associated proteins, CLASPs (chapter 5) [156]. It is shown that CLASP bind to both CLIP-115 and CLIP-170 and localize at microtubule distal ends. Overexpression of CLASP induces microtubule stabilization and inhibition of CLASP by antibody injections prevents the stabilization of microtubules in motile fibroblasts. This suggests that CLIPs and CLASPs act together to regulate microtubule dynamics. CLASP might even act as a anti-catastrophe factor as proposed from the tip1p study by Brunner and Nurse (2000) [131].

To summarize, four lines of evidence suggest that CLIPs of class Ia en Ib are involved in the regulation of microtubule dynamics. 1) The dynamic localization of CLIP-70, CLIP-115 and tip1p at the tips of growing microtubules. 2) Tip1p is involved in the suppression of microtubule catastrophe. 3) Bik1p regulates the assembly or stabilization of microtubules. 4) CLIP-associated proteins induce local stabilization of microtubules.

Role of CLIPs in vesicle transport

Waterman-Storer et al., (1995) [157] showed that membranous vesicles selectively attach to dynamic plus ends of microtubules. The unidentified molecules that bind to the membrane region and the microtubule tip were collectively named the tip attachment complex (TAC). Since CLIP-170 has been observed at the tip of microtubules and has been shown to bind endosomes *in vitro*, it was suggested that CLIPs are candidate proteins to be present in the TAC [126]. CLIPs may provide a specialized binding site for membranous organelles at the tubulin distal ends. In this scenario, CLIP-170 may link endocytic organelles to microtubules and facilitate the

transport of endocytotic vesicles [108]. Evidence for the role of CLIPs in organelle movement comes from *Drosophila* studies on actin-based motor proteins, where CLIP-190 has been shown to interact with the myosin VI [129]. Since myosin VI was shown to function as a vesicle motor, it was suggested that CLIP-190 and myosin may link microtubule plus ends to cortical actin cables and coordinate the microtubule and actin-based transport of vesicles from or to the plasma membrane [158,159]. Further more compelling evidence for a role of CLIPs in organelle movements has emerged from recent studies on the minus-end-directed microtubule-based motor dynein and its activator dynactin. Dynein itself can bind membrane lipids, but dynein is also thought to bind cargo via dynactin (see section 2.4.2). Immunofluorescent and immunoelectron microscopy studies in cultured cells reveal that dynactin and dynein colocalize with CLIP-170 at microtubule distal ends [160,161]. Overexpression of CLIP-170 recruits dynactin to CLIP-170-induced patches [162]. It has been proposed that CLIP-170 targets dynactin and dynein to microtubule plus ends to generate an early vesicle loading site for minus end directed organelle transport [13,160,162]. In this view, dynactin is targeted, with the help of CLIP-170, to the microtubule tip which extends into the periphery of the cell. Vesicles, such as endosomes may be loaded on microtubule plus end carrying CLIP-170/dynactin. While the vesicle is docked to the microtubule, dynactin may provide a dynein binding site. When the conditions are right for motility, dynein becomes activated and takes off to power minus end directed transport. Subsequently, the CLIP-170 microtubule link is severed, perhaps by phosphorylation.

2.5.2 EB1 and APC family proteins

The adenomatous polyposis coli protein (APC) and its binding protein, EB1, have both been found at microtubule ends and represent another example of microtubule plus end binding proteins [163-168]. The APC protein was originally identified as a tumor suppressor and the gene was found mutated in patients with familial adenomatous polyposis, a syndrome characterized by multiple colonic polyps and colorectal carcinoma [169]. APC is a 310 kDa protein which has multiple domains and is thought to be a protein scaffold that binds numerous protein partners at distinct sites along its length [170]. The N-terminal region contains an alpha-helical domain and seven armadillo repeats and binds to phosphatase 2A [171]. The middle part of APC contains amino acid repeats that interact with β-catenin, glycogen synthase kinase 3β (GSK-3β) and axin. The C-terminal part of APC associates with microtubules, with EB1 and with the disc large (DLG) tumour suppressor protein [172]. The APC protein is part of the Wingless (Wnt) signal transduction pathway and is involved in the regulation of the stability of β-catenin [173,174]. In the absence of Wnt signal, β-catenin is targeted for destruction by the APC/Axin/GSK-3β complex. Mutations in the APC gene disable the destruction complex, leading to β-catenin accumulation and activation of Wnt target genes. The APC protein may also have

additional cellular roles. In migrating cells, APC is localized to the leading edges, were it is concentrated as granules at the microtubule plus ends [165,168]. Recently, it has been shown that binding of APC to microtubules increases microtubule stability [164,175,176]. Together these data lead to the hypothesis that APC present at the leading edge is involved in the stabilization of microtubule plus ends and may play a role in the stabilization of polarized cellular extensions. Since EB1 family proteins interact with the C-terminal region of APC and are concentrated at the ends of microtubules, it is likely that APC is targeted to the microtubule ends via EB1. In line with this, APC mutants which lack the EB1 binding domain in the C-terminal tail still associate with microtubules but are not targeted to plus ends [164,166,176].

EB1 was isolated from a yeast-two hybrid screen using APC [177]. Although the 30 kDa EB1 protein has been found to associate with microtubules it does not show any homology to a known microtubule binding motif. Instead, the protein contains coiled-coil structures in the middle and C-terminal part and bears a domain with weak similarity to a calponin motif, at its N-terminus. EB1 family members have been found from yeast to mammals. In budding yeast the EB1 homologue is named binding to microtubules 1 protein, Bim1p [178] and in fission yeast, mal3 [179]. Interestingly, Bim1p interacts, like the CLIP-170 homologue Alf1p, with α-tubulin in a yeast two hybrid assay, suggesting that both proteins use similar mechanisms for the binding to tubulin [178]. *C. elegans* has two EB1 related genes and *Drosophila* three EB1 family members. In humans the EB1 family is called MAPRE (microtubule associated protein members) and consist of at least three members, EB1, EB2 (RP1) and EB3 (EBF3) [180].

Perhaps best understood is the function of Bim1p. Bim1p localizes, like its mammalian homologue EB1, to microtubule tips. Cells lacking the Bim1 gene show reduced microtubule dynamics, which results in shorter microtubules. In addition, cells without Bim1p fail to orient microtubules towards the bud in mating cells and are defective in mitotic spindle positioning [181]. The spindle orientation process in budding yeast is unique, because it must actively line the mitotic spindle in parallel to the mother-bud axis to segregate one nucleus to each progeny cell (see section 1.4.4) (chapter 1 Fig. 4c). Bim1p is a key regulator for the interaction between the microtubules and cell cortex in positioning the mitotic spindle [182]. By interacting with Kar9p, which is a cortical protein present in the bud tip, Bim1p establishes a link between the microtubule ends and the cell cortex [183,184]. These studies suggest a mechanism for the capture of microtubules at the cortex of the bud during spindle positioning. Bim1p increases microtubule dynamicity, which enhances the search by microtubules for cortical binding sites. An interaction between Bim1p and Kar9p causes attachment of the microtubule to the cortex. Next, spindle movement is mediated by microtubule plus end depolymerization, which generates a pulling force towards the cortex. The capture complex may maintain the contact with the shortening end. No homologue of Kar9p has been found in other species. So, it is tempting to

speculate that a similar microtubule capture mechanism exists in flies and mammals which relies on the APC-EB1 interaction [185].

Since EB1-GFP localizes dynamically to growing microtubule plus ends in a manner very similar to CLIP-170, this suggests that both proteins use the same mechanism to preferentially interact with the microtubule plus ends [167]. However, EB1 family proteins and CLIPs show no similarity in microtubule binding domains. In addition to its interaction with APC and tubulin, EB1 also associates with the dynactin complex and cytoplasmic dynein [186]. It has been proposed that EB1, like CLIP-170, may help to load dynactin onto the microtubules[186]. How all these proteins interact with each other and the microtubule plus ends remains unclear.

References

1. Solomon, F., Magendantz, M., and Salzman, A. (1979) Identification with cellular microtubules of one of the co-assemlbing microtubule-associated proteins. *Cell* **18**(2): 431-8.
2. Desai, A., Verma, S., Mitchison, T. J., and Walczak, C. E. (1999) Kin I kinesins are microtubule-destabilizing enzymes. *Cell* **96**(1): 69-78.
3. Fuchs, E., and Yang, Y. (1999) Crossroads on cytoskeletal highways. *Cell* **98**(5): 547-50.
4. Bashour, A. M., and Bloom, G. S. (1998) 58K, a microtubule-binding Golgi protein, is a formiminotransferase cyclodeaminase. *J Biol Chem* **273**(31): 19612-7.
5. Gao, Y. S., Alvarez, C., Nelson, D. S., and Sztul, E. (1998) Molecular cloning, characterization, and dynamics of rat formiminotransferase cyclodeaminase, a Golgi-associated 58-kDa protein. *J Biol Chem* **273**(50): 33825-34.
6. Rajas, F., Gire, V., and Rousset, B. (1996) Involvement of a membrane-bound form of glutamate dehydrogenase in the association of lysosomes to microtubules. *J Biol Chem* **271**(47): 29882-90.
7. Drewes, G., Ebneth, A., and Mandelkow, E. M. (1998) MAPs, MARKs and microtubule dynamics. *Trends Biochem Sci* **23**(8): 307-11.
8. Mandelkow, E., and Mandelkow, E. M. (1995) Microtubules and microtubule-associated proteins. *Curr Opin Cell Biol* **7**(1): 72-81.
9. Hirokawa, N. (1998) Kinesin and dynein superfamily proteins and the mechanism of organelle transport. *Science* **279**(5350): 519-26.
10. Lane, J., and Allan, V. (1998) Microtubule-based membrane movement. *Biochim Biophys Acta* **1376**(1): 27-55.
11. Cassimeris, L. (1999) Accessory protein regulation of microtubule dynamics throughout the cell cycle. *Curr Opin Cell Biol* **11**(1): 134-41.
12. Andersen, S. S. (2000) Spindle assembly and the art of regulating microtubule dynamics by MAPs and Stathmin/Op18. *Trends Cell Biol* **10**(7): 261-7.
13. Schroer, T. A. (2001) Microtubules don and doff their caps: dynamic attachments at plus and minus ends. *Curr Opin Cell Biol* **13**(1): 92-6.
14. Schuyler, S. C., and Pellman, D. (2001) Microtubule "plus-end-tracking proteins": the end is just the beginning. *Cell* **105**(4): 421-4.
15. Tirnauer, J. S., and Bierer, B. E. (2000) EB1 proteins regulate microtubule dynamics, cell polarity, and chromosome stability. *J Cell Biol* **149**(4): 761-6.
16. Hirokawa, N. (1994) Microtubule organization and dynamics dependent on microtubule- associated proteins. *Curr Opin Cell Biol* **6**(1): 74-81.
17. Kreis, T., and Vale, R. (1999) Guidebook to the cytoskeletal and motor proteins, 2nd Ed., Oxford University Press, Oxford ; New York
18. Chen, J., Kanai, Y., Cowan, N. J., and Hirokawa, N. (1992) Projection domains of MAP2 and tau determine spacings between microtubules in dendrites and axons. *Nature* **360**(6405): 674-7.
19. Hammarback, J. A., Obar, R. A., Hughes, S. M., and Vallee, R. B. (1991) MAP1B is encoded as a polyprotein that is processed to form a complex N- terminal microtubule-binding domain. *Neuron* **7**(1): 129-39.
20. Togel, M., Wiche, G., and Propst, F. (1998) Novel features of the light chain of microtubule-associated protein MAP1B: microtubule stabilization, self interaction, actin filament binding, and regulation by the heavy chain. *J Cell Biol* **143**(3): 695-707.

21. Meixner, A., Haverkamp, S., Wassle, H., Fuhrer, S., Thalhammer, J., Kropf, N., Bittner, R. E., Lassmann, H., Wiche, G., and Propst, F. (2000) MAP1B is required for axon guidance and Is involved in the development of the central and peripheral nervous system. *J Cell Biol* **151**(6): 1169-78.
22. Roos, J., Hummel, T., Ng, N., Klambt, C., and Davis, G. W. (2000) Drosophila Futsch regulates synaptic microtubule organization and is necessary for synaptic growth. *Neuron* **26**(2): 371-82.
23. Hummel, T., Krukkert, K., Roos, J., Davis, G., and Klambt, C. (2000) Drosophila Futsch/22C10 is a MAP1B-like protein required for dendritic and axonal development. *Neuron* **26**(2): 357-70.
24. Lee, G., Neve, R. L., and Kosik, K. S. (1989) The microtubule binding domain of tau protein. *Neuron* **2**(6): 1615-24.
25. Gustke, N., Trinczek, B., Biernat, J., Mandelkow, E. M., and Mandelkow, E. (1994) Domains of tau protein and interactions with microtubules. *Biochemistry* **33**(32): 9511-22.
26. Kaech, S., Ludin, B., and Matus, A. (1996) Cytoskeletal plasticity in cells expressing neuronal microtubule- associated proteins. *Neuron* **17**(6): 1189-99.
27. Harada, A., Oguchi, K., Okabe, S., Kuno, J., Terada, S., Ohshima, T., Sato-Yoshitake, R., Takei, Y., Noda, T., and Hirokawa, N. (1994) Altered microtubule organization in small-calibre axons of mice lacking tau protein. *Nature* **369**(6480): 488-91.
28. Takei, Y., Teng, J., Harada, A., and Hirokawa, N. (2000) Defects in axonal elongation and neuronal migration in mice with disrupted tau and map1b genes. *J Cell Biol* **150**(5): 989-1000.
29. Spittaels, K., Van den Haute, C., Van Dorpe, J., Bruynseels, K., Vandezande, K., Laenen, I., Geerts, H., Mercken, M., Sciot, R., Van Lommel, A., Loos, R., and Van Leuven, F. (1999) Prominent axonopathy in the brain and spinal cord of transgenic mice overexpressing four-repeat human tau protein. *Am J Pathol* **155**(6): 2153-65.
30. Heutink, P. (2000) Untangling tau-related dementia. *Hum Mol Genet* **9**(6): 979-86.
31. Garcia, M. L., and Cleveland, D. W. (2001) Going new places using an old MAP: tau, microtubules and human neurodegenerative disease. *Curr Opin Cell Biol* **13**(1): 41-8.
32. Mandelkow, E. M., and Mandelkow, E. (1998) Tau in Alzheimer's disease. *Trends Cell Biol* **8**(11): 425-7.
33. Hall, G. F., Chu, B., Lee, G., and Yao, J. (2000) Human tau filaments induce microtubule and synapse loss in an in vivo model of neurofibrillary degenerative disease. *J Cell Sci* **113**(Pt 8): 1373-87.
34. Ebneth, A., Godemann, R., Stamer, K., Illenberger, S., Trinczek, B., and Mandelkow, E. (1998) Overexpression of tau protein inhibits kinesin-dependent trafficking of vesicles, mitochondria, and endoplasmic reticulum: implications for Alzheimer's disease. *J Cell Biol* **143**(3): 777-94.
35. Gotz, J., Probst, A., Spillantini, M. G., Schafer, T., Jakes, R., Burki, K., and Goedert, M. (1995) Somatodendritic localization and hyperphosphorylation of tau protein in transgenic mice expressing the longest human brain tau isoform. *Embo J* **14**(7): 1304-13.
36. Duff, K., Knight, H., Refolo, L. M., Sanders, S., Yu, X., Picciano, M., Malester, B., Hutton, M., Adamson, J., Goedert, M., Burki, K., and Davies, P. (2000) Characterization of pathology in transgenic mice over-expressing human genomic and cDNA tau transgenes. *Neurobiol Dis* **7**(2): 87-98.
37. Lewis, J., McGowan, E., Rockwood, J., Melrose, H., Nacharaju, P., Van Slegtenhorst, M., Gwinn-Hardy, K., Paul Murphy, M., Baker, M., Yu, X., Duff, K., Hardy, J., Corral, A., Lin, W. L., Yen, S. H., Dickson, D. W., Davies, P., and Hutton, M. (2000) Neurofibrillary tangles, amyotrophy and progressive motor disturbance in mice expressing mutant (P301L) tau protein. *Nat Genet* **25**(4): 402-5.
38. Probst, A., Gotz, J., Wiederhold, K. H., Tolnay, M., Mistl, C., Jaton, A. L., Hong, M., Ishihara, T., Lee, V. M., Trojanowski, J. Q., Jakes, R., Crowther, R. A., Spillantini, M. G., Burki, K., and Goedert, M. (2000) Axonopathy and amyotrophy in mice transgenic for human four-repeat tau protein. *Acta Neuropathol (Berl)* **99**(5): 469-81.
39. Ishihara, T., Hong, M., Zhang, B., Nakagawa, Y., Lee, M. K., Trojanowski, J. Q., and Lee, V. M. (1999) Age-dependent emergence and progression of a tauopathy in transgenic mice overexpressing the shortest human tau isoform. *Neuron* **24**(3): 751-62.
40. McNally, F. J. (1999) Microtubule dynamics: Controlling split ends. *Curr Biol* **9**(8): R274-6.
41. Walczak, C. E. (2000) Microtubule dynamics and tubulin interacting proteins. *Curr Opin Cell Biol* **12**(1): 52-6.
42. Pryer, N. K., Walker, R. A., Skeen, V. P., Bourns, B. D., Soboeiro, M. F., and Salmon, E. D. (1992) Brain microtubule-associated proteins modulate microtubule dynamic instability in vitro. Real-time observations using video microscopy. *J Cell Sci* **103**(Pt 4): 965-76.
43. Drechsel, D. N., Hyman, A. A., Cobb, M. H., and Kirschner, M. W. (1992) Modulation of the dynamic instability of tubulin assembly by the microtubule-associated protein tau. *Mol Biol Cell* **3**(10): 1141-54.
44. Gard, D. L., and Kirschner, M. W. (1987) A microtubule-associated protein from Xenopus eggs that specifically promotes assembly at the plus-end. *J Cell Biol* **105**(5): 2203-15.

45. Tournebize, R., Popov, A., Kinoshita, K., Ashford, A. J., Rybina, S., Pozniakovsky, A., Mayer, T. U., Walczak, C. E., Karsenti, E., and Hyman, A. A. (2000) Control of microtubule dynamics by the antagonistic activities of XMAP215 and XKCM1 in Xenopus egg extracts. *Nat Cell Biol* **2**(1): 13-9.
46. Wang, P. J., and Huffaker, T. C. (1997) Stu2p: A microtubule-binding protein that is an essential component of the yeast spindle pole body. *J Cell Biol* **139**(5): 1271-80.
47. Nabeshima, K., Kurooka, H., Takeuchi, M., Kinoshita, K., Nakaseko, Y., and Yanagida, M. (1995) p93dis1, which is required for sister chromatid separation, is a novel microtubule and spindle pole body-associating protein phosphorylated at the Cdc2 target sites. *Genes Dev* **9**(13): 1572-85.
48. Matthews, L. R., Carter, P., Thierry-Mieg, D., and Kemphues, K. (1998) ZYG-9, a Caenorhabditis elegans protein required for microtubule organization and function, is a component of meiotic and mitotic spindle poles. *J Cell Biol* **141**(5): 1159-68.
49. Cullen, C. F., Deak, P., Glover, D. M., and Ohkura, H. (1999) mini spindles: A gene encoding a conserved microtubule-associated protein required for the integrity of the mitotic spindle in Drosophila. *J Cell Biol* **146**(5): 1005-18.
50. Charrasse, S., Schroeder, M., Gauthier-Rouviere, C., Ango, F., Cassimeris, L., Gard, D. L., and Larroque, C. (1998) The TOGp protein is a new human microtubule-associated protein homologous to the Xenopus XMAP215. *J Cell Sci* **111**(Pt 10): 1371-83.
51. Spittle, C., Charrasse, S., Larroque, C., and Cassimeris, L. (2000) The interaction of TOGp with microtubules and tubulin. *J Biol Chem* **275**(27): 20748-53.
52. Belmont, L. D., and Mitchison, T. J. (1996) Identification of a protein that interacts with tubulin dimers and increases the catastrophe rate of microtubules. *Cell* **84**(4): 623-31.
53. Endow, S. A., Kang, S. J., Satterwhite, L. L., Rose, M. D., Skeen, V. P., and Salmon, E. D. (1994) Yeast Kar3 is a minus-end microtubule motor protein that destabilizes microtubules preferentially at the minus ends. *Embo J* **13**(11): 2708-13.
54. Saunders, W., Hornack, D., Lengyel, V., and Deng, C. (1997) The Saccharomyces cerevisiae kinesin-related motor Kar3p acts at preanaphase spindle poles to limit the number and length of cytoplasmic microtubules. *J Cell Biol* **137**(2): 417-31.
55. Hartman, J. J., Mahr, J., McNally, K., Okawa, K., Iwamatsu, A., Thomas, S., Cheesman, S., Heuser, J., Vale, R. D., and McNally, F. J. (1998) Katanin, a microtubule-severing protein, is a novel AAA ATPase that targets to the centrosome using a WD40-containing subunit. *Cell* **93**(2): 277-87.
56. Charbaut, E., Curmi, P. A., Ozon, S., Lachkar, S., Redeker, V., and Sobel, A. (2001) Stathmin family proteins display specific molecular and tubulin binding properties. *J Biol Chem* **276**(19): 16146-54.
57. Curmi, P. A., Nogues, C., Lachkar, S., Carelle, N., Gonthier, M. P., Sobel, A., Lidereau, R., and Bieche, I. (2000) Overexpression of stathmin in breast carcinomas points out to highly proliferative tumours. *Br J Cancer* **82**(1): 142-50.
58. Jeha, S., Luo, X. N., Beran, M., Kantarjian, H., and Atweh, G. F. (1996) Antisense RNA inhibition of phosphoprotein p18 expression abrogates the transformed phenotype of leukemic cells. *Cancer Res* **56**(6): 1445-50.
59. Marklund, U., Larsson, N., Gradin, H. M., Brattsand, G., and Gullberg, M. (1996) Oncoprotein 18 is a phosphorylation-responsive regulator of microtubule dynamics. *Embo J* **15**(19): 5290-8.
60. Howell, B., Deacon, H., and Cassimeris, L. (1999) Decreasing oncoprotein 18/stathmin levels reduces microtubule catastrophes and increases microtubule polymer in vivo. *J Cell Sci* **112**(Pt 21): 3713-22.
61. Arnal, I., Karsenti, E., and Hyman, A. A. (2000) Structural transitions at microtubule ends correlate with their dynamic properties in Xenopus egg extracts. *J Cell Biol* **149**(4): 767-74.
62. Walczak, C. E., and Mitchison, T. J. (1996) Kinesin-related proteins at mitotic spindle poles: function and regulation. *Cell* **85**(7): 943-6.
63. Sharp, D. J., Rogers, G. C., and Scholey, J. M. (2000) Microtubule motors in mitosis. *Nature* **407**(6800): 41-7.
64. Endow, S. A. (1999) Determinants of molecular motor directionality. *Nat Cell Biol* **1**(6): E163-7.
65. Vale, R. D., Reese, T. S., and Sheetz, M. P. (1985) Identification of a novel force-generating protein, kinesin, involved in microtubule-based motility. *Cell* **42**(1): 39-50.
66. Schnapp, B. J., and Reese, T. S. (1989) Dynein is the motor for retrograde axonal transport of organelles. *Proc Natl Acad Sci U S A* **86**(5): 1548-52.
67. Schnapp, B. J. (1997) Retroactive motors. *Neuron* **18**(4): 523-6.
68. Vale, R. D., and Milligan, R. A. (2000) The way things move: looking under the hood of molecular motor proteins. *Science* **288**(5463): 88-95.
69. Howard, J. (1997) Molecular motors: structural adaptations to cellular functions. *Nature* **389**(6651): 561-7.
70. Moore, J. D., and Endow, S. A. (1996) Kinesin proteins: a phylum of motors for microtubule-based motility. *Bioessays* **18**(3): 207-19.

71. Terada, S., and Hirokawa, N. (2000) Moving on to the cargo problem of microtubule-dependent motors in neurons. *Curr Opin Neurobiol* **10**(5): 566-73.
72. Manning, B. D., and Snyder, M. (2000) Drivers and passengers wanted! the role of kinesin-associated proteins. *Trends Cell Biol* **10**(7): 281-9.
73. Nonaka, S., Tanaka, Y., Okada, Y., Takeda, S., Harada, A., Kanai, Y., Kido, M., and Hirokawa, N. (1998) Randomization of left-right asymmetry due to loss of nodal cilia generating leftward flow of extraembryonic fluid in mice lacking KIF3B motor protein. *Cell* **95**(6): 829-37.
74. Rattner, J. B., Rees, J., Arnett, F. C., Reveille, J. D., Goldstein, R., and Fritzler, M. J. (1996) The centromere kinesin-like protein, CENP-E. An autoantigen in systemic sclerosis. *Arthritis Rheum* **39**(8): 1355-61.
75. Dupuis, L., de Tapia, M., Rene, F., Lutz-Bucher, B., Gordon, J. W., Mercken, L., Pradier, L., and Loeffler, J. P. (2000) Differential screening of mutated SOD1 transgenic mice reveals early up-regulation of a fast axonal transport component in spinal cord motor neurons. *Neurobiol Dis* **7**(4): 274-85.
76. Zhao, C., Takita, J., Tanaka, Y., Setou, M., Nakagawa, T., Takeda, S., Yang, H. W., Terada, S., Nakata, T., Takei, Y., Saito, M., Tsuji, S., Hayashi, Y., and Hirokawa, N. (2001) Charcot-marie-tooth disease type 2a caused by mutation in a microtubule motor kif1bbeta. *Cell* **105**(5): 587-97.
77. Verhey, K. J., Lizotte, D. L., Abramson, T., Barenboim, L., Schnapp, B. J., and Rapoport, T. A. (1998) Light chain-dependent regulation of Kinesin's interaction with microtubules. *J Cell Biol* **143**(4): 1053-66.
78. Gho, M., McDonald, K., Ganetzky, B., and Saxton, W. M. (1992) Effects of kinesin mutations on neuronal functions. *Science* **258**(5080): 313-6.
79. Hall, D. H., and Hedgecock, E. M. (1991) Kinesin-related gene unc-104 is required for axonal transport of synaptic vesicles in C. elegans. *Cell* **65**(5): 837-47.
80. Tanaka, Y., Kanai, Y., Okada, Y., Nonaka, S., Takeda, S., Harada, A., and Hirokawa, N. (1998) Targeted disruption of mouse conventional kinesin heavy chain, kif5B, results in abnormal perinuclear clustering of mitochondria. *Cell* **93**(7): 1147-58.
81. Vallee, R. B., and Sheetz, M. P. (1996) Targeting of motor proteins. *Science* **271**(5255): 1539-44.
82. Kumar, J., Yu, H., and Sheetz, M. P. (1995) Kinectin, an essential anchor for kinesin-driven vesicle motility. *Science* **267**(5205): 1834-7.
83. Kamal, A., Stokin, G. B., Yang, Z., Xia, C. H., and Goldstein, L. S. (2001) Axonal transport of amyloid precursor protein is mediated by direct binding to the kinesin light chain subunit of kinesin-I. *Neuron* **28**(2): 449-59.
84. Takeda, S., Yamazaki, H., Seog, D. H., Kanai, Y., Terada, S., and Hirokawa, N. (2000) Kinesin superfamily protein 3 (KIF3) motor transports fodrin- associating vesicles important for neurite building. *J Cell Biol* **148**(6): 1255-65.
85. Verhey, K. J., Meyer, D., Deehan, R., Blenis, J., Schnapp, B. J., Rapoport, T. A., and Margolis, B. (2001) Cargo of kinesin identified as JIP scaffolding proteins and associated signaling molecules. *J Cell Biol* **152**(5): 959-70.
86. Epstein, E., Sela-Brown, A., Ringel, I., Kilav, R., King, S. M., Benashski, S. E., Yisraeli, J. K., Silver, J., and Naveh-Many, T. (2000) Dynein light chain binding to a 3'-untranslated sequence mediates parathyroid hormone mRNA association with microtubules. *J Clin Invest* **105**(4): 505-12.
87. Karki, S., and Holzbaur, E. L. (1999) Cytoplasmic dynein and dynactin in cell division and intracellular transport. *Curr Opin Cell Biol* **11**(1): 45-53.
88. Allan, V. J., and Schroer, T. A. (1999) Membrane motors. *Curr Opin Cell Biol* **11**(4): 476-82.
89. Asai, D. J., and Koonce, M. P. (2001) The dynein heavy chain: structure, mechanics and evolution. *Trends Cell Biol* **11**(5): 196-202.
90. Tynan, S. H., Gee, M. A., and Vallee, R. B. (2000) Distinct but overlapping sites within the cytoplasmic dynein heavy chain for dimerization and for intermediate chain and light intermediate chain binding. *J Biol Chem* **275**(42): 32769-74.
91. Vaughan, K. T., and Vallee, R. B. (1995) Cytoplasmic dynein binds dynactin through a direct interaction between the intermediate chains and p150Glued. *J Cell Biol* **131**(6 Pt 1): 1507-16.
92. Harada, A., Takei, Y., Kanai, Y., Tanaka, Y., Nonaka, S., and Hirokawa, N. (1998) Golgi vesiculation and lysosome dispersion in cells lacking cytoplasmic dynein. *J Cell Biol* **141**(1): 51-9.
93. Gill, S. R., Schroer, T. A., Szilak, I., Steuer, E. R., Sheetz, M. P., and Cleveland, D. W. (1991) Dynactin, a conserved, ubiquitously expressed component of an activator of vesicle motility mediated by cytoplasmic dynein. *J Cell Biol* **115**(6): 1639-50.
94. King, S. J., and Schroer, T. A. (2000) Dynactin increases the processivity of the cytoplasmic dynein motor. *Nat Cell Biol* **2**(1): 20-4.

95. Schafer, D. A., Gill, S. R., Cooper, J. A., Heuser, J. E., and Schroer, T. A. (1994) Ultrastructural analysis of the dynactin complex: an actin-related protein is a component of a filament that resembles F-actin. *J Cell Biol* **126**(2): 403-12.
96. Paschal, B. M., Holzbaur, E. L., Pfister, K. K., Clark, S., Meyer, D. I., and Vallee, R. B. (1993) Characterization of a 50-kDa polypeptide in cytoplasmic dynein preparations reveals a complex with p150GLUED and a novel actin. *J Biol Chem* **268**(20): 15318-23.
97. Eckley, D. M., Gill, S. R., Melkonian, K. A., Bingham, J. B., Goodson, H. V., Heuser, J. E., and Schroer, T. A. (1999) Analysis of dynactin subcomplexes reveals a novel actin-related protein associated with the arp1 minifilament pointed end. *J Cell Biol* **147**(2): 307-20.
98. Burkhardt, J. K., Echeverri, C. J., Nilsson, T., and Vallee, R. B. (1997) Overexpression of the dynamitin (p50) subunit of the dynactin complex disrupts dynein-dependent maintenance of membrane organelle distribution. *J Cell Biol* **139**(2): 469-84.
99. Echeverri, C. J., Paschal, B. M., Vaughan, K. T., and Vallee, R. B. (1996) Molecular characterization of the 50-kD subunit of dynactin reveals function for the complex in chromosome alignment and spindle organization during mitosis. *J Cell Biol* **132**(4): 617-33.
100. Swaroop, A., Swaroop, M., and Garen, A. (1987) Sequence analysis of the complete cDNA and encoded polypeptide for the Glued gene of Drosophila melanogaster. *Proc Natl Acad Sci U S A* **84**(18): 6501-5.
101. Reddy, S., Jin, P., Trimarchi, J., Caruccio, P., Phillis, R., and Murphey, R. K. (1997) Mutant molecular motors disrupt neural circuits in Drosophila. *J Neurobiol* **33**(6): 711-23.
102. Fan, S. S., and Ready, D. F. (1997) Glued participates in distinct microtubule-based activities in Drosophila eye development. *Development* **124**(8): 1497-507.
103. McGrail, M., Gepner, J., Silvanovich, A., Ludmann, S., Serr, M., and Hays, T. S. (1995) Regulation of cytoplasmic dynein function in vivo by the Drosophila Glued complex. *J Cell Biol* **131**(2): 411-25.
104. Lacey, M. L., and Haimo, L. T. (1994) Cytoplasmic dynein binds to phospholipid vesicles. *Cell Motil Cytoskeleton* **28**(3): 205-12
105. Tai, A. W., Chuang, J. Z., Bode, C., Wolfrum, U., and Sung, C. H. (1999) Rhodopsin's carboxy-terminal cytoplasmic tail acts as a membrane receptor for cytoplasmic dynein by binding to the dynein light chain Tctex-1. *Cell* **97**(7): 877-87.
106. Sawin, K. E. (2000) Microtubule dynamics: the view from the tip. *Curr Biol* **10**(23): R860-2.
107. Schroer, T. A. (2000) Motors, clutches and brakes for membrane traffic: a commemorative review in honor of Thomas Kreis. *Traffic* **1**(1): 3-10.
108. Pierre, P., Scheel, J., Rickard, J. E., and Kreis, T. E. (1992) CLIP-170 links endocytic vesicles to microtubules. *Cell* **70**(6): 887-900.
109. Vale, R. D., Schnapp, B. J., Mitchison, T., Steuer, E., Reese, T. S., and Sheetz, M. P. (1985) Different axoplasmic proteins generate movement in opposite directions along microtubules in vitro. *Cell* **43**(3 Pt 2): 623-32.
110. Rickard, J. E., and Kreis, T. E. (1990) Identification of a novel nucleotide-sensitive microtubule-binding protein in HeLa cells. *J Cell Biol* **110**(5): 1623-33.
111. Rickard, J. E., and Kreis, T. E. (1991) Binding of pp170 to microtubules is regulated by phosphorylation. *J Biol Chem* **266**(26): 17597-605.
112. Scheel, J., and Kreis, T. E. (1991) Motor protein independent binding of endocytic carrier vesicles to microtubules in vitro. *J Biol Chem* **266**(27): 18141-8.
113. Scheel, J., Pierre, P., Rickard, J. E., Diamantopoulos, G. S., Valetti, C., van der Goot, F. G., Haner, M., Aebi, U., and Kreis, T. E. (1999) Purification and analysis of authentic CLIP-170 and recombinant fragments. *J Biol Chem* **274**(36): 25883-91.
114. Bilbe, G., Delabie, J., Bruggen, J., Richener, H., Asselbergs, F. A., Cerletti, N., Sorg, C., Odink, K., Taresay, L., Wiesendanger, W., and et al. (1992) Restin: a novel intermediate filament-associated protein highly expressed in the Reed-Sternberg cells of Hodgkin's disease. *Embo J* **11**(6): 2103-13.
115. de Waegh, S. M., Lee, V. M., and Brady, S. T. (1992) Local modulation of neurofilament phosphorylation, axonal caliber, and slow axonal transport by myelinating Schwann cells. *Cell* **68**(3): 451-63.
116. Delabie, J., Shipman, R., Bruggen, J., De Strooper, B., van Leuven, F., Taresay, L., Cerletti, N., Odink, K., Diehl, V., Bilbe, G., and et al. (1992) Expression of the novel intermediate filament-associated protein restin in Hodgkin's disease and anaplastic large-cell lymphoma. *Blood* **80**(11): 2891-6.
117. Delabie, J., Bilbe, G., Bruggen, J., Van Leuven, F., and De Wolf-Peeters, C. (1993) Restin in Hodgkin's disease and anaplastic large cell lymphoma. *Leuk Lymphoma* **12**(1-2): 21-6.
118. Griparic, L., Volosky, J. M., and Keller, T. C., 3rd. (1998) Cloning and expression of chicken CLIP-170 and restin isoforms. *Gene* **206**(2): 195-208.

119. Pierre, P., Pepperkok, R., and Kreis, T. E. (1994) Molecular characterization of two functional domains of CLIP-170 in vivo. *J Cell Sci* **107**(Pt 7): 1909-20.
120. Riehemann, K., and Sorg, C. (1993) Sequence homologies between four cytoskeleton-associated proteins. *Trends Biochem Sci* **18**(3): 82-3.
121. Webb, J. R., and McMaster, W. R. (1993) Molecular cloning and expression of a Leishmania major gene encoding a single-stranded DNA-binding protein containing nine "CCHC" zinc finger motifs. *J Biol Chem* **268**(19): 13994-4002.
122. Curtis, D., Treiber, D. K., Tao, F., Zamore, P. D., Williamson, J. R., and Lehmann, R. (1997) A CCHC metal-binding domain in Nanos is essential for translational regulation. *Embo J* **16**(4): 834-43.
123. Berg, J. M., and Shi, Y. (1996) The galvanization of biology: a growing appreciation for the roles of zinc. *Science* **271**(5252): 1081-5.
124. Bavoso, A., Ostuni, A., Battistuzzi, G., Menabue, L., Saladini, M., and Sola, M. (1998) Metal ion binding to a zinc finger peptide containing the Cys-X2-Cys-X4- His-X4-Cys domain of a nucleic acid binding protein encoded by the Drosophila Fw-element. *Biochem Biophys Res Commun* **242**(2): 385-9.
125. Dujardin, D., Wacker, U. I., Moreau, A., Schroer, T. A., Rickard, J. E., and De Mey, J. R. (1998) Evidence for a role of CLIP-170 in the establishment of metaphase chromosome alignment. *J Cell Biol* **141**(4): 849-62.
126. Rickard, J. E., and Kreis, T. E. (1996) CLIPs for organelle-microtubule interactions. *Trends Cell Biol* **6**: 178-182
127. Infante, C., Ramos-Morales, F., Fedriani, C., Bornens, M., and Rios, R. M. (1999) GMAP-210, A cis-Golgi network-associated protein, is a minus end microtubule-binding protein. *J Cell Biol* **145**(1): 83-98.
128. Thiemann, M., Schrader, M., Volkl, A., Baumgart, E., and Fahimi, H. D. (2000) Interaction of peroxisomes with microtubules. In vitro studies using a novel peroxisome-microtubule binding assay. *Eur J Biochem* **267**(20): 6264-75.
129. Lantz, V. A., and Miller, K. G. (1998) A class VI unconventional myosin is associated with a homologue of a microtubule-binding protein, cytoplasmic linker protein-170, in neurons and at the posterior pole of Drosophila embryos. *J Cell Biol* **140**(4): 897-910.
130. Berlin, V., Styles, C. A., and Fink, G. R. (1990) BIK1, a protein required for microtubule function during mating and mitosis in Saccharomyces cerevisiae, colocalizes with tubulin. *J Cell Biol* **111**(6 Pt 1): 2573-86.
131. Brunner, D., and Nurse, P. (2000) CLIP170-like tip1p spatially organizes microtubular dynamics in fission yeast. *Cell* **102**(5): 695-704.
132. Jannatipour, M., and Rokeach, L. A. (1998) A Schizosaccharomyces pombe gene encoding a novel polypeptide with a predicted alpha-helical rod structure found in the myosin and intermediate-filament families of proteins. *Biochim Biophys Acta* **1399**(1): 67-72.
133. De Zeeuw, C. I., Hoogenraad, C. C., Goedknegt, E., Hertzberg, E., Neubauer, A., Grosveld, F., and Galjart, N. (1997) CLIP-115, a novel brain-specific cytoplasmic linker protein, mediates the localization of dendritic lamellar bodies. *Neuron* **19**(6): 1187-99.
134. Consortium, T. C. e. S. (1998) Genome sequence of the nematode C. elegans: a platform for investigating biology. The C. elegans Sequencing Consortium. *Science* **282**(5396): 2012-8.
135. Hoogenraad, C. C., Akhmanova, A., Grosveld, F., De Zeeuw, C. I., and Galjart, N. (2000) Functional analysis of CLIP-115 and its binding to microtubules. *J Cell Sci* **113**(Pt 12): 2285-97.
136. Yamashita, A., Watanabe, Y., and Yamamoto, M. (1997) Microtubule-associated coiled-coil protein Ssm4 is involved in the meiotic development in fission yeast. *Genes Cells* **2**(2): 155-66.
137. Kahana, J. A., Schlenstedt, G., Evanchuk, D. M., Geiser, J. R., Hoyt, M. A., and Silver, P. A. (1998) The yeast dynactin complex is involved in partitioning the mitotic spindle between mother and daughter cells during anaphase B. *Mol Biol Cell* **9**(7): 1741-56.
138. Radcliffe, P. A., Hirata, D., Vardy, L., and Toda, T. (1999) Functional dissection and hierarchy of tubulin-folding cofactor homologues in fission yeast. *Mol Biol Cell* **10**(9): 2987-3001.
139. Tian, G., Huang, Y., Rommelaere, H., Vandekerckhove, J., Ampe, C., and Cowan, N. J. (1996) Pathway leading to correctly folded beta-tubulin. *Cell* **86**(2): 287-96.
140. Tian, G., Lewis, S. A., Feierbach, B., Stearns, T., Rommelaere, H., Ampe, C., and Cowan, N. J. (1997) Tubulin subunits exist in an activated conformational state generated and maintained by protein cofactors. *J Cell Biol* **138**(4): 821-32.
141. Feierbach, B., Nogales, E., Downing, K. H., and Stearns, T. (1999) Alf1p, a CLIP-170 domain-containing protein, is functionally and physically associated with alpha-tubulin. *J Cell Biol* **144**(1): 113-24.

142. Adams, M. D., Celniker, S. E., Holt, R. A., Evans, C. A., Gocayne, J. D., Amanatides, P. G., Scherer, S. E., Li, P. W., and et al. (2000) The genome sequence of Drosophila melanogaster. *Science* **287**(5461): 2185-95.
143. Li, H. P., Liu, Z. M., and Nirenberg, M. (1997) Kinesin-73 in the nervous system of Drosophila embryos. *Proc Natl Acad Sci U S A* **94**(4): 1086-91.
144. Hanada, T., Lin, L., Tibaldi, E. V., Reinherz, E. L., and Chishti, A. H. (2000) GAKIN, a novel kinesin-like protein associates with the human homologue of the Drosophila discs large tumor suppressor in T lymphocytes. *J Biol Chem* **275**(37): 28774-84.
145. Budnik, V., Koh, Y. H., Guan, B., Hartmann, B., Hough, C., Woods, D., and Gorczyca, M. (1996) Regulation of synapse structure and function by the Drosophila tumor suppressor gene dlg. *Neuron* **17**(4): 627-40.
146. Guan, B., Hartmann, B., Kho, Y. H., Gorczyca, M., and Budnik, V. (1996) The Drosophila tumor suppressor gene, dlg, is involved in structural plasticity at a glutamatergic synapse. *Curr Biol* **6**(6): 695-706.
147. Jamain, S., Quach, H., Fellous, M., and Bourgeron, T. (2001) Identification of the Human KIF13A Gene Homologous to Drosophila kinesin-73 and Candidate for Schizophrenia. *Genomics* **74**(1): 36-44.
148. Venter, J. C., Adams, M. D., Myers, E. W., Li, P. W., Mural, R. J., Sutton, G. G., Smith, H. O., Yandell, M., and et al. (2001) The sequence of the human genome. *Science* **291**(5507): 1304-51.
149. Bignell, G. R., Warren, W., Seal, S., Takahashi, M., Rapley, E., Barfoot, R., Green, H., Brown, C., Biggs, P. J., Lakhani, S. R., Jones, C., Hansen, J., Blair, E., Hofmann, B., Siebert, R., Turner, G., Evans, D. G., Schrander-Stumpel, C., Beemer, F. A., van Den Ouweland, A., Halley, D., Delpech, B., Cleveland, M. G., Leigh, I., Leisti, J., and Rasmussen, S. (2000) Identification of the familial cylindromatosis tumour-suppressor gene. *Nat Genet* **25**(2): 160-5.
150. Perez, F., Diamantopoulos, G. S., Stalder, R., and Kreis, T. E. (1999) CLIP-170 highlights growing microtubule ends in vivo. *Cell* **96**(4): 517-27.
151. Sammak, P. J., and Borisy, G. G. (1988) Direct observation of microtubule dynamics in living cells. *Nature* **332**(6166): 724-6.
152. Diamantopoulos, G. S., Perez, F., Goodson, H. V., Batelier, G., Melki, R., Kreis, T. E., and Rickard, J. E. (1999) Dynamic localization of CLIP-170 to microtubule plus ends is coupled to microtubule assembly. *J Cell Biol* **144**(1): 99-112.
153. Goode, B. L., Drubin, D. G., and Barnes, G. (2000) Functional cooperation between the microtubule and actin cytoskeletons. *Curr Opin Cell Biol* **12**(1): 63-71.
154. Mata, J., and Nurse, P. (1997) tea1 and the microtubular cytoskeleton are important for generating global spatial order within the fission yeast cell. *Cell* **89**(6): 939-49.
155. Vega, L. R., and Solomon, F. (1997) Microtubule function in morphological differentiation: growth cones and growth cones. *Cell* **89**(6): 825-8.
156. Akhmanova, A., Hoogenraad, C. C., Drabek, K., Stepanova, T., Dortland, B., Verkerk, T., Vermeulen, W., Burgering, B. M., De Zeeuw, C. I., Grosveld, F., and Galjart, N. (2001) Clasps are CLIP-115 and -170 associating proteins involved in the regional regulation of microtubule dynamics in motile fibroblasts. *Cell* **104**(6): 923-35.
157. Waterman-Storer, C. M., Gregory, J., Parsons, S. F., and Salmon, E. D. (1995) Membrane/microtubule tip attachment complexes (TACs) allow the assembly dynamics of plus ends to push and pull membranes into tubulovesicular networks in interphase Xenopus egg extracts. *J Cell Biol* **130**(5): 1161-9.
158. Mermall, V., Post, P. L., and Mooseker, M. S. (1998) Unconventional myosins in cell movement, membrane traffic, and signal transduction. *Science* **279**(5350): 527-33.
159. Wu, X., Jung, G., and Hammer, J. A., 3rd. (2000) Functions of unconventional myosins. *Curr Opin Cell Biol* **12**(1): 42-51.
160. Vaughan, K. T., Tynan, S. H., Faulkner, N. E., Echeverri, C. J., and Vallee, R. B. (1999) Colocalization of cytoplasmic dynein with dynactin and CLIP-170 at microtubule distal ends. *J Cell Sci* **112**(Pt 10): 1437-47.
161. Habermann, A., Schroer, T. A., Griffiths, G., and Burkhardt, J. K. (2001) Immunolocalization of cytoplasmic dynein and dynactin subunits in cultured macrophages: enrichment on early endocytic organelles. *J Cell Sci* **114**(Pt 1): 229-240.
162. Valetti, C., Wetzel, D. M., Schrader, M., Hasbani, M. J., Gill, S. R., Kreis, T. E., and Schroer, T. A. (1999) Role of dynactin in endocytic traffic: effects of dynamitin overexpression and colocalization with CLIP-170. *Mol Biol Cell* **10**(12): 4107-20.
163. Morris, N. R. (2000) Nuclear migration. From fungi to the mammalian brain. *J Cell Biol* **148**(6): 1097-101.

164. Munemitsu, S., Souza, B., Muller, O., Albert, I., Rubinfeld, B., and Polakis, P. (1994) The APC gene product associates with microtubules in vivo and promotes their assembly in vitro. *Cancer Res* **54**(14): 3676-81.
165. Nathke, I. S., Adams, C. L., Polakis, P., Sellin, J. H., and Nelson, W. J. (1996) The adenomatous polyposis coli tumor suppressor protein localizes to plasma membrane sites involved in active cell migration. *J Cell Biol* **134**(1): 165-79.
166. Askham, J. M., Moncur, P., Markham, A. F., and Morrison, E. E. (2000) Regulation and function of the interaction between the APC tumour suppressor protein and EB1. *Oncogene* **19**(15): 1950-8.
167. Mimori-Kiyosue, Y., Shiina, N., and Tsukita, S. (2000) The dynamic behavior of the APC-binding protein EB1 on the distal ends of microtubules. *Curr Biol* **10**(14): 865-8.
168. Mimori-Kiyosue, Y., Shiina, N., and Tsukita, S. (2000) Adenomatous polyposis coli (APC) protein moves along microtubules and concentrates at their growing ends in epithelial cells. *J Cell Biol* **148**(3): 505-18.
169. Kinzler, K. W., and Vogelstein, B. (1996) Lessons from hereditary colorectal cancer. *Cell* **87**(2): 159-70.
170. Polakis, P. (1999) The oncogenic activation of beta-catenin. *Curr Opin Genet Dev* **9**(1): 15-21.
171. Seeling, J. M., Miller, J. R., Gil, R., Moon, R. T., White, R., and Virshup, D. M. (1999) Regulation of beta-catenin signaling by the B56 subunit of protein phosphatase 2A. *Science* **283**(5410): 2089-91.
172. Matsumine, A., Ogai, A., Senda, T., Okumura, N., Satoh, K., Baeg, G. H., Kawahara, T., Kobayashi, S., Okada, M., Toyoshima, K., and Akiyama, T. (1996) Binding of APC to the human homolog of the Drosophila discs large tumor suppressor protein. *Science* **272**(5264): 1020-3.
173. Cadigan, K. M., and Nusse, R. (1997) Wnt signaling: a common theme in animal development. *Genes Dev* **11**(24): 3286-305.
174. Gumbiner, B. M. (1998) Propagation and localization of Wnt signaling. *Curr Opin Genet Dev* **8**(4): 430-5.
175. Zumbrunn, J., Kinoshita, K., Hyman, A. A., and Nathke, I. S. (2001) Binding of the adenomatous polyposis coli protein to microtubules increases microtubule stability and is regulated by GSK3 beta phosphorylation. *Curr Biol* **11**(1): 44-9.
176. Deka, J., Kuhlmann, J., and Muller, O. (1998) A domain within the tumor suppressor protein APC shows very similar biochemical properties as the microtubule-associated protein tau. *Eur J Biochem* **253**(3): 591-7.
177. Su, L. K., Burrell, M., Hill, D. E., Gyuris, J., Brent, R., Wiltshire, R., Trent, J., Vogelstein, B., and Kinzler, K. W. (1995) APC binds to the novel protein EB1. *Cancer Res* **55**(14): 2972-7.
178. Schwartz, K., Richards, K., and Botstein, D. (1997) BIM1 encodes a microtubule-binding protein in yeast. *Mol Biol Cell* **8**(12): 2677-91.
179. Beinhauer, J. D., Hagan, I. M., Hegemann, J. H., and Fleig, U. (1997) Mal3, the fission yeast homologue of the human APC-interacting protein EB-1 is required for microtubule integrity and the maintenance of cell form. *J Cell Biol* **139**(3): 717-28.
180. Su, L., and Qi, Y. (2001) Characterization of human mapre genes and their proteins. *Genomics* **71**(2): 142-9.
181. Tirnauer, J. S., O'Toole, E., Berrueta, L., Bierer, B. E., and Pellman, D. (1999) Yeast Bim1p promotes the G1-specific dynamics of microtubules. *J Cell Biol* **145**(5): 993-1007.
182. Bloom, K. (2000) It's a kar9ochore to capture microtubules. *Nat Cell Biol* **2**(6): E96-8.
183. Korinek, W. S., Copeland, M. J., Chaudhuri, A., and Chant, J. (2000) Molecular linkage underlying microtubule orientation toward cortical sites in yeast. *Science* **287**(5461): 2257-9.
184. Lee, L., Tirnauer, J. S., Li, J., Schuyler, S. C., Liu, J. Y., and Pellman, D. (2000) Positioning of the mitotic spindle by a cortical-microtubule capture mechanism. *Science* **287**(5461): 2260-2.
185. Bienz, M. (2001) Spindles cotton on to junctions, APC and EB1. *Nat Cell Biol* **3**(3): E67-8.
186. Berrueta, L., Tirnauer, J. S., Schuyler, S. C., Pellman, D., and Bierer, B. E. (1999) The APC-associated protein EB1 associates with components of the dynactin complex and cytoplasmic dynein intermediate chain. *Curr Biol* **9**(8): 425-8.

Chapter 3

CLIP-115, A NOVEL BRAIN-SPECIFIC CYTOPLASMIC LINKER PROTEIN, MEDIATES THE LOCALIZATION OF DENDRITIC LAMELLAR BODIES

Chris I. De Zeeuw[2*], Casper C. Hoogenraad[1,2*], Erika Goedknegt[2], Elliot Hertzberg[3], Andrea Neubauer[1], Frank Grosveld[1], Niels Galjart[1]

MGC Departments of [1]Cell Biology and Genetics, [2]Anatomy, Erasmus Univerisity, P.O. Box 1738, 3000 DR Rotterdam, The Netherlands. [3]Department of Neuroscience, Albert Einstein College of Medicine, New York. *These authors contributed equally to the results described in this paper.

CLIP-115, a Novel Brain-Specific Cytoplasmic Linker Protein, Mediates the Localization of Dendritic Lamellar Bodies

Chris I. De Zeeuw,*§‖ Casper C. Hoogenraad,†§ Erika Goedknegt,* Elliot Hertzberg,‡ Andrea Neubauer,† Frank Grosveld,† and Niels Galjart†‖
*Department of Anatomy
†Department of Cell Biology
Erasmus University Rotterdam
P. O. Box 1738
3000 DR Rotterdam
The Netherlands
‡Department of Neuroscience
Albert Einstein College of Medicine
New York, New York 10461

Summary

Intracellular localization of organelles may depend in part on specific cytoplasmic linker proteins (CLIPs) that link membranous organelles to microtubules. Here, we characterize rat cDNAs encoding a novel, brain-specific CLIP of 115 kDa. This protein contains two N-terminal microtubule-binding domains and a long coiled-coil region; it binds to microtubules and is homologous to CLIP-170, a protein mediating the binding of endosomes to microtubules. CLIP-115 is enriched in the dendritic lamellar body (DLB), a recently discovered organelle predominantly present in bulbous dendritic appendages of neurons linked by dendrodendritic gap junctions. Local microtubule depolymerization leads to a temporary reduction of DLBs. These results suggest that CLIP-115 operates in the control of brain-specific organelle translocations.

Introduction

Microtubules are components of the cytoskeleton of eukaryotic cells that play an important role, for example, in the establishment of cell polarity (Wade and Hyman, 1997). Neurons are the most obvious example of a polarized cell type, with a myriad of dendrites that receive signals from the environment and their axon that can extend long distances. This polarized cell structure, which is not static but continuously subjected to plastic changes, requires neuronal microtubules to form an intraneuronal framework under precise temporal and spatial control. The adjustment of the microtubule cytoskeleton is partly mediated by microtubule-associated proteins (MAPs), which have been shown to determine the rate of growth of the microtubules by stabilizing their polymerization (Maccioni and Cambiazo, 1995). In neurons, MAP2 and tau are the dendrite- and axon-enriched prototypes of MAP, respectively (Craig and Banker, 1994). This differential distribution is in line with the different orientation patterns of the microtubules in dendrites and axons; axons have their microtubules organized with their plus ends pointed away from the cell body, while dendrites have microtubules oriented in both directions (Sharp et al., 1995; Schnapp, 1997).

Several lines of evidence indicate that microtubules also provide tracks for efficient organelle translocations and that they are essential for the general organization of membrane structures in a cell. For example, the endoplasmic reticulum forms a reticular network that colocalizes with microtubules, and the Golgi apparatus clusters around the region of the microtubule-organizing center (Cole and Lippincott-Schwartz, 1995). In addition, it has been demonstrated that depolymerization of microtubules, induced by application of nocodazole, can affect not only the movements and localization of membranous organelles but also their formation (Matteoni and Kreis, 1987; Cole et al., 1996).

The transport of organelles along microtubules is mediated by microtubule-based motor proteins, which serve as the engines of the translocation (Hirokawa, 1996; Vallee and Sheetz, 1996). Motor proteins are categorized according to the direction of the membrane movement that they carry out with respect to the plus and minus ends of microtubules. In general, plus end–directed transport is catalyzed by kinesins, while minus end–directed transport is catalyzed by cytoplasmic dynein (Hirokawa, 1996; Ogawa and Mohri, 1996). Recent characterization of ten kinesin superfamily proteins (KIFs) suggests that each member can, apart from some redundancy, convey a specific organelle or cargo. For example, KIFC2 has been reported to be a neuron-specific kinesin superfamily motor for dendritic transport of multivesicular body–like organelles (Saito et al., 1997; cf. Hanlon et al., 1997).

In the process of membrane trafficking, the motor proteins presumably interact with accessory factors that are required to guide each individual organelle to the appropriate motor protein. For example, kinectin has been identified as a putative kinesin receptor on membranes (Toyoshima et al., 1992; Burkhardt, 1996), and the dynactin complex is essential for the activity of dynein (Allan, 1996). One of the proteins of the dynactin complex is $p150^{glued}$ (Swaroop et al., 1987); it is supposed to link cytoplasmic dynein to its membranous cargo through interactions with a number of other components. This protein is a member of a novel family of microtubule-binding proteins, which is characterized by an N-terminal globular region with a novel type of microtubule-binding domain (MTB domain) and by a large coiled-coil region for protein–protein interactions (Vaughan and Vallee, 1995). Another member of this family is CLIP-170 (Pierre et al., 1992). This protein with an apparent M_r of 170 kDa has two MTB domains similar to the one of $p150^{glued}$, in addition to a long coiled-coil region. It was referred to as a cytoplasmic linker protein (CLIP) because it was shown to link endocytotic carrier vesicles to microtubules. On the basis of these findings, it was proposed that other CLIPs exist that could mediate the interaction of specific cytoplasmic organelles with microtubules (Rickard and Kreis, 1996).

Recently, a new membranous organelle, the dendritic

§These authors contributed equally to this work.
‖To whom correspondence should be addressed.

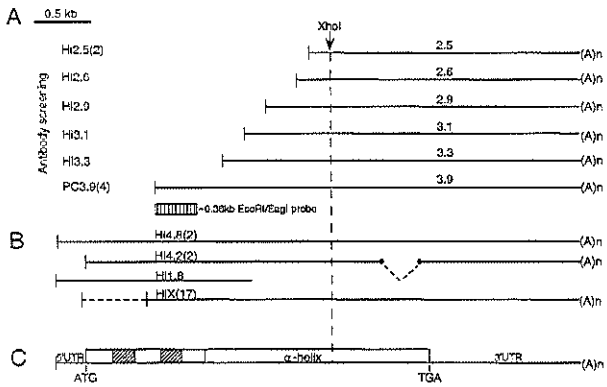

Figure 1. Cloning Strategy of *CLIP-115* cDNAs

(A) Ten cDNA clones isolated with antiserum α12B/18 from expression libraries of the hippocampus (Hi2.5, Hi2.6, Hi2.9, Hi3.1, Hi3.3) and piriform cortex (PC3.9). Clone Hi2.5 and clone PC3.9 were independently isolated two and four times, respectively.

(B) Twenty-two cDNA clones isolated from the hippocampus library with the use of a 0.36 kb EcoRI/EagI probe (striped box) from PC3.9; two nonidentical clones (Hi4.8) have an open reading frame that is preceded by an in-frame stop codon, while two other nonidentical clones (Hi4.2) miss 378 bp, presumably due to alternative splicing (stippled line).

(C) Structure of the composite 4.8 kb mRNA, including its 5′ and 3′ UTRs and the encoded novel protein product. The striped boxes within the open reading frame indicate the position of two repeated motifs within the protein.

lamellar body (DLB), was discovered (De Zeeuw et al., 1995). It occurs exclusively in bulbous dendritic appendages of neurons in particular brain regions such as the inferior olive, hippocampus, piriform cortex, and olfactory bulb. The function of DLBs remains to be elucidated, but several observations suggest it is related to that of dendrodendritic gap junctions, which are membrane specializations mediating electrotonic coupling between neurons. For example, during development, DLBs and dendrodendritic gap junctions arise simultaneously, while during adulthood, DLBs are present in all brain areas where gap junctions between dendrites of neurons are prominent. Moreover, the densities of both DLBs and dendrodendritic gap junctions in the inferior olive can be down-regulated concomitantly by removal of the cerebellar GABAergic afferents to electrotonically coupled olivary dendrites (De Zeeuw et al., 1997). In addition, the density of DLBs in olivary subnuclei can be correlated to the level of synchronous firing of these neurons. DLBs were discovered because they can be specifically labeled by batch #18 of antiserum α12B (α12B/18), which is an antiserum originally raised against a peptide (α12B) of the extracellular loop of gap junction protein connexin 43 (cx43) (De Zeeuw et al., 1995). Although this initially suggested the presence of cx43 in DLBs, we noted that DLB labeling is only observed with α12B/18, not with earlier batches of the antiserum or with other antibodies against cx43. Also, antiserum α12B/18, preabsorbed with matrix-linked peptide α12B, provides the same DLB immunoreactivity as nonpreabsorbed antiserum, and the affinity-purified antibody of α12B/18, eluted from the peptide α12B column, does not give DLB labeling. Therefore, we concluded that an antibody population is present in antiserum α12B/18 that is not directed against cx43 but against an unknown antigen component of DLBs (De Zeeuw et al., 1995).

In the present study, we used antiserum α12B/18 to isolate cDNAs encoding the DLB-specific antigen by expression screening of cDNA libraries of the brain areas with a high density of DLBs. All cDNAs are derived from the same mRNA and encode a novel, brain-specific protein, which is named CLIP-115 because of its strong similarity with CLIP-170 and its M_r of 115 kDa. Like its larger relative, CLIP-115 contains two MTB domains and a long coiled-coil region. Newly raised antibodies against CLIP-115 immunoreact with microtubules and DLBs. Depolymerization of the microtubules of neurons in the inferior olive by local application of nocodazole dramatically reduces the density of DLBs. We conclude that CLIP-115 is a protein constituent of DLBs, and we hypothesize that it determines the stucture and precise cytoplasmic location of DLBs. CLIP-115 and CLIP-170 may define a novel subfamily of proteins designed for the interaction of specific membranous organelles with microtubules.

Results

Expression Cloning of a Novel, Brain-Specific Cytoplasmic Linker Protein, CLIP-115

To isolate the α12B/18 antigen expressed in DLBs, λZAP expression libraries were made of areas with high densities of DLBs. A first screen of amplified hippocampus and piriform cortex cDNA libraries with antiserum α12B/18 resulted in the isolation of 68 positives. Secondary screening led to the positive identification of 10 clones, some of which are duplicates (Figure 1A). All clones were subsequently shown to have overlapping restriction enzyme maps and cross hybridizing inserts (data not shown). Six clones were characterized in detail, five from the hippocampus library with insert sizes of 2.5–3.3 kb (Hi2.5–3.3) and one clone from the piriform cortex library with an insert of 3.9 kb (PC3.9). Sequence analysis demonstrated that all clones come from the same transcript, suggesting that the antigenic determinant present in these clones reacts specifically with α12B/18. Since the 5′ end of the novel mRNA is not present in any of the clones, another screen of the hippocampus library was performed using a 0.36 kb DNA fragment as a probe; the fragment was subcloned from the 5′ end of PC3.9 (see Figure 1A). In this hybridization, 40 independent clones were isolated; 18 were later shown to encode rat CLIP-170, while 22 were 5′ end extensions of the clones isolated with α12B/18. Two of the latter have inserts of 4.8 kb (clones Hi4.8, Figure

1B). Hi1.8 starts more upstream than the two Hi4.8 fragments; the extra 50 bp sequence in the 5′ end of clone Hi1.8 is included in Figure 2. Two clones (Hi4.2) lack an internal fragment of 378 bp, presumably because of alternative splicing of primary transcripts. The structure and sequence of the composite 4.85 kb mRNA and the predicted secondary structure of the largest open reading frame (ORF) within the transcript are shown in Figures 1C and 2. The cDNA consists of a 5′ untranslated region (5′ UTR) of 288 nt, with a stop codon 42 bp upstream of and in-frame with the ATG that forms the translation start of a large ORF of 3141 bp. Deletion of the internal fragment of 378 bp from this ORF results in the removal of 126 amino acids from the predicted C-terminal end of the protein product, but the reading frame is maintained. A 3′ UTR of 1.3 kb follows the ORF. It contains two polyadenylation sites upstream of a poly(A)$^+$ tract (Figure 2). Translation of the ORF results in a protein of 1046 amino acids with a predicted molecular mass of 115 kDa. Its secondary structure suggests the presence of a globular N-terminal domain, which contains a doubly repeated motif of 69 amino acids and has runs of serine residues. Numerous sites for posttranslational modifications, such as casein kinase II–dependent phosphorylation, are scattered throughout the N-terminal domain. The N-terminal region also contains a small hydrophobic segment, which is located at amino acids 306–333 and which might form a transmembrane domain (Hofmann and Stoffel, 1993). It is followed by a large α-helical region of 699 amino acids, which contains stretches of heptad repeats. This domain is predicted to form a coiled-coil structure (Lupas, 1996).

Comparison of the amino acid sequence presented in Figure 2 to DNA/protein databases revealed we have cloned a novel cDNA encoding a protein with a striking homology to CLIP-170 (Pierre et al., 1992). CLIP-170 is identical to a protein called restin except for a 35 amino acid insert (Bilbe et al., 1992). Our novel protein, which we named CLIP-115, also contains the extra sequence present in restin. The overall identity and similarity between CLIP-115 and CLIP-170/restin are 45% and 67%, respectively (Figure 3A). When only the N-terminal regions are compared, these numbers rise to 58% and 77%. Immediately downstream of the repeats, CLIP-115 and CLIP-170/restin remain quite similar, but as the long coiled-coil regions are reached, similarity drops considerably. Moreover, the rod domain of CLIP-115 is much shorter than that of CLIP-170/restin, and the putative metal binding structure at the C terminus of CLIP-170/restin is not present in CLIP-115.

The doubly repeated motif in the N-terminal domain of CLIP-115, described above, corresponds to the MTB domains in CLIP-170/restin (Pierre et al., 1992, 1994). These domains, which differ from the MTB domains in MAPs (Lewis et al., 1988), can also be found in various other proteins from different organisms; these include DP-150 (Holzbaur et al., 1991), p150^{glued} (Swaroop et al., 1987), BIK1 (Trueheart et al., 1987), CKAP1 (Watanabe et al., 1996), Ssm4 (Yamashita et al., 1997), and kinesin-73 (Li et al., 1997). Rat DP-150 and its Drosophila melanogaster homolog p150^{glued} are part of the dynactin complex and are involved in dynein-dependent vesicle movements along microtubules (Gill et al., 1991). Kinesin-73 is a motor protein in Drosophila with an MTB domain located in the C-terminal region of the protein (Li et al., 1997). BIK1, a 60 kDa protein from Saccharomyces cerevisiae, is required for microtubule-related functions during mitosis (Berlin et al., 1990), while Ssm4 is a protein that modifies the structure and/or function of nuclear microtubules in order to promote meiotic nuclear division (Yamashita et al., 1997). In addition, approximately 60 mammalian expressed sequence tags (ESTs) with this novel domain can be found in the databases. Thus, the type of motif present twice in the N-terminal domain of CLIP-115 and CLIP-170 occurs as a single domain in numerous proteins involved in a variety of intracellular processes and is highly conserved throughout evolution. It is noteworthy, however, that the number of proteins with such a presumptive MTB domain has expanded particularly in mammals.

Alignment of the motifs in the N-terminal domain of CLIP-115 to those of CLIP-170/restin and other proteins with homologous domains (Figure 3B) allows us to extend the size of the consensus MTB domain in comparison to previous reports (e.g., Pierre et al., 1992; Watanabe et al., 1996). This extension appears valid because glycine and valine, which are characteristic amino acid residues in the consensus motif, are also present at the boundaries of the extended domain. The alignment emphasizes two other points. First, it shows that the CLIP-115 repeats best resemble those of CLIP-170/restin. The identity between the first MTB domain of CLIP-115 and CLIP-170/restin is 78% (similarity 93%), while for the second MTB domain, this number equals 86% (similarity 97%). These data strongly suggest that CLIP-115 indeed also binds to microtubules. Second, CLIP-115 and CLIP-170/restin are so far the only proteins with two MTB domains instead of one. This observation emphasizes the high degree of similarity between these proteins and suggests a specific function might be assigned to CLIP-115 and CLIP-170.

Northern blot analysis of rat and mouse tissues, using rat *CLIP-115* cDNA fragments as probes, revealed the presence in both organisms of transcripts of ~5 kb (Figure 4). Thus, the rat *CLIP-115* cDNA sequence, depicted in Figure 2, is probably full-length, and rat and mouse mRNAs must be highly homologous. In the adult rat, mRNA is detected not only in areas like the hippocampus, inferior olive, and piriform cortex, where DLBs are prominent, but also in the cerebellum, where DLBs have not been shown to occur (Figure 4A) (De Zeeuw et al., 1995). In the adult mouse, *CLIP-115* mRNA is detected in the brain but not in testis, thymus, liver, spleen, and heart. *CLIP-115* is present at very low doses in kidney, and a weakly hybridizing band of ~6–7 kb is also detected in lung; *CLIP-115* thus appears to be quite specific for neurons and/or glia cells. No difference in expression level is seen between male and female adult brain. During development, expression of *CLIP-115* oscillates (Figure 4B). Message is undetectable in embryonic stem cells, but at E10.5, the first embryonic time point tested, transcript is readily detected. As development proceeds, message levels appear to decline until birth, after which *CLIP-115* mRNA suddenly increases. Subsequently, the message gradually decreases until postnatal day 10, the day when DLBs start to occur (De

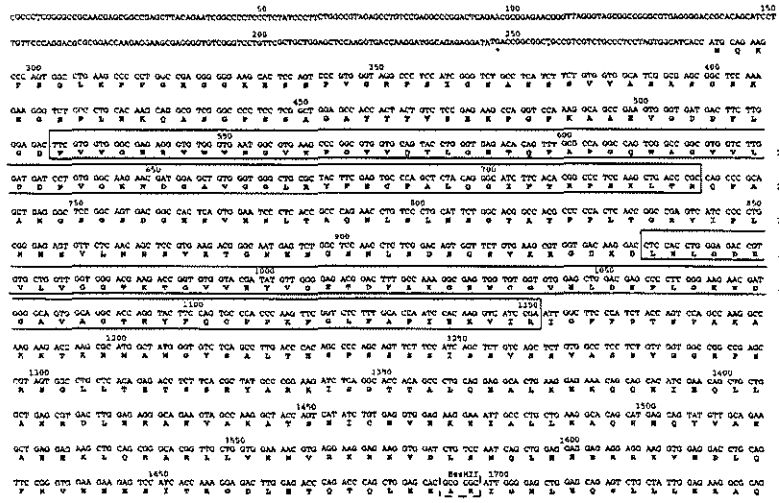

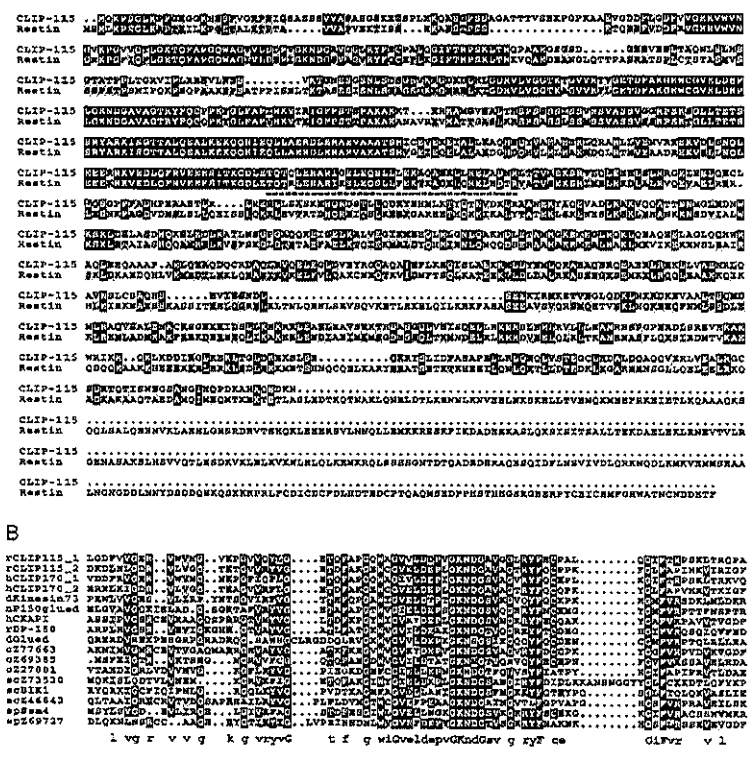

Figure 3. CLIP-115 and Its Similarity to Other Proteins

(A) Alignment of rat CLIP-115 with restin, which is identical to human CLIP-170 except for an additional 35 amino acids (dashed line). Note the very high degree of similarity in the N-terminal regions of CLIP-115 and CLIP-170/restin.

(B) Alignment of the MTB domains of CLIP-115 with those of other fully sequenced proteins, i.e., h(uman) CLIP-170, r(at) 150k DAP, d(rosophila) Glued, n(eurospora) p150 Glued, h CKAPI, S(accharomyces) c(erevisiae) BIK1, S(accharomyces) p(ombe) Ssm4, and the yeast (sc/sp) and C. elegans (c) hypothetical proteins with accession numbers Z73530, Z46843, Z69727, Z77663, Z69385, and Z27081. Sequences were taken from the SwissProt database and aligned using ClustalW and GCG software packages. Black boxes indicate that more than 50% of the aligned sequence contains a particular amino acid, while conserved amino acid substitutions are represented by a gray outline. The consensus sequence for the MTB domain is given below the alignment: capital letters indicate complete conservation, while small letters indicate a preference for a particular residue.

Zeeuw et al., 1995). At that point, the message increases again and reaches the levels present in adult brain. Thus, the variation in *CLIP-115* mRNA levels seems to reflect a differential need for the protein during mouse development.

In conclusion, using antiserum α12B/18, we have cloned cDNAs, which encode a protein with homology to CLIP-170/restin. The similarity is most prominent in two MTB domains, suggesting that the novel protein CLIP-115 can bind to microtubules. The fact that all cDNAs from the two expression libraries are derived from a single, brain-specific message strongly suggests that we cloned the DLB-specific antigen detected by α12B/18. However, *CLIP-115* mRNA is present in the

Figure 2. Nucleotide and Deduced Amino Acid Sequence of *CLIP-115* cDNAs

Sequence of the composite cDNA depicted in Figure 1C. Nucleotide numbering is shown above the sequence, while amino acid numbering is indicated in the right margin. The plain boxed sequences indicate the MTB domains; the BssHII site is indicated to show how the CLIP-115$_{1-468}$ sequence for the GFP experiments in Figure 5 was generated; dashed lines underscore the 16 or 17 amino acid peptides (dlb-2 and dlb-1, respectively) that were used for raising antibodies. Asterisks denote stop codons; brackets indicate the region of presumed alternative splicing; the dashed boxes indicate polyadenylation sites.

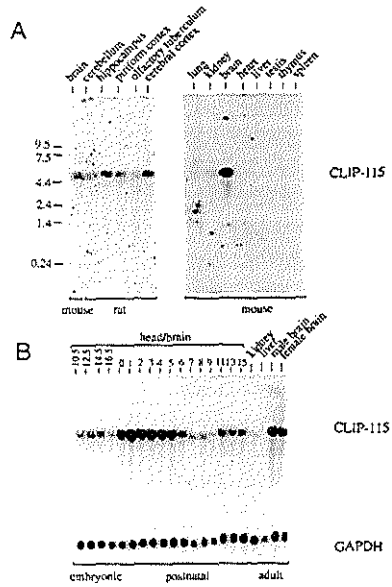

Figure 4. Expression of *CLIP-115* mRNA

(A) Northern blots, containing ~15 μg of total RNA from different tissues, were screened with *CLIP-115*-specific DNA probes.

(B) Comparable amounts of total mouse RNA, isolated from embryonic or postnatal heads/brains at the indicated time points during development, were screened for *CLIP-115* message as in (A). To control for RNA quantity, the developmental blot was reprobed with a cDNA encoding the glycolytic enzyme GAPDH. The variation in *CLIP-115* mRNA level was normalized to that of GAPDH with phosphorimage analysis.

cerebellum, while DLBs are not, and *CLIP-115* mRNA occurs during development before the final formation of DLBs. Thus, we set out experiments to determine whether CLIP-115 can indeed bind to microtubules and to find out whether it is a protein constituent of DLBs.

Localization of CLIP-115 In Vitro

To characterize CLIP-115 at the protein level, different antibodies were raised against peptides derived from the unique coiled-coil domain of the protein (antisera #2131 and #2133; see Figure 2) or against the MTB domain (α-MTCLIP115). The specificity of the new antisera against CLIP-115 was tested on Western blot and in fluorescence experiments. COS1 cells were transfected with normal, full-length CLIP-115, with a protein lacking the alternatively spliced sequence (δCLIP-115), or with CLIP-115 linked to green fluorescent protein (GFP-CLIP-115). As a control, mock transfected cells were included. Two days after transfection, cells were harvested and total protein extracts were made. Proteins were run alone or next to total protein homogenates from mouse kidney, liver, and brain, Western blotted, and incubated with antibodies against GFP and MTCLIP115 (Figure 5A) or affinity-purified #2133 antibodies (Figure 5B). The experiments demonstrate that CLIP-115, δCLIP-115, and GFP-CLIP-115 are produced in the COS1 cells as proteins of the expected size. Each protein is subjected to partial proteolytic degradation; this is particularly evident with the α-GFP antibody. The anti-MTCLIP115 antibodies recognize each CLIP variant, but in addition, other common proteins are detected. Therefore, we used affinity-purified anti-peptide antibodies against a unique stretch of the coiled-coil region of CLIP-115 to detect the protein in vivo (Figure 5B). This antiserum recognizes two proteins of approximately 110–140 kDa specifically in brain tissue, which is consistent with the Northern blot expression results. In addition, the anti-peptide antibodies recognize CLIP-115 in transfected COS1 cells. The mouse proteins comigrate with the rat-derived CLIP-115 isoforms produced in COS1 cells, suggesting that the sizes of the two isoforms of CLIP-115 produced in mouse brain are similar to those of the rat and that the antibodies are specific for CLIP-115.

In the fluorescence experiments, both transfected COS1 cells (Figures 5C–5J) and cultured neurons from the hippocampus (Figures 5K and 5L) were investigated. In the COS1 cells transfected with the CLIP-115 isoforms, a clear fluorescent labeling pattern, which appears as long centrifugal fine wires in the cytoplasm, can be observed with both antisera #2131 (data not shown) and #2133 (Figure 5E); no immunolabeling is detected in nontransfected cells (Figures 5C and 5D). The labeling pattern of CLIP-115 revealed with antiserum #2133 completely overlaps with that obtained with anti-β-tubulin antibodies (Figure 5F). From these data, we conclude that CLIP-115, overexpressed in COS1 cells, colocalizes with the microtubule cytoskeleton.

This association was further confirmed by experiments in which COS1 cells were transfected with GFP-CLIP-115, GFP-δCLIP-115, or GFP linked to a truncated N-terminal mutant spanning amino acid residues 1–468 (GFP-CLIP$_{1-468}$). GFP-CLIP-115 fluorescent labeling in transfected COS1 cells is still very strong after mild fixation with paraformaldehyde, and it is virtually identical to that obtained with antisera #2131 and #2133 in CLIP-115–transfected cells (compare Figures 5E and 5G). This finding emphasizes the specificity of the new antisera against CLIP-115. The labeling extends into the long and thin outgrowths of the COS1 cells when these are present (data not shown). When GFP-CLIP$_{1-468}$ is used, the labeling of the cytoplasmic microtubules of the COS1 cells intensifies, and the microtubules appear to be clustered in thick bundles (for comparison with distribution of β-tubulin, see Figures 5I and 5J). Thus, expression of the MTB domains of CLIP-115 without the large coiled-coil region leads to enhanced bundling of the cytoskeletal microtubule network. This phenomenon has been observed previously in experiments using CLIP-170 or p150^{glued} deletion constructs and could be due to cross-linking of the microtubules (Pierre et al., 1994; Waterman-Storer et al., 1995).

Finally, to demonstrate that CLIP-115 is also associated with microtubules in neurons, we investigated the distributions of CLIP-115 and MAP2 in a monolayer of differentiating cultured neurons from the hippocampus. As shown in Figures 5K and 5L, CLIP-115 colocalizes with MAP2 in all (i.e., both proximal and distal) dendritic

components of these neurons. Taken together, these experiments suggest that (1) CLIP-115 indeed binds to microtubules; (2) the microtubule-binding property of CLIP-115 is mediated by the two MTB domains in its N-terminal region; and (3) the peptide antisera against CLIP-115 are specific and can be further employed on tissue sections.

Localization of CLIP-115 In Vivo

To determine whether CLIP-115 is located in DLBs, the newly raised antisera #2131 and #2133 were used for immunocytochemistry on adult rat brain sections. Both light microscopic and electron microscopic analyses were carried out (Figures 6 and 7). In general, both antisera revealed the same labeling pattern in the three areas of the brain with the highest density of DLBs, i.e., the inferior olive, hippocampus, and piriform cortex. Since these antisera are raised against different regions of CLIP-115, this suggests that the labeling seen is specific for CLIP-115. In the light microscopic analysis, we observed that in the inferior olive, the most prominent labeling is, apart from some weak cytoplasmic dendritic staining, an overall punctate labeling ubiquitously distributed in the neuropil of all its subnuclei (Figures 6A and 6C; for comparison with labeling obtained with antiserum α12B/18, see Figure 8B); this labeling is abolished by preincubation of the antisera with bacterially produced GST-CLIP115 (Figure 6B), strongly suggesting the antibodies specifically recognize CLIP-115. In the hippocampus and piriform cortex, the most prominent staining is found in the dendrites of the pyramidal cells (Figure 6D), while modest punctate labeling can be seen in the neuropil. In the cerebellum, we observed a specific labeling of the fiber extensions of all Bergmann glia cells in the molecular layer of the cerebellar cortex (Figures 6E and 6F). The proximal parts of the cytoplasm of the

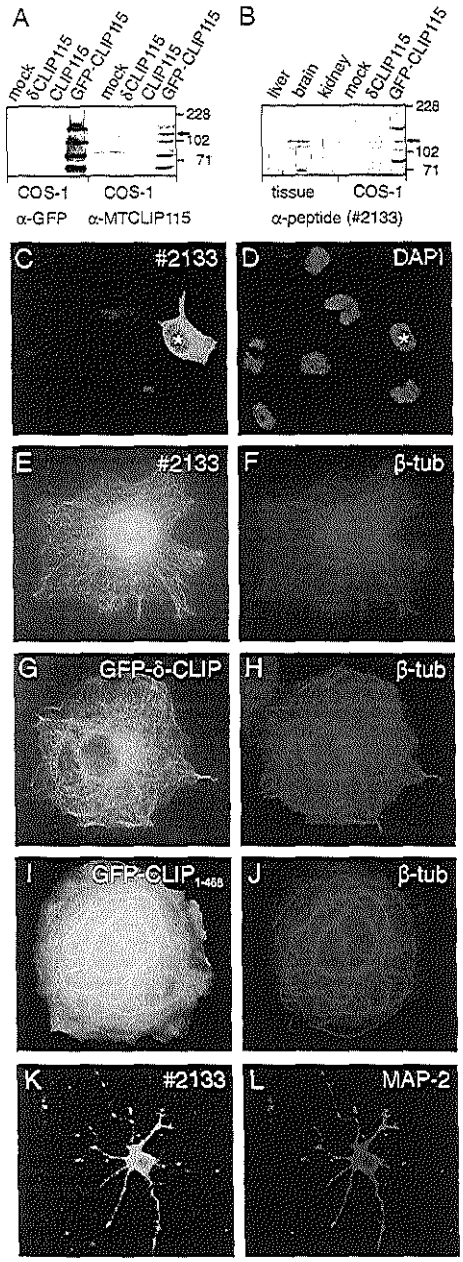

Figure 5. CLIP-115 Expression in Tissue Extracts, COS1 Cells, and Cultured Neurons

(A and B) CLIP-115 expression analyzed on Western blot. In (A), protein extracts from mock transfected COS1 cells or from cells transfected with CLIP-115, δCLIP-115, and GFP-CLIP-115 were run on gel, blotted, and incubated with α-GFP or α-MTCLIP115 antibodies. CLIP-115, δCLIP-115, and GFP-CLIP-115 proteins of the correct size are produced. The arrow indicates full-length CLIP-115 in the GFP-CLIP115 lane incubated with α-MTCLIP115 antibodies; proteolytic processing leads to the appearance of this protein, as it is not recognized by α-GFP. In (B), protein extracts from mouse brain, liver, and kidney as well as COS1 cells were tested for the presence of CLIP-115 with the use of affinity-purified #2133. The arrow points at the position of presumptive CLIP-115 generated by proteolytic processing in the GFP-CLIP115 lane.

(C–J) Fluorescence study of CLIP-115 expression in COS1 cells. In (C) and (E), the pattern of CLIP-115 as detected with antiserum #2133 consists of a centrifugal fine wire network in the cytoplasm. In (C), one transfected cell (asterisk) is surrounded by non-transfected cells that are identified by DAPI staining of their nuclei in (D). (F) The CLIP labeling pattern colocalizes with the microtubule network as revealed by β-tubulin labeling. CLIP-115 expression was also investigated in COS1 cells transfected with constructs expressing GFP, linked to δCLIP-115 (G) and $CLIP_{1-465}$ (I). Note that the labeling pattern obtained in (G) is virtually identical to that in (E). (I) Expression of mutant $GFP\text{-}CLIP_{1-465}$ causes thickening of the microtubule bundles. GFP signals colocalize with anti-β-tubulin staining pattern in both (H) and (J).

(K and L) CLIP-115 expression in cultured neurons. CLIP-115 (K) is expressed in all the dendritic components of differentiating hippocampal neurons that contain the microtubule-associated protein MAP2 (L).

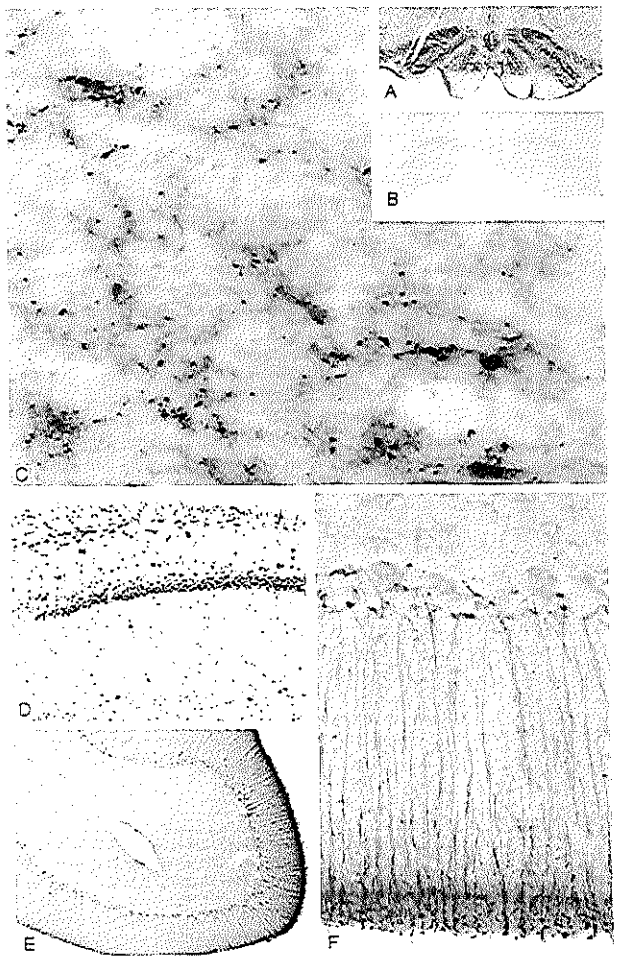

Figure 6. Distribution of CLIP-115 in the Rat Brain

Labeling patterns of CLIP-115 obtained with antiserum #2131 and #2133.

(A) Labeling in the ventral medulla oblongata. Note the ubiquitous immunolabeling in all subnuclei of the inferior olive.

(B) Labeling of the same structure with antiserum #2133 preabsorbed with bacterially produced CLIP-115.

(C) High magnification of the rostral medial accessory olive, the olivary subnucleus with the highest density of immunoreactive puncta.

(D) Labeled dendrites of pyramidal cells in the CA1 area of the hippocampus. This micrograph was taken from a section counterstained with cresyl violet.

(E) Labeled Bergmann glia fibers in the molecular layer of the cerebellar cortex.

(F) Same fibers at a higher magnification; note that the cell bodies of the Bergmann glia cells are not labeled, whereas the proximal parts of the fibers are densely stained. The labeled fibers extend into the extreme outer part of the molecular layer.

Bergmann fibers are more prominently labeled than the peripheral parts. The cell bodies of the Bergmann glia cells are not labeled. Identical results were obtained with affinity-purified #2133 antiserum both on rat and mouse brain sections (data not shown), again suggesting that the labeling with the peptide antisera on brain sections is specific for CLIP-115.

In the electron microscopic analysis, we found that the punctate labeling in the inferior olive corresponds to DLBs (Figure 7); the morphology of the DLBs, as revealed with the new antisera against CLIP-115, is the same as that of the DLBs labeled with antiserum α12B/18 (compare Figures 7B and 7D). The preimmune sera of #2131 and #2133 as well as antisera against CLIP-170 (Pierre et al., 1992, 1994) do not label DLBs. Within DLBs, the most abundant labeling occurs in the electron dense depositis in between the lamellar stacks, which are approximately 60 nm apart from one another. Most of the cytoplasmic labeling in dendrites of olivary neurons, on the other hand, corresponds to clusters of microtubules (for labeling with antiserum #2133, see Figures 7C and 7E; with antiserum #2131, see Figure 7F). Apparently, antisera #2131 and #2133 do not only detect microtubules in vitro, as described above for COS1 cells and cultured hippocampal neurons, but also in vivo. The dendrites containing labeled microtubules belong to all possible categories, i.e., proximal, intermediate, and distal dendrites. Interestingly, the microtubules labeled with antisera #2131 or #2133 are frequently located in the vicinity of labeled vesicles, while the nonlabeled microtubules within the same dendritic profile are not associated with vesicles (e.g., Figure 7C). Therefore, it appears possible that CLIP-115 establishes a link between microtubules and membranous vesicles.

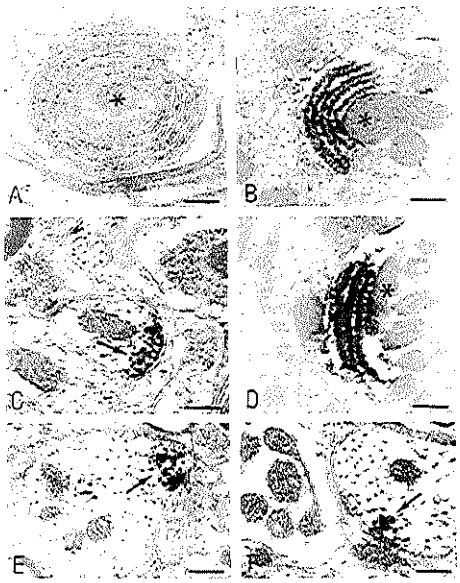

Figure 7. CLIP-115 Is Localized in DLBs and Microtubules

Detailed analysis of the punctate labeling in the inferior olive as presented in Figures 6A and B demonstrates that the dots and cytoplasmic dendritic labeling correspond to DLBs and clusters of microtubules, respectively.

(A) Shows the characteristic morphology of a DLB following standard electron microscopy. Note that the lamella are surrounding a mitochondrion (asterisk) located in the center of the organelle.

(B) Shows a DLB labeled with antiserum α12B/18 ([A] and [B] are modified from De Zeeuw et al., 1995).

(C) Shows a cluster of labeled microtubules in a distal dendrite following immunocytochemistry with antiserum #2133 against CLIP-115. Note that the labeled microtubules indicated by the arrow surround a labeled vesicle.

(D) Shows a DLB labeled with antiserum #2133; this DLB is highly similar to the DLB labeled by antiserum α12B/18 in (B).

(E and F) Show intermediate dendrites with clusters of microtubules labeled with the use of antisera #2133 and #2131, respectively. Scale bars in (A), (B), (C), (D), (E), and (F) indicate 26 μm, 26 μm, 0.25 μm, 0.27 μm, 31 μm, and 30 μm, respectively.

These vesicles in turn, then, might be specifically involved in the formation or turnover of the DLBs.

The Effect of Microtubule Depolymerization on the Density of DLBs

Above, it is shown that CLIP-115 can bind to microtubules and that DLBs are detected with antisera against CLIP-115. To find out whether and to what extent microtubules are necessary for the localization of DLBs in vivo, we investigated the effects of depolymerization of microtubules on the distribution of DLBs by local application of nocodazole and taxol (Kolodney and Elson, 1995). Eight and sixteen hours after unilateral extracellular application of nocodazole to the rat inferior olive (for electrophysiological identification, see Figure 8A), the density of olivary DLBs was reduced to 14% and

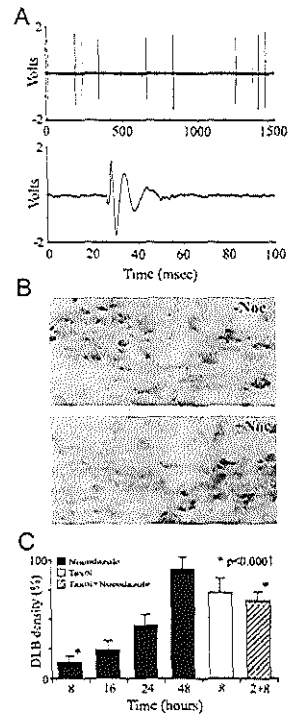

Figure 8. Microtubule Depolymerization In Vivo Affects the Density of DLBs

The density of DLBs in the inferior olive of the rat brainstem was investigated after several periods of survival time following local injection of nocodazole.

(A) Shows the electrophysiological identification of a neuron in the rat inferior olive. Olivary neurons can be recognized by their low firing frequency of 0.5–1 Hz (top) and by the characteristic wave shape of their action potential (bottom).

(B) Shows the effect of nocodazole on the density of DLBs in the rostral medial accessory olive of the rat 8 hrs after the injection. Note the reduction in immunoreactive puncta (revealed with antiserum α12B/18).

(C) Shows the densities of DLBs in the olive at different survival times following local application of nocodazole, taxol, or both drugs. Following nocodazole alone, the density of DLBs was reduced to 14%, 24%, 46%, and 94% of the normal density after 8, 16, 24, and 48 hrs of survival, respectively. Although taxol itself evoked a mild reducing effect on the density of DLBs, it practically abolished the reducing effect of nocodazole; when the inferior olive was injected with taxol 2 hrs prior to the nocodazole application, the density of DLBs 8 hrs after the nocodazole injection was reduced to 73% instead of 14%. This difference was significant ($p < 0.0001$; Wilcoxon rank-sum test).

24% of normal values (Figures 8B and 8C) (for an overview of absolute densities of DLBs in different olivary subnuclei, see De Zeeuw et al., 1995). The number of Nissl-stained neurons in the inferior olive, quantified as a control, remained the same. Twenty-four and forty-eight hours after intraolivary injection of nocodazole,

the DLBs reappeared (46% and 94% of normal values, respectively). Injection of the carrier alone, i.e., 25% DMSO, did not result in reduction of DLBs. When the inferior olive was injected with the microtubule stabilizing drug taxol 2 hrs prior to nocodazole application, the density of DLBs 8 hrs after the nocodazole injections was reduced to 73% instead of 14% (Figure 8C). This difference strongly suggests that the DLB reducing effect of nocodazole is caused by depolymerization of the microtubules. These experiments indicate that the formation of DLBs, as detected by α12B/18, is dependent on the presence of normal polymerized microtubules, and they suggest there is a continuous and rapid turnover of DLBs in olivary neurons.

Discussion

Recently, we discovered a new neuronal organelle, the dendritic lamellar body (DLB), which is exclusively located in the bulbous appendages of dendrites of neurons with dendrodendritic gap junctions (De Zeeuw et al., 1995). This organelle can be specifically labeled with antiserum α12B/18, which was raised against one of the extracellular loops of the gap junction protein cx43. However, until now, it was not clear what epitope is detected by this antiserum. Here, we determined the identity of the epitope by producing cDNA libraries of brain areas with high densities of DLBs and screening these with α12B/18. We characterized ten clones from two different cDNA libraries, yet we showed that all clones are derived from the same mRNA. These data strongly suggest that the isolation of these clones is due to the presence of a specific antibody population in α12B/18 directed against the protein product encoded by the different cDNAs. This protein is brain-specific and is referred to as CLIP-115 because of its homology with CLIP-170. Newly raised antisera against CLIP-115 were found to label DLBs. Thus, we conclusively demonstrated that we have isolated the antigen in the α12B/18 antiserum that is specific for DLBs, and thereby we identified a novel protein component of this intriguing neuronal organelle. By using (parts of) CLIP-115 in yeast two-hybrid screens, other protein constituents of DLBs can now be isolated.

Previously, we showed that α12B/18 antibodies detect proteins in rat brain of 110–140 kDa on Western blots, which are present only in those areas of the brain that contain DLBs (De Zeeuw et al., 1995). The sizes calculated from those SDS-PAGE experiments correlate well with the predicted molecular mass of CLIP-115, and the fact that two proteins were detected on Western blots can be explained by assuming that specific post-translational modifications take place on CLIP-115 and/or that different brain areas express either one of the two alternative splice products of CLIP-115. Interestingly, two isoforms of CLIP-115 are also specifically detected in mouse brain, using anti-peptide antibodies against rat CLIP-115. The finding that CLIP-115 is detected in the cerebellum, in both rat and mouse and at both mRNA and protein level, whereas the DLB-specific antigen in α12B/18 is not, is probably due to the stringent conditions under which incubatons with α12B/18 were done. The same conditions were used for screening the cDNA libraries with α12B/18 and yielded only one type of clone. Thus, it is presumably the high local concentration of CLIP-115 in DLBs and recombinant CLIP in phage lysates that permits its clean detection by α12B/18 under stringent conditions, both in tissue sections and on nitrocellulose filters.

Within DLBs, most of the CLIP-115 labeling occurs in the electron-dense depositis between the lamellar stacks. This observation raises the possibility that CLIP-115 is not only necessary for the localization of DLBs in dendrites but also for the appropriate distance between the membraneous stacks within a DLB; this distance is approximately 60 nm and could correspond to the length of the coiled-coil domain in CLIP-115 (Moore and Endow, 1996). CLIP-115 would therefore have a role as a structural determinant of DLB morphology in addition to its more general function as a membrane–microtubule linking molecule. Because of the morphological resemblance between DLBs and calciosomes (Villa et al., 1991), we have tested whether CLIP-115 is expressed in calciosomes but found no evidence for the presence of the protein there. Interestingly, calciosomes have more closely packed membranous stacks than DLBs, a feature that may be due to the lack of CLIP-115 (or the presence of a shorter unknown CLIP). We have also attempted to label DLBs with markers for IP3 and ryanodine receptors, which are found on calciosomes (Takei et al., 1992), but none of these receptors was found to colocalize with DLBs (data not shown). In spite of these findings, DLBs might still operate as a special type of intracellular calcium storage site. This possibility is supported not only by their morphologic resemblance with calciosomes but also by the fact that dendritic calcium spikes have been identified in most, if not all, of the brain areas with DLBs (e.g., Llinás and Yarom, 1981; Andreasen and Nedergaard, 1996).

DLBs have been associated with dendrodendritic gap junctions because of their overlapping distribution in the brain and their simultaneous occurrence during development (De Zeeuw et al., 1995). In addition, DLBs and dendrodendritic gap junctions can be down-regulated concomitantly, and the level of electrotonic coupling of neurons can be correlated to the density of DLBs (De Zeeuw et al., 1997). Based upon these observations, we have proposed that DLBs are necessary for the turnover and/or assembly of dendrodendritic gap junction channels, which are usually being replaced in only a few hours (Laird et al., 1991). Since CLIP-115 is a structural component of DLBs in dendritic varicosities, and the turnover of DLBs following application of nocodazole is as rapid as that of gap junctions, it is possible that CLIP-115 is also involved in the maintenance of dendrodendritic gap junctions. In this respect, it is interesting to note that Bergmann glia cells, which do not contain DLBs but prominently express CLIP-115, are coupled by extremely extensive gap junction plaques (Palay and Chan-Palay, 1974). Moreover, CLIP-170 has also been associated with membrane specializations, i.e., desmosomal plaques (Wacker et al., 1992). Thus, both these observations are compatible with a proposed role of CLIP-115 in the formation and/or turnover of gap junctions.

The definition of cytoplasmic linker proteins implies their involvement in the translocation of cytoplasmic organelles as well as their proper intracellular localization. Similar to the hypothesis that each member of the kinesin superfamily of motor proteins conveys a specific organelle (Hirokawa, 1996; Saito et al., 1997), it has been proposed that for each type of membrane, a different CLIP might exist (Rickard and Kreis, 1996). However, whereas ten different members of the kinesin superfamily have already been identified (Hirokawa, 1996), CLIP-170, which links endocytotic vesicles to microtubules, is so far the only protein that has been identified as a cytoplasmic binding factor in vivo (Pierre et al., 1992). In the present study, we demonstrate that its close relative CLIP-115 is associated with the membranes of DLBs, that CLIP-115 contains MTB domains that function as such both in vitro and in vivo, and that depolymerization of microtubules by nocodazole application in vivo influences the (trans)location of DLBs. Thus, CLIP-115 indeed appears to mediate the interaction between microtubules and a highly specific neuronal organelle with a particular localization. It is noteworthy that of the large family of proteins with the novel MTB domain described to date, only CLIP-115 and ~170 have a tandem motif and also are the only proteins that have been shown to associate directly with particular membranes and microtubules. Therefore, a repeated MTB domain might be characteristic for proteins directly interacting with membranous organelles and microtubules. By cloning CLIP-115 and determining its distribution, we lend support to the theory that multiple CLIPs exist and that they are involved in the localization of organelles (Rickard and Kreis, 1996), but it remains to be shown whether each type of membranous organelle has its own CLIP and to what extent each CLIP binds to specific organelles.

Experimental Procedures

cDNA Libraries

Brain regions highly enriched for hippocampus, piriform cortex, inferior olive, frontal cortex, cerebellum, and olfactory bulb were collected from 20 adult male Wistar rats, and total cellular RNA was extracted (Auffray and Rougeon, 1980). Five micrograms of poly(A)$^+$ mRNA was isolated from the three brain areas with the highest density of DLBs (i.e., hippocampus, piriform cortex, and inferior olive) with the use of magnetic oligo(dT)$_{25}$ Dynabeads (Dynal, Oslo, Norway). Double-stranded cDNAs were made, and fragments longer than 500 bp were force cloned into lambda ZAP Express (Stratagene). Libraries were packaged with Gigapack II Gold (Stratagene).

Cloning and Sequencing of *CLIP-115* cDNAs

The hippocampus and piriform cortex libraries (complexity of 1.1×10^6 and 0.7×10^6 independent clones, respectively) were plated and screened using antiserum α12B/18 (1:1000) according to standard procedures (Sambrook et al., 1989). Positive clones were plaque purified, and inserts were excised using the Rapid Excision kit (Stratagene). To obtain full-length cDNAs, the hippocampus library was replated and screened with a DNA probe, which was a labeled 0.36 kb EcoRI-EagI fragment from the 5′ end of clone PC3.9 (Figure 1A) (Feinberg and Vogelstein, 1983). The CLIP-115 nucleotide sequence was determined on both strands with ^{35}S-dATP and Sequenase (Amersham).

Northern Blot Analysis

Total RNA from mouse and rat tissues was isolated as described above. RNA samples were electrophoresed on a 0.8% agarose gel containing 0.66 M formaldehyde (Fourney et al., 1988), blotted onto Hybond N$^+$ nylon membranes (Amersham), and hybridized according to standard procedures (Sambrook et al., 1989) with different *CLIP-115* DNA probes, labeled as above. Filters were exposed to PhosphorImager screens and images acquired through Imagequant (Molecular Dynamics).

Generation of Antisera

Full-length CLIP-115 and the N-terminal region including the MTB domains (MTCLIP115) were fused to glutathione S-transferase (GST) using pGEX2T (Pharmacia). Both GST fusion proteins were induced in bacteria and purified (Smith et al., 1988). In addition, two peptides of 17 (dlb-1) or 16 (dlb-2) amino acids were synthesized, and 0.5 mg of each peptide was conjugated to 2 mg of thyroglobulin (Sigma) using 0.15% glutaraldehyde in phosphate buffer. Purified GST-MTCLIP-115 and the conjugated dialyzed peptides were injected into New Zealand White rabbits in a suspension of Freund's incomplete adjuvans. Serum from rabbit #2131 is against peptide dlb-1, and serum from #2133 is against peptide dlb-2 (see Figure 2). Serum #2133 was affinity purified on filter strips containing GST-CLIP-115. The unbound or depleted antibody population was used in the experiments shown in Figure 6B. The bound antibody pool was eluted from the filter using 0.1 M glycine (pH 2.3) and 1 M NaCl. After elution, the pH was quickly restored with unbuffered Tris. Affinity-purified antibodies were concentrated on centricon-30 membranes (Amicon) and stored in the presence of 0.1 mg/ml BSA.

Western Blot Analysis

Total protein extracts from COS1 cells were obtained 2 days after transfection. After sonication, cell lysates were boiled in SDS sample buffer in the presence of DTT. Mouse brain, liver, and kidney were homogenized in PBS in the presence of protease inhibitors (Boehringer Mannheim) and further treated as above. Equal amounts of protein homogenates were analyzed on 7% SDS-polyacrylamide gels and by Western blots (Sambrook et al., 1989). Blots were blocked for 1 hr in 10 mM Tris (pH 7.6), 100 mM NaCl, 0.05% Tween (TNT) containing 3 mg/ml BSA and incubated with α-GFP (Clontech; 1:4000), α-MTCLIP115 (1:1000), or affinity-purified #2133 (1:50) for 2 hrs at room temperature. After washing in TNT buffer, goat-anti rabbit antibody coupled to alkaline phosphatase (Sigma, 1:2000) was added to the blots in TNT/BSA buffer for 2 hrs. Enzymatic detection of antigen–antibody interactions was carried out using the Sigma Fast BCIP/NBT system.

Transfection Studies In Vitro

For the immunocytochemical detection of CLIP-115 in COS1 cells, full-length *CLIP-115* (HI4.8) and δ*CLIP-115* (HI4.2) cDNAs were excised from λZAP and transfected into COS1 cells. Two days after transfection, the cells were fixed in 100% methanol/1 mM EGTA, blocked in 0.5% BSA/0.02% glycine in PBS, and immunoreacted with antiserum #2131 or #2133 (1:100) and anti-β-tubulin (1:200; Sigma). After washing, sections were incubated with FITC-labeled secondary antibodies (Nordic Laboratories, The Netherlands; 1:80) to detect δCLIP-115 and with rhodamine-labeled sheep anti-mouse (1:20; Boehringer Mannheim) to detect β-tubulin. For direct detection of CLIP-115, three proteins were fused to GFP (Chalfie et al., 1994): these included δCLIP-115, full-length CLIP-115, and CLIP-115$_{1-468}$, a construct that contains a large part of the N-terminal domain with the two MTB domains (upstream of the BssHII site indicated in Figure 2). All constructs were transfected into COS1 cells, and after two days, cells were fixed in 2% paraformaldehyde/PBS and processed for GFP/β-tubulin codetection. To detect CLIP-115 in differentiating neuronal cultures in vitro, hippocampi were dissected from newborn mouse brains, and cells were resuspended and grown on coated glass slides in neurobasal medium (Life Technologies). After 5 days in culture, cells were fixed and processed for immunocytochemistry with #2133 (1:100) and α-MAP2 (1:200; Boehringer Mannheim). Cells were analyzed on an Olympus inverted microscope equipped with GFP/TXR filter blocks, and images were captured with the use of a Sony 3CCD camera (model DXP-950).

Immunocytochemistry In Vivo: Light Microscopy

For analysis of CLIP-115 expression in adult rat brain, Sprague-Dawley rats were anesthetized with sodium pentobarbital (75 mg/kg, intraperitoneally), and perfused with 0.5% zinc salicylate and 4% paraformaldehyde in 0.9% NaCl (pH 5.0). The brains were cryoprotected in saline containing 30% sucrose and cut into 20 μm thick transverse sections on a freezing microtome. All sections were collected in 0.5 M Tris buffer (pH 7.6) with 0.25% Triton-X, blocked in 5% nonfat dry milk in the same buffer for 4 hrs, and incubated for 48 hrs at 4°C with antisera #2131 or #2133 (1:500) or with the affinity-purified antibody (1:20) in 1% nonfat dry milk in 0.5 M Tris buffer with 0.25% Triton. After the primary incubations, sections were rinsed and processed with the use of the avidin–biotin complex method (ABC Elite kit, Vector Laboratories). Finally, the sections were incubated in 0.05% 3,3-diaminobenzidine (DAB) and 0.01% H_2O_2 in 0.05 M Tris buffer, mounted, and coverslipped.

Immunocytochemistry In Vivo: Electron Microscopy

For electron microscopy, adult Sprague-Dawley rats were sacrificed as described above and processed according to published protocols (De Zeeuw et al., 1995). In short, the animals were perfused transcardially, and the brains were sectioned on a Vibratome. These sections were processed for preembedding immunocytochemistry as described above with the use of antisera #2131, #2133, or preimmune sera. Some sections were processed with an antiserum against CLIP-170 (kindly provided by Dr. J. Rickard; for details, see Pierre et al., 1992, 1994; Wacker et al., 1992). Subsequently, sections were osmicated, stained in uranyl acetate, dehydrated in dimethoxypropane, and embedded in Araldite. Guided by semithin sections, we prepared pyramids of the hippocampus and inferior olive. From these tissue blocks, ultrathin sections were cut, counterstained, and examined in a Philips CM 100 electron microscope.

Nocodazole and Taxol Treatment of Olivary Neurons

The effect of microtubule depolymerization on the presence of DLBs was investigated by injecting nocodazole and/or taxol unilaterally into the inferior olive of ketamine anesthetized rats. Prior to the injections, the inferior olive was identified electrophysiologically by the characteristic low firing frequency and waveshape of the action potentials of its neurons (Llinás and Yarom, 1981). Eight adult male Wistar rats received a pressure injection of 5 μg of nocodazole in 20 μl of 25% DMSO through glass micropipettes, two rats received an injection of 1 μg of taxol in 1 μl of DMSO, four rats received both a taxol and nocodazole injection, while four littermates received the drug vehicle only. In the group of eight rats that received only nocodazole, two rats were sacrificed 8 hrs after the injection, two rats after 16 hrs, two rats after 24 hrs, and two rats 48 hrs after the injection. The taxol-treated animals were sacrificed 8 hrs after drug application, while the rats treated with both drugs received taxol 2 hrs prior to nocodazole and were sacrificed 8 hrs later. In all animals, the density of DLBs was investigated immunocytochemically with the use of antiserum α12B/18. Sections were counterstained for cresyl violet, and the neurons were counted and compared to the number of neurons in control animals.

Acknowledgments

We would like to thank Dr. A. Hoogeveen for peptide synthesis and T. Verkerk, R. Hawkins, J. v.d. Burg, M. Kuit, and E. Dalm for their excellent technical assistance. In addition, we thank Dr. J. E. Rickard for kindly providing antisera against CLIP-170. This research was supported by grants from the Netherlands Organization for Scientific Research (NWO; GB-MW 903-68-361), the Life Sciences Foundation (SLW; 805.33.310), and the Royal Dutch Academy of Sciences (KNAW).

Received July 25, 1997; revised October 31, 1997.

References

Allan, V. (1996). Motor proteins: a dynamic duo. Curr. Biol. *6*, 630–633.

Andreasen, M., and Nedergaard, S. (1996). Dendritic electrogenesis in rat hippocampal CA1 pyramidal neurons: functional aspects of Na^+ and Ca^{2+} currents in apical dendrites. Hippocampus *6*, 79–95.

Auffray, C., and Rougeon, F. (1980). Nucleotide sequence of a cloned cDNA corresponding to secreted mu chain of mouse immunoglobulin. Gene *12*, 77–86.

Berlin, V., Styles, C.A., and Fink, G.R. (1990). BIK1, a protein required for microtubule function during mating and mitosis in Saccharomyces cerevisiae, colocalizes with tubulin. J. Cell Biol. *111*, 2573–2586.

Bilbe, G., Delabie, J., Bruggen, J., Richener, H., Asselbergs, F.A., Cerletti, N., Sorg, C., Odink, K., Tarcsay, L., Wiesendanger, W., et al. (1992). Restin: a novel intermediate filament-associated protein highly expressed in the Reed-Sternberg cells of Hodgkin's disease. EMBO J. *11*, 2103–2113.

Burkhardt, J.K. (1996). In search of membrane receptors for microtubule-based motors - is kinectin a kinesin receptor? Trends Cell Biol. *6*, 127–131.

Chalfie, M., Tu, Y., Euskirchen, G., Ward, W.W., and Prasher, D.C. (1994). Green fluorescent protein as a marker for gene expression. Science *263*, 802–805.

Cole, N.B., and Lippincott-Schwartz, J. (1995). Organization of organelles and membrane traffic by microtubules. Curr. Opin. Cell Biol. *7*, 55–64.

Cole, N.B., Sciaky, N., Marotta, A., Song, J., and Lippincott-Schwartz, J. (1996). Golgi dispersal during microtubule disruption: regeneration of Golgi stacks at peripheral endoplasmic reticulum exit sites. Mol. Biol. Cell *7*, 631–650.

Craig, A.M., and Banker, G. (1994). Neuronal polarity. Annu. Rev. Neurosci. *17*, 267–310.

De Zeeuw, C.I., Hertzberg, E.L., and Mugnaini, E. (1995). The dendritic lamellar body: a new neuronal organelle putatively associated with dendrodendritic gap junctions. J. Neurosci. *15*, 1587–1604.

De Zeeuw, C.I., Koekkoek, S.K.E., Wylie, D.R.W., and Simpson, J.I. (1997). Association between dendritic lamellar bodies and complex spike synchrony in the olivocerebellar system. J. Neurophysiol. *77*, 1747–1758.

Feinberg, A.P., and Vogelstein, B. (1983). A technique for radiolabeling DNA restriction endonuclease fragments to high specific activity. Anal. Biochem. *132*, 6–13.

Fourney, R.M., Miyakoshi, J., Day, R.S., and Paterson, M.C. (1988) Northern blotting: efficient RNA staining and transfer. Focus *10*, 5–7.

Gill, S.R., Schroer, T.A., Szilak, I., Steuer, E.R., Sheetz, M.P., and Cleveland, D.W. (1991). Dynactin, a conserved, ubiquitously expressed component of an activator of vesicle motility mediated by cytoplasmic dynein. J. Cell Biol. *115*, 1639–1650.

Hanlon, D.W., Yang, Z., and Goldstein, L.S. (1997). Characterization of KIFC2, a neuronal kinesin superfamily member in mouse. Neuron *18*, 439–451.

Hirokawa, N. (1996). The molecular mechanism of organelle transport along microtubules: the identification and characterization of KIFs (kinesin superfamily proteins). Cell Struct. Funct. *21*, 357–367.

Hofmann, K., and Stoffel, W. (1993). TMbase- a database of membrane spanning proteins segments. Biol. Chem. Hoppe-Seyler *347*, 166.

Holzbaur, E.L., Hammarback, J.A., Paschal, B.M., Kravit, N.G., Pfister, K.K., and Vallee, R.B. (1991). Homology of a 150K cytoplasmic dynein-associated polypeptide with the Drosophila gene Glued. Nature *351*, 579–583. Erratum: Nature *360(6405)*.

Kolodney, M.S., and Elson, E.L. (1995). Contraction due to microtubule disruption is associated with increased phosphorylation of myosin regulatory light chain. Proc. Natl. Acad. Sci. USA *92*, 10252–10256.

Laird, D.W., Puranam, K.L., and Revel, J.P. (1991). Turnover and phosphorylation dynamics of connexin43 gap junction protein in cultured cardiac myocytes. Biochem. J. *273*, 67–72.

Lewis, S.A., Wang, D.H., and Cowan, N.J. (1988). Microtubule-associated protein MAP2 shares a microtubule binding motif with tau protein. Science *242*, 936–939.

Li, I., Liu, Z.-M., and Nirenberg, M. (1997). Kinesin-73 in the nervous

system of Drosophila embryos. Proc. Natl. Acad. Sci. USA *94*, 1086–1091.

Llinas, R., and Yarom, Y. (1981). Properties and distribution of ionic conductances generating electroresponsiveness of mammalian inferior olivary neurones in vitro. J. Physiol. *315*, 569–584.

Lupas, A. (1996). Coiled coils: new structures and new functions. Trends Biochem. Sci. *21*, 375–382.

Maccloni, R.B., and Cambiazo, V. (1995). Role of microtubule-associated proteins in the control of microtubule assembly. Physiol. Rev. *75*, 835–864.

Matteoni, R., and Kreis, T.E. (1987). Translocation and clustering of endosomes and lysosomes depends on microtubules. J. Cell Biol. *105*, 1253–1265.

Moore, J.D., and Endow, S.A. (1996). Kinesin proteins: a phylum of motors for microtubule-based motility. Bioessays *18*, 207–219.

Ogawa, K., and Mohri, H. (1996). A dynein motor superfamily. Cell Struct. Funct. *21*, 343–349.

Palay, S.L., and Chan-Palay, V. (1974). Cerebellar Cortex: Cytology and Organization (New York: Springer-Verlag).

Pierre, P., Scheel, J., Rickard, J.E., and Kreis, T.E. (1992). CLIP-170 links endocytic vesicles to microtubules. Cell *70*, 887–900.

Pierre, P., Pepperkok, R., and Kreis, T.E. (1994). Molecular characterization of two functional domains of CLIP-170 in vivo. J. Cell Sci. *107*, 1909–1920.

Rickard, J.E., and Kreis, T.E. (1996). CLIPs for organelle-microtubule interactions. Trends Cell Biol. *6*, 178–183.

Saito, N., Okada, Y., Noda, Y., Kinoshita, Y., Kondo, S., and Hirokawa, N. (1997). KIFC2 is a novel neuron-specific C-terminal type kinesin superfamily motor for dendritic transport of multivesicular body-like organelles. Neuron *18*, 425–438.

Sambrook, J., Fritsch, E.F., and Maniatis, T. (1989). Molecular Cloning: A Laboratory Manual, 2nd Ed. (New York: Cold Spring Harbor Laboratory Press).

Schnapp, B.J. (1997). Retroactive motors. Neuron *18*, 523–526.

Sharp, D.J., Yu, W., and Baas, P.W. (1995). Transport of dendritic microtubules establishes their nonuniform polarity orientation. J. Cell Biol. *130*, 93–103.

Smith, P.K., Krohn, R.I., Hermanson, G.T., Mallia, A.K., Gartner, F.H., Provenzano, M.D., Fujimoto, E.K., Goeke, N.M., Olson, B.J., and Klenk, D.C. (1985). Measurement of protein using bicinchoninic acid. Anal. Biochem. *150*, 76–85.

Swaroop, A., Swaroop, M., and Garen, A. (1987). Sequence analysis of the complete cDNA and encoded polypeptide for the Glued gene of Drosophila melanogaster. Proc. Natl. Acad. Sci. USA *84*, 6501–6505.

Takei, K., Stukenbrok, H., Metcalf, A., Mignery, G.A., Sudhof, T.C., Volpe, P., and De Camilli, P. (1992). Ca^{2+} stores in Purkinje neurons: endoplasmic reticulum subcompartments demonstrated by the heterogeneous distribution of the InsP3 receptor, Ca(2+)-ATPase, and calsequestrin. J. Neurosci. *12*, 489–505.

Toyoshima, I., Yu, H., Steuer, E.R., and Sheetz, M.P. (1992). Kinectin, a major kinesin-binding protein on ER. J. Cell Biol. *118*, 1121–1131.

Trueheart, J., Boeke, J.D., and Fink, G.R. (1987). Two genes required for cell fusion during yeast conjugation: evidence for a pheromone-induced surface protein. Mol. Cell. Biol. *7*, 2316–2328.

Vallee, R.B., and Sheetz, M.P. (1996). Targeting of motor proteins. Science *271*, 1539–1544.

Vaughan, K.T., and Vallee, R.B. (1995). Cytoplasmic dynein binds dynactin through a direct interaction between the intermediate chains and p150Glued. J. Cell Biol. *131*, 1507–1516.

Villa, A., Podini, P., Clegg, D.O., Pozzan, T., and Meldolesi, J. (1991). Intracellular Ca^{2+} stores in chicken Purkinje neurons: differential distribution of the low affinity-high capacity Ca^{2+} binding protein, calsequestrin, of Ca^{2+} ATPase and of the ER lumenal protein, Bip. J. Cell Biol. *113*, 779–791.

Wacker, I.U., Rickard, J.E., De Mey, J.R., and Kreis, T.E. (1992). Accumulation of a microtubule-binding protein, pp170, at desmosomal plaques. J. Cell Biol. *117*, 813–824.

Wade, R.H., and Hyman, A.A. (1997). Microtubule structure and dynamics. Curr. Opin. Cell Biol. *9*, 12–17.

Watanabe, T.K., Shimizu, F., Nagata, M., Kawai, A., Fujiwara, T., Nakamura, Y., Takahashi, E., and Hirai, Y. (1996). Cloning, expression, and mapping of CKAP1, which encodes a putative cytoskeleton-associated protein containing a CAP-GLY domain. Cytogenet. Cell Genet. *72*, 208–211.

Waterman-Storer, C.M., Karki, S., and Holzbaur, E.L. (1995). The p150Glued component of the dynactin complex binds to both microtubules and the actin-related protein centractin (Arp-1). Proc. Natl. Acad. Sci. USA *92*, 1634–1638.

Yamashita, A., Watanabe, Y., and Yamamoto, M. (1997). Microtubule-associated coiled-coil protein Ssm4 is involved in the meiotic development in fission yeast. Genes Cells *2*, 155–166.

GenBank Accession Number

The EMBL accession number of the *CLIP-115* cDNA sequence is AJ000485.

Chapter 4

FUNCTIONAL ANALYSIS OF CLIP-115 AND ITS BINDING TO MICROTUBULES

Casper C. Hoogenraad[1,2], Anna Akmanova[1], Frank Grosveld[1], Chris I. De Zeeuw[2], Niels Galjart[1]

MGC Departments of [1]Cell Biology and Genetics, [2]Anatomy, Erasmus Univerisity, P.O. Box 1738, 3000 DR Rotterdam, The Netherlands.

Functional analysis of CLIP-115 and its binding to microtubules

Casper C. Hoogenraad[1,2], Anna Akhmanova[1], Frank Grosveld[1], Chris I. De Zeeuw[2] and Niels Galjart[1,*]

[1]MGC Department of Cell Biology and Genetics and [2]Department of Anatomy, Erasmus University, PO Box 1738, 3000 DR Rotterdam, The Netherlands

*Author for correspondence (e-mail: galjart@ch1.fgg.eur.nl)

Accepted 4 April; published on WWW 25 May 2000

SUMMARY

Cytoplasmic linker proteins (CLIPs) bind to microtubules and are proposed to link this cytoskeletal network to other intracellular structures. We are interested in CLIP-115, since this protein is enriched in neuronal dendrites and may operate in the control of brain-specific organelle translocations. Each CLIP monomer is characterized by two microtubule-binding (MTB) motifs, surrounded by basic, serine-rich regions. This head domain is connected to the C-terminal tail through a long coiled-coil structure. The MTB domains are conserved as a single domain in other proteins involved in microtubule based transport and dynamics, such as p150^{Glued}. Here we provide evidence that efficient binding of CLIP-115 to microtubules is sensitive to phosphorylation and is not mediated by the conserved MTB domains alone, but requires the presence of the basic, serine rich regions in addition to the MTB motifs. In transfected COS-1 cells, CLIP-115 initially accumulates at the distal ends of microtubules and coincides with CLIP-170, indicating that both proteins mark growing microtubule ends. However, when expressed at higher levels, CLIP-115 and -170 affect the microtubule network differently. This might be partly due to the divergent C-termini of the two proteins. We demonstrate that, similar to CLIP-170, CLIP-115 forms homodimers, which, at least in vitro, are linked by disulfide bridges. Cysteine^{391} of CLIP-115, however, is specific in that it controls the microtubule bundling capacity of certain mutant CLIP-115 molecules. Therefore, both similar and specific mechanisms appear to regulate the conformation of CLIPs as well as their binding to microtubules.

Key words: Cytoplasmic linker protein, Disulfide bridge, Phosphorylation, Microtubule plus end, Microtubule binding protein

INTRODUCTION

Numerous types of membranous organelles depend on an intact, polarized network of interphase microtubules and a complex protein machinery for their proper intracellular transport and delivery. Microtubules provide a directional track for organelle movement, whereas microtubule-based motors of the kinesin and dynein families provide the motive force. Molecular studies have revealed the structures and many characteristics of these motors, and mechanistic aspects of microtubule-motor interactions are beginning to emerge (Hirokawa, 1998). In contrast, the mechanisms that coordinate the subcellular distribution and temporal and spatial activity of individual motors remain largely unknown (Vallee and Sheetz, 1996).

Accessory proteins with a potential role in targeting the motor proteins to the appropriate organellar sites have been identified for dynein and kinesin family members. For example, cytoplasmic dynein has been shown to interact with a macromolecular complex, termed the dynactin complex, through the polypeptide, p150^{Glued} (Vaughan and Vallee, 1995). This protein binds to microtubules as well, whereas another component of dynactin, an actin-related protein termed centractin or Arp1, is postulated to mediate the membrane association required for vesicle motility (Waterman-Storer et al., 1995).

Cytoplasmic linker proteins (CLIPs) are another type of accessory proteins, that were originally defined in a functional manner and proposed to link specific organelle membranes to microtubules (Pierre et al., 1992; Rickard and Kreis, 1996). The prototype member of the small CLIP family is CLIP-170, a protein that may be involved in the binding of endocytotic vesicles to microtubules (Pierre et al., 1992). However, recently CLIP-170 has also been found to associate with kinetochores of prometaphase chromosomes, suggesting it may be a linker for cargo in mitosis (Dujardin et al., 1998). In addition, enrichment of CLIP-170 at the plus ends of microtubules has been described (Diamantopoulos et al., 1999; Rickard and Kreis, 1990) and, using a GFP-tagged version of the protein, it was shown that CLIP-170 highlights the growing microtubule tip and may have a function in the dynamics of this network (Perez et al., 1999). Recently, the CLIP-170 homologue in *Drosophila melanogaster* was cloned and named D-CLIP-190 (Lantz and Miller, 1998). This protein was found to coimmunoprecipitate with a class VI unconventional myosin. Together these data suggest that CLIPs may be involved in linking microtubules to multiple types of intracellular cargo and in the regulation of the dynamics of the growing microtubule.

We have cloned a rat cDNA encoding CLIP-115, a protein that is mainly expressed in the brain (De Zeeuw et al., 1997).

With the exception of Bergmann glia cells of the cerebellum, CLIP-115 is primarily present in the dendritic compartment of many different types of neurons. In dendrites, CLIP-115 is found associated to microtubules and vesicles as well as a very specialized membrane structure, that is called the dendritic lamellar body (DLB) and which resembles a stack of Golgi membranes (De Zeeuw et al., 1995). DLBs are detected in the dendrites of those neurons that are connected by dendrodendritic gap junctions. Although the exact function of DLBs remains to be elucidated, they may be involved in the formation and/or turnover of gap junction channels. The localization and structure of CLIP-115 suggest that this protein operates in the control of DLB formation and/or translocation. However, since CLIP-115 is more widely distributed than DLBs and appears earlier in embryonic development, it is likely to be involved in additional processes.

The gene encoding CLIP-115 is named CYLN2 (cytoplasmic linker protein gene 2); it was mapped in mice to the telomeric end of chromosome 5 and in man to the Williams Syndrome Critical Region (WSCR) region on chromosome 7q11.23 (Hoogenraad et al., 1998). Williams Syndrome (WS) is a contiguous gene deletion disorder caused by haploinsufficiency of genes at 7q11.23 and characterized by supravalvular aortic stenosis, infantile hypercalcemia and unique cognitive and behavioral features (Bellugi et al., 1990). The most common deletion involves a region of 1.5 Mb on chromosome 7q11.23 (Meng et al., 1998) and we have shown that one allele of the CYLN2 gene is absent in the 8 WS patients that we tested (Hoogenraad et al., 1998). This observation has lead to the hypothesis that haploinsufficiency of CLIP-115 may contribute to some of the neurological features observed in WS patients.

The structure predicted for CLIP-115 is quite similar to that of CLIP-170 and D-CLIP-190. The latter two proteins are characterized by three domains: a basic N-terminal domain, containing two microtubule binding (MTB) motifs, surrounded by basic, serine-rich stretches; a long alpha-helical region with the disposition to form coiled-coils; and a C-terminal domain, which could bind metal ions. For CLIP-170 the C-terminal domain has been proposed to be responsible for targeting the protein to endocytic membranes and kinetochores (Dujardin et al., 1998; Perez et al., 1999; Pierre et al., 1992). Recently, the structure of human CLIP-170 was investigated by electron microscopy, which showed that native CLIP-170 is a thin molecule of approximately 135 nm, with two kinks in its central rod domain (Scheel et al., 1999). Thus, the N-terminal (MTB) and C-terminal (cargo interaction) domains are at opposite ends of a highly elongated dimeric coiled-coil. Interestingly, the C-terminal tail of CLIP-115 is quite short and the potential metal binding residues which are present in the tails of the two other CLIPs are absent from CLIP-115.

The most conserved regions among the various CLIPs are the two, aforementioned microtubule-binding (MTB) motifs. For example, the similarity between MTB domain 1 and 2 of CLIP-115 and -170 is 93% and 97%, respectively (De Zeeuw et al., 1997). The MTB domain (or CAP-GLY motif) has a length of approximately 69 amino acids and is found as a single motif in various other proteins from different organisms, for example p150^{Glued}, tubulin-folding factor, BIK1, Ssm4 and kinesin-73 (Feierbach et al., 1999; Li et al., 1997; Pierre et al., 1992). The domain is rich in glycine and valine residues and contains a core sequence of PXGKND. Mutation analysis of MTB domains 1 and 2 of CLIP-170 confirmed the importance of both motifs in microtubule binding (Pierre et al., 1992, 1994). However, no studies have yet addressed the issue of whether other regions are important for the interaction of CLIPs with microtubules.

In order to analyze the function and intracellular distribution of CLIP-115, we generated a number of deletion and/or point mutation constructs and coupled these to green fluorescent protein (GFP). Intact and mutant forms of CLIP-115 were tested for their conformation and microtubule binding capacity in transfected cells and in in vitro assays. The data indicate that the MTB domains in CLIP-115 are not sufficient to bind microtubules, but that the adjacent basic, serine rich regions are also required for efficient binding. Furthermore, we show that overexpressed CLIP-115 forms homodimers, which might utilize intermolecular disulfide bridges to stabilize different protein conformations. These findings suggest common and specific mechanisms by which CLIP functions are regulated.

MATERIALS AND METHODS

GST-CLIP115 constructs and antibodies

Full-length CLIP-115, the N-terminal region of the protein (amino acid residues 1-333) and the C-terminal region of a putative splice variant of CLIP-115 (residues 755-899/1026-1046), were fused to glutathione S-transferase (GST) using pGEX-2T and pGEX-3X (Pharmacia). GST fusion proteins were induced in BL21 *Escherichia coli* cells as described (Smith and Johnson, 1988) and purified on glutathione-Sepharose 4B beads (Pharmacia) according to the instructions of the manufacturer. For antibody production, bacterially expressed N- and C-terminal proteins were purified by preparative SDS-PAGE using a Bio-Rad Prep Cell. Pooled fractions of GST fusion proteins were dialyzed, concentrated using Centricon-30 (Amicon) and injected into New Zealand White rabbits in a suspension of Ribi Adjuvant (RIBI Immunochem Research). Sera from rabbits #2220 and #2221 are against the N terminus of CLIP-115, and sera from rabbits #2238 and #2239 are against its C terminus. Monoclonal anti-HA antibodies were purchased from BAbCO (Ca, USA), polyclonal anti-GFP antibodies were purchased from Clontech (Ca, USA).

Western blot analysis and immunoprecipitations

Brains and livers were obtained from adult mice and used for protein extract preparation immediately. Total protein extracts were prepared by homogenization in PBS/1% Triton X-100, in the presence of protease inhibitors (Boehringer Mannheim), followed by sonication and boiling in SDS sample buffer (Sambrook et al., 1989) in the presence or absence of DTT. Equal amounts of protein homogenate were analyzed on SDS-polyacrylamide gels (Sambrook et al., 1989). Western blots were blocked for 2 hours in PBS/2% BSA/0.05% Tween-20 and incubated with anti-GFP (1:2500) or anti-CLIP-115 (#2220, #2221, #2238 and #2239, all used at 1:1000) overnight at room temperature. After washing, the blots were incubated with secondary goat anti-rabbit antibodies, coupled to alkaline phosphatase (Sigma, 1:2000) and enzyme detection was carried out using the Sigma Fast BCIP/NBT system.

Immunoprecipitations were carried out on total protein extracts, prepared from transfected COS-1 cells. Cells were lysed in buffer containing 30 mM HEPES (pH 7.4), 100 mM KCl, 1% NP40, supplemented with protease inhibitors (Boehringer) and incubated at 4°C for 30 minutes, to depolymerize microtubules. All subsequent steps were also carried out at 4°C. Cell lysates were centrifuged at 13,000 rpm for 10 minutes, and the supernatant was precleared with

Protein A-agarose beads for 30 minutes, after which beads were removed by low speed centrifugation. Precleared supernatants were incubated with the anti-HA or -GFP antibodies for 2 hours, in the presence of Protein A-agarose beads. Immunoprecipitated material was collected on the beads, washed extensively and purified proteins were eluted in SDS-PAGE sample buffer. Precipitated proteins were analyzed on western blot as described above.

Transfections and immunocytochemistry

The fusion of full length CLIP-115 and that of truncated CLIP-115^{1-468} to green fluorescent protein (GFP) has previously been described (De Zeeuw et al., 1997). The same mammalian expression vectors (pEGFP-C1, pEGFP-C2 and pEGFP-C3; Clontech), were used to construct all other truncated forms of GFP-CLIP115. For the immunoprecipitation experiments, described below, we linked the HA epitope tag in-frame at the N terminus of CLIP-115. The integrity of the coding sequences was confirmed by nucleotide sequencing and western blot analysis of the transfected constructs. Transfections with CLIP-170 were carried out with human GFP-CLIP170 (a kind gift from Dr Griparic), or with a novel, brain-specific form of rat CLIP-170, linked in-frame to the HA epitope tag, or to EGFP (C. C. Hoogenraad, A. Akhmanova, F. Grosveld and N. Galjart, unpublished). COS-1 cells were transfected by the DEAE-dextran method (Sambrook et al., 1989). For western blotting, cultures were maintained for 40 hours after transfection, harvested and protein extracts prepared as described above. For immunofluorescence experiments, transfected cells were grown in Lab-Tek chamber slides (Nunc) for 18 or 40 hours after transfection. In the microtubule depolymerization experiment, 10 μM of nocodazole (Sigma) was added to the cells for 30 minutes prior to fixation. Cells were either fixed in 100% methanol/1 mM EGTA for 10 minutes at −20°C, or in 2% paraformaldehyde (20 minutes at room temperature, or at 37°C) followed by 5 minutes in 0.1% Triton X-100/PBS. Slides were blocked in 0.5% BSA/0.02% glycine/PBS and then labeled with anti-β-tubulin antiserum (1:200, Sigma) for 1 hour. After washing in 0.05% Tween-20/PBS sections were incubated with rhodamine-labeled sheep anti-mouse (1:20, Boehringer). Slides were mounted using Vectashield mounting medium (Vector laboratories) and 4',6-diamidino-2-phenylindole (DAPI; Sigma).

All signals were captured with a Leica DMRBE fluorescence microscope, equipped with a Hamamatsu C4880 DCC camera. To quantify the GFP fluorescence, cells were imaged using fixed data collection times: 100 milliseconds for highly expressing cells, 600 milliseconds for moderately expressing cells and 1200 milliseconds for cells expressing low levels of GFP fusion protein.

In vitro transcription-translation and in vitro microtubule binding assays

Constructs of GFP-CLIP115 for in vitro transcription and translation were generated using PCR (Saiki et al., 1988). The sense primer contained a T7 polymerase recognition sequence and 21 nucleotides complementary to GFP, including a translation initiation codon. The antisense primer contained translational stop sequences. PCR products were transcribed and translated in vitro using the TnT coupled transcription-translation system (Promega). Following a 1:2 dilution in PEM buffer (100 mM PIPES-KOH, 2 mM EGTA, 1 mM $MgCl_2$, pH 6.8), translation products were centrifuged at 25,000 *g* for 30 minutes at 4°C. The supernatant was split in two and incubated at room temperature for 30 minutes with or without 20 μg of purified, taxol stabilized bovine brain microtubules (Molecular Probes). The samples were layered over 100 μl of 30% sucrose in PEM and centrifuged at 25,000 *g* for 30 minutes at 20°C. Supernatant and pellets (washed once with PEM buffer) were analyzed by SDS-PAGE and western blotting. In some experiments, 2 mM ATP and/or 5 μM okadaic acid (Sigma) was added for 1 hour at 37°C, prior to the addition of the microtubules, to phosporylate GFP-CLIP115 proteins.

The ability of CLIP-115 from brain extracts to cosediment with microtubules was tested as described above. Brain extracts were made in PEM buffer and spun in a microcentrifuge for 30 minutes at 4°C and subsequently at 25,000 *g* for 30 minutes at 4°C. To induce microtubule polymerization 20 μM taxol (Sigma) and 0.5 mM GTP and/or 20 μg taxol-stabilized microtubules were added to 50 μl of the supernatant and incubated for 30 minutes at 37°C.

Physical characterization of CLIP-115

COS-1 cells, transfected with CLIP-115, were harvested in PBS, pelleted and resuspended in PBS/0.2% Triton-X100, containing protease inhibitors. After 30 minutes at 4°C the lysate was centrifuged at 13000 rpm for 10 minutes and the supernatant was recovered. The sedimentation coefficient, $S_{20,w}$, of overexpressed CLIP-115 was measured by sucrose gradient centrifugation of the COS-1 cell supernatants. Samples of 50 μl were loaded onto a 4-ml sucrose gradient (5-20% in PBS) and spun at 33000 rpm for 16 hours at 4°C, in a SW60 rotor (Beckman). Standard proteins and their sedimentation coefficients ($\times 10^{13}$ s) were: albumin (4.4), catalase (11.3) and thyroglobulin (19.0). Fractions of 0.3 ml were collected from the top of the gradient. They were analysed for standard protein content by the BCA protein assay (Smith et al., 1985) and by SDS-PAGE and western blotting for CLIP-115. The diffusion coefficient, $D_{20,w}$, was measured by gel filtration chromatography (SMART system, Pharmacia) using a superose 6 column (PC3.2/3.0 Pharmacia), equilibrated with PBS. A sample of 50 μl was loaded and 50 μl fractions were collected. They were analyzed by OD measurements at 280 nm for standard proteins and by SDS-PAGE and western blotting for CLIP-115. Standard proteins and their diffusion coefficients ($\times 10^7$ cm^2/second) were thyroglobulin (2.50), catalase (4.10) and albumin (6.90). The void volume (V_0) was measured with blue dextran. The native molecular mass of CLIP-115 was calculated as previously published (Bloom et al., 1988).

RESULTS

Comparison of CLIP-115 and -170 binding to microtubules

Human GFP-CLIP170 was recently shown to preferentially associate with the growing (plus) ends of microtubules in cultured cells, when expressed at low levels (Perez et al., 1999). To determine whether CLIP-115 behaves similarly, we transfected GFP-CLIP115 (De Zeeuw et al., 1997) and GFP-CLIP170 in COS-1 cells and compared the staining patterns of these proteins (Fig. 1). Cells were fixed at various time points after transfection, to analyze different levels of overexpression. We divided the cells into low, moderate and highly overexpressing cells, based on the intensity of the GFP signal (see Materials and Methods for the exposure times used). As shown in Fig. 1, both GFP-CLIP115 and GFP-CLIP170 accumulate at the distal ends of the microtubule network in cells expressing low amounts of fusion protein (Fig. 1A,B, compare to tubulin staining in 1C,D). In cells expressing moderate to high levels of GFP-CLIP115 (Fig. 1E,G, respectively), the fusion protein is detected over all microtubules and this even distribution of CLIP-115 eventually causes the bundling of the microtubule network into fibers, which are often circular. In contrast, in cells expressing medium levels of GFP-CLIP170, a number of aggregates of fusion protein appear at the cell periphery, which capture the distal ends of most microtubules and might be responsible for the longitudinal extension of the cell cytoplasm (Fig. 1F). In cells expressing high levels of GFP-CLIP170, the same, lengthwise extended cell morphology is seen, but the peripheral patches of GFP-CLIP170 are not

prominent, since microtubules are labeled along their entire length with the fluorescent fusion protein and circular bundles are also observed (Fig. 1H). The staining patterns described here for CLIP-170 are in agreement with previous data (Perez et al., 1999; Pierre et al., 1994). When we scored 100 cells with high levels of CLIP-115 for the presence of more prominent circular bundles versus peripheral microtubule aggregates, this revealed that 99 preferentially contained circular aggregates of microtubules and only one cell showed a microtubule aggregate at the periphery, while for 100 cells expressing high levels of CLIP-170 these numbers were 5 (mainly circular) and 95 (mainly peripheral), respectively. These results demonstrate that both CLIP-115 and CLIP-170 initially accumulate at the plus ends of microtubules, suggesting that this behavior is not a property unique to CLIP-170. However, when expressed at higher levels, CLIP-115 affects the microtubule network differently from full length CLIP-170.

To analyze whether CLIP-115 and -170 associate with the same distal ends of microtubules, COS-1 cells were cotransfected with GFP-CLIP115 and HA-tagged CLIP-170. Immunofluorescence analysis of fixed cells, expressing low amounts of both fusion proteins, reveals a striking colocalization of CLIP-115 and -170 within the microtubule arrays (Fig. 2), although at higher magnification it is clear that CLIP-115 and -170 staining is variable in intensity along single microtubule ends (Fig. 2D-F). Since CLIP-170 has been shown to mark the growing microtubule ends specifically (Perez et al., 1999), our results indicate that CLIP-115 has similar properties.

Microtubule binding properties of CLIP-115 in cultured cells

Having established that the microtubule-binding properties of CLIP-115 resemble those of CLIP-170, we next tested which domains directly regulate the interaction of CLIP-115 with microtubules. Therefore, a series of truncated forms of CLIP-115, in fusion with GFP, was generated and transiently overexpressed in COS-1 cells. Each mutant was scored for its microtubule binding capacity by direct (GFP) and indirect (anti-tubulin antiserum) immunofluorescence analysis. For these studies COS-1 cells were analyzed 18 and 40 hours after transfection to obtain low, medium and high levels of expression. In Fig. 3 the set of mutants is listed, together with a summary of their behavior in transfected cells. Selected examples of GFP-CLIP-microtubule interactions are shown in Fig. 4. Western blot analysis with a GFP antiserum showed that all fusion proteins are made in comparable quantities and that these proteins migrate according to their predicted molecular size, under reducing conditions (data not shown).

These mutagenesis and transfection studies show that the N-terminal domain of CLIP-115 is essential for microtubule binding, since the mutant lacking this head domain (GFP-CLIP115$^{852\text{-}1046}$) has a diffuse cytoplasmic

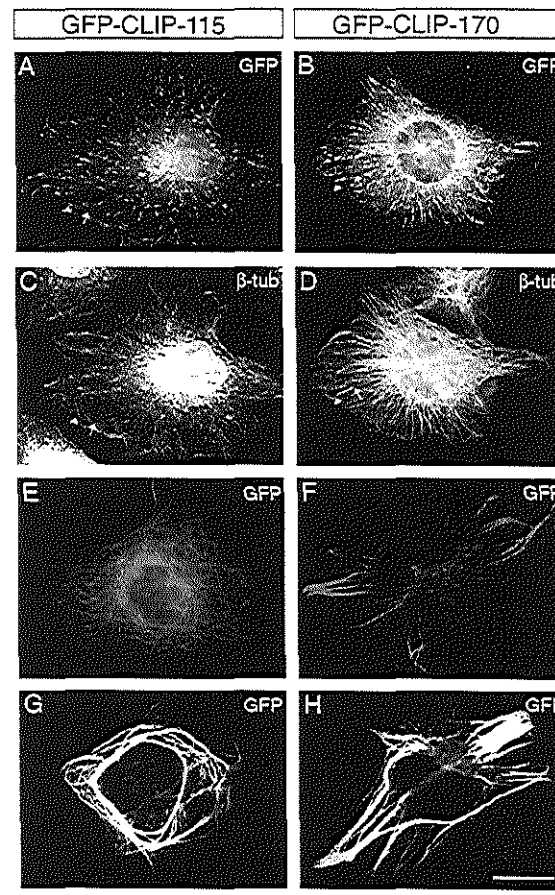

Fig. 1. Expression of GFP-CLIP115 and GFP-CLIP170 in transfected COS-1 cells. COS-1 cells were transfected with GFP-CLIP115 (A,C,E,G) or GFP-CLIP170 (B,D,F,H). Cells were processed 18 (A-D) or 40 hours (E-H) after transfection. After fixation and permeabilization, cells were incubated with anti-β-tubulin antibodies, followed by secondary, rhodamine-conjugated antibodies. In A and B, examples of transfected cells are shown with low levels of CLIP-115 and -170, respectively (the fluorescence signals were enhanced in order to visualize CLIP accumulation at distal ends). The tubulin staining pattern of the cells in A and B, is shown in C and D. Note the accumulation of both CLIPs at the plus ends of microtubules. For each protein one example of such an accumulation (indicated by the arrowheads) on the microtubule filament (indicated by arrows) is highlighted. In the other examples, medium (E,F) and high (G,H) levels of expression of CLIP-115 (E,G) and -170 (F,H) are shown. Exposure time for E-H: 100 milliseconds. The microtubule staining in E-H is not shown, since the distribution is identical to the GFP signal. Bar, 10 μm.

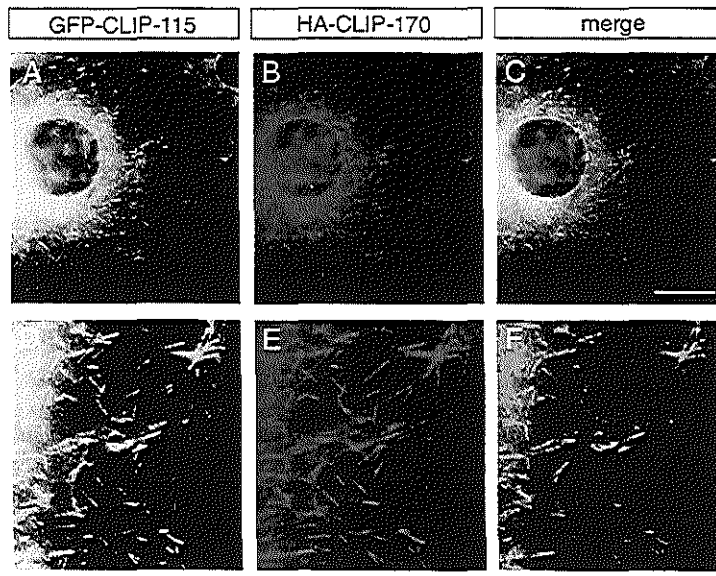

Fig. 2. Colocalization of CLIP-115 and -170 at microtubule distal ends. COS-1 cells were cotransfected with GFP-CLIP115 and HA-CLIP170 and cells expressing low levels of both proteins were processed for immunofluorescence, using a monoclonal anti-HA antibody, followed by rhodamine-conjugated anti-mouse IgG secondary antibodies. In (A,D) GFP-CLIP115 is detected, while in (B,E) HA-CLIP170 is visualized (the fluorescence signals were enhanced in order to visualize CLIP accumulation at distal ends). In (D-F) enlargements of A-C are shown. In (C,F) the green and red signals are merged to demonstrate that the CLIPs colocalize at the distal ends of microtubules, but that within a given microtubule tip there may be local differences in the level of each protein. Bar, 10 μm.

staining, while the GFP-CLIP115$^{1-359}$ mutant, containing the complete N-terminal domain but lacking the coiled-coil, decorates microtubules (Fig. 4A). Interestingly, the microtubule binding capacity of CLIP-115 appears to be greatly enhanced by the basic, serine-rich regions surrounding the MTB motifs, e.g. GFP-CLIP115$^{75-152/219-292}$, which has two MTB motifs but no surrounding sequences, only labels microtubules weakly and only in cells expressing high levels of the truncated protein, while GFP-CLIP115$^{75-292}$, which has the two MTB motifs and the basic region in between these domains, binds microtubules quite well (Fig. 4B).

CLIP-115 mutants with only a single MTB motif, have completely lost the capacity to bind to microtubules (e.g. GFP-CLIP115$^{219-292}$, Fig. 4C); they are cytosolic and weakly nuclear, like GFP. However, mutants containing an MTB motif with serine-rich domain 2 and/or 3, bind microtubules (e.g. GFP-CLIP115$^{147-292}$ and GFP-CLIP115$^{219-359}$, Fig. 3). These data indicate that the MTB motifs bind microtubules efficiently only in the presence of serine-rich domains 2 and/or 3. This conclusion is supported by the observation that GFP-CLIP115$^{75-221}$, which contains serine-rich domain 2 coupled to MTB domain 1, binds microtubules, although only in highly expressing cells, while GFP-CLIP115$^{1-152}$, a mutant containing serine rich-domain 1 and MTB motif 1, does not label the microtubules at all (Fig. 3).

The result that the basic regions surrounding the MTB motifs are required for efficient microtubule binding by CLIP-115, is novel, but it is likely to apply to CLIP-170 as well, since the N terminus of this protein is highly similar to that of CLIP-115. In addition, we find that, in the presence of the same basic serine-rich stretch, MTB domain 2 binds microtubules better than domain 1 (Fig. 3, compare GFP-CLIP-115$^{147-292}$ with -115$^{75-221}$), indicating that the MTB motifs 1 and 2 each have a slightly different affinity for microtubules. A similar result has been documented for CLIP-170 (Pierre et al., 1992). Taken together these results suggest that CLIP-115 and -170 have comparable microtubule binding properties and that similar mechanisms regulate the targeting of these proteins to the distal ends of the microtubule network.

As shown in Fig. 1, microtubule bundles are formed, when full length GFP-CLIP115 is overexpressed in COS-1 cells. Microtubule bundling is also induced when the truncated proteins GFP-CLIP115$^{1-899/1026-1046}$ and GFP-CLIP115$^{1-468}$ (De Zeeuw et al., 1997) are transfected, or when GFP-CLIP115$^{1-743}$ is overexpressed (see summary in Fig. 3). Coupling MTB domain 1 or 2 to serine rich domain 3 and a small coiled-coil region in GFP-CLIP115$^{75-152/286-470}$ and GFP-CLIP115$^{219-468}$, respectively, gives rise to strong microtubule binding proteins and to bundling of the microtubule filaments. The same constructs without serine rich domain 3, i.e. GFP-CLIP115$^{75-152/360-470}$ and GFP-CLIP115$^{219-292/360-470}$, are cytosolic and do not affect the microtubule network. Taken together, these studies suggest that microtubule bundling in transiently transfected COS-1 cells is induced when a high affinity microtubule binding site and the first part of the coiled-coil region of CLIP-115 are present within the GFP-CLIP115 mutant protein.

In vitro characterization of the microtubule binding domains of CLIP-115

An in vitro cosedimentation assay was employed to analyze the microtubule binding properties of selected GFP-CLIP115

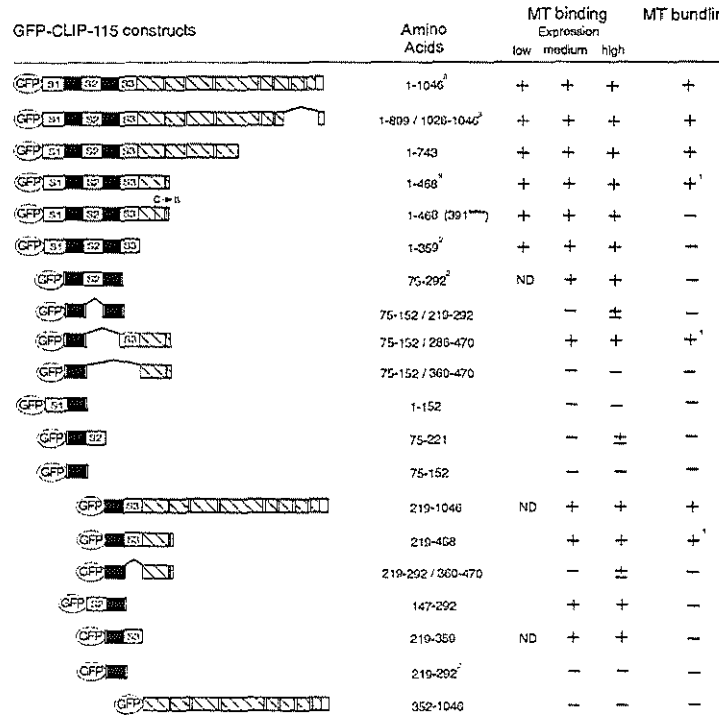

Fig. 3. GFP-CLIP115 deletion mutants and their microtubule binding capacity. COS-1 cells were transfected with the GFP-CLIP115 mutants, whose structure is depicted to the left (black bars: MTB domains, hatched bars: coiled-coil regions, S1-S3; basic, serine-rich regions). The numbering indicates which CLIP-115 amino acids are present in the GFP fusion proteins. C→S represents the point mutation, which changes cys[391] to serine. Cells were fixed at various time points after transfection to determine CLIP-115 binding to microtubules at different levels of expression. Staining with anti-β-tubulin antiserum, followed by rhodamine-conjugated secondary antibodies, was used to localize the microtubules. Microtubule binding and bundling activity in transfected cells with low, medium and high expression levels, as determined by GFP fluorescence (see Materials and Methods) are indicated (+ indicates good, ± indicates moderate and – means no binding or bundling). At low levels of expression accumulation of various mutant proteins to the microtubule distal ends was detected (indicated by +), while for other mutants tested, this was not detectable (ND). This is either due to an intrinsic incapacity to accumulate at the distal ends, or to a high cytoplasmic fluorescence, generated by the cytoplasmic pool of mutant proteins. [1]Bundling of microtubules, as observed in Fig. 8A. [2]These mutants are shown in Fig. 4. [3]These GFP-fusion proteins were made previously (de Zeeuw et al., 1997).

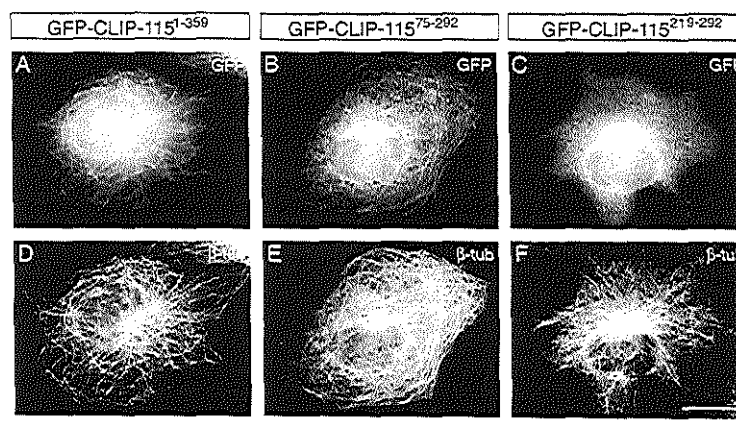

Fig. 4. Transient transfection of CLIP-115 mutant proteins in COS-1 cells. COS-1 cells, transfected with the GFP-CLIP115 mutants depicted in Fig. 3, were fixed 18 or 40 hours after transfection and stained with anti-β-tubulin antibodies (D-F). Shown here are the transfections with GFP-CLIP115[1-359] (A,D), GFP-CLIP115[75-292] (B,E) and GFP-CLIP115[219-292] (C,F). Note that the latter fusion protein, although it contains an MTB motif, fails to attach to microtubules, as judged by the tubulin staining. Bar, 10 μm.

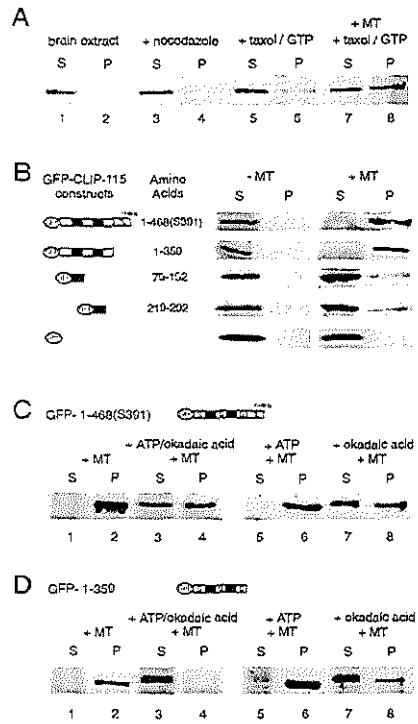

Fig. 5. In vitro microtubule binding of CLIP-115. (A) Soluble CLIP-115 from brain extracts was cosedimented with endogenous microtubules, either alone (lanes 1, 2), in the presence of nocodazole (lanes 3, 4), with GTP and taxol (lanes 5, 6), or with GTP and taxol-stabilized microtubules (+MT; lanes 7, 8). Microtubule binding is demonstrated by the appearance of CLIP-115 in the pellet (P), while lack of association results in the protein remaining in the supernatant (S). CLIP-115 was detected on western blot with anti-CLIP-115 antiserum (#2221, see Fig. 6). (B) Microtubule binding of in vitro translated GFP-CLIP115 constructs. The constructs used are indicated to the left. Western blots of the GFP-CLIP115 proteins, incubated with (+) or without (-) microtubules (MT), are shown to the right. Cosedimentation with microtubules is demonstated by the appearance of the GFP protein in the pellet (P). Coommassie staining of the gel was done to confirm pelleting of α- and β-tubulin (data not shown). (C,D) Microtubule binding of in vitro translated GFP-CLIP115$^{1\text{-}468(S391)}$ (C) and GFP-CLIP115$^{1\text{-}359}$ (D). Assays were performed with or without 2 mM ATP and/or 5 μM okadaic acid. Notice the different relative molecular mass of the proteins bound to MTs, versus those that are not bound.

mutants, in order to validate the GFP-microtubule experiments in COS-1 cells. We first looked whether brain-derived CLIP-115 could be cosedimented with microtubules. When brain microtubules are incubated with or without the microtubule depolymerizing agent nocodazole, hardly any endogenous CLIP-115 is pelleted (Fig. 5A, lanes 1-4). When brain microtubules are allowed to polymerize by adding GTP and taxol, a small fraction of endogenous CLIP-115 is pelleted along with the microtubules (Fig. 5A, lanes 5, 6). Further addition of purified, taxol-stabilized microtubules to the brain extracts results in more CLIP-115 cosedimentation with microtubules (Fig. 5A, lanes 7, 8). These data suggest that brain-derived CLIP-115 binds microtubules in vitro. We subsequently tested whether different in vitro translated GFP-CLIP115 constructs (Fig. 5B) cosediment with taxol-stabilized microtubules. However, GFP-CLIP115$^{1\text{-}468}$ is already pelleted without addition of microtubules (data not shown), indicating it forms protein aggregates in vitro. GFP-CLIP115$^{1\text{-}468(S391)}$ and GFP-CLIP115$^{1\text{-}359}$ on the other hand, remain soluble and cosediment efficiently with microtubules, while fragments with only the first or second MTB domain hardly come down (Fig. 5B). These results correlate well with the transfection data, and suggest again that the MTB motifs of CLIP-115 alone do not have the ability to bind to microtubules with high affinity.

It has been shown that binding of CLIP-170 to microtubules in vitro is inhibited by phosphorylation (Rickard and Kreis, 1991). To investigate whether this applies to CLIP-115, we used the constructs GFP-CLIP115$^{1\text{-}468(S391)}$ (Fig. 5C) and GFP-CLIP115$^{1\text{-}359}$ (Fig. 5D) for in vitro microtubule binding, in the presence of 2 mM ATP and/or 5 μM of the serine phosphatase inhibitor okadaic acid, a concentration sufficient to inhibit both type 1 and 2A phosphatases (Cohen et al., 1989). Under these conditions none of the GFP-CLIP115$^{1\text{-}359}$ (Fig. 5D, lanes 3, 4) and ~50% of the GFP-CLIP115$^{1\text{-}468(S391)}$ (Fig. 5C, lanes 3, 4) proteins bind microtubules. The effect of okadaic acid alone is similar to that of ATP and okadaic acid (Fig. 5C and D, compare lanes 3, 4 with lanes 7, 8). Addition of ATP alone has no effect on cosedimentation with microtubules (Fig. 5C and D, lanes 1, 2 and 5 and 6). Strikingly, the proteins detected in the supernatant, i.e. the non-bound fraction, have an increased molecular mass compared to microtubule-sedimented proteins, suggesting they are phosphorylated forms of CLIP-115. These results are consistent with the hypothesis that phosphorylation of CLIP-115 negatively influences the capacity of the protein to bind to microtubules. Dephosphorylation via an okadaic acid-sensitive phosphatase appears to allow the binding of CLIP-115 to microtubules.

Dimerization and immunological detection of CLIP-115

CLIP-170 has recently been shown to form parallel homodimers, in which the N-terminal head is separated from the C-terminal tail by an elongated coiled-coil domain, which contains only two kinks (Scheel et al., 1999). Like CLIP-170, CLIP-115 contains stretches of residues that are predicted to form α-helical coiled-coils; they run from amino acid 360 towards its C terminus (Fig. 6A). Based on its type of coiled-coil (Lupas, 1996) and on its similarity to CLIP-170, we have proposed that CLIP-115 also forms parallel homodimers (De Zeeuw et al., 1997). To validate this hypothesis we determined the state of oligomerization of COS-1-cell transfected CLIP-115, by calculating the native molecular mass of the protein, based on measurements of diffusion ($D_{20,w}$) and sedimentation ($S_{20,w}$) coefficients. The sedimentation coefficient of

transfected CLIP-115, determined by sucrose gradient centrifugation, is 6.45 S (range: 5.70-7.20) and the diffusion coefficient, measured by gel filtration, is 2.59×10^7 cm^2/s (range: 2.54-2.62). Calculation of the native molecular mass of CLIP-115 from these values, according to the Svedberg equation (Bloom et al., 1988), gives a value of 220 kDa (range: 190-250). This corresponds well to a homodimerized form of CLIP-115. As a second test for CLIP-115 dimerization, we transfected COS-1 cells with HA-CLIP115, with GFP-tagged CLIP-115, or with a combination of these two proteins and determined whether in the latter transfection heterodimers could be detected by co-immunoprecipitation with anti-HA, or anti-GFP, antisera. As shown in Fig. 6B, in the double transfected cells, HA-CLIP115 is coprecipitated with GFP-CLIP115, using the anti-GFP antiserum and GFP-CLIP115 is coprecipitated with HA-tagged CLIP-115, using the anti-HA antibodies. Taken together, these data suggest that native CLIP-115 is a homodimer and that HA-CLIP115 and GFP-CLIP115 form heterodimers, most likely via an interaction in their common coiled-coil regions.

Analysis of the coiled-coil region of CLIP-115 reveals it to be more often interrupted by non-helical regions than the same domain of CLIP-170 (data not shown), suggesting that the rod domain of CLIP-115 may be more flexible than the one of CLIP-170. Of the 7 cysteine residues within the CLIP-115 rod (see Fig. 6A), cysteines at positions 391, 725, 801 and 860 are within presumptive coiled-coil stretches and could potentially be used to establish intermolecular disulfide bridges between CLIP-115 monomers, to stabilize coiled-coils. To test this hypothesis, three GST-fusion proteins were constructed and expressed in bacteria (Fig. 6C) and analyzed by SDS-PAGE, both under non-reducing and under reducing conditions (Fig. 6D). These results show that GST-CLIP115 and GST-CLIP115$^{755\text{-}899/1026\text{-}1046}$ migrate at a position approximately twice the size of the respective proteins, measured under reducing conditions, suggesting that both fusion proteins exist

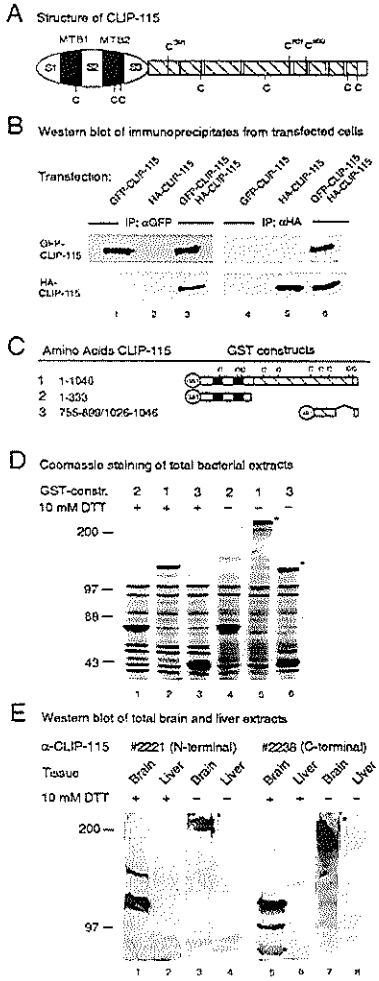

Fig. 6. Structure and immunological detection of CLIP-115.
(A) Structure of CLIP-115. Depicted is a CLIP-115 monomer, which is characterized by an N-terminal domain (ellipse), with two MTB motifs (black bars), surrounded by basic serine-rich regions (S1, S2, S3). The short C terminus (white bar) is connected to the N-terminal domain by a long rod, in which several coiled-coil stretches are present (hatched bars), which are interrupted by small regions with a low probability to form a coiled-coil (white areas between hatched bars). The rod domain of CLIP-170 contains less of these latter regions (not shown). The positions of all cysteines within CLIP-115 are indicated: cysteines pointing upward are conserved in CLIP-115 forms from different organisms and they are in a presumptive coiled-coil stretch. Cysteines pointing downward are either not conserved (725 and 996; see (Hoogenraad et al., 1998), or they are not in a coiled-coil (MTB-residues and cysteines 526 and 1017).
(B) Immunoprecipitation of tagged, transfected CLIP-115. COS-1 cells were transfected with a cDNA encoding either GFP-CLIP115 or HA-CLIP115, or with both cDNAs and protein homogenates were immunoprecipitated (IP) with monoclonal anti-GFP (αGFP) or anti-HA (αHA) antibodies. The precipitated proteins were resolved by SDS-PAGE, blotted and immunoprecipitated material was detected with the polyclonal anti-CLIP115 antiserum (#2221) described below. (C) Structure of bacterially expressed GST-CLIP115 proteins. The amino acid portions of CLIP-115, that were cloned in-frame with GST, are indicated to the left. Cysteine residues, MTB motifs (black boxes) and coiled-coil region (hatched box) are indicated. The presumptive alternatively spliced rat sequence (De Zeeuw et al., 1997) is indicated by a line. (D) SDS-polyacrylamide gel electrophoresis of full length and truncated GST-CLIP115 constructs. Bacterial extracts of construct 1 (GST-CLIP115: lanes 2 and 5), 2 (GST-CLIP115$^{1\text{-}333}$: lanes 1 and 4) and 3 (GST-CLIP115$^{755\text{-}1046}$: lanes 3 and 6) were run with (+) or without (−) DTT. After electrophoresis, gels were fixed and stained with Coomassie brilliant blue. Dimers are indicated by an asterisk. Molecular mass markers are on the left. (E) Western blot analysis of brain and liver extracts, incubated with antibodies against GST-CLIP115$^{1\text{-}333}$ (#2221) or GST-CLIP115$^{755\text{-}1046}$ (#2238). Dimers of CLIP-115 are marked by an asterisk. Molecular mass markers are on the left.

as disulfide linked dimers and that cysteines 801 and/or 860, which are present in GST-CLIP115$^{755\text{-}899/1026\text{-}1046}$, are able to form intermolecular disulfide bonds.

To investigate whether CLIP-115 undergoes disulfide-mediated linkage in tissue extracts, western blots of mouse brain and liver homogenates, run under non-reducing and reducing conditions, were incubated with novel anti-CLIP-115 antibodies, raised against GST-CLIP115$^{1\text{-}333}$ (#2220 and #2221) and GST-CLIP115$^{755\text{-}899/1026\text{-}1046}$ (#2238 and #2239). Under reducing conditions, all antisera react most strongly with a protein of approximately 115 kDa (Fig. 6E, lanes 1, 5 and data not shown), that is present in the brain extract and which represents CLIP-115. In the absence of DTT, only protein complexes larger than 200 kDa are detected (#2221; Fig. 6E, lane 3 and #2238; Fig. 6E lane 7), indicating that CLIP-115 may form intermolecular disulfide bridges. However, whether these bridges are formed in vivo, or after homogenization of the tissue, and whether they occur between CLIP-115 monomers, or between CLIP-115 and other proteins, can not be determined from this analysis.

The novel antisera against CLIP-115 also react with proteins, different in size compared to CLIP-115. Proteins of approximately 100 kDa and 80 kDa, recognized both by #2238 (Fig. 6E, lane 5) and #2239 (data not shown), may be C-terminal proteolytic cleavage forms or alternative translation initiation products of CLIP-115. Interestingly, C-terminal fragments of similar size are also recognized in a rat brain lysate by affinity-purified anti-peptide antibodies (De Zeeuw et al., 1997), as well as by a commercially available monoclonal antibody, raised against the C terminus of CLIP-115 (Transduction Laboratories, USA). The protein of ~160 kDa, recognized by #2220 (data not shown) and #2221 (Fig. 6E, lane 1) antisera, represents a brain-specific isoform of rat CLIP-170 (C. C. Hoogenraad, A. Akhmanova, F. Grosveld and N. Galjart, unpublished). The cross reaction, which is due to the fact that the antibodies were raised against the region of CLIP-115 that includes the highly conserved MTB-domains, was confirmed by performing western blot and immunoprecipitation analyses of COS-1 cells, transiently transfected with rat brain CLIP-170 (data not shown). In the same experiments it was shown that CLIP-170, which has 2 cysteines within its coiled-coil domain (Pierre et al., 1992), forms intermolecular disulfide bridges, as does CLIP-115. This explains the western blot results of Fig. 6E, lane 3, where, under non-reducing conditions, brain CLIP-170 is not detected as a monomer.

Cysteine^{391} controls microtubule bundling induced by CLIP-115 deletion mutants

The results presented here indicate that CLIP-115 and -170 monomers might be linked by intermolecular disulfide bridges. The bacterial fusion proteins suggest that in the case of CLIP-115 C-terminal cysteines could be involved in this process. We therefore analyzed whether N-terminal cysteine residues could also contribute to disulfide linkage of CLIP-115 monomers. A series of GFP-deletion mutants (Fig. 7A), harvested from transfected COS-1 cells, was electrophoresed under reducing and non-reducing conditions, blotted and probed with a GFP antiserum. As shown in Fig. 7B, under non-reducing conditions the molecular mass of CLIP-115 mutants with the complete coiled-coil domain is approximately twice that of the same mutants, run under reducing conditions (Fig. 7B, lanes 3-8). Because in each transfection only a protein of twice the size is detected in the non-reduced samples, these data argue against the formation of non-specific disulfide links between GFP-CLIP115 and other proteins in the extract. Instead the data indicate that CLIP-115 homodimers are formed, which are then stabilized by intermolecular disulfide bridges.

When CLIP-115 mutants, in which residue cys^{391} is the only coiled-coil cysteine present, are transfected to COS-1 cells, the mutant proteins are in part linked by disulfide bridges (Fig. 7B, lanes 9, 10, 17, 18). Replacement of cys^{391} residue with serine, gives rise to a protein (GFP-CLIP115$^{1\text{-}468(S391)}$) that migrates as a monomer under non-reducing conditions (Fig. 7B, lanes 11, 12). In addition, proteins with the complete N-terminal domain of CLIP-115, but without coiled-coils (GFP-CLIP115$^{1\text{-}359}$) or with only the MTB-domains (GFP-CLIP115$^{75\text{-}152}$, GFP-CLIP115$^{219\text{-}292}$, and GFP-CLIP115$^{219\text{-}359}$) migrate as monomers and do not form intermolecular disulfide bridges. Taken together, these data show that cys^{391} may be involved in intermolecular disulfide bridge formation.

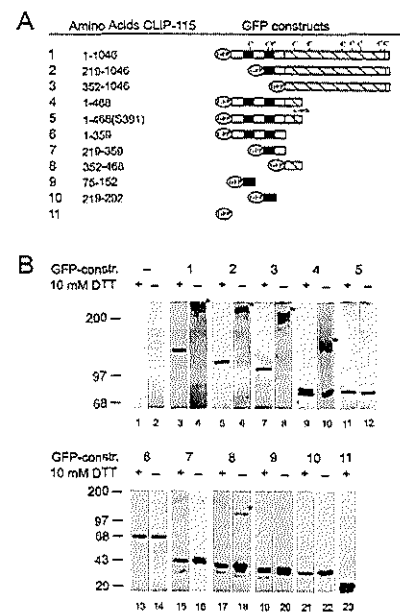

Fig. 7. Disulfide bridges in CLIP-115 mutants from transfected COS-1 cells. (A) Structures of GFP-CLIP115 constructs. The scheme is set up as in Fig. 3. (B) Western blot of COS-1 cell extracts transfected with GFP-CLIP115 constructs. Six (upper) and ten (lower) percent SDS-polyacrylamide gels were run with (+) or without (–) DTT. The GFP constructs were detected using anti-GFP antibodies. Dimers of CLIP-115 are indicated by an asterisk. Molecular mass markers are on the left. Note the aberrant migration of 'dimeric' CLIP-115$^{352\text{-}468}$ in lane 18.

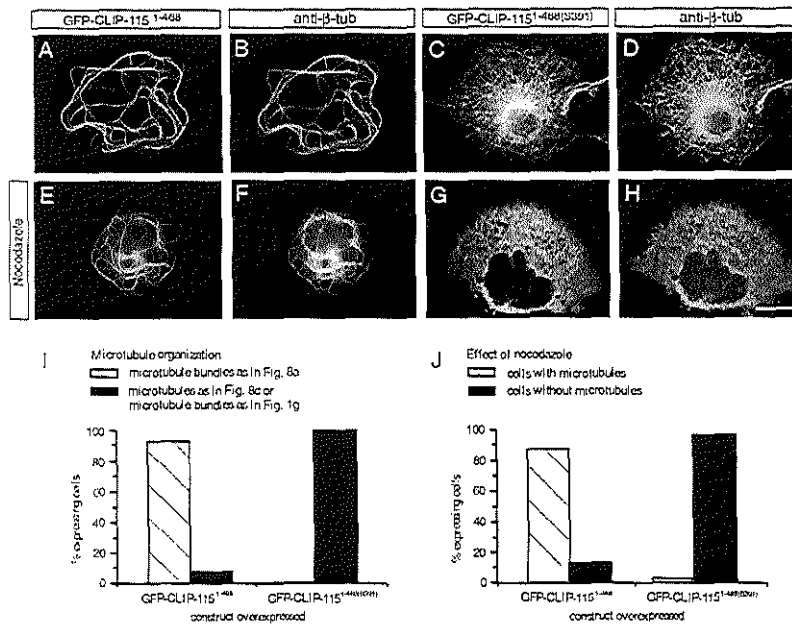

Fig. 8. Influence of cys[391] on microtubule bundling by CLIP-115 mutants in transfected COS-1 cells. (A-H) COS-1 cells were transfected with GFP-CLIP115$^{1-468}$ (A,B,E,F), or GFP-CLIP115$^{1-468(S391)}$ (C,D,G,H) and processed for GFP (A,E,C,G) or β-tubulin (B,F,D,H) staining. (E-H) Cells were treated with 10 μM nocodazole for 30 minutes prior to fixation. Data collection time for capture of the GFP fluorescence is identical in all pictures. Note that GFP-CLIP115$^{1-468(S391)}$ binds microtubules efficiently, but fails to cause bundling of the network, in sharp contrast to GFP-CLIP115$^{1-468}$, which causes bundling at low expression levels. Bar, 10 μm. (I,J) Microtubule bundling and nocodazole resistance effects, documented in A-H, were quantified by counting 100 transfected cells for each construct, with and without nocodazole.

whereas the 3 cysteine residues within the MTB domains are not.

The mutant protein GFP-CLIP115$^{1-468}$ causes a profound bundling of the microtubule network in transfected cells (De Zeeuw et al., 1997). This effect is already seen at low expression levels (Fig. 8A,B). Surprisingly, GFP-CLIP115$^{1-468(S391)}$, which can not form intermolecular disulfide bonds, binds microtubules well but does not cause bundling of the network (Fig. 8C,D). Nocodazole treatment of cells, separately transfected with each construct, demonstrates that cells expressing GFP-CLIP115$^{1-468}$ resist microtubule depolymerization better than cells transfected with GFP-CLIP115$^{1-468(S391)}$ (Fig. 8E,F and G,H, respectively). Both the bundling of microtubules and their resistance to nocodazole were quantified in cells expressing the two mutants (Fig. 8I,J), which demonstrates the differential effect of these two fusion proteins on the microtubule network. Taken together, these data indicate that the bundling and nocodazole resistance of microtubules, induced by the GFP-CLIP115$^{1-468}$ mutant, are mediated by cys[391]. One possible explanation for the specific bundling of the microtubule network in cells expressing GFP-CLIP115$^{1-468}$ is that intermolecular disulfide-bridges stabilize CLIP-115 homodimers and/or multimers, which in turn create a high affinity microtubule binding lattice.

DISCUSSION

CLIP-115 is a member of a small, emerging family of microtubule binding proteins with two MTB motifs and a long coiled-coil region, to which CLIP-170 and D-CLIP-190 also belong. CLIP-115 is interesting because of its restricted expression pattern, its association in the brain with microtubules and a highly specialized membranous organelle, the DLB, and because the gene encoding CLIP-115 is hemizygously deleted in patients with WS. In addition, CLIP-115 lacks a prominent, cysteine-rich tail domain, which distinguishes CLIP-170 and -190. To correlate CLIP-115 function and structure, we investigated what mechanisms regulate its interaction with microtubules in cultured cells and what features distinguish it from CLIP-170.

The N-terminal domain of CLIP-115 is characterized by two MTB motifs and three basic, serine-rich regions. We show that efficient microtubule binding activity requires the presence of

at least one MTB motif together with basic, serine-rich domain 2 or 3. This indicates that the in vivo interaction of CLIP-115 with microtubules is mediated by the combined action of relatively weak MTB motifs and elements in the sequence surrounding these motifs. This is comparable to the mode of microtubule binding by tau proteins, which have three (or four) 31-residue MTB repeats, that bind microtubules tightly only in conjunction with regions flanking the repeats (Gustke et al., 1994). Like in tau, the basic residues in the serine-rich domains of CLIP-115 could function as positively charged amino acid stretches, which engage in electrostatic interactions with the acidic tubulin molecule(s), thereby acting as 'jaws' for the MTB motifs and allowing a tight binding of CLIP-115 to microtubules.

The capacity of CLIP-115 to interact with microtubules is controlled by phosphorylation. This is analogous to the situation for CLIP-170 (Rickard and Kreis, 1991), $p150^{Glued}$ (Farshori and Holzbaur, 1997) and tau (Drewes et al., 1998), which are also released from microtubules upon phosphorylation. The negatively charged phosphate groups in the serine rich regions might simply mask the basic stretches and prevent an efficient interaction with microtubules. However, for tau the effect of phosphorylation on microtubule binding at sites flanking the MTB repeats is weak, while phosphorylation by MARK at the single ser^{261} within the repeat, completely abolishes tau binding to microtubules (Drewes et al., 1998). A MARK consensus phosphorylation site is not present in CLIP-115, but it remains possible that phosphorylation within the MTB motif is the critical event for microtubule release. Site-specific phosphorylation of the CLIPs might underlie their differential distribution over the microtubule network.

As shown here, at low expression levels, CLIP-115 and -170 colocalize at the distal ends of microtubules, indicating that CLIP-115, like CLIP-170, has a preference for microtubule plus ends. Since these proteins do not associate with each other (data not shown), CLIP-115 is targeted to the growing ends by a CLIP-170-independent mechanism. In fact, the minimal truncated CLIP-115 construct that could be detected at these ends contains 2 MTB domains and the surrounding basic, serine-rich regions. Thus, a monomeric CLIP-115 mutant is capable of plus-end accumulation, similar to what has been reported for CLIP-170 (Perez et al., 1999). High levels of overexpression of full length CLIP-115 and -170, however, result in differently organized microtubule cytoskeletons. Interestingly, a CLIP-170 mutant lacking the C-terminal metal binding motif distributes evenly over microtubules, when overexpressed (Pierre et al., 1994) and appears to have a similar distribution and effect on microtubule organization in overexpressing cells when compared to GFP-CLIP115. Therefore, the differential organization of the microtubule network in cells, transfected with CLIP-115 or -170, could be in part related to the lack of a cysteine-rich, C-terminal domain in the first.

The amino acid residues within a single heptad repeat unit in an α-helix are designated a through g, with a and d being generally hydrophobic and forming the coiled-coil interface (i.e. facing inward), while b, c, e, f and g are often hydrophilic and form the solvent-exposed part of the coiled-coil (i.e. facing outward). In a parallel coiled-coil, a cysteine at position a or d, i.e. inside the α-helix of the coiled-coil domain, could form a disulfide bond with a cysteine in the neighbouring molecule. In vitro, these disulfide bridges between coiled-coils have been shown to occur, for example in vimentin, where they stabilize coiled-coil interactions (Rogers et al., 1996). Of the 7 cysteine residues present in the coiled-coil region of CLIP-115, residues 391, 801 and/or 860 were shown to be involved in disulfide

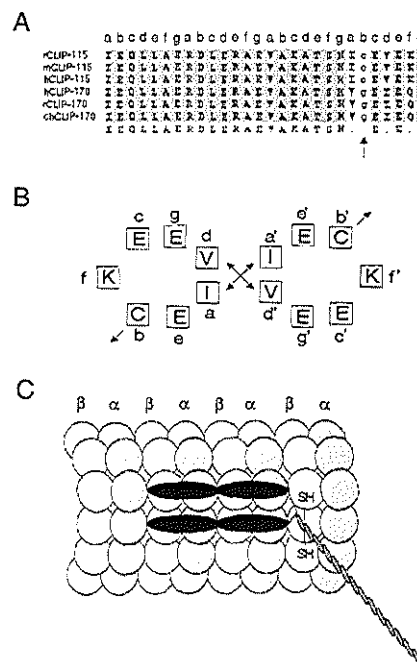

Fig. 9. Model for CLIP-115 structure. (A) Amino acid comparison of the initial segment of the coiled-coil domain of CLIP-115 and -170 proteins from different organisms, demonstrates that this region is highly conserved, except for cys^{391}. The position of heptad repeat residues (A-G) is indicated above the comparison. The position of cys^{391} in CLIP-115, which is replaced by glycine in CLIP-170, is indicated by an arrow. M = mouse; r = rat; h = human; ch = chicken. (B) Helical wheel representation of the putative heptad repeat region surrounding cys^{391}. Note that this residue points outward. (C) Hypothetical model of the mode of binding of CLIP-115 to microtubules. The α- and β-tubulin subunits within part of a microtubule polymer are indicated. In CLIP-115, each MTB motif with surrounding basic, serine rich region, is indicated by an ellipse and the rod domain points away from the microtubule, towards the reader. The free SH-groups from cys^{391} are indicated. It needs to be emphasized that other modes of microtubule binding are possible and that no specificity of CLIP-115 for either α- or β-tubulin has been drawn. However, binding of a CLIP-115 homodimer is likely to be directional, i.e. the complete N-terminal domain will point in one direction. With four MTB domains, CLIP-115 is predicted to have a strong preference for (sheets of) protofilaments and not for free tubulin.

bond formation in vitro. Interestingly, the cysteines at positions 801 and 860 have an inward facing position and could therefore stabilize homodimers of CLIP-115. Whether these disulfide bridges are formed in vivo remains to be demonstrated, since it is generally believed that the cytoplasmic environment inhibits crosslinks of this type. However, keratins of the suprabasal layer of the esophageal epithelium form an exception to this rule, since these intermediate filament proteins have been shown to undergo extensive disulfide crosslinking in vivo, in their coiled-coil region (Pang et al., 1993). Thus, although we can not exclude the possibility that the disulfide crosslinks on CLIP dimers, observed in our experiments, may have arisen when exposing CLIP molecules to the oxidizing environment of the test tube, these crosslinks might actually serve to stabilize CLIP dimers in vivo.

Cys^{391}, which is located within the initial segment of the α-helical coiled-coil region of CLIP-115, endows the CLIP-115^{1-468} mutant protein with a profound microtubule bundling capacity. Comparison of the initial α-helical coiled-coil segments of all CLIP-115 and CLIP-170 proteins cloned to date, shows that this portion is quite well conserved, except for cys^{391} itself, which is replaced by glycine in CLIP-170 (Fig. 9A). Thus, cys^{391} confers a property, which is unique to CLIP-115. In contrast to the cysteines at positions 801 and 860, cys^{391} is in position 'b' of the heptad repeat unit and would face the outside of the predicted coiled-coil dimer (Fig. 9B). Cysteines in the intermediate filament protein vimentin, which occupy the same position, were shown to crosslink coiled-coil dimers into multimers in vitro (Rogers et al., 1996). Thus, two outward facing cys^{391} residues in a GFP-$CLIP115^{1-468}$ homodimer might generate CLIP-115^{1-468} multimers, by forming disulfide bridges with the free cys^{391} of neighboring dimer molecules. Such an arrangement would explain the profound bundling of microtubules, observed in GFP-$CLIP115^{1-468}$ expressing cells and the lack of bundling in cells expressing mutants without cys^{391}. However, as mentioned above, disulfide bridges do not normally form in the cytoplasm. Because of this reason and because we have only tested the influence of cys^{391} in the CLIP-115^{1-468} mutant, it remains to be shown that cys^{391} is critical for multimerization of CLIP-115 in vivo.

Microtubules are cytoskeletal filaments, composed of heterodimers of α- and β-tubulin. Assembly of the tubulin dimer requires a specific chaperonin supercomplex, which also contains a set of tubulin folding cofactors (Tian et al., 1996). Alf1p is the yeast ortholog of mammalian cofactor b; it associates with α-tubulin through a single MTB motif that is similar to the MTBs present in the CLIPs (Feierbach et al., 1999). These results raise the possibility that the MTB-motifs found in CLIP-115 and -170 also have an intrinsic preference for the α-tubulin subunit, within the context of the microtubule polymer. This hypothesis is supported by the fact that each dimeric head domain of CLIP-170 (with four MTB regions) binds to microtubules in vitro with a stoichiometry of one dimeric head to four tubulin heterodimers, while one monomeric head domain binds two tubulin heterodimers (Scheel et al., 1999). If the MTB motifs in CLIP-170 had equal preference for either α- or β-tubulin, each monomeric molecule would be expected to bind one α/β-tubulin heterodimer, leading to ratios of 1:2 and 1:1, respectively.

A simple, hypothetical model for the mode of interaction of CLIP-115 with microtubules, is presented in Fig. 9C. The model predicts that if all four MTB motifs and surrounding 'jaws' are to be accomodated on a microtubule, binding can only occur on microtubule oligomers and/or assembled filaments. At the same time, the binding of all four MTB regions of a CLIP-115 dimer to microtubules provides stabilization to tubulin protofilaments and, laterally, to tubulin sheets. We hypothesize that the specificity of the binding of CLIP-115 to microtubules originates in the MTB motifs, while the affinity for microtubules is enhanced by the serine-rich regions. Binding might be cooperative, i.e. once the first MTB motif (perhaps motif 2, which has a higher affinity than motif 1) recognizes its specific target on the microtubule, the second MTB motif and the 'jaws' enhance a further and tighter binding. Local clustering of CLIP-115 on particular sites of dendritic microtubules (De Zeeuw et al., 1997) may then lead to the association of CLIP-115 dimers with other proteins.

We thank Dr L. Griparic for sending us the human GFP-CLIP170 construct and Dr D. van Gent for help with the gel filtration experiments. This research was supported by grants from the Netherlands Organization for Scientific Research (NWO; GB-MW 903-68-361), the Life Sciences Foundation (SLW; 805.33.310) and the Royal Dutch Academy of Sciences (KNAW).

REFERENCES

Bellugi, U., Bihrle, A., Jernigan, T., Trauner, D. and Doherty, S. (1990). Neuropsychological, neurological, and neuroanatomical profile of Williams syndrome. *Am. J. Med. Genet. Suppl.* **6**, 115-125.

Bloom, G. S., Wagner, M. C., Pfister, K. K. and Brady, S. T. (1988). Native structure and physical properties of bovine brain kinesin and identification of the ATP-binding subunit polypeptide. *Biochemistry* **27**, 3409-3416.

Cohen, P., Klumpp, S. and Schelling, D. L. (1989). An improved procedure for identifying and quantitating protein phosphatases in mammalian tissues. *FEBS Lett.* **250**, 596-600.

De Zeeuw, C. I., Hertzberg, E. L. and Mugnaini, E. (1995). The dendritic lamellar body: a new neuronal organelle putatively associated with dendrodendritic gap junctions. *J. Neurosci.* **15**, 1587-1604.

De Zeeuw, C. I., Hoogenraad, C. C., Goedknegt, E., Hertzberg, E., Neubauer, A., Grosveld, F. and Galjart, N. (1997). CLIP-115, a novel brain-specific cytoplasmic linker protein, mediates the localization of dendritic lamellar bodies. *Neuron* **19**, 1187-1199.

Diamantopoulos, G. S., Perez, F., Goodson, H. V., Batelier, G., Melki, R., Kreis, T. E. and Rickard, J. E. (1999). Dynamic localization of CLIP-170 to microtubule plus ends is coupled to microtubule assembly. *J. Cell Biol.* **144**, 99-112.

Drewes, G., Ebneth, A. and Mandelkow, E. M. (1998). MAPs, MARKs and microtubule dynamics. *Trends Biochem. Sci.* **23**, 307-311.

Dujardin, D., Wacker, U. I., Moreau, A., Schroer, T. A., Rickard, J. E. and De Mey, J. R. (1998). Evidence for a role of CLIP-170 in the establishment of metaphase chromosome alignment. *J. Cell Biol.* **141**, 849-862.

Farshori, P. and Holzbaur, E. L. (1997). Dynactin phosphorylation is modulated in response to cellular effectors. *Biochem. Biophys. Res. Commun.* **232**, 810-816.

Feierbach, B., Nogales, E., Downing, K. H. and Stearns, T. (1999). Alf1p, a CLIP-170 domain-containing protein, is functionally and physically associated with alpha-tubulin. *J. Cell Biol.* **144**, 113-124.

Gustke, N., Trinczek, B., Biernat, J., Mandelkow, E. M. and Mandelkow, E. (1994). Domains of tau protein and interactions with microtubules. *Biochemistry* **33**, 9511-9522.

Hirokawa, N. (1998). Kinesin and dynein superfamily proteins and the mechanism of organelle transport. *Science* **279**, 519-526.

Hoogenraad, C. C., Eussen, B. H., Langeveld, A., van Haperen, R., Winterberg, S., Wouters, C. H., Grosveld, F., De Zeeuw, C. I. and Galjart, N. (1998). The murine CYLN2 gene: genomic organization, chromosome localization, and comparison to the human gene that is located

within the 7q11.23 Williams syndrome critical region. *Genomics* **53**, 348-358.

Lantz, V. A. and Miller, K. G. (1998). A class VI unconventional myosin is associated with a homologue of a microtubule-binding protein, cytoplasmic linker protein-170, in neurons and at the posterior pole of Drosophila embryos. *J. Cell Biol.* **140**, 897-910.

Li, H. P., Liu, Z. M. and Nirenberg, M. (1997). Kinesin-73 in the nervous system of Drosophila embryos. *Proc. Nat. Acad. Sci. USA* **94**, 1086-1091.

Lupas, A. (1996). Coiled coils: new structures and new functions. *Trends Biochem. Sci.* **21**, 375-382.

Meng, X., Lu, X., Li, Z., Green, E. D., Massa, H., Trask, B. J., Morris, C. A. and Keating, M. T. (1998). Complete physical map of the common deletion region in Williams syndrome and identification and characterization of three novel genes. *Hum. Genet.* **103**, 590-599.

Pang, Y. Y., Schermer, A., Yu, J. and Sun, T. T. (1993). Suprabasal change and subsequent formation of disulfide-stabilized homo- and hetero-dimers of keratins during esophageal epithelial differentiation. *J. Cell Sci.* **104**, 727-740.

Perez, F., Diamantopoulos, G. S., Stalder, R. and Kreis, T. E. (1999). CLIP-170 highlights growing microtubule ends in vivo. *Cell* **96**, 517-527.

Pierre, P., Scheel, J., Rickard, J. E. and Kreis, T. E. (1992). CLIP-170 links endocytic vesicles to microtubules. *Cell* **70**, 887-900.

Pierre, P., Pepperkok, R. and Kreis, T. E. (1994). Molecular characterization of two functional domains of CLIP-170 in vivo. *J. Cell Sci.* **107**, 1909-1920.

Rickard, J. E. and Kreis, T. E. (1990). Identification of a novel nucleotide-sensitive microtubule-binding protein in HeLa cells. *J. Cell Biol.* **110**, 1623-1633.

Rickard, J. E. and Kreis, T. E. (1991). Binding of pp170 to microtubules is regulated by phosphorylation. *J. Biol. Chem.* **266**, 17597-17605.

Rickard, J. E. and Kreis, T. E. (1996). CLIPs for organelle-microtubule interactions. *Trends Cell Biol.* **6**, 178-182.

Rogers, K. R., Herrmann, H. and Franke, W. W. (1996). Characterization of disulfide crosslink formation of human vimentin at the dimer, tetramer, and intermediate filament levels. *J. Struct. Biol.* **117**, 55-69.

Saiki, R. K., Gelfand, D. H., Stoffel, S., Scharf, S. J., Higuchi, R., Horn, G. T., Mullis, K. B. and Erlich, H. A. (1988). Primer-directed enzymatic amplification of DNA with a thermostable DNA polymerase. *Science* **239**, 487-491.

Sambrook, J., Fritsch, E. F. and Maniatis, T. (1989). *Molecular Cloning: a Laboratory Manual*. New York: Cold Spring Harbor Laboratory Press.

Scheel, J., Pierre, P., Rickard, J. E., Diamantopoulos, G. S., Valetti, C., van der Goot, F. G., Hüner, M., Aebi, U. and Kreis, T. E. (1999). Purification and analysis of authentic CLIP-170 and recombinant fragments. *J. Biol. Chem.* **274**, 25883-25891.

Smith, D. B. and Johnson, K. S. (1988). Single-step purification of polypeptides expressed in Escherichia coli as fusions with glutathione S-transferase. *Gene* **67**, 31-40.

Smith, P. K., Krohn, R. I., Hermanson, G. T., Mallia, A. K., Gartner, F. H., Provenzano, M. D., Fujimoto, E. K., Goeke, N. M., Olson, B. J. and Klenk, D. C. (1985). Measurement of protein using bicinchoninic acid. *Anal. Biochem.* **150**, 76-85.

Tian, G., Huang, Y., Rommelaere, H., Vandekerckhove, J., Ampe, C. and Cowan, N. J. (1996). Pathway leading to correctly folded beta-tubulin. *Cell* **86**, 287-296.

Vallee, R. B. and Sheetz, M. P. (1996). Targeting of motor proteins. *Science* **271**, 1539-1544.

Vaughan, K. T. and Vallee, R. B. (1995). Cytoplasmic dynein binds dynactin through a direct interaction between the intermediate chains and p150Glued. *J. Cell Biol.* **131**, 1507-1516.

Waterman-Storer, C. M., Karki, S. and Holzbaur, E. L. (1995). The p150Glued component of the dynactin complex binds to both microtubules and the actin-related protein centractin (Arp-1). *Proc. Nat. Acad. Sci. USA* **92**, 1634-1638.

Chapter 5

CLASPS ARE CLIP-115 AND -170 ASSOCIATING PROTEINS INVOLVED IN THE REGIONAL REGULATION OF MICROTUBULE DYNAMICS IN MOTILE FIBROBLASTS

Anna Akhmanova[1*], Casper C. Hoogenraad[1,2*], Ksenija Drabek[1], Tatiana Stepanova[1], Bjorn Dortland[1], Ton Verkerk[1], Wim Vermeulen[1], Boudewijn M. Burgering[3], Chris I. de Zeeuw[2], Frank Grosveld[1], Niels Galjart[1]

MGC Departments of [1]Cell Biology and Genetics, [2]Anatomy, Erasmus Univerisity, P.O. Box 1738, 3000 DR Rotterdam, The Netherlands. [3]Laboratory for Physiological Chemistry and Centre for Biomedical Genetics. University of Utrecht. *These authors contributed equally to the results described in this paper.

CLASPs Are CLIP-115 and -170 Associating Proteins Involved in the Regional Regulation of Microtubule Dynamics in Motile Fibroblasts

Anna Akhmanova,*‖ Casper C. Hoogenraad,*†‖
Ksenija Drabek,* Tatiana Stepanova,*
Bjorn Dortland,* Ton Verkerk,* Wim Vermeulen,*
Boudewijn M. Burgering,‡ Chris I. De Zeeuw,†
Frank Grosveld,* and Niels Galjart*§
*MGC Department of Cell Biology and Genetics and
†MGC Department of Anatomy
Erasmus University
P.O. Box 1738
3000 DR Rotterdam
The Netherlands
‡Laboratory for Physiological Chemistry and Centre for Biomedical Genetics
University of Utrecht
Universiteitsweg 100
3584 CG Utrecht
The Netherlands

Summary

CLIP-170 and CLIP-115 are cytoplasmic linker proteins that associate specifically with the ends of growing microtubules and may act as anti-catastrophe factors. Here, we have isolated two *CLIP-associated proteins* (CLASPs), which are homologous to the *Drosophila* Orbit/Mast microtubule-associated protein. CLASPs bind CLIPs and microtubules, colocalize with the CLIPs at microtubule distal ends, and have microtubule-stabilizing effects in transfected cells. After serum induction, CLASPs relocalize to distal segments of microtubules at the leading edge of motile fibroblasts. We provide evidence that this asymmetric CLASP distribution is mediated by PI3-kinase and GSK-3β. Antibody injections suggest that CLASP2 is required for the orientation of stabilized microtubules toward the leading edge. We propose that CLASPs are involved in the local regulation of microtubule dynamics in response to positional cues.

Introduction

Microtubules (MTs) constitute an important part of the cellular cytoskeleton. They are essential for chromosome segregation in mitosis and for organelle movement and positioning in interphase cells. MTs are inherently polarized structures, with a fast-growing end (the plus end) and a slow growing end (the minus end). In fibroblasts, the majority of MTs is attached with the minus end to the MT organizing center (MTOC), while the plus ends are directed to the cell periphery. Both in vitro and in vivo, the MT plus ends alternate between phases of elongation and shrinkage. This phenomenon is called dynamic instability (reviewed by Desai and Mitchison, 1997).

MT dynamics in living cells is regulated by a variety of protein factors. These include MT destabilizing proteins, such as stathmin/Op18 and XKCM1, as well as factors that promote MT elongation, such as XMAP215/TOG1 (for review, see Wittmann et al., 2001). Some of the proteins involved in regulating MT growth, depolymerization, and/or MT interaction with the cellular cortex are localized specifically at the MT plus end. For example, the yeast protein BIM1p, which increases MT dynamicity, localizes to dots at the distal ends of cytoplasmic MTs (Tirnauer et al., 1999), as does its mammalian homolog EB1 (Mimori-Kiyosue et al., 2000). Another protein demonstrated to be present at the plus ends is mammalian CLIP-170. Using a fusion of CLIP-170 to the green fluorescent protein (GFP), it was shown that CLIP-170 moves together with the tips of growing MTs in living cells (Perez et al., 1999). However, CLIP-170 was previously also implicated in the attachment of endosomes to MTs (Pierre et al., 1992) and, in addition, it was found at the kinetochores of the prometaphase chromosomes (Dujardin et al., 1998). In fibroblasts, CLIP-170 colocalizes with cytoplasmic dynein and dynactin at the distal ends of MTs (Valetti et al., 1999; Vaughan et al., 1999). It was suggested, therefore, that these regions represent the cargo-loading sites for the minus end directed organelle movement by dynein, and that CLIP-170 might be involved in this process. However, no association of CLIP-170 with dynein and dynactin has been demonstrated. To resolve CLIP-170 function at MT plus ends, it is essential to define with what proteins it interacts directly.

The closest homolog of CLIP-170 in mammals is CLIP-115 (De Zeeuw et al., 1997). Both CLIP-170 and CLIP-115 contain two MT binding (MTB) domains at their N termini, surrounded by positively charged, serine rich regions. One such MTB motif, together with one serine rich region, is sufficient for MT binding (Hoogenraad et al., 2000). The middle part of both proteins contains a long region of heptad repeats, which form a coiled-coil and mediate homodimerization of these proteins (Scheel et al., 1999; Hoogenraad et al., 2000). While CLIP-170 is expressed in many different cell lines and tissues, CLIP-115 appears to be predominantly present in neurons, where it is localized in dendrites (De Zeeuw et al., 1997). When expressed in fibroblasts at low levels, CLIP-115 localizes at the MT plus ends, similar to CLIP-170 (Hoogenraad et al., 2000). This suggests that in neurons, the function of CLIP-115 might be related to some aspect of MT dynamics.

Given the common properties of the two CLIPs, we hypothesized that they might have overlapping functions and, therefore, common protein partners. We searched for such partners (*CLIP-associating proteins*, or CLASPs) with the aid of a yeast two-hybrid system, using a conserved part of the coiled-coil region of CLIP-115 as bait. We identified two mammalian proteins, CLASP1 and CLASP2, with similarity to regulators of MT dynamics. CLASPs bind both to CLIPs and to MTs and

§To whom correspondence should be addressed (e-mail: galjart@ch1.fgg.eur.nl).
‖These authors contributed equally to the results described in this paper.

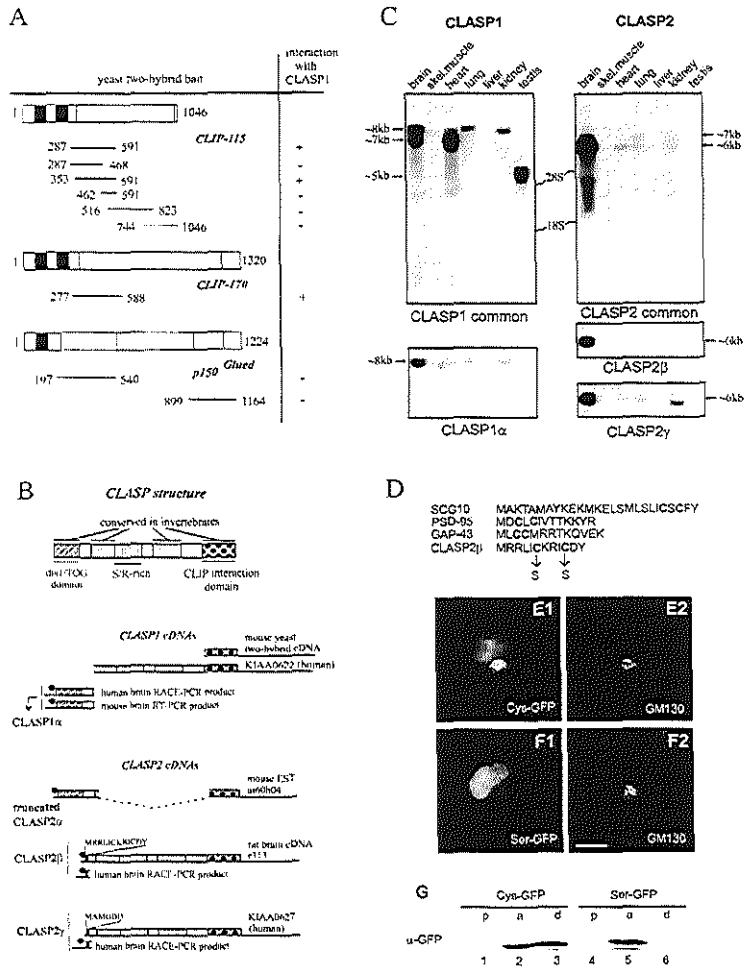

Figure 1. CLASP Isolation and Structure

(A) The region spanning amino acids 287–591 of CLIP-115 was used in a yeast two-hybrid screen of an E14.5 day mouse cDNA library. Mouse *CLASP1* cDNA, isolated in this screen, was next tested in yeast two-hybrid assays with protein fragments from CLIP-115, CLIP-170, and $p150^{Glued}$. The domain structure of these three proteins, with MT binding motifs (black bars) and coiled-coil regions (gray bars), is represented. The amino acids covered by each fragment are indicated; their interaction with mCLASP1 is shown to the right (+: positive interaction, −: no interaction).

(B) Schematic representation of CLASP structure and the CLASP-encoding cDNAs. Protein-coding regions are represented by bars and untranslated regions by lines. The top bar represents the largest CLASP ORF, encoded by CLASP1/2α cDNAs. Above the CLASP2β and -γ cDNAs, the sequence of the alternatively spliced, N-terminal domain is shown. A vertical line with a filled circle on top indicates a stop codon upstream and in-frame with the translational start codon, suggesting the presence of a full-length ORF. The stippled line in the mouse EST clone ui60h04 indicates the position of a deletion, which is probably an artifact, because it could not be confirmed by Northern blotting or RT-PCR.

(C) *CLASP* expression profile. Northern blots with total RNA from different mouse tissues (~20 μg per lane) were hybridized with probes, encompassing the CLIP binding domain of CLASP1 and -2 ("common" probes), or with 5′ probes, specific for particular CLASP variants. Approximate sizes of the different CLASP transcripts and positions of the 18S and 28S rRNAs are indicated.

(D) Comparison of the N terminus of CLASP2β with known palmitoylation motifs. Fatty acylated cysteine residues are in bold. Amino acid substitutions are indicated.

(E and F) Intracellular distribution of GFP, fused either to the first 40 amino acids of wild-type CLASP2β (Cys-GFP) or to the sequence with two serine substitutions (Ser-GFP). Transfected COS-1 cells were fixed and stained with antibodies to the *cis*-Golgi marker GM130. GFP

have a MT stabilizing effect in transfected cells. Using motile fibroblasts as a model system, we find that CLASPs specifically mark the distal ends of MTs at the leading edge of the cell and are involved in organizing stabilized MTs. Thus, CLASPs may play a role in local MT stabilization in response to positional cues.

Results

Characterization of CLIP-Associating Proteins (CLASPs)

Within the coiled-coil region of CLIP-115 and -170, the N-terminal portion is best conserved. This part of CLIP-115 (amino acids 287–591; Figure 1A) was therefore used as bait in a yeast two-hybrid screen to identify common *CLIP-associating proteins* (CLASPs). We found one clone, which interacted both with CLIP-115 and with the corresponding region of CLIP-170 and which was therefore named CLASP1. This clone did not interact with vector alone, with other portions of CLIP-115, or with the coiled-coil domains of $p150^{Glued}$, a dynactin subunit that structurally resembles CLIP-170 (Pierre et al., 1992). Deletion analysis demonstrated that the whole coiled-coil part of the CLIP-115 bait construct is necessary and sufficient for binding to CLASP1 (Figure 1A).

Mouse *CLASP1* cDNA (*mCLASP1*) contains a 5′ truncated open reading frame (ORF) with very high similarity to the C termini of the proteins encoded by the incomplete human brain cDNAs KIAA0622 (98% identity, hCLASP1) and KIAA0627 (75% identity, hCLASP2). We searched for complete ORFs of CLASP1 and -2 by cDNA library screening, RACE-PCR, and EST database analysis. This yielded several cDNAs, named *CLASP1/2*α, -2β, and -2γ, which encode different protein isoforms (Figure 1B). Northern blot analysis with probes to the common C-terminal domains of *CLASP1* and -2 shows that differently sized *CLASP* mRNAs are present in various tissues (Figure 1C), indicating that *CLASP* transcripts undergo alternative splicing. *CLASP1* shows highest expression in brain, heart, and testis, while *CLASP2* mRNAs are enriched in the brain. Interestingly, the *CLASP2*β transcript appears to be brain specific (Figure 1C). Using probes, specific for *CLASP1*α (Figure 1C) or *CLASP2*α (data not shown), we only detect hybridization to the longest transcript of each *CLASP* (~8 kb for *CLASP1*α and ~7 kb for *CLASP2*α, respectively). The presence of 5 and 7 kb *CLASP1* transcripts indicates that there are additional N-terminal variants of CLASP1, similar to CLASP2.

The different *CLASP1* and *-2* cDNAs encode proteins with a predicted molecular mass of ~170 kDa (α isoforms) and ~140 kDa (β/γ isoforms). A database search revealed a striking similarity of the CLASPs to a protein called either Orbit or Mast, which is an essential MT-associated protein (MAP) from *D. melanogaster*, involved in the regulation of MT behavior during mitosis (Inoue et al., 2000; Lemos et al., 2000). Three putative CLASPs are also present in *C. elegans* (ZC84.3, R107.6, and C07h6.3). The domains of CLASP that are conserved in invertebrates are schematically indicated in Figure 1B. Interestingly, our 5′ RACE analysis demonstrates that an N-terminal ~200 amino acid domain in Mast, which is similar to a repeated motif in the dis1/TOG family of vertebrate MT stabilizing proteins (Lemos et al., 2000), is also present in CLASP1α and -2α. These observations indicate that CLASPs might bind MTs.

CLASP2β is represented by the rat hippocampus cDNA clone r313 (Figure 1B). Instead of the dis1/TOG-homologous domain, this isoform contains a short N-terminal motif, which is conserved in humans (Figure 1B). It is characterized by two cysteines, surrounded by positively charged and hydrophobic residues (Figures 1B and 1D). Similar motifs in other proteins were shown to cause membrane anchoring, due to palmitoylation of the cysteine residues (Resh, 1999). Fusion of the N terminus of CLASP2β to GFP gives rise to a protein that accumulates in the region of the Golgi complex in transfected COS-1 cells (Figure 1E1, compare to the Golgi marker GM130 in Figure 1E2). Substitution of cysteine residues for serines (Figure 1F) or alanines (not shown) abolishes targeting to the Golgi, supporting the idea that fatty acylation of the cysteines within the N-terminal peptide stretch of CLASP2β causes membrane targeting. Triton-X114 partitioning experiments (Hancock et al., 1989), in which the cysteine-containing, but not the serine-containing, GFP fusion is partially retained in the detergent enriched (i.e., the membranous) phase (Figure 1G, compare lanes 1–3 and 4–6, respectively), further support this notion. Subsequent shortening of the CLASP2β N terminus within the fusion construct demonstrated that the first 14 amino acids of this CLASP isoform are sufficient for membrane association (data not shown).

In contrast to the α- and β-isoforms, CLASP2γ, represented by KIAA0627 cDNA, contains an inconspicuous peptide (MAMGDD) at its N terminus (Figure 1B). In conclusion, CLASPs appear to be the mammalian counterparts of the *D. melanogaster* protein Orbit/Mast. They exist as a family of widely distributed isoforms, each with a CLIP interaction domain but with variable N termini, and are likely to have MT binding properties.

CLASPs Colocalize with CLIPs at MT Distal Ends

We raised antibodies against the conserved C-terminal domain of hCLASP2 (antiserum #2358) in order to investigate the intracellular distribution of different CLASP isoforms. These studies were carried out both in COS-1 cells and in 3T3 fibroblasts, to compare results in different systems and to take advantage of the fact that COS-1 cells are easily transfected, whereas in 3T3 cells MT dynamics have been extensively studied. Interestingly, COS-1 cells express only CLIP-170, while in 3T3 fibroblasts, both CLIP-115 and CLIP-170 are present at MT distal ends. The specificity of antiserum #2358 was

fluorescence is shown in (E1) and (F1), and the antibody labeling of the same cells in (E2) and (F2). Bar, 10 μm.

(G) COS-1 cells, transfected with Cys-GFP or Ser-GFP, were lysed using Triton X-114. After pelleting of the insoluble fraction (lanes marked "p"), the lysate was partitioned into an aqueous phase ("a") and a detergent-enriched phase ("d"). The volumes of the three fractions were equalized before loading on gel and proteins were analyzed by Western blotting with anti-GFP serum.

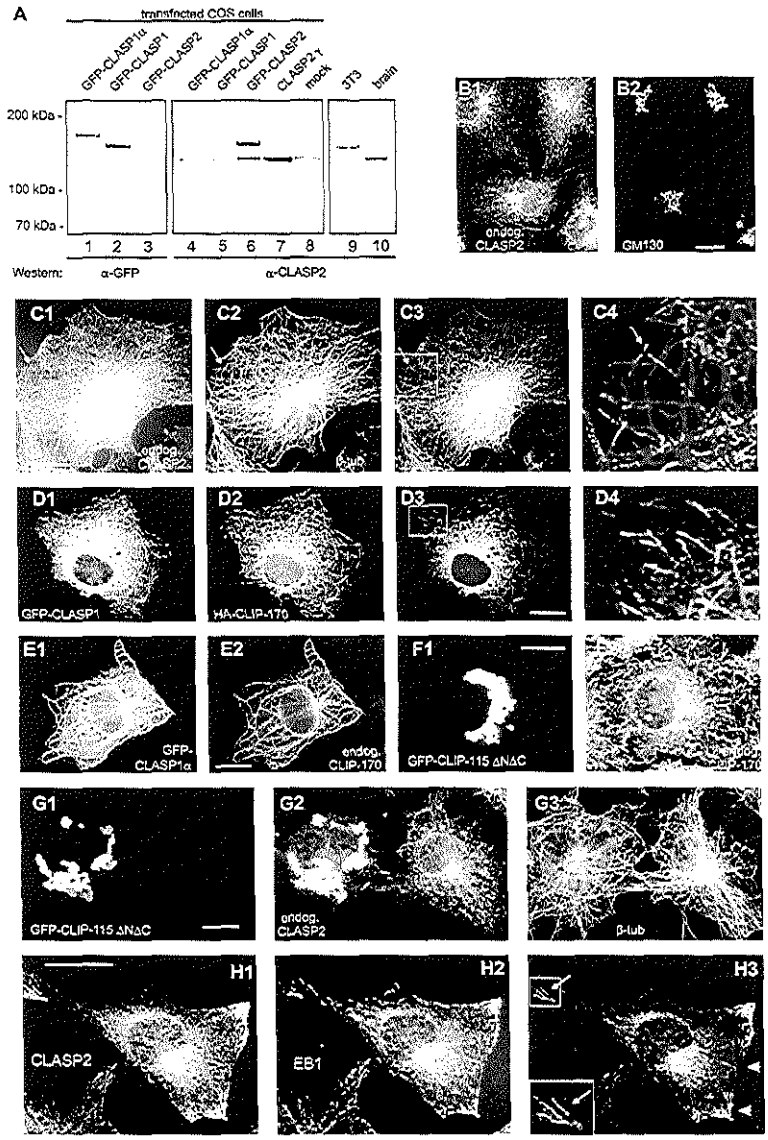

Figure 2. Localization of CLASPs in Cultured Cells

(A) Specificity of #2358 antibodies. Protein extracts from COS-1 cells, transiently transfected with the indicated CLASP expression constructs (lanes 1–7) or mock transfected (lane 8), and from 3T3 cells (lane 9) or mouse brain (lane 10) were analyzed by Western blotting, using antibodies against GFP (lanes1–3, α-GFP) or with the #2358 antiserum (lanes 4–10, α-CLASP2). Notice that GFP-CLASP1 fusions are more abundantly expressed than GFP-CLASP2 (lanes 1–3), but less well recognized by #2358 antibodies (lanes 4–6).

(B and C) Untransfected COS-1 cells, immunostained with #2358 antiserum and anti-GM130 (B) or anti-β-tubulin (C). In (C3) and (C4), signals of (C1) (green) and (C2) (red) are merged. (C4) is an enlargement of the indicated area in (C3) to demonstrate the MT plus end labeling of CLASP2 (indicated by an arrow). Bar, 10 μm.

(D–G) COS-1 cells, transfected with different cDNA constructs, fixed 24 hr after transfection and immunostained using specific antisera. Bar, 10 μm.

first analyzed by Western blotting in transfected COS-1 cells using different GFP-CLASP1 and -2 fusion proteins or untagged CLASP2γ (Figure 2A). In these cells, the #2358 antibodies react strongly with GFP-CLASP2 and with untagged CLASP2γ (Figure 2A, lanes 6 and 7, respectively). Weak cross-reactivity with GFP-CLASP1 proteins is also observed (Figure 2A, lanes 4 and 5). In agreement with these Western blot data, immunofluorescence experiments in transfected COS-1 cells with #2358 antibodies show very strong reaction with GFP-CLASP2 proteins and a weak reaction with GFP-CLASP1 fusions (data not shown). Based on these observations, we conclude that antiserum #2358 recognizes CLASPs specifically, but that use of these antibodies predominantly reflects the distribution of CLASP2 isoforms. Thus, the #2358 antiserum is also named anti-CLASP2 antiserum.

In mock transfected COS-1 cells, #2358 antibodies detect proteins of ~170 and ~140 kDa (Figure 2A, lane 8), which are the expected lengths for CLASP2α and -β/γ, respectively. Surprisingly, Western blot analysis of 3T3 cell lysates with antiserum #2358 reveals only a protein of ~170 kDa (Figure 2A, lane 9), whereas in mouse brain, the tissue with highest expression of CLASP2, proteins of ~140 and ~170 kDa are detected (Figure 2A, lane 10). These Western blots results with antiserum #2358 were verified by Northern blot analysis (data not shown). Together, the data demonstrate that CLASP2β and -γ are not highly expressed in 3T3 cells, whereas in brain they are more abundant than CLASP2α.

CLASP2 distribution was next examined using immunofluorescence microscopy. In COS-1 cells, prominent labeling is detected in the perinuclear region, corresponding to the Golgi apparatus (Figure 2B). In addition, anti-CLASP2 antibodies stain MT plus ends (Figure 2C), in a pattern similar to that described previously for CLIP-170 (Pierre et al., 1992; Perez et al., 1999). Both types of CLASP staining are completely inhibited by preincubation of the antibodies with the antigen used for their generation, while affinity-purified antibodies produce the same signal as the crude serum (data not shown). Thus, CLASP2 distribution in COS-1 cells overlaps with that of CLIP-170 at the distal ends of MTs.

Using GFP-CLASP1 (containing the 5′ truncated ORF from KIAA0622), GFP-CLASP1α, and GFP-CLASP2 (derived from KIAA0627), we next investigated the distribution of individual, overexpressed CLASP1 and -2 isoforms and the effect of coexpression with the CLIPs. At low expression levels, all three GFP-CLASP fusions colocalize with CLIP-170 or CLIP-115 at MT plus ends (Figure 2D and data not shown). When GFP-CLASPs are highly overexpressed, they accumulate along the whole length of MTs, causing MT rearrangement and bundling and CLIP-170 relocalization to these MT bundles (Figure 2E). At low expression levels in live transfected cells, GFP-CLASP2 behaves very similar to GFP-CLIP-170 (see Supplemental Information for live GFP-CLASP2 and GFP-CLIP-170 behavior in COS-1 cells at http://www.cell.com/cgi/content/full/104/6/923/DC1), which was shown to move with the growing ends of MTs (Perez et al., 1999). Taken together, these data verify the distribution of endogenous CLASP2, as detected with #2358 antibodies and establish CLASPs as a novel family of proteins that bind to the distal ends of interphase MTs.

A GFP fusion protein, containing the CLASP-interacting region of CLIP-115 (GFP-CLIP-115ΔNΔC, including amino acids 353–756 of CLIP-115), is unable to bind MTs, since it lacks the MTB domains. Instead, it forms cytoplasmic aggregates, which contain no significant amount of tubulin (Figures 2G1 and 2G3). Strikingly, in cells overexpressing this mutant protein, endogenous CLASP is titrated away from the Golgi complex as well as from MT distal ends and is detected in the aggregates (Figure 2G2). In contrast, both CLIP-170 (Figure 2F) and EB1 (data not shown) remain bound to MT distal ends. These results validate the yeast two-hybrid interaction between CLIPs and CLASPs. In addition, they indicate that CLIP-170 and EB1 are able to associate with MT distal ends in the absence of CLASP.

In 3T3 cells, CLASP2 distribution is similar to that in COS-1 cells. However, we noted that in cells with a shape characteristic of motile fibroblasts, intense labeling of MT distal segments is detected at the leading edge, but not in the cell body (Figures 2H1 and 2H3). This asymmetric distribution is particularly apparent when CLASP2 localization is compared to that of EB1, which marks MT tips throughout 3T3 cells (Figures 2H2 and 2H3). When a distal segment of an MT appears positive for both CLASP2 and EB1, the highest concentration of EB1 is often observed at the tip, while a more proximal portion of the MT is strongly stained with anti-CLASP2 antibodies (see insets in Figure 2H3). Thus, the MT labeling by CLASP2 at the periphery of subconfluent 3T3 cells is often nonuniform.

CLASPs Bind to CLIPs and MTs

To verify the CLIP–CLASP interactions, we tested their association in vitro. Radioactively labeled hCLASP1 and hCLASP2, generated by in vitro transcription-translation, bind to bacterially produced GST fusions of full-length CLIP-115 and the yeast two-hybrid fragment (CLIP-115-TH), but not to control GST fusion proteins (Figure 3C). Alternatively, in vitro translated CLIP-115 specifically binds to the GST fusion of the mCLASP1 C terminus (GST-CLASP1-C; Figure 3D). A GST pulldown assay with mouse brain extracts shows that both CLIP-115 and CLIP-170 are retained by GST-CLASP1-C, but not by GST alone (Figure 3E). Since all GST fusion pro-

(D) Cotransfection of GFP-CLASP1 (low level of expression) and HA-tagged CLIP-170, staining with antibody against the HA tag. (D4) is an enlargement of the indicated area in (D3).

(E) Transfection with GFP-CLASP1α, staining with antibodies against CLIP-170. The MTOC is indicated by an arrow.

(F and G) Transfections with GFP-CLIP-115ΔNΔC, staining with antibodies against CLASP2 (G2) and tubulin (G3), or with antibodies against CLIP-170 (F2).

(H) Intracellular distribution of CLASP2 in Swiss 3T3 fibroblasts. Cells were stained with anti-CLASP2 (H1) and anti-EB1 (H2) antisera. The overlay is shown in (H3) (CLASP2 is green, EB1 red). The arrow in (H3) indicates an example of MT distal ends with a high concentration of EB1 at the tip and CLASP2 at a more proximal segment. Arrowheads indicate the leading edge.

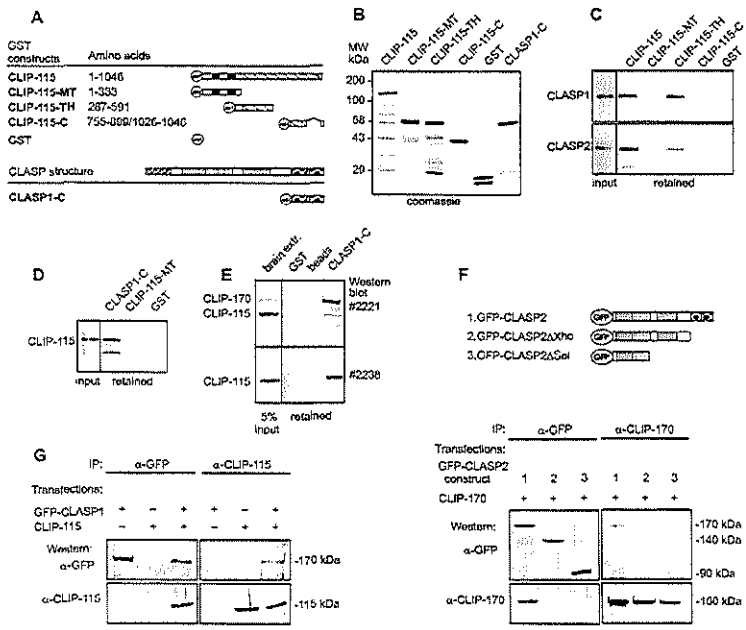

Figure 3. Analysis of CLIP–CLASP Interactions

(A) Schematic representation of bacterial GST fusion proteins of CLIP-115 and mCLASP1.

(B) SDS-PAGE analysis of purified GST fusions. All proteins are soluble and have the expected size. Molecular weight markers are indicated on the left.

(C) In vitro binding of ^{35}S-methionine-labeled CLASP1 and CLASP2 (see lanes, marked "input") to the GST fusion proteins, depicted in (A) and (B). Radioactive proteins were visualized by X-ray film exposure of dried gels.

(D) In vitro binding of ^{35}S-methionine-labeled CLIP-115 to GST fusion proteins. The experiment was performed as in (C).

(E) GST pulldown assay using mouse brain extract. Proteins, retained by glutathione-sepharose beads alone, beads decorated with GST, or with GST-mCLASP1-C, were analyzed by Western blotting, using antibody #2221, which recognizes both CLIP-115 and CLIP-170, or antibody #2238, which is specific for CLIP-115.

(F) Immunoprecipitations (IP) from COS-1 cells, transiently expressing rat brain CLIP-170, together with GFP-CLASP2, or C-terminal deletion mutants of CLASP2 (see scheme above the Western). Precipitated proteins were analyzed by Western blotting with antibodies against GFP or CLIP-170.

(G) Immunoprecipitations (IP) from COS-1 cells, transiently expressing GFP-CLASP1, CLIP-115, or both proteins. Precipitated proteins were analyzed by Western blotting with antibodies against GFP or CLIP-115.

teins (Figure 3A) are soluble and produced in comparable quantities (Figure 3B), these data suggest that the retention of CLASP1 and -2 by GST-CLIP-115 and GST-CLIP-115-TH and that of CLIP-115 and -170 by GST-CLASP1-C is specific.

We next immunoprecipitated different transfected GFP-CLASP fusion proteins from COS-1 cells, cotransfected with the CLIPs. Both full-length GFP-CLASP1 and -2 coprecipitate with CLIP-115 and -170 (Figures 3F and 3G and data not shown). These immunoprecipitates of CLIPs and CLASPs contain neither tubulin nor EB1 or dynactin (data not shown), indicating that these proteins do not mediate the CLIP–CLASP interaction. In addition, truncated GFP-CLASP2 proteins, where the C-terminal CLIP binding domain (GFP-CLASP2ΔXho) or the whole C-terminal half of the protein (GFP-CLASP2ΔSal) is deleted (Figure 3F), do not coprecipitate with CLIP-170 (Figure 3F) or CLIP-115 (data not shown) while being present in similar quantities as full-length GFP-CLASP2 (Figure 3F). Since these mutants still bind MTs (see below) but fail to bind CLIPs, these data strongly suggest that the CLIP–CLASP interaction is not mediated via tubulin, but occurs directly through the C-terminal CLIP-interacting domain of the CLASPs.

A sedimentation assay, whereby in vitro translated CLASPs were tested for their ability to cosediment with purified, taxol-stabilized MTs, reveals that only a small proportion of the CLASPs comes down with MTs (Figure 4A, left panels). This could be partially due to phosphorylation of CLASPs in the translation mix since this has been shown to inhibit MT binding of CLIP-115 and CLIP-170 (Pierre et al., 1992; Hoogenraad et al., 2000). To reduce the extent of phosphorylation of the CLASPs, after translation the system was depleted of ATP with apyrase. This caused a considerable increase in the proportion of CLASPs pelleted with MTs (Figure 4A,

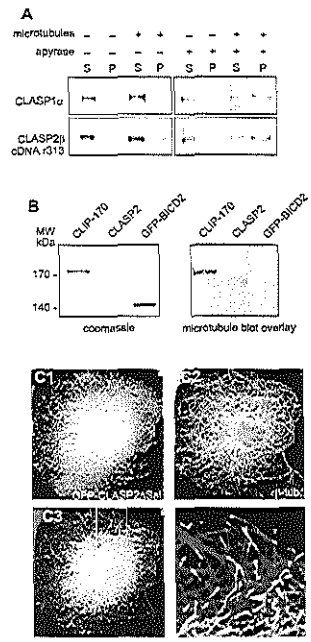

Figure 4. CLASPs Bind MTs Directly and Independently of CLIPs

(A) In vitro binding of CLASPs to MTs. ^{35}S-methionine-labeled CLASP1 and -2 were polleted in the absence or in the presence of MTs, and the supernatants (lanes marked "S") and pellets (lanes marked "P") were analyzed by SDS-PAGE and autoradiography. In some cases, translation products were incubated with apyrase prior to the addition of MTs.

(B) MT blot overlay. CLIP-170, immunoprecipitated with antibodies #2221 from HeLa cells (500 ng), CLASP2, immunoprecipitated with antibodies #2358 from 3T3 cells (100 ng), and GFP-BICD2, immunoprecipitated from transfected COS-1 cells with GFP-specific antibodies (500 ng) were analyzed by SDS-PAGE or transferred to a Western blot, which was incubated with taxol-stabilized MTs (50 mg/ml). MTs, retained on the blot, were detected with anti-tubulin antibodies.

(C) COS-1 cells, transfected with GFP-CLASP2ΔSal (GFP signal shown in [C1]) were stained with anti-tubulin antibodies (C2). In (C3) and (C4), signals of (C1) (green) and (C2) (red) are merged. In (C4), an enlargement of the area indicated in (C3) is shown to demonstrate MT plus end labeling. Bar, 10 μm.

right panels). In MT blot overlays, immunoprecipitated CLASP2 and CLIP-170 bind MTs, whereas a Golgi-associated GFP fusion protein of similar size and quantity (GFP-BICD2; C. Hoogenraad et al., submitted) does not (Figure 4B). Thus, these results suggest that CLASPs bind MTs directly and this binding may be influenced by phosphorylation.

The GFP-CLASP2ΔSal mutant binds neither CLIP-115 nor CLIP-170 (Figure 3F) due to the absence of the C-terminal CLIP interaction domain. However, this protein does contain a presumptive MT binding domain (Inoue et al., 2000; Lemos et al., 2000). At low expression levels in transfected cells, this fusion protein localizes to the distal ends of MTs (Figure 4C) and colocalizes with CLIP-170 and EB1, while at high expression levels, GFP-CLASP2ΔSal is detected along the MTs (data not shown). These results suggest that CLASPs can accumulate on distal ends of MTs independently of their binding to CLIPs.

CLASP2 Localization in 3T3 Fibroblasts Correlates with the Orientation of Stabilized MTs

Since we observed that CLASP2 distribution in 3T3 cells with a representative motile shape is asymmetric, we investigated CLASP2 function further using the in vitro wound healing model (Liao et al., 1999). Swiss 3T3 fibroblasts were grown to confluence and a stripe of cells was scraped off, creating a "wound" in the monolayer. Cells at the edge of the wound polarize in such a way that their leading edges face the cell-free area. A subset of MTs, oriented in the direction of the wound along the polarization axis, becomes stabilized (Liao et al., 1999) and accumulates posttranslationally modified forms of tubulin, such as detyrosinated (Glu) tubulin and acetylated (Ac) tubulin, which can be visualized using specific antibodies (Bulinski and Gundersen, 1991).

Selective stabilization of MTs, oriented toward the leading edge, does not occur in serum-starved 3T3 cells, but can be quickly induced by the addition of serum (Cook et al., 1998). In agreement with these data, we find that after 24–48 hr of serum starvation, fibroblasts contain very few detyrosinated and acetylated MTs, which are concentrated in the region occupied by the Golgi complex (Figure 5A). Under these conditions, CLASP2 is mainly detected in the region of the Golgi complex, although weak staining with anti-CLASP2 antibodies is observed at the MT tips, which are also positive for EB1 (Figure 5B). Addition of serum induces formation of detyrosinated and acetylated MTs directed toward the edge of the wound (Figure 5C). The distribution of the two different posttranslationally modified forms of tubulin shows a strong correlation (but not a complete colocalization). MT tips at the leading edge and in the cell body are still stained with anti-EB1 antiserum as well as with anti-CLIP antibodies, which produce a highly similar staining pattern (Figure 5D).

In contrast to the MT distribution of EB1 and CLIP, anti-CLASP2 antibodies mainly stain the distal segments of MTs at the leading edge of the cell (Figure 5E). Very little MT bound CLASP2 is observed in the cell body and at the lateral edges of the cells, in areas of intercellular contacts (compare Figure 5E5 to 5E4). When CLASP2 localization is compared to that of acetylated tubulin, it becomes clear that many stabilized, acetylated MT bundles display a high accumulation of CLASP2 at their distal ends (Figure 5F).

MT stabilization at the leading edge of fibroblasts is induced rapidly (~5 min) in response to serum factors, although it takes about 30 min before posttranslationally modified tubulin isoforms have accumulated (Cook et al., 1998). Redistribution of CLASP2 in response to serum addition can be observed already after 5 min (data not shown), although all cells at the edge of the monolayer acquire a highly polarized CLASP2 staining pattern only after 15–20 min. Taken together, these data suggest that serum addition to wounded monolayers of 3T3 cells causes the rapid and asymmetric redistribution of CLASP2 to a subset of MT distal ends.

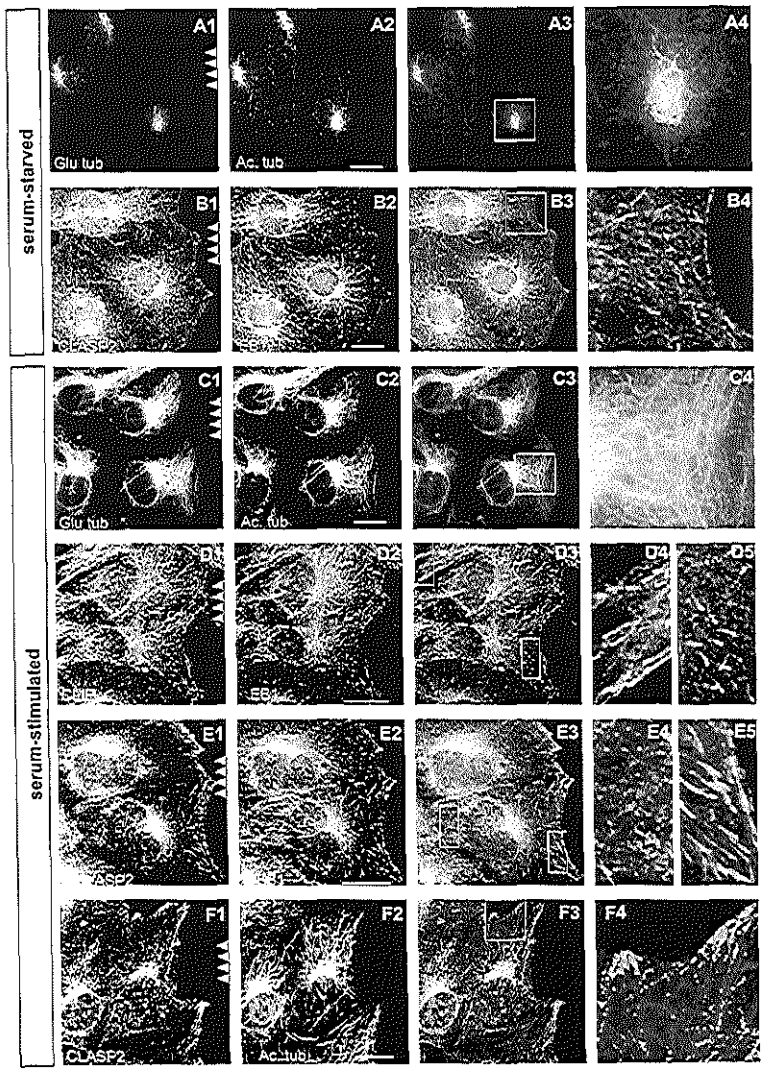

Figure 5. Localization of CLASP2 at the Leading Edge of Serum-Stimulated 3T3 Cells

3T3 cells were grown to 95% confluence in serum-containing medium and then incubated with serum-free medium for 30 hr. Narrow stripes of cells were removed by scraping, and after incubating for 2 more hr without serum, cells were fed either serum-free (A and B) or serum-containing medium (C–F) for an additional 30 min. Cells were fixed and costained with antibodies against Glu tubulin and acetylated tubulin (A and C), CLASP2 and EB1 (B and E), CLIP-115/CLIP-170 (#2221) and EB1 (D), and CLASP2 and acetylated tubulin (F). Images (A3)–(F3) represent overlays of images (A1)–(F1) (green) with images (A2)–(F2) (red). Panels on the right show an enlargement of part of the overlays (indicated by white rectangles). MT tips from the trailing part of the cell are shown in (D4) and (E4). MT tips from the leading edge in (D5) and (E5). The position of the wound is indicated (arrowheads; in [F], the leading edge also extends towards the top). Bar, 10 μm.

CLASPs Stabilize MTs

The similarity of CLASPs to Orbit/Mast and their asymmetric distribution in motile fibroblasts suggests that these proteins might be involved in the regulation of MT dynamics. We examined the MT-stabilizing effect of CLASPs first in COS-1 cells, which normally have few stabilized MTs, as determined by Glu tubulin antibody staining (Figure 6B). Overexpression of GFP-CLASP fu-

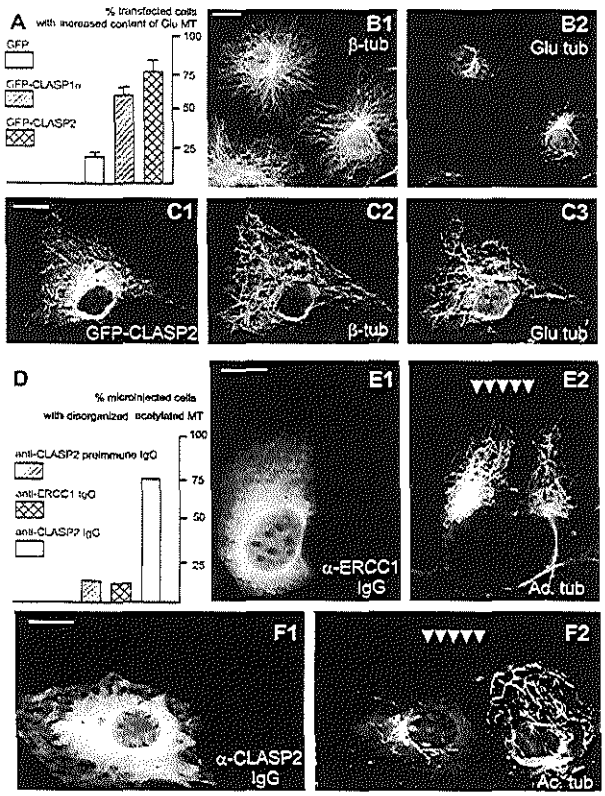

Figure 6. CLASPs Have an MT-Stabilizing Effect

(A) COS-1 cells were transfected with constructs, expressing GFP, GFP-CLASP1α, or GFP-CLASP2, and stained with Glu tubulin antibodies to detect stabilized MTs. The percentage of transfected cells, displaying a significant amount of Glu tubulin at the cell periphery, is shown in (A) (three experiments performed per construct, 100 cells counted per experiment, standard deviation indicated). Cells with very low GFP levels (not visible at data collection times below 600 ms, see Experimental Procedures) or high expression levels (visible at data collection times of 150 ms) were excluded from the analysis.

(B and C) Examples of tubulin (β-tub) and Glu tubulin (Glu tub) staining in untransfected COS-1 cells (B), or in cells expressing moderate levels of GFP-CLASP2 (C). The data collection time was 600 ms in (C1). Bar, 10 μm.

(D–F) Serum-starved 3T3 fibroblasts were injected with anti-CLASP2 or control antibodies, induced with serum for 2 hr, and stained for rabbit IgG (E1 and F1) and acetylated tubulin (E2 and F2). Position of the wound is indicated (arrowheads).

(D) The percentage of injected cells, displaying few or disorganized acetylated MTs, was determined for cells injected with control (#2358 preimmune and anti-ERCC1) antibodies or with anti-CLASP2 antibodies.

(E) 3T3 fibroblast injected with control antibodies.

(F) 3T3 fibroblast injected with anti-CLASP2 antibodies. Bar, 10 μm.

sions induces highly increased levels of detyrosinated MTs (Figures 6A and 6C). In the GFP-CLASP transfected cells, almost all cells contain many stabilized MTs outside the Golgi region, while in a control transfection, GFP alone does not have this effect. Importantly, MT stabilization occurs already at moderate levels of CLASP overexpression, when the distal segments of MTs are decorated by CLASPs (Figure 6C).

In the MT stabilizing assay, GFP-CLASP1α and GFP-CLASP2 fusions show comparable induction of detyrosinated MTs (Figure 6A), indicating that both CLASP1 and -2 have MT-stabilizing properties. In cells displaying an increased number of detyrosinated MTs, also the level of acetylated MTs is increased (data not shown). Such accumulation of two independent posttranslationally modified forms of tubulin argues in favor of an effect of GFP-CLASP overexpression on MT longevity rather than on the tubulin modification machinery itself. In agreement with a stabilizing function of CLASPs, the whole MT cytoskeleton becomes much more dense and entangled in GFP-CLASP-expressing cells (compare Figure 6B1 to Figure 6C2).

In a second experiment, we examined the effect of injected anti-CLASP2 antibodies on the orientation of stabilized MTs at the leading edge. A very high proportion of cells, injected with purified anti-CLASP2 antibodies, show reduced and disorganized stabilized MTs (Figures 6D and 6F) as compared to cells injected with control antibodies (Figures 6D and 6E). The fact that not all cells are affected by anti-CLASP2 injection might be due to variations in the amount of antibody injected, to variations in the state of polarization of motile fibroblasts that were injected, and/or to differences in the expression levels of CLASP1 and -2 within individual cells. Taken together, both the overexpression and antibody inhibition analyses point to a crucial role for CLASPs in the regulation of MT dynamics, in particular in the stabilization of MTs in polarized fibroblasts.

Regulation of CLASP-MT Association by Phosphorylation

The relocalization of CLASP2 upon serum stimulation suggests that CLASPs associate with MTs in a spatially regulated manner. Recently, it was documented that spatial sensing in fibroblasts is mediated by 3′ phosphoinositides (Haugh et al., 2000), implying the involvement of phosphoinositide (PI)-3 kinase at the leading edge. We therefore tested whether inhibition of PI-3 kinase activity affects polarized localization of CLASP2. Serum stimulation in the presence of the PI-3 kinase inhibitors

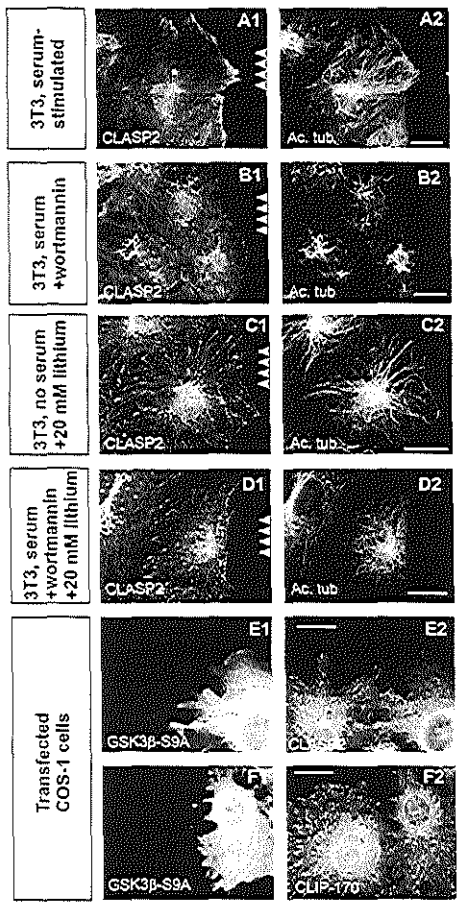

Figure 7. Regulation of Asymmetric CLASP2 Distribution

(A–D) A wounded monolayer of 3T3 cells (see Figure 5) was serum stimulated (A, B, and D) or kept on serum-free medium (C). To inhibit PI-3 kinase or GSK3β, either wortmannin (B and D) or LiCl (C and D) were added, respectively. Cells were fixed and costained with antibodies against CLASP2 and acetylated tubulin. White arrowheads mark the position of the wound in the monolayer.

(E and F) COS-1 cells, transfected with constitutively active, HA-tagged GSK3β-S9A, were fixed and costained with anti-HA antibodies (E1 and F1) and antibodies against CLASP2 (E2) or CLIP-170 (F2). Bar, 10 μm.

wortmannin or LY294002 indeed reduces the normal serum-induced accumulation of CLASP2 at the leading edge (compare Figure 7B to Figure 7A, or 5E). Absence of CLASP accumulation correlates with lack of polarized arrays of acetylated MTs (Figure 7B2). We next tested if glycogen synthase kinase (GSK)-3β, one of the downstream targets of PI-3 kinase, plays a role in regulating CLASP-MT distal end association. Treatment of serum-starved 3T3 cells (which normally do not contain much MT bound CLASP, Figure 5B) with lithium chloride, a direct inhibitor of GSK-3β, results in a significant increase in CLASP2 signal at distal MT ends (Figure 7C1) and in the appearance of extended acetylated MTs (Figure 7C2), which, like CLASP2, are localized throughout the cell. A similar result is observed in lithium-treated cells, which are serum stimulated in the presence of wortmannin (Figure 7D), indicating that GSK-3β inhibition is critical in regulating CLASP–MT interactions. This idea is supported by the observation that overexpression of a constutively active form (GSK-3β-S9A, where serine 9 is replaced by alanine) significantly inhibits CLASP2 localization to MT plus ends in transfected COS-1 cells (Figure 7E), but not that of CLIP-170 (Figure 7F).

Discussion

CLASPs Induce Local Stabilization of MTs

The MT network is a highly dynamic structure that is capable of quick rearrangements in response to environmental cues (Kirschner and Mitchison, 1986). Proteins, which bind to MT tips are of particular interest, since they are likely to be involved in regulation of MT dynamics and/or the interaction of MTs with the cellular cortex. CLIP-170 and CLIP-115 are such plus end binding proteins (Perez et al., 1999; Hoogenraad et al., 2000). Recently, a CLIP-170-like protein from fission yeast, tip1p, was shown to function as an anti-catastrophe factor (Brunner and Nurse, 2000), indicating that CLIP-115 and -170 might have a similar role in mammals. In this study, we identified CLASP1 and -2 as common protein partners of CLIP-115 and -170, which, similar to CLIPs, localize to MT tips. CLASPs are homologous along their entire length to the *Drosophila* MAP Orbit/Mast (Inoue et al., 2000; Lemos et al., 2000). Like Orbit/Mast, CLASPs directly bind MTs. Overexpression of CLASPs in COS-1 cells induces MT stabilization, while inhibition of CLASP2 function by antibody injections prevents the formation of aligned and stabilized MTs in motile fibroblasts. CLASP2 is predominantly bound to MTs at the leading edge of 3T3 cells, where they tend to grow or become stabilized, and not in the cell body, where MTs are unstable and often depolymerize. Taken together, this evidence strongly suggests that CLASPs are MAPs that regulate MT dynamics in polarized cells.

Potential Role of CLASP Isoform Variability

CLASPs exist as a family of isoforms, distinguished by their N-terminal sequences. The domain present in the long CLASP1/2α isoforms (and in Orbit/Mast) is similar to protein sequences in the MT stabilizing proteins of the dis1/TOG family. Although this suggests a function for the dis1/TOG domain of CLASPα in MT stabilization, deletion of the domain did not make a difference in the MT stabilization assay in transfected COS-1 cells. Interestingly, the dis1/TOG members ZYG-9 and Mini Spindles associated with spindle poles and centrosomes (Matthews et al., 1998; Cullen et al., 1999) and transfected GFP-CLASP1α preferentially accumulated in centrosomally originating MT bundles, while the other isoforms did not. It is therefore possible that the N-terminal domain of CLASPα plays a role in centrosomal MT nucleation.

The N terminus of CLASP2β is a membrane-targeting domain, similar to the dual palmitoylation module identified in several other proteins (Resh, 1999). Palmitoylation plays an essential role in protein sorting; for example, it is required to target the membrane-associated guanylate kinase PSD-95 to the postsynaptic density (El-Husseini et al., 2000). The existence of a brain-specific CLASP isoform with a membrane-targeting signal, together with more widely expressed isoforms lacking such a signal, is reminiscent of a situation described for the stathmin protein family. Stathmin is a small cytosolic phosphoprotein, which destabilizes MTs and which is the prototype member of a family, that includes the nervous system proteins SCG10, SCLIP, and RB3 (Gavet et al., 1998). These proteins can associate with membranes through their dually palmitoylated N termini and at least one of them, SCG10, is specifically localized to neuronal growth cones (Di Paolo et al., 1997). The existence of both stabilizing (CLASP) and destabilizing (stathmin) factors with similar targeting properties could provide a mechanism for the fine regulation of MT dynamics in particular neuronal compartments.

Regulation of CLASP–MT Interactions at Distal Ends

Different from other MT-stabilizing factors, such as XMAP215, which bind along the whole length of MTs, CLASPs can induce MT stabilization when present only at the distal ends of MTs. Both in CLASP-overexpressing COS-1 cells and at the leading edge of 3T3 fibroblasts, this stabilization is associated with the presence of a "coat" of CLASP at distal segments. Our findings indicate that PI-3 kinase signaling through GSK3β is an important mediator of the asymmetric CLASP2–MT interactions in 3T3 fibroblasts. These results are consistent with the observation that PI-3 kinase plays an essential role in the polarization of fibroblasts (Haugh et al., 2000) and that one of the biological responses of PI-3 kinase activation is the inactivation of GSK3β (van Weeren et al., 1998). The latter actually fulfills all the requirements for being a negative regulator of CLASP2–MT interactions. First, our in vitro studies suggest that MT binding by CLASPs is negatively influenced by phosphorylation. Second, unlike many other kinases, GSK3β is constitutively active in resting cells (such as serum-starved cells) and is inhibited when cells are stimulated by a number of growth factors. These results are in line with the fact that CLASP binding to distal ends is reduced in serum-starved cells (or in cells overexpressing a constitutively active form of GSK3β) and stimulated by serum (or by inactivation of GSK3β with lithium chloride). Thus, the polarized accumulation of CLASPs is subject to regulation by positional cues and by serum, which distinguishes CLASPs from other MT plus end binding proteins, such as CLIPs and EB1.

Functional Significance of the CLIP–CLASP Interaction

We have shown that the C-terminal domain of CLASPs specifically binds to a portion of the coiled-coil domain of CLIP-115 and -170. In vivo, this CLIP–CLASP interaction might be transient since the distribution of CLIPs and CLASPs shows only partial overlap in interphase fibroblasts. There is a substantial Golgi-associated pool of CLASPs, while CLIP-170 and CLIP-115 do not accumulate significantly in the Golgi. Also, in serum-stimulated 3T3 cells, only a subset of EB1/CLIP-positive MT tips are labeled strongly with anti-CLASP2 antibodies. In serum-grown 3T3 cells, CLIPs and EB1 are most concentrated at the very tip of an MT, while longer and more proximal MT segments are stained by anti-CLASP2 antibodies. A transient CLIP–CLASP interaction would account for previous failures to copurify CLASPs (or any other protein) with CLIP-170 (Scheel et al., 1999). Also, in our hands, no significant amounts of CLIP-170 could be coprecipitated with CLASP from untransfected COS-1 cells.

The affinity of CLASPs for MT tips is not solely dependent on interaction with CLIPs since a CLASP2 mutant, lacking the CLIP binding domain, is still targeted to MT plus ends. In spite of this fact and the putative transient nature of the CLIP–CLASP interaction, these proteins are highly likely to influence the affinity of each other for MTs and thereby affect the fate of MTs. For example, CLIPs could stimulate the loading of (membrane bound) CLASPs onto the MT plus ends. Conversely, accumulation of CLASPs on distal segments of a subset of MTs might serve to attract CLIP-170 (or CLIP-115) to the tips of MTs, even under conditions of MT shrinkage and/or pausing, conditions that normally cause dissociation of CLIP-170 from the distal ends (Perez et al., 1999). Attraction of the CLIPs by a CLASP-positive segment may rescue pausing/retracting MTs and revert them to a state of growth and may be one of the mechanisms by which CLASPs stabilize MTs. This model is both in line with the proposed anti-catastrophe role of tip1p (Brunner and Nurse, 2000) and with the observation that CLIP-170 treadmills on the growing ends of MTs by copolymerization with tubulin and could thus be an inherent part of the MT polymerization machinery (Diamantopoulos et al., 1999; Perez et al., 1999). It also would explain the increased longevity of a subset of MTs at the leading edge (Cook et al., 1998) and why these MTs still have their tips decorated with EB1/CLIP. In conclusion, we propose that CLIP–CLASP interactions constitute part of a regulatory device on the distal ends of MTs that is needed to target or modulate MT dynamics in polarized cells. The partnership between CLIPs and CLASPs bears a striking resemblance to that of APC and EB1, two proteins which bind to each other, accumulate at MT plus ends, and regulate MT dynamics in polarized cells (for review, see Tirnauer and Bierer, 2000). It will be interesting to investigate to what extent CLIP–CLASP and APC–EB1 pathways interact.

Experimental Procedures

Yeast Two-Hybrid Screen

A mouse E14.5 day embryonic cDNA library (Chevray and Nathans, 1992) was screened by the yeast two-hybrid assay (Wolthuis et al., 1996). Fragments of rat CLIP-115, rat brain CLIP-170, and chicken $p150^{Glued}$ were cloned into the pPC97 yeast two-hybrid vector (see Figure 1A). Production of yeast proteins was verified by Western blotting using monoclonal antibodies against GAL4 DNA binding and activation domains (Clontech). Mouse CLASP1 cDNA, derived from the yeast two-hybrid screen, corresponds to the 3′ portion of KIAA0622, starting from position 3010 (see Figure 1B). Interaction of mCLASP1 with CLIP-115 was verified by exchanging the inserts of bait and fish vectors.

cDNA Isolation and Northern Blotting

The CLIP-170 clone used here is a rat brain cDNA encoding a CLIP-170 isoform with a 115 amino acid deletion in the C-terminal portion of the coiled-coil region (accession number AJ237670). Human KIAA0622 (CLASP1) and KIAA0627 (CLASP2) cDNAs (Ishikawa et al., 1998) were obtained from the Kazuza DNA Research Institute. To complete the 5′ ends of these cDNAs, we used RACE-PCR with human adult brain poly(A)$^+$ RNA (Clontech) or mouse brain RNA as a template. Mouse EST ui60h04 (truncated CLASP2α) is an IMAGE clone. Rat cDNA clone r313 (CLASP2β) was isolated by screening of a rat hippocampus cDNA library (De Zeeuw et al., 1997). Accession numbers are: AJ288057 (human brain 5′ end CLASP1α), AJ288058, and AJ288059 (human brain 5′ end CLASP2γ and -β, respectively); AJ288060 (clone r313); AJ288061 (mouse yeast two-hybrid CLASP1); AJ276961 (ui60h04), and AJ276962 (mouse brain 5′ end CLASP1α). Northern blots were prepared and hybridized using standard protocols (Sambrook et al., 1989).

GST Fusion Constructs and Generation of CLASP Antisera

Glutathione S-transferase (GST) fusions were generated using plasmids pGEX-2T and pGEX-3X (Pharmacia). GST-mCLASP1-C contains the whole coding part of the mouse yeast two-hybrid CLASP1 cDNA. GST-hCLASP2 contains the corresponding C terminus of human CLASP2 (nucleotide positions 3074–3976 of the KIAA0627 cDNA). The GST-CLIP fusion proteins are explained in Figure 3A. Purification of GST fusion proteins and immunization of rabbits were performed as described (Hoogenraad et al., 2000). Antiserum #2358 is against GST-hCLASP2.

Western Blot Analysis and Immunoprecipitations

Protein extract preparation, Western blotting, and CLIP antisera have been described (Hoogenraad et al., 2000). Proteins were detected using rabbit polyclonal anti-GFP (1:2500; Clontech) or anti-CLIP and CLASP antibodies (all used at 1:2500). The Triton-X114 partitioning assay was performed as published (Hancock et al., 1989).

In the immunoprecipitation experiments, transfected COS-1 cells were lysed in buffer containing 30 mM HEPES (pH 7.4), 100 mM KCl, 1% NP-40, supplemented with protease inhibitors (Boehringer Mannheim), and incubated at 4°C for 30 min to depolymerize MTs. All subsequent steps were carried out as described (Hoogenraad et al., 2000).

GST Pulldown and MT Binding Assays

KIAA0622, KIAA0627, and CLIP-115 cDNAs were transcribed and translated in vitro using the TnT-coupled transcription-translation system (Promega) and ^{35}S-methionine (Trans35S label, ICN). Aliquots of radiolabeled proteins were incubated with different GST fusion proteins in NETT buffer (100 mM NaCl, 50 mM Tris (pH 7.5), 5 mM EDTA, 0.5% Triton X-100) for 2 hr at room temperature. Afterwards, samples were washed five times in NETT buffer. Proteins were eluted by boiling in sample buffer and analyzed by SDS-PAGE. Dried gels were exposed to film.

Mouse brains were homogenized in NETT buffer containing protease inhibitors. After removing insoluble material by centrifugation for 10 min at 10,000 × g, protein extract was used for the GST pulldown assay, as described above. Bound proteins were detected by Western blotting.

For the MT binding assays (Hoogenraad et al., 2000), CLASP1α and r313 plasmids were transcribed and translated. Some samples were treated for 15 min at 30°C with apyrase (1 U, Sigma) immediately after translation. The MT blot overlay was performed as described (Brunner and Nurse, 2000).

Expression Constructs

GFP-CLASP1 contains the whole open reading frame of KIAA0622, subcloned in-frame into pEGFP-C1 (Clontech). CLASP1α was constructed from KIAA0622 and an overlapping human brain RACE product, encoding the XMAP215-homologous domain, by using a unique AvrII site at position 580 in KIAA0622. Fusing the CLASP1α insert into pEGFP-C1 produced GFP-CLASP1α. Untagged CLASP2γ consists of the whole insert of KIAA0627, cloned into pCI-neo (Promega). GFP-CLASP2 was made by inserting KIAA0627 cDNA from the BspEI site at position 184 into pEGFP-C1; it therefore lacks the first 29 amino acids encoded by KIAA0627. In the GFP-CLASP2 C-terminal deletion constructs, the CLASP2 coding sequence was abrogated at nucleotide positions 1830 (GFP-CLASP2ΔSal) and 3138 (GFP-CLASP2ΔXho) of the KIAA0627 sequence. The GSK-3β (S9A) construct has been described (van Weeren et al., 1998).

Cell Culture Manipulations and Immunofluorescence

COS-1 cells were cultured and transfected as described (Hoogenraad et al., 2000). Swiss 3T3 fibroblasts were cultured in DMEM medium with 8% fetal calf serum. Serum starvation and monolayer wounding were as reported (Gundersen et al., 1994). For PI3-kinase inhibition, 100 nM wortmannin or 300 μM LY294002 (Sigma) was used. For GSK-3β inhibition, 10–20 mM LiCl was added to the culture medium. Antibody injections into fibroblasts on the edge of the stripes were performed as published previously (van Vuuren et al., 1994). Injections were done 2 hr prior to serum induction using IgG-purified antibodies at 5 mg/ml. Injected cells were detected using fluorescently labeled rabbit secondary antibodies. The percentage of cells with reduced or disorganized stabilized MTs was determined by staining with antibodies against acetylated tubulin. Stabilized MTs were scored as disorganized if their amount was highly reduced (see example in Figure 6F) and/or if they displayed random orientation with respect to the loading edge. Percentages were determined by counting 79 cells injected with control #2358 preimmune IgG (16% disorganized), 86 cells injected with control anti-ERCC1 antibodies (van Vuuren et al., 1994; 14% disorganized), and 233 cells injected with anti-CLASP2 antibodies (results from the two independent experiments with the different control antibodies; 76% disorganized).

Immunofluorescence experiments (Hoogenraad et al., 2000) were performed using rabbit anti-CLASP2 antiserum, antiserum #2221, which recognizes both CLIP-115 and CLIP-170 and antiserum #2238, which is specific for CLIP-115 (Hoogenraad et al., 2000). In a dilution of 1:300. Rabbit antibodies against Glu tubulin (a gift from Dr. J. C. Bulinski) were diluted at 1:500. Mouse monoclonal antibodies against the HA tag (BABCO), β-tubulin, acetylated tubulin and vinculin (Sigma), EB1, and GM130 (Transduction Laboratories) were diluted 1:100. Secondary antibodies used were rhodamine-conjugated sheep anti-mouse (1:25, Boehringer Mannheim), Alexa 594-conjugated goat anti-rabbit (1:500, Molecular Probes), FITC-conjugated goat anti-rabbit (1:100, Nordic Laboratories), and Alexa 350-conjugated sheep anti-mouse (1:250, Molecular Probes).

Signals were captured with a Leica DMRBE fluorescence microscope equipped with a Hamamatsu C4880 DCC camera. To quantify the GFP fluorescence, cells were imaged using fixed data collection times: 150 ms for highly expressing cells, 600 ms for moderately expressing cells, and 1200 ms for cells expressing low levels of GFP fusion protein.

Acknowledgments

We are grateful to Dr. T. A. Schroer for sending the chicken p150^{Glued} cDNA, to Dr. J. C. Bulinski for sending anti-Glu tubulin antiserum, and to Dr. T. Nagase for providing KIAA0622 and KIAA0627 cDNAs. This research was supported by grants from the Netherlands Organization for Scientific Research (NWO; GB-MW 903-68-361), the Life Sciences Foundation (SLW; 805.33.310; 803.33.311), and the Royal Dutch Academy of Sciences (KNAW).

Received June 23, 2000; revised January 25, 2001.

References

Brunner, D., and Nurse, P. (2000). CLIP170-like tip1p spatially organizes microtubular dynamics in fission yeast. Cell *102*, 695–704.

Bulinski, J.C., and Gundersen, G.G. (1991). Stabilization of post-translational modification of microtubules during cellular morphogenesis. Bioessays *13*, 285–293.

Chevray, P.M., and Nathans, D. (1992). Protein interaction cloning in yeast: identification of mammalian proteins that react with the leucine zipper of Jun. Proc. Natl. Acad. Sci. USA *89*, 5789–5793.

Cook, T.A., Nagasaki, T., and Gundersen, G.G. (1998). Rho guano-

sine triphosphatase mediates the selective stabilization of microtubules induced by lysophosphatidic acid. J. Cell Biol. *141*, 175–185.

Cullen, C.F., Deak, P., Glover, D.M., and Ohkura, H. (1999). Mini spindles: a gene encoding a conserved microtubule-associated protein required for the integrity of the mitotic spindle in Drosophila. J. Cell Biol. *146*, 1005–1018.

Desai, A., and Mitchison, T.J. (1997). Microtubule polymerization dynamics. Annu. Rev. Cell Dev. Biol. *13*, 83–117.

De Zeeuw, C.I., Hoogenraad, C.C., Goedknegt, E., Hertzberg, E., Neubauer, A., Grosveld, F., and Galjart, N. (1997). CLIP-115, a novel brain-specific cytoplasmic linker protein, mediates the localization of dendritic lamellar bodies. Neuron *19*, 1187–1199.

Di Paolo, G., Lutjens, R., Pellier, V., Stimpson, S.A., Bouchat, M.H., Catsicas, S., and Gronningloh, G. (1997). Targeting of SCG10 to the area of the Golgi complex is mediated by its NH2-terminal region. J. Biol. Chem. *272*, 5175–5182.

Diamantopoulos, G.S., Perez, F., Goodson, H.V., Batelier, G., Melki, R., Kreis, T.E., and Rickard, J.E. (1999). Dynamic localization of CLIP-170 to microtubule plus ends is coupled to microtubule assembly. J. Cell Biol. *144*, 99–112.

Dujardin, D., Wacker, U.I., Moreau, A., Schroer, T.A., Rickard, J.E., and De Mey, J.R. (1998). Evidence for a role of CLIP-170 in the establishment of metaphase chromosome alignment. J. Cell Biol. *141*, 849–862.

El-Husseini, A.E., Craven, S.E., Chetkovich, D.M., Firestein, B.L., Schnell, E., Aoki, C., and Bredt, D.S. (2000). Dual palmitoylation of PSD-95 mediates its vesiculotubular sorting, postsynaptic targeting, and ion channel clustering. J. Cell Biol. *148*, 159–172.

Gavet, O., Ozon, S., Manceau, V., Lawler, S., Curmi, P., and Sobel, A. (1998). The stathmin phosphoprotein family: intracellular localization and effects on the microtubule network. J. Cell Sci. *111*, 3333–3346.

Gundersen, G.G., Kim, I., and Chapin, C.J. (1994). Induction of stable microtubules in 3T3 fibroblasts by TGF-beta and serum. J. Cell Sci. *107*, 645–659.

Hancock, J.F., Magee, A.I., Childs, J.E., and Marshall, C.J. (1989). All ras proteins are polyisoprenylated but only some are palmitoylated. Cell *57*, 1167–1177.

Haugh, J.M., Codazzi, F., Teruel, M., and Meyer, T. (2000). Spatial sensing in fibroblasts mediated by 3′ phosphoinositides. J. Cell Biol. *151*, 1269–1280.

Hoogenraad, C.C., Akhmanova, A., Grosveld, F., De Zeeuw, C.I., and Galjart, N. (2000). Functional analysis of CLIP-115 and its binding to microtubules. J. Cell Sci. *113*, 2285–2297.

Inoue, Y.H., do Carmo Avides, M., Shiraki, M., Deak, P., Yamaguchi, M., Nishimoto, Y., Matsukage, A., and Glover, D.M. (2000). Orbit, a novel microtubule-associated protein essential for mitosis in Drosophila melanogaster. J. Cell Biol. *149*, 153–166.

Ishikawa, K., Nagase, T., Suyama, M., Miyajima, N., Tanaka, A., Kotani, H., Nomura, N., and Ohara, O. (1998). Prediction of the coding sequences of unidentified human genes. X. The complete sequences of 100 new cDNA clones from brain which can code for large proteins in vitro. DNA Res. *5*, 169–176.

Kirschner, M., and Mitchison, T. (1986). Beyond self-assembly: from microtubules to morphogenesis. Cell *45*, 329–342.

Lemos, C.L., Sampaio, P., Maiato, H., Costa, M., Omel'yanchuk, L.V., Liberal, V., and Sunkel, C.E. (2000). Mast, a conserved microtubule-associated protein required for bipolar mitotic spindle organization. EMBO J. *19*, 3668–3682.

Liao, G., Kroltzer, G., Cook, T.A., and Gundersen, G.G. (1999). A signal transduction pathway involved in microtubule-mediated cell polarization. Fasob. J. *13*, S257–S260.

Matthews, L.R., Carter, P., Thierry-Mieg, D., and Kemphues, K. (1998). ZYG-9, a Caenorhabditis elegans protein required for microtubule organization and function, is a component of meiotic and mitotic spindle poles. J. Cell Biol. *141*, 1159–1168.

Mimori-Kiyosue, Y., Shiina, N., and Tsukita, S. (2000). The dynamic behavior of the APC-binding protein EB1 on the distal ends of microtubules. Curr. Biol. *10*, 865–868.

Perez, F., Diamantopoulos, G.S., Stalder, R., and Kreis, T.E. (1999). CLIP-170 highlights growing microtubule ends in vivo. Cell *96*, 517–527.

Pierre, P., Scheel, J., Rickard, J.E., and Kreis, T.E. (1992). CLIP-170 links endocytic vesicles to microtubules. Cell *70*, 887–900.

Resh, M.D. (1999). Fatty acylation of proteins: new insights into membrane targeting of myristoylated and palmitoylated proteins. Biochim. Biophys. Acta *1451*, 1–16.

Sambrook, J., Fritsch, E.F., and Maniatis, T. (1989). Molecular Cloning: A Laboratory Manual, 2nd Edition (New York: Cold Spring Harbor Laboratory Press).

Scheel, J., Pierre, P., Rickard, J.E., Diamantopoulos, G.S., Valetti, C., van der Goot, F.G., Haner, M., Aebi, U., and Kreis, T.E. (1999). Purification and analysis of authentic CLIP-170 and recombinant fragments. J. Biol. Chem. *274*, 25883–25891.

Timauer, J.S., and Bloror, B.E. (2000). EB1 proteins regulate microtubule dynamics, cell polarity, and chromosome stability. J. Cell Biol. *149*, 761–766.

Timauer, J.S., O'Toole, E., Berrueta, L., Bloror, B.E., and Pellman, D. (1999). Yeast Bim1p promotes the G1-specific dynamics of microtubules. J. Cell Biol. *145*, 993–1007.

Valetti, C., Wetzel, D.M., Schrader, M., Hasbani, M.J., Gill, S.R., Kreis, T.E., and Schroer, T.A. (1999). Role of dynactin in endocytic traffic: effects of dynamitin overexpression and colocalization with CLIP-170. Mol. Biol. Cell *10*, 4107–4120.

van Vuuren, A.J., Vermeulen, W., Ma, L., Weeda, G., Appeldoorn, E., Jaspers, N.G., van der Eb, A.J., Bootsma, D., Hoeijmakers, J.H., Humbert, S., et al. (1994). Correction of xeroderma pigmentosum repair defect by basal transcription factor BTF2 (TFIIH). EMBO J. *13*, 1645–1653.

van Weeren, P.C., de Bruyn, K.M., de Vries-Smits, A.M., van Lint, J., and Burgering, B.M. (1998). Essential role for protein kinase B (PKB) in insulin-induced glycogen synthase kinase 3 inactivation. Characterization of dominant-negative mutant of PKB. J. Biol. Chem. *273*, 13150–13156.

Vaughan, K.T., Tynan, S.H., Faulkner, N.E., Echeverri, C.J., and Vallee, R.B. (1999). Colocalization of cytoplasmic dynein with dynactin and CLIP-170 at microtubule distal ends. J. Cell Sci. *112*, 1437–1447.

Wittmann, T., Hyman, A., and Desai, A. (2001). The spindle: a dynamic assembly of microtubules and motors. Nat. Cell Biol. *3*, E28–E34.

Wolthuis, R.M., Bauer, B., van't Veer, L.J., de Vries-Smits, A.M., Cool, R.H., Spaargaren, M., Wittinghofer, A., Burgering, B.M., and Bos, J.L. (1996). RalGDS-like factor (Rlf) is a novel Ras and Rap 1A-associating protein. Oncogene *13*, 353–362.

GenBank Accession Numbers

The GenBank accession numbers for the eight sequences reported in this paper are: AJ237670 (rat brain CLIP-170); AJ288057 (human brain 5′ end CLASP1α); AJ288058 and AJ288059 (human brain 5′ end CLASP2γ and -β, respectively); AJ288060 (clone r313); AJ288061 (mouse yeast two-hybrid CLASP1); AJ276961 (ui60h04) and AJ276962 (mouse brain 5′ end CLASP1α).

Chapter 6

COMPARATIVE ANALYSIS OF CLIP-115 AND CLIP-170: EXPRESSION PATTERNS AND BINDING PARTNERS IN THE BRAIN

Casper C. Hoogenraad[1,2*], Anna Akhmanova[1*], Yvonne Krom[1], Bjorn R. Dortland[1], Chris I. De Zeeuw[2], Tama Hasson[3], Frank Grosveld[1], Niels Galjart[1]

MGC Departments of [1]Cell Biology and Genetics, [2]Anatomy, Erasmus Univerisity, P.O. Box 1738, 3000 DR Rotterdam, The Netherlands. [3]Department of Biology, University of California at San Diego, La Jolla *These authors contributed equally to the results described in this paper.

Summary

CLIP-115 and CLIP-170 are two structurally similar mammalian proteins, which localize to the ends of growing microtubules. Here we describe a novel splicing variant of CLIP-170, CLIP-170-br, which represents the predominant brain isoform of this protein. In vivo localization of CLIP-170-br and CLIP-115 in mouse brain reveals distinct but overlapping expression patterns. Coexpression experiments show that both CLIPs can compete with each other for the binding to microtubule tips. CLIP-115 and CLIP-170-br can interact with CLASP1 and 2, while some muscle-enriched splicing isoforms of CLIP-170 show reduced affinity for these proteins, suggesting that CLIP-CLASP interactions might be more important in the brain than in the muscle. We also analyzed a potential interaction between both CLIPs and myosin VI, because their *Drosophila* homologues, D-CLIP-190 and myosin 95F were shown to associate with each other, but found no evidence to support such an interaction in mammals. Finally, we show that CLIP-170, but not CLIP-115, is able to enhance the accumulation of dynactin and LIS1 at the microtubule tips. Our results suggest that CLIP-170 may act as a scaffold to mediate the recruitment of both LIS1 and dynactin to the microtubule tips. CLIP-115 might partially inhibit this function by reducing CLIP-170 concentration at these sites.

Introduction

The formation of a highly specific pattern of connections in the nervous system proceeds by the extension of long processes from the neuronal cell bodies. Neurites must elongate, find the appropriate pathway, branch and finally establish connections [1]. Changes in the organization of microtubules in axons and dendrites are strongly implicated in the mechanism of neuronal growth and maintenance [2-4]. In addition, microtubules also play a central role in intracellular membrane transport and cell polarity [5]. Microtubules are themselves polarized tubular structures, with a plus and minus end, and are formed by the polymerization of tubulin. Microtubule plus ends undergo phases of growing and shortening, referred to as dynamic instability [6]. Microtubule polymerization or depolymerization as well as switching between theses phases are regulated by multiple cellular factors.

It is likely that microtubule plus end dynamics depends on regulatory factors which specifically bind to the microtubule tip. CLIP-170 and CLIP-115 are microtubule binding proteins present at the plus ends of growing microtubules [7,8]. The two CLIPs are structurally similar: their N-terminal part consists of two conserved microtubule binding domains (MTB) surrounded by basic serine-rich regions, while a long coiled-coil segment in the middle of each protein allows dimerization [8,9]. The C-terminal domain of CLIP-170 contains two metal binding motifs, which are not present in CLIP-115.

In fission yeast, the CLIP-170 homologue, tip1p, has been shown to suppress microtubule catastrophes specifically when the microtubules contact the cell cortex in certain cell areas [10]. In addition, we recently showed that CLIP-115 and -170

associated proteins, CLASP1 and -2, localize at microtubule distal ends at the leading edge of the motile fibroblasts and participate in local stabilization of microtubules in these polarized cells [11]. These studies suggest that CLIPs, most likely in concert with associating proteins, are involved in the local regulation of microtubule dynamics.

The specific localization of CLIPs at the growing microtubule plus ends may also promote the interactions of microtubules with the cellular cortex or cargoes, destined for transport, such as membrane organelles. In favor of this latter view, CLIP-170 was initially described as linking microtubules to endosomes in vitro [12]. In addition, *Drosophila* CLIP-170, D-CLIP-190, is found to be associated with a class VI unconventional myosin [13]. The association of a myosin and a microtubule binding protein suggests that these two proteins may link microtubule plus ends to cortical actin cables and coordinate the microtubule and actin-based transport of vesicles [14,15]. However, it needs to be determined whether this interaction is conserved in vertebrates. Further more compelling evidence for the role of CLIP-170 in organelle transport has emerged from recent studies on the minus end directed motor protein dynein and its activator dynactin. CLIP-170 has been colocalized with both complexes at the microtubule plus ends [16]. Overexpression of CLIP-170 relocalizes the components of the dynactin complex, which is dependent on the C-terminus of CLIP-170 [17]. It was proposed that CLIP-170 first targets dynactin to the microtubule tip and subsequently dynein is loaded to this site and becomes activated to perform minus end directed transport [16-18].

Another potential participant in dynein-mediated transport is an evolutionary conserved protein LIS1. It was originally identified as the mutated gene responsible for the brain abnormalities in type 1 lissencephaly [19]. Genetic analyses in flies and fungi implicated LIS1 and dynein-mediated processes, such as nuclear migration [20-23]. Mammalian LIS1 co-immunoprecipitates with both cytoplasmic dynein and dynactin [24-26]. LIS-1 and its homologue in *Aspergillus*, NudF, localize to microtubule tips [27,28] and overexpression of LIS1 abolishes the localization of dynactin to the microtubule plus ends [25], suggesting that LIS1 has a function in the dynein-dynactin pathway at the microtubule tips. The role of CLIPs in the LIS1/dynein/dynactin pathway is not yet clear.

In the present study we isolated an isoform of CLIP-170, named CLIP-170-br, which is predominately expressed in the brain. We analyzed the distribution of CLIP-170 and CLIP-115 in the brain and, since CLIP-170 and CLIP-115 are coexpressed in many neuronal types, we tested the competition of CLIP-115 and -170 at the microtubule plus ends. Furthermore, we compared the interaction between CLIP-170 isoforms and CLIP-115 with some of their potential brain protein partners, such as CLASP, myosin VI, dynactin, LIS1 and LIS1-associating proteins NudE, NudEL and NudC. The functional implications of our findings will be discussed.

Results

Isolation and characterization of an alternatively spliced CLIP-170 isoform, which is predominately expressed in the brain

We have screened a rat hippocampus cDNA library using as a probe a CLIP-115 cDNA fragment, encoding the MTBs [29]. In addition to CLIP-115 cDNAs, we have isolated overlapping cDNA clones encoding the rat homologue of CLIP-170/restin. Three longest clones contained an open reading frame (ORF) of 3963 bp, preceded by an in-frame stop codon, suggesting that these cDNAs cover the complete coding region (Fig 1a).

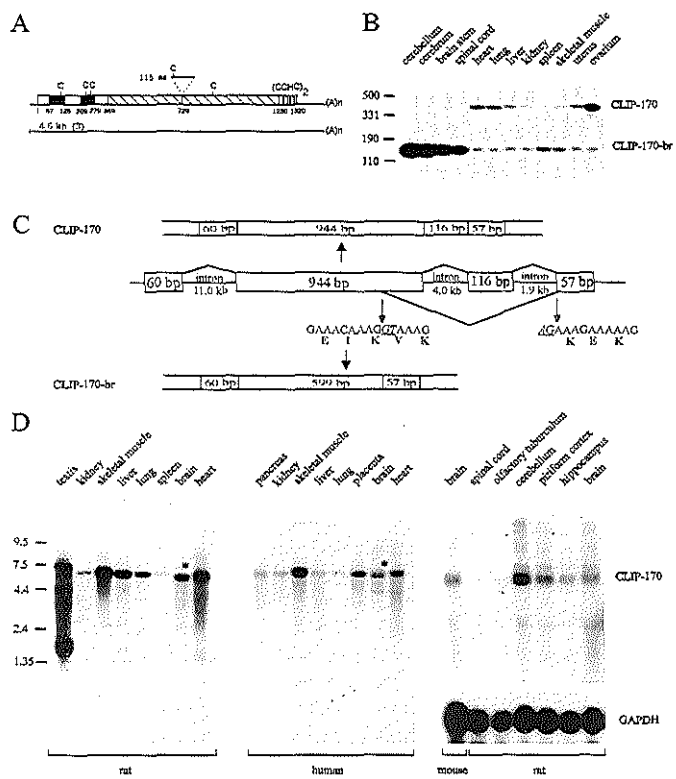

Figure 1. Cloning and expression of CLIP-170-br (**a**)Schematic representation of the longest CLIP-170-br-encoding cDNA. The structure of the CLIP-170-br protein is depicted (black bars: MTB domains; hatched bar: coiled-coil region; gray bars with $(CCHC)_2$: metal binding motifs). The amino acid positions and all cysteine residues are indicated below and above the protein structure, respectively. The position of the CLIP-170-br-specific deletion is indicated. (**b**) RT-PCR analysis of rat RNA from various tissues. Samples were resolved in a 2% agarose gel and stained with ethidium bromide. PCR amplification with primers common for CLIP-170 (458 bp product) and CLIP-170-br (113 bp product) reveals expression of the two isoforms in various tissues. (**c**) The genomic organization of the part of the human CLIP-170 gene covering the 345 bp fragment lacking in CLIP-170-br and the possible alternative splicing events. Exons are shown as boxes and introns as horizontal lines. The 345 bp fragment is covered by a part of the 944 bp exon and the 116 bp exon. Alternative splice sites, used to generate the CLIP-170-br transcript are indicated by open arrows, with the nucleotide and amino acid sequences around these sites shown below. Conserved dinucleotides that match the consensus sites are shown in italic and underlined, and amino acids, present in CLIP-170-br protein are shown in bold. (**d**) Analysis of CLIP-170 expression by Northern blotting. Northern blots containing RNA from human and rat tissues were hybridized with rat CLIP-170-br cDNA. Northern blots in the left and middle panels contained equal amounts of polyA(+) mRNA in all lanes, in the right panel GAPDH probe was used as a loading control.

Rat brain CLIP-170 sequence is very similar (83 % identity) to human restin and includes the restin-specific 35 amino acid insertion (see below). However, in contrast to both human CLIP-170 and restin, it contains a 345 bp long in-frame deletion in the middle part of the ORF (Fig. 1a,c). We named this splicing isoform CLIP-170-br. Comparison of the CLIP-170-br cDNA with the sequence of the human CLIP-170 gene [30] indicates that this splicing isoform results from an alternative 5' splice site usage and exon skipping (Fig. 1c).

To determine the expression profile of CLIP-170-br, we performed RT-PCR and northern blot analyses on multiple tissues. RT-PCR analysis with primers flanking the 345 bp deletion yields 458 bp product for CLIP-170/restin and 113 bp product for CLIP-170-br (Fig. 1b). This analysis reveals that CLIP-170-br is predominantly present in the brain.

Northern blots with total rat and human RNA, a CLIP-170 transcript of approximately 6 kb is present in all tissues examined (Fig. 1d). CLIP-170 is highly expressed in skeletal muscle, heart, brain and testis. The CLIP-170 transcript detected in human and rat brain is slightly smaller compared to the other tissues and is likely to correspond to the CLIP-170-br isoform. CLIP-170 is transcribed in different regions of the adult brain, displaying highest levels in the cerebellum (Fig 1d).

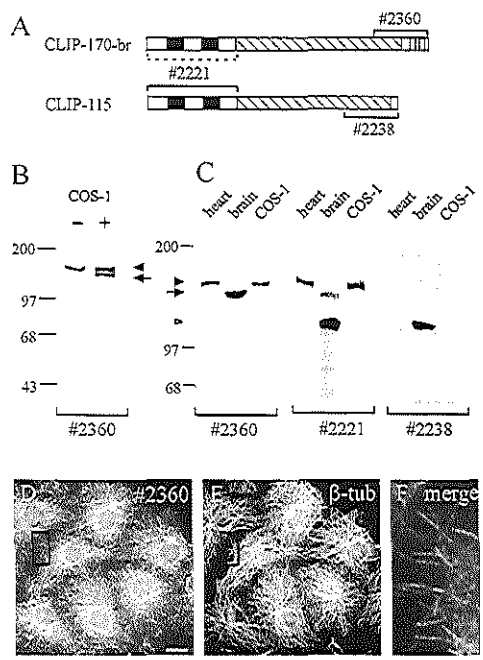

Figure 2. Characterization of the CLIP-170-specific antibodies
(**a**) Structure of CLIP-115 and CLIP-170-br proteins (depicted in the same way as in Fig.1a) and the position of the antigens used to generate anti-CLIP antibodies.(**b**) Western blots of cell extracts, prepared from untransfected COS-1 cells, or cells, transfected with CLIP-170-br. Blots are probed with the anti-CLIP-170 antibody (#2360). (**c**) Western blots of heart, brain and COS-1 cell homogenates were incubated with the antibodies, indicated under the blots. In (b) and (c) the band, corresponding to the full-length CLIP-170 is indicated by a black arrowhead, CLIP-170-br – by an arrow and CLIP-115 – by an open arrowhead. (**d-f**) Immunofluorescence staining of COS-1 cells with antibodies #2360 against CLIP-170 (d, green in merged picture) and β-tubulin (e, red in merged picture). Higher magnification view of the indicated part of the merged picture is shown in (f). Bar: 10 μm.

To investigate the in vivo distribution of the CLIP-170 in mouse or rat tissues, we have raised polyclonal antibodies against the C-terminus of the rat CLIP-170-br (antiserum #2360) (Fig. 2a). In COS-1 cell extracts, this antiserum reacts with a single protein band of ~160 kDa (Fig. 2b), which is the expected molecular mass of the full-length CLIP-170. In extracts of COS-1 cells, transfected with a CLIP-170-br-encoding expression vector, a second protein species of ~150 kDa is detected, which is in agreement with the expected size of this CLIP-170 isoform (148 kDa). A protein of ~150 kDa was also detected on western blots of brain tissue, while a protein of ~160 kDa was present in heart extracts (Fig.2c). These results were confirmed using our previously described antibodies, which recognize the N-termini of both CLIP-115 and CLIP-170 (#2221) and the C-terminal domain of CLIP-115 (#2238) [8] (Fig. 2a,c). Since both CLIP-170 antibodies (#2221 and #2360) detect a single CLIP-170 protein species in brain extracts, we conclude that the major CLIP-170 isoform in the brain is CLIP-170-br.

In immunofluorescence experiments in COS-1 cells, anti-CLIP-170 antibodies stains stretches of distal ends of microtubules (Fig. 2d-f), as has been described previously [7,12]. In transiently transfected COS-1 cells, CLIP-170-br shows the same distribution patterns as a full-length CLIP-170 (compare data in Fig. 4 to [7,31]), indicating that the brain-specific deletion has no apparent effect in this assay. The 345 bp deletion removes a part of the coiled-coil "stalk" of CLIP-170 and generates an amino acid motif KKEK (Fig. 1a,c). Interestingly, this motif is present in proteins that bind actin or actin-related proteins, such as the Arp1 subunit of the dynactin complex [32-34]. Interaction between CLIP-170-br and Arp1 could be relevant, because CLIP-170 is involved in targeting dynactin to the plus ends of microtubules ([16,17] and see below). However, by using yeast two-hybrid and in vitro binding assays we could detect no interaction between Arp1 and KKEK-containing part of the CLIP-170-br coiled coil region (data not shown). Overexpressed CLIP-170-br or its KKEK-containing tail did not colocalise with overexpressed Arp1 or with actin fibers and had no visible effect on the organization or distribution of the actin cytoskeleton (data not shown). Still, we cannot exclude that KKEK motif contributes to the CLIP-170-br interaction with dynactin or with actin filaments.

Distribution CLIP-170-br and CLIP-115 proteins in the brain

Northern blotting indicated that both CLIPs are present throughout the brain (Fig.1d and [29]). To determine in which brain cells and subcellular compartments CLIP-170-br and CLIP-115 are localized, an immunofluorescence and a light microscopy analysis on the brain sections from adult mouse were performed. Using anti-CLIP-115 antibody #2238, we observed strong labeling of the Purkinje cell bodies and dendrites in the molecular layer of the cerebellum (Fig. 3a-d). Anti-CLIP-170 antibody #2360 showed staining in the granular layer of the cerebellar cortex and not in the Purkinje cells (Fig. 3g,h). The CLIP-170-specific staining in the granular layer is concentrated in bright immunoreactive dots (arrowheads in Fig. 3h). Since they do not completely coincide with the bodies of the granular cells and often appear to be located

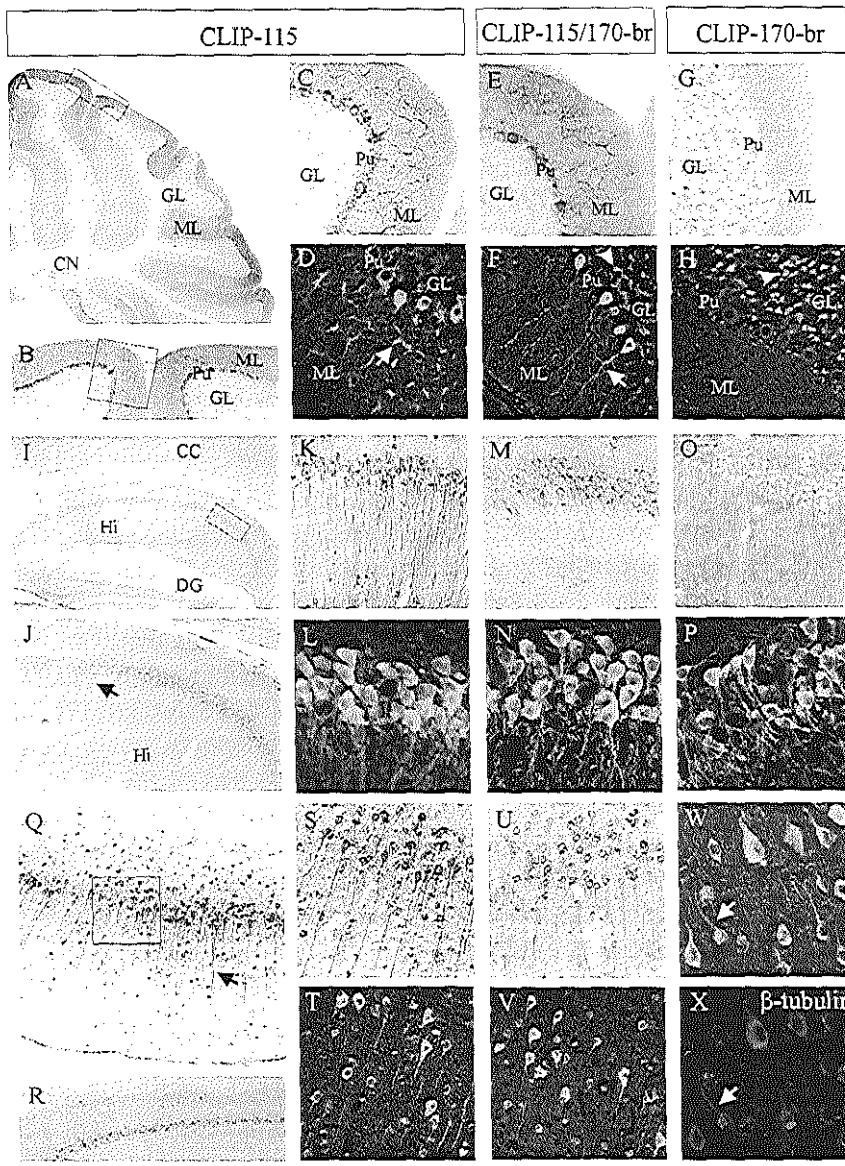

Figure 3. Localization of CLIP-115 and CLIP-170-br in mouse brain.
Sections of cerebellum (a-h), hippocampus (i-m), cerebral cortex (q, s-x) and olfactory bulb (r) immunostained for CLIP-115 (antiserum #2238), CLIP-115/CLIP-170 (antiserum #2221), and CLIP-170 (antiserum #2360). (a-c,e,g,i-k,m,o,r) are immunocytochemistry images of sagittal and (q,s,u) of transversal sections. (d,f,h,l,m,p,t,v-x) are immunofluorescence images of transversal sections. (w,x) Double staining of the cerebral cortex for CLIP-170 and β-tubulin. CLIP-115 and –170 – positive dendritic processes are indicated by arrows, and CLIP-170-specific staining in the granular layer of the cerebellum is indicated by arrowheads. CC, cerebral cortex; CN, cerebellum nuclei; GL, granular layer; Hi, Hippocampus; ML, molecular layer, Pu, Purkinje cell. Bar: 100 μm.

next to the these cells, these dots may represent axon terminals from the mossy fibers. Antibodies #2221, which are directed against both CLIP-115 and CLIP-170, stain Purkinje cells as well as the granular layer (Fig. 3e,f). Both CLIPs are also detected at high levels in the cerebral cortex, hippocampus, olfactory bulb and amygdala, where they are localized to the cell bodies and the dendrites of neurons (Fig. 3i-w). Thus, in these brain regions the expression of CLIP-115 overlaps with that of CLIP-170-br, while in the cerebellum these proteins localize in different cell types.

Since the CLIPs are microtubule binding proteins, we analyzed their colocalization with microtubules in brain sections by double staining with antibodies against CLIPs and β-tubulin. In all CLIP-115 and CLIP-170-br-positive neurons there is a clear colocalization of CLIPs and microtubules (Fig. 3w,x and data not shown). Taken together, these data indicate that in the brain both CLIP-115 and CLIP-170-br are predominantly found in neurons, where they have overlapping but distinct expression patterns and colocalize with microtubules.

CLIP-115 and CLIP-170-br can compete with each other for the microtubule plus ends

Having shown that CLIP-115 and CLIP-170-br have an overlapping distribution in the brain and can both be found in the same intracellular compartments, we next tested the effect of having both CLIPs in transfected cells. CLIP-170 is endogenously present in COS-1 cells (Fig. 2d) and at low expression levels GFP-CLIP-115 colocalizes with it at the microtubule plus ends ([8] and data not shown). At higher levels, GFP-CLIP-115 localizes along the microtubules and displaces endogenous CLIP-170 from microtubule tips (Fig. 4 a,b).

Next, we cotransfected COS-1 cells with CLIP-115 and CLIP-170-br, which were bearing a GFP- or a HA-tag, and looked at individual cells with different expression levels of both CLIPs. When both HA-CLIP-115 and GFP-CLIP-170-br are coexpressed at low levels, they colocalize and associate with the same distal ends of microtubules [8]. Cells expressing medium levels of HA-CLIP-115 and low levels of GFP-CLIP-170-br show HA-CLIP-115 labeling along the length of the microtubule and a prominent staining of GFP-CLIP-170-br at microtubule plus ends (Fig. 4c,d). The same effect is seen in cotransfections with GFP-CLIP-115 and HA-CLIP-170-br (Fig. 4e,f), indicating that the protein tag and immunological detection do not influence the difference observed between the two CLIPs. When HA-CLIP-115 is expressed at very high levels and forms microtubule bundles within the cell [8], GFP-CLIP-170-br is no longer present at microtubule plus ends, but codistributes with CLIP-115 (data not shown). On the other hand, cells expressing medium levels of GFP-CLIP-170-br and low levels of HA-CLIP-115 show that the latter colocalizes with GFP-CLIP-170-br along the microtubules and does not accumulate at the microtubule tips (Fig.4g,h).

Taken together, the data show that CLIP-115 and CLIP-170-br can associate with the same microtubule plus tips and compete with each other for these tips.

However, at intermediate expression levels, when CLIP-115 is found along the microtubules, CLIP-170-br can be still present predominantly at microtubules plus ends, indicating that CLIP-170-br has higher affinity for these sites (or lower affinity for the rest of the microtubule cytoskeleton).

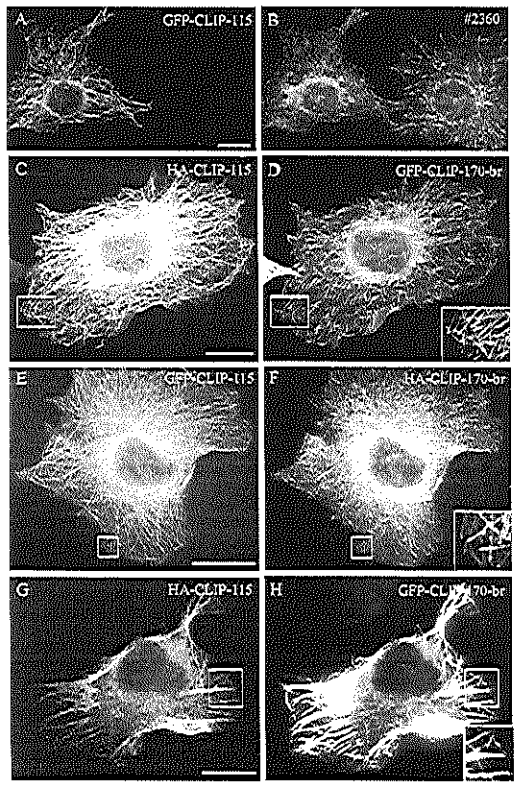

Figure 4. Competition between CLIP-115 and CLIP-170-br at microtubule plus ends.
COS-1 cells were transfected with GFP-CLIP-115 (a) or cotransfected with HA-CLIP-115 and GFP-CLIP-170-br (c,d,g,h) or GFP-CLIP-115 and HA-CLIP-170-br (e,f). Cells were stained with anti-CLIP-170 antibody #2360 (b) or an anti-HA antibody (c,f). Bar: 10 μm.

Alternative splicing in CLIP-170 modulates its affinity for CLASP proteins

Recently, we have identified two binding partners of the CLIP proteins, which were named CLASP1 and –2. The 345 bp deletion, specific for CLIP-170-br, is located downstream of the CLASP-binding domain in CLIP-170 (Fig.5a) and has no apparent effect on the CLIP-CLASP interaction (data not shown).

However, in addition to the CLIP-170-br isoform in the brain, CLIP-170 is present as a mixture of different isoforms in several other tissues [35-37]. In particular, a stretch of 35 amino acids (which is specific for the CLIP-170 isoform called restin) can be either excluded or included at position 457 within the CLIP-170 coiled-coil region in different tissues (Fig. 5a and [36]). In muscle tissue, an 11 amino acid insert is present in some CLIP-170 transcripts at the same place and instead of or together with the 35 amino acid insert (Fig.5a and [35]). These CLIP-170 isoforms are named, CLIP-170(+11), CLIP-170(+11+35), CLIP-170(+35) (restin) and CLIP-170. These alternative splicing patterns of CLIP-170 are conserved between human, chicken and

rat, indicating their functional significance (Fig. 5b and [36]). The fact that the +11/+35 insert is part of the CLASP-binding portion of the CLIP-170 rod domain [11] prompted us to investigate whether the different CLIP-170 isoforms bind to CLASPs with the same affinity. Therefore, the 35 amino acids stretch in rat CLIP-170-br was either deleted or substituted with the 11 amino acid stretch. The affinity of the three CLIP-170 fragments for CLASPs was tested by GST pull down (Fig. 5c,d) and yeast two-hybrid assays (Fig. 5e). The results of both experiments indicate that the (+35) isoform displays higher affinity for CLASPs than the isoform, which does not contain this insert, while the (+11) insertion completely abolishes the interaction. The 35 amino acid insert increases the length of the CLIP-170 coiled-coil region, but does not interrupt it [35]. On the other hand, the 11 amino acid exon contains an evolutionary conserved proline residue, which is likely to induce a kink in the CLIP-170 rod (Fig. 5b). Since CLASPs bind optimally to the (+35) isoform and do not bind to the (+11) isoform, we conclude that the stalk-like structure of this portion of CLIP-170 is important for the CLASP binding, while a bend within this region is incompatible with it.

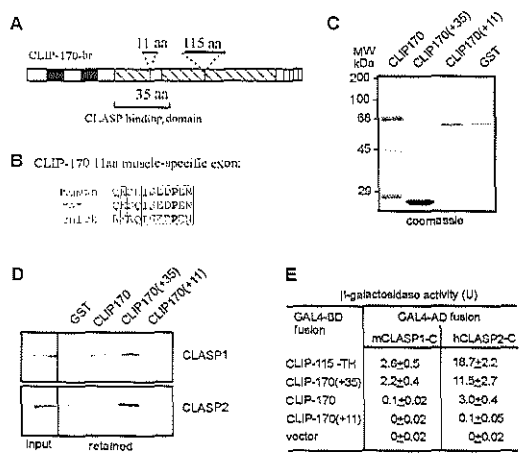

Figure 5. Alternative splicing in CLIP-170 modulates its affinity for CLASP proteins

(**a**) Structure of the CLIP-170-br protein (depicted in the same way as in Fig.1a) and the position of the alternatively spliced exons and the CLASP-binding domain. (**b**) Alignment of the sequence of the 11 amino acid exon of CLIP-170, obtained from rat skeletal muscle RNA by RT-PCR, with the corresponding human and chicken sequences. The conserved proline residue is shown in bold. (**c**) SDS-PAGE analysis of the purified GST fusion proteins, containing the rat CLIP-170 fragment 277-588 (CLIP-170(+35)), the same fragment without the 35 amino acid exon (CLIP-170), or the same fragment with the 35 amino acid exon substituted for the 11 amino acid muscle-specific exon (CLIP-170(+11)). All proteins have the expected size. Molecular weight markers are indicated. (**d**) In vitro binding of the ^{35}S-labeled CLASP1 and CLASP2 to the GST fusion proteins, shown in (c). Radioactive proteins were analyzed by X-ray film exposure of dried SDS-gels. (**e**) Interaction between CLASP1 and CLASP2 determined by measuring the β-galactosidase activity in yeast cultures, coexpressing indicated GAL4-BD and GAL4-AD fusions. The CLIP-115 fragment has been described by Akhmanova et al. (2001) [11] and CLIP-170 fragments used are the same as in the GST-fusions. The activity values obtained for CLASP1 and CLASP2 are not directly comparable, because a long 3' UTR sequence is present in the first, but not in the second construct. All CLIP constructs are exactly in the same sequence context and can be compared.

CLIP-170-br does not associate with myosin VI

Another potential binding partner of the CLIPs, present in neurons, has been identified in *Drosophila*. The *Drosophila* homologue of CLIP-170, D-CLIP-190, was

found to be associated with the 95F unconventional myosin VI [13]. Colocalization of these proteins is particularly prominent in the central nervous system. To test whether the interaction between CLIP-170 and the myosin VI is conserved in vertebrates, several experiments have been carried out.

First, co-immunoprecipitations from transfected COS-1 cells and brain extracts were performed. Expression vectors encoding myosin VI and GFP-myosin VI were constructed and tested by transfection and western blotting with anti-myosin VI antibodies. COS-1 cell extracts show an endogenous protein of ~150 kDa, consistent with the predicted molecular weight of myosin VI [38] (Fig. 6a). Extracts from COS-1 cells transfected with myosin VI and GFP-myosin VI expression constructs contain a protein of expected size (Fig. 6a). To test whether myosin VI and CLIP-170-br could be co-immunoprecipitated, cells were cotransfected with myosin VI and GFP-CLIP-170-br or with GFP-myosin and CLIP-170-br and protein extracts were immunoprecipitated using antibodies against myosin VI, GFP or CLIP-170. While we could easily observe precipitation of myosin VI or CLIP-170-br, no coprecipitation of these proteins was detected (data not shown). Also using mouse brain extracts, we could find no coprecipitation of myosin VI with either CLIP-170 or CLIP-115 (data not shown).

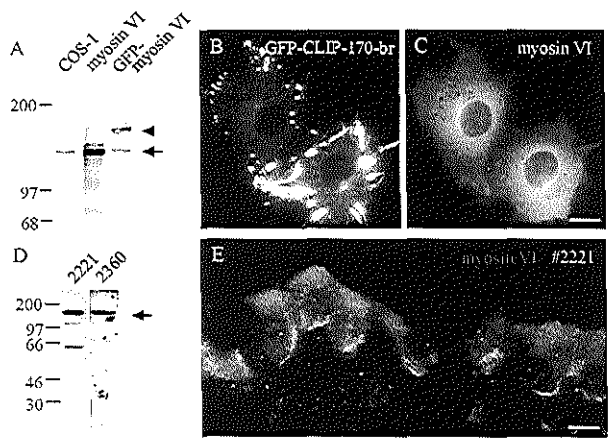

Figure 6. Analysis of a potential interaction between CLIP-170 and myosin VI
(**a**) Western blot of extracts of COS-1 cells, transfected with myosin VI or GFP-myosin VI expressing constructs or mock-transfected, were probed with anti-myosin VI antibodies. Untagged myosin VI protein is indicated by an arrow, and GFP- myosin VI with an arrowhead. Molecular weight markers are indicated. (**b,c**) COS-1 cells were cotransfected with GFP-CLIP-170-br (b) and myosin VI (c) and incubated with anti-myosin VI antibodies. Myosin VI is not redistributed to the CLIP-170-positive patches. Bar: 10 μm. (**d**) Western blots of chicken cochlea incubated with anti-CLIP-115/170 antibody #2221and anti-CLIP-170 antibody #2360. Position of the CLIP-170-specific band is indicated by an arrow. Molecular weight markers are indicated. (**e**) Immunofluorescence staining for CLIP-170 (red) and myosin VI (green) in the sensory epithelium of chicken cochlea. Double labeling shows myosin VI in the cochlear hair cells and CLIP-170 in nerve terminals contacting these hair cells. Bar: 10 μm.

Second, immunofluorescence analyses of transfected COS-1 cells were performed using different fixation procedures. It has been shown that proteins, which associate with CLIP-170, are redistributed to patchy aggregates in CLIP-170 overexpressing cells (Fig. 6b and [11,17]). However, in cells transfected with CLIP-170-br and stained for endogenous myosin VI, no redistribution of myosin VI to these

CLIP-170-positive structures have been observed (data not shown). Similar results were obtained when cells were cotransfected with myosin VI and GFP-CLIP-170-br (Fig. 6b,c) or GFP-myosin VI and CLIP-170-br (data not shown). Also in cells co-expressing myosin VI and full length GFP-CLIP-170 [7] or CLIP-115 no colocalization was observed (data not shown).

Since colocalization of myosin VI and CLIP-170 is lacking in cultured cells we next investigated colocalization in tissue sections. Although myosin VI is ubiquitously expressed in vertebrates, it is found highly concentrated within the hair cells of the ear [38,39]. To examine the presence and distribution of CLIP-170 in the cells of the inner ear, immunoblotting and immunohistochemistry analyses were performed on chicken cochlea. Western blots with both anti-CLIP-115/170 antibodies #2221 and #2360 showed that CLIP-170 is the most abundant CLIP present in the cochlea (Fig. 6d). Double labeling with anti-myosin VI antibodies and anti-CLIP antibodies #2221 or #2360 showed no colocalization between CLIP-170 and myosin VI and revealed that CLIP-170 is not detectable in the hair cells (Fig. 6e). Interestingly, all CLIP-170 labeling in the sensory epithelium apparently is associated with nerve fibers. CLIP-170 immunoreactivity is mainly present at nerve synaptic terminals contacting the base of the hair cells (Fig. 6e). Taken together these results argue against a direct association between mammalian myosin VI and CLIP-170.

CLIP-170, but not CLIP-115 recruits dynactin and Lis-1 to microtubule tips

There is increasing evidence that CLIP-170 and the dynein/dynactin motor system may work in concert at the microtubule plus ends. Dynactin colocalizes with CLIP-170 at microtubule plus ends and can redistribute to CLIP-170-positive patches in CLIP-170-overexpressing cells [16,17]. Deletion of the C-terminal domain of CLIP-170 abolishes this effect [17]. We have tested whether CLIP-170-br overexpression affects dynactin localization. Similar to the full-length CLIP-170, GFP-CLIP-170-br forms patchy aggregates, which also accumulate dynactin (Fig. 7a,b). When a deletion mutant of GFP-CLIP-170-br, lacking the C-terminal 79 amino acids (named CLIP-170-br (-tail), (Fig. 7e) is overexpressed, dynactin is lost from the microtubule plus ends, apparently due to displacement of the endogenous, C-terminus-containing CLIP-170 (Fig. 7c,d). These results corroborate the findings of [17] and indicate that CLIP-170-br behaves identically to CLIP-170 with respect to the recruitment of dynactin.

Overexpressed GFP-CLIP-115 produces an effect very similar to that of GFP-CLIP-170-br(-tail), since it displaces both CLIP-170 and dynactin from the microtubule tips (Fig. 7f-h). To determine, whether the C-terminal tail of CLIP-170 is able to interact with dynactin when it is placed in the context of CLIP-115, the last 159 amino acids of CLIP-170-br were attached to the end of GFP-CLIP-115 (GFP-CLIP-115(+tail), see Fig.7e). At low levels of expression, GFP-CLIP-115(+tail) is present at microtubule plus ends and at higher levels it accumulates in patchy (Fig.7i) or spherical (Fig.8e) aggregates, which also recruit dynactin (Fig. 7k). This indicates that the last 159 amino acids of CLIP-170 are sufficient to confer to CLIP-115 a capacity to relocalize dynactin.

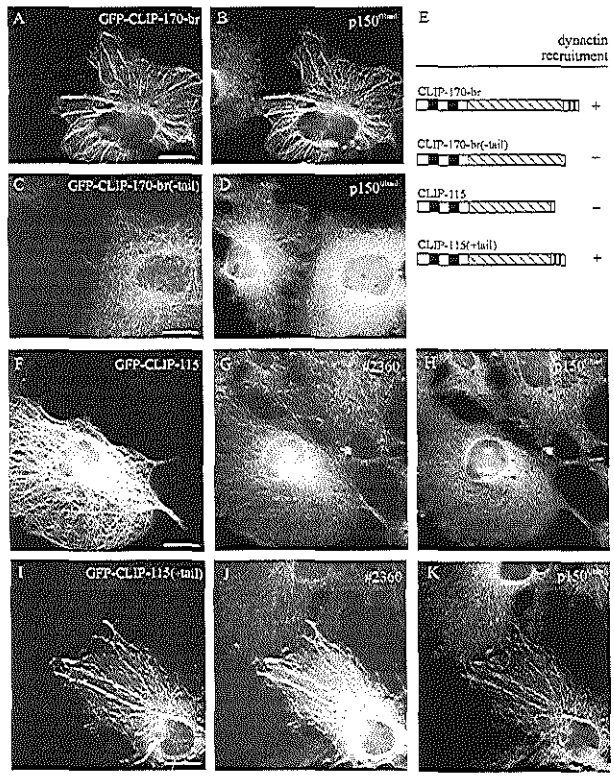

Figure 7. CLIP-170, but not CLIP-115, recruits dynactin to microtubule-associated patches
COS-1 cells were transfected with GFP-CLIP-170-br (a,b), GFP-CLIP-170-br(-tail) (c,d), GFP-CLIP-115 (f-h) or GFP-CLIP-115 (+tail) (I-K). Cells were stained for endogenous dynactin (b,d,h,k) and CLIP-170 (g,j). Structure of the different CLIP constructs and their ability to recruit dynactin are shown in (e). Bar: 10 μm.

Since LIS1 also has been shown to abolish dynactin accumulation at the microtubule plus ends [25], we have tested if overexpression of the two CLIPs can influence the microtubule plus end targeting of the GFP fusions of LIS1 and LIS1-associating proteins NudE, NudEL and NudC, which are implicated in dynein/dynactin pathway [18,27,40]. When expressed alone in COS-1 cells, all these GFP fusion proteins displayed mainly cytoplasmic staining (as well as some accumulation at the centrosome in case of LIS1, NudE and NudEL), but none of them showed specific localization to the microtubule ends (data not shown). Medium overexpression levels of GFP- or HA-CLIP-115 did not change the LIS1 localization (Fig. 8a-b). However, GFP- or HA-CLIP-170-br or GFP-CLIP-115(+tail), induced accumulation of tagged LIS1 proteins at the tips of microtubules (Fig. 8c-f). Together these data indicate that the C-terminal domain of CLIP-170 is sufficient to relocalize LIS1. GFP-fusion proteins of NudE, NudEL and NudC were not recruited to microtubules by any of the CLIPs (either in double transfections with HA-CLIP fusions or in triple transfections with an untagged CLIP and an HA-LIS1-expressing construct, Fig. 8g,h and data not shown). In addition, none of the NudE/EL/C constructs had an apparent influence on the localization of dynactin to microtubule tips (data not shown). We conclude that the LIS1 associated proteins, NudE, NudEL and NudC are not involved in the targeting of LIS1 (and dynactin) to microtubule plus ends.

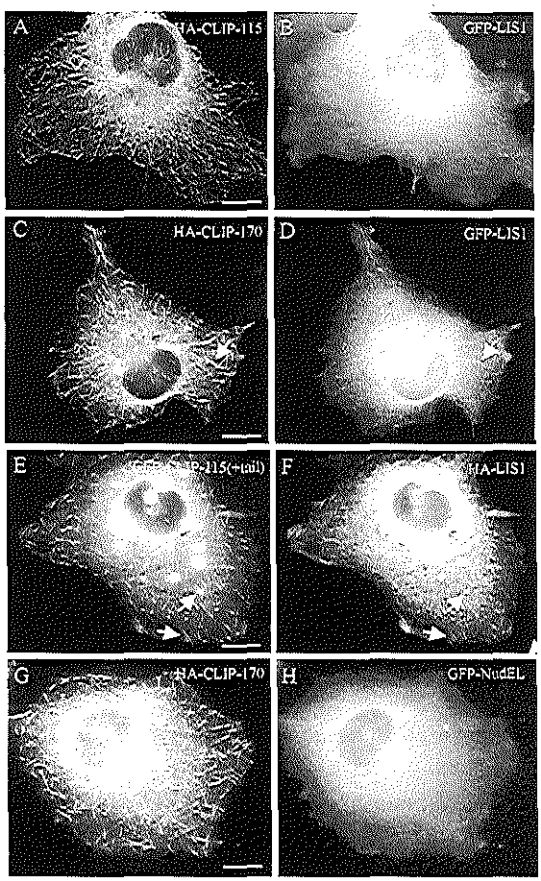

Figure 8. CLIP-170, but not CLIP-115, recruits LIS1 to microtubule distal ends
COS-1 cells were cotransfected with HA-CLIP-115 and GFP-LIS1 (a,b), HA-CLIP-170-br and GFP-LIS1 (c,d), GFP-CLIP-115(+tail) and HA-LIS1 (e,f) and HA-CLIP-170-br and GFP-NudEL (g,h). LIS1, recruited to the CLIP-positive structures, is indicated by arrows. Bar: 10 μm.

Discussion

Functional significance of CLIP-170-br and other CLIP isoforms

We report here the identification of CLIP-170-br, the predominant brain variant of CLIP-170. CLIP-170-br lacks a fragment of 115 amino acids in the coiled-coil region of the protein due to alternative splicing, which results in the generation of a KKEK motif. This motif have been found in actin binding proteins, such as villin [32,33] and a CLIP homologue, $p150^{Glued}$ [34] and was suggested to be involved in binding actin or actin-related proteins. We could find no experimental support for interaction of CLIP-170-br with actin or Arp1. However, since the human genome sequence has revealed that in addition to 6 actin genes, there are seven genes that code for divergent actin proteins and sixteen different genes for actin-related proteins [30,41], it remains possible that CLIP-170-br associates with one the members of the actin family.

Recently, we have shown that CLIP-115 forms homodimers which can be stabilized by cysteine residues in the coiled–coil stalk [8]. CLIP-170 has two cysteines

within the coiled-coiled stretches that could potentially be used to form intermolecular disulfide bridges between the monomers. Because of the deletion in CLIP-170-br, one of the conserved cysteines is removed, which could result in a less stable coiled-coil structure. This could have consequences for the interactions of CLIP-170-br with other proteins.

In addition to the CLIP-170-br isoform in the brain, CLIP-170 is present as a mixture of different isoforms in several other tissues [35-37]. Here we show that alternative splicing in CLIP-170 influences the affinity of this protein for CLASPs. CLIP-170(+35) isoform, which has the highest affinity for CLASP proteins, is the most abundant in the brain [35]. This suggests that the CLIP-CLASP interaction might be particularly important in this tissue. In line with this observation, CLIP-115, which is highly expressed in the brain, exists exclusively as the (+35) isoform. On the other hand, the (+11) isoform of CLIP-170 is very prominent in skeletal muscle, the tissue where CLASP1/2 transcription is low [11]. Since CLIP-170 is an abundant muscle protein (Fig. 1c), it is likely that CLIP-170(+11) has some specific, CLASP- unrelated function in this tissue. Finally, it would be particularly interesting to investigate the relationship between CLIP-170 and CLASP in the heart, since different CLIP-170 variants, including the CLIP-170(+11) isoform, are present in cardiac muscle, and CLASP2 is also abundantly transcribed there (Fig. 1c and [11]).

CLIP-115 and CLIP-170-br localization in the brain

De Zeeuw et al. (1997) [29] have reported immunolocalization of CLIP-115 in the brain. Polyclonal anti-peptide antisera, which were raised against the coiled-coil region of the CLIP-115, were found to label neuronal cell bodies and membranous organelles, called dendritic lamellar bodies (DLBs) in the dendritic appendages of these neurons. To verify the CLIP-115 localization we incubated mouse brain sections with the new CLIP-115-specific antibodies. Both anti-peptide antibodies and anti-CLIP-115 antiserum #2238 prominently label neurons in the hippocampus and cerebral cortex (compare [29] with Fig. 3). However, while the anti-peptide antibodies showed an intense staining in the inferior olive, including a puntate labeling that might represent DLBs ([29]), no such labeling is found with antibodies #2238 or #2221 in this brain area (data not shown). These data indicate that the newly raised antibodies against CLIP-115 do not recognize the DLBs. Furthermore, immuno-EM studies, have thus far failed to demonstrate staining of DLBs by #2221 and #2238 antisera. Finally, labeling of Bergmann glia cells previously described with the anti-peptide is not very pronounced with the newly raised antisera against CLIP-115 and conversely Purkinje-cell staining was less pronounced using anti-peptide antibodies. Since the new CLIP-115 antibodies recognize CLIP-115 with a much higher affinity on Western blot compared to the anti-peptide antibodies, we believe that the expression pattern described here reflects better the CLIP-115 distribution. However, verification of these results is only possible when knock out mice are available.

In addition, we determined the brain localization of CLIP-170 and found that both CLIPs are present in neurons in the hippocampus, cerebral cortex, olfactory bulb and cerebellum. However, within the cerebellum, the expression patterns of the two CLIPs differ. While CLIP-115 is mainly present in the Purkinje cells, CLIP-170 is found in the granular layer of the cerebellar cortex, where it is apparently concentrated in the axon terminals of the mossy fibers (Fig. 3g,h). In line with this observation, we find CLIP-170 staining in the axon terminals of neurons, which project on the hair cells in the cochlea. Interestingly, CLASP2β, a brain-specific isoform of the CLIP partner CLASP2, can associate with membranes [11]. An intriguing possibility is that CLIP-170-br and CLASP2β may function together as regulators of microtubule dynamics or membrane transport within presynaptic terminals.

The two CLIPs are coexpressed in the cell bodies and dendrites of many types of neurons. CLIP-170 and CLIP-115 can compete with each other for the microtubule tips, and such competition might play a role in their respective functions. For example, high levels of CLIP-115 in certain cellular compartments may reduce the concentration of CLIP-170 at the microtubule ends. This, in its turn, will diminish the occupancy of microtubule tips by protein complexes, which are targeted there via the C-terminal domain of CLIP-170, such as dynactin and LIS1. In this way, CLIP-115 may actively influence CLIP-170 dependent processes.

No evidence for association between CLIP-170 and myosin VI

Experiments in *Drosophila* have shown that the CLIP-170 homologue, D-CLIP-190, is present within a complex which also contains the 95F unconventional myosin VI [13]. Based on this, it has been speculated that CLIPs may act to coordinate actin- and microtubule base organelle movements or target microtubules to cortical actin foci ([14,15]. However, we could find no experimental support for the association between vertebrate CLIPs and myosin VI, suggesting that this interaction may be not conserved in evolution. It should be noted that a direct nature of the interaction between D-CLIP-190 and myosin 95F has not been established. It is possible, therefore, that additional factors, present in the complexes which include these two proteins in flies are not conserved in mammals (or at least in the cell systems which we have tested), or that for some reason these complexes are more difficult to obtain by immunoprecipitation from a vertebrate, rather that an insect system.

Association between LIS1, dynactin and CLIP-170 at microtubule plus ends

Our findings corroborate the study by Valleti et al. (1999), which suggested that dynactin is targeted to the ends of growing microtubules by interactions involving the C-terminal metal-binding domain of CLIP-170. The displacement of dynactin from microtubule tips by a CLIP-170 mutant with deleted C-terminus probably occurs due to competing away the endogenous, non-mutated CLIP-170. We show here that CLIP-115 produces a similar effect, suggesting that in terms of dynactin association it behaves like a "tailless" CLIP-170.

LIS1 and LIS1-associated proteins were proposed to function as regulators of microtubule end-dependent processes [18,27]. We have shown here that LIS1 protein can be recruited to the ends of microtubules in a manner, dependent on the C-terminal domain of CLIP-170. The interaction between LIS1 and CLIP-170 is supported by genetic studies on their homologues Pac1p and Bik1p in fission yeast [42]. We have attempted to corroborate our cytological observations by immunoprecipitations, but in our hands similar amounts of LIS1 were coprecipitated from transfected cells with both CLIP-115 and CLIP-170, indicating that the specificity of interactions at the microtubule tips was not reflected in these experiments (data not shown). The exact role of CLIP-170 in microtubule targeting of dynactin and LIS1 is unclear. Since both the large subunit of dynactin, $p150^{Glued}$, and LIS1 can bind microtubules directly [34,43], it is likely that CLIP-170 provides specificity for the freshly assembled microtubule ends [44]. LIS1-associating proteins NudE, NudEL and NudC [26,40,45-47] displayed no specific localization to microtubule tips in our experiments, suggesting that they might be involved in other aspects of LIS1 functioning and dynein-based motility (see Table 1 and [18,27]).

Table 1

Possible CLIP-115 and CLIP-170- interacting proteins

Protein	CLIP-115 interaction	CLIP-170-br interaction	methods used	references
CLASP1/2	+	+	yth, ip, ox, col	[11]
Myosin VI	-	-	ip, ox, col	this study
Dynactin	-	+	ox, col, (ip negative)	[16,17], this study
LIS1	-	+	ox, col, (ip negative)	this study
NudC	-	-	ox	this study
NudE	-	-	ox	this study
NudEL	-	-	ox	this study

yth: yeast two hybrid; ip: immunoprecipitation; ox: overexpression; col; colocalization;
+ positive; - negative

Overexpression of LIS1 removes dynactin from the microtubule plus ends ([25] and data not shown). This could be explained by proposing that dynactin and LIS1 bind to microtubule tips as a complex, the stoichiometry of which is disrupted by LIS1 overexpression. Alternatively, dynactin and LIS1 might compete for the association with CLIP-170. If microtubule plus ends function as cargo-loading sites [16,17], competition between LIS1 and dynactin could serve a regulatory role in the minus end-directed motility. The contacts between the ends of microtubules and cargo could be initiated by dynactin, targeted to microtubule tips through an interaction with CLIP-170. Subsequent binding of LIS1 (and dynein) could cause the release of the complex, resulting in actual transport. Such a view is consistent with the proposed role of LIS1 in the activation of dynein-mediated motility [27].

An interesting observation is that LIS1 can be localized at cortical sites of the cell [23,25]. This raises the possibility that LIS1 interacts with CLIP-170 when the

microtubule reaches the periphery of the cell. This could result in a mobile LIS1/dynactin/dynein complex at the cellular cortex, which would create a pulling force at the microtubule. Such forces are believed to play an important role in cellular and nuclear migration [48,49]. The potential role of CLIPs and their protein partners in cellular (especially neuronal) migration is an exiting avenue for future investigation.

Materials and Methods

cDNA isolation and expression constructs.

A rat hippocampus λZAP expression library was screened, using as a probe a 0.36 kb CLIP-115 DNA fragment, encoding CLIP-115 MTB [29]. In addition to the CLIP-115 cDNAs, we isolated 18 CLIP-170 cDNA clones, the longest of which has been sequenced (accession number AJ237670). The mammalian expression vectors pEGFP-C (Clontech) were used to construct GFP-CLIP-115 and GFP-CLIP-170-br (Hoogenraad et al., 2000). These vectors were also used to construct GFP-CLIP-170(-tail), in which the last 79 amino acids CLIP-170-br are deleted and GPF-CLIP-115(+tail), which contains the C-terminal 159 amino acids of CLIP-170 linked in frame to CLIP-115 in front of its stop codon, GFP-LIS1 (mouse LIS1 cDNA was obtained by RT-PCR from total mouse brain RNA), GFP-NudC (mouse NudC cDNA is an IMAGE clone 2646247, accession number AW322862), GFP-NudE (human NudE cDNA is an IMAGE clone 2820974, accession number AW249237) and GFP-NudEL (mouse NudEL cDNA is an IMAGE clone 2646029, accession number AW322683). Human cDNA KIAA0389, containing the open reading frame of myosin VI was obtained from Kazuza DNA Research Institute [50], was subcloned in the expression vector pCI-neo and in frame with GFP in vector pEGFP-C3. To generate HA-CLIP-115 and HA-CLIP-170-br fusions pMT2SM-HA vector was used; HA-LIS1 was produced by substituting GFP for HA-tag in the corresponding fusion construct.

RT-PCR and Northern blotting

Isolation of total RNA and Northern blotting were performed as described by [29]. Multiple tissue Northern blots from Clontech were also used. cDNA was synthesized with Superscript II reverse transcriptase (GIBCO BRL) using 0.5 μg of total RNA from each source and oligo(dT) and random primers. RT-PCR analysis was performed using oligonucleotides 5'- GCTGGACACGGCG GAAGACC and 5'-GAGACGGCCTCCTCTGA-AGC.

GST fusion constructs, generation of CLIP-170 antibodies and GST pull down assays

To generate CLIP-170-specific antibodies (#2360), the C-terminal region of the CLIP-170-br (amino acids 1029-1320) was expressed in bacteria as a GST fusion, purified by preparative SDS-PAGE and injected into rabbits as described [8].

The rat CLIP-170 fragment (amino acids 277-588, CLIP-170(+35)) which binds to CLASP proteins was fused to glutathione S-transferase (GST) [11]. This fragment was used to construct GST-CLIP-170, by deleting the 35 amino acids exon and GST-CLIP-170(+11), by substitution of the 35 amino acid exon for the 11 amino acid exon. The two three GST fusion proteins were prepared as described by [8]. KIAA0622 (CLASP1) and KIAA0627 (CLASP2) were transcribed and translated in vitro using the TnT coupled transcription-translation system (Promega) and incubated with the GST-fusion proteins as described by [11]. Antiserum #2238 is against the C-terminus of CLIP-115 and antiserum #2221 is against the N-terminus of CLIP-115 [8].

Yeast two-hybrid assay

The yeast two-hybrid assay was performed as described previously [11]. Fragments of the rat CLIP-170 cDNA, identical to those used in the GST fusions (see above) and the rat CLIP-115 cDNA (amino acids 287-591, CLIP-115-TH), which binds to CLASP proteins were linked to the GAL4 DNA-BD in the pPC97 yeast two hybrid vector. The C-terminal domains of CLASP1 and CLASP2 (positions 3077-3976 of KIAA0627) were linked to the GAL4 AD in the pPC86 yeast two-hybrid vector [11]. Production of the yeast fusion proteins of correct size was verified by western blotting, using antibodies against GAL4 DNA-BD and GAL4 AD (Clontech). β-galactosidase activity

measurements (expressed in arbitrary units) were performed in triplicate from two independent experiments, as described [51].

Cell culture, transfection and immunofluorescence

Culturing and transfection of COS-1 cells was performed as described previously (Hoogenraad et al., 2000). For immunofluorescence, cells were fixed in 100% methanol/1 mM EGTA for 10 min at –20°C followed by 15 min fixation in 4% paraformaldehyde in phosphate-buffered saline (PBS). Cells were washed for 5 min in 0.15% TritonX-100/PBS, blocked in PBS /1% BSA/0.1% Tween (PBT) and labeled with different antibodies for 1 hour at room temperature. Following antibodies were used: rabbit anti-CLIP-170 antibodies #2360 (1:300), rabbit anti-CLIP-115 antibodies #2238 (1:300), rabbit anti-CLIP-115/170 antibody #2221 (1:300) (Hoogenraad et al., 2000), mouse anti-myosin VI antibody (1: 500) [38], mouse anti-β-tubulin (Sigma 1:100), mouse anti-HA (BAbCO 1:100), mouse anti-$p150^{Glued}$ (Transduction Laboratories, 1:100). After washing in 0.05% Tween-20/PBS sections were incubated with secondary antibodies: rhodamine-labeled sheep anti-mouse (Boehringer, 1:25), FITC-conjugated goat anti-rabbit (Nordic Laboratories; 1:100), Alexa 594-conjugated goat anti-rabbit (Molecular probes, 1:500) and Alexa 350-conjugated sheep anti-mouse (Molecular probes, 1:250). Slides were mounted using Vectashield mounting medium (Vector laboratories) with DAPI (Sigma) and analyzed on a Leica DMRBE fluorescence microscope, equipped with a Hamamatsu C4880 DCC camera. Quantification of GFP fluorescence was described previously [8]

Immunocytochemistry and immunofluorescence microscopy of brain sections

To analyze CLIP expression in the brain of adult mice, Fvb mice were anaesthetized with Nembutal (3,5 µl/kg intraperitoneally). The mice were perfused with 4% paraformaldehyde and the brains were fixed for another 2 hours. For immunocytochemistry, the brains were cryoprotected in saline containing 30% sucrose and cut into 20 µm thick transversal or sagittal sections on a freezing microtome. All sections were collected in 50 mM Tris-HCl buffer, pH 7.5, containing 0.9% NaCl, blocked in 10% normal goat serum in the same buffer for 4 hours and incubated for 48 hours at 4°C with antibodies #2360, #2238 and #2221, diluted 1:1000 in 2% normal goat serum in the same buffer. The sections were subsequently processed with the use of the avidin-biotin complex method (ABC Elite kit, Vector Laboratories). Finally, the sections were incubated in 0.05% 3,3 diaminobenzidine (DAB) and 0.01% H_2O_2 in 0.05 M sodium phosphate buffer and mounted.

For immunofluorescence, 7 µm paraffin sections of mouse brains were prepared and microwave-treated in 10 mM Na-citrate buffer pH 5.5 as described by Akhmanova et al., 2000 [11]. The sections were blocked with PBT for 1 hour at 20°C. Primary antibody incubations were performed in the same buffer overnight at 4°C and secondary antibody incubations for 2 hours at 20°C. Antibody dilutions, mounting and microscopy were performed in the same way as for staining cultured cells (see above).

Western blot Analysis

Protein extracts of chicken cochlea were made as described [38]. Total protein extracts of mouse brain and heart was prepared by homogenization in PBS/1% Triton X-100 in the presence of protease inhibitors (Boehringer Mannheim), sonicated and boiled in SDS sample buffer in the presence of DTT. Total protein extracts from COS-1 cells were obtained two days after transfection and treated as above. Equal amounts of protein homogenate were loaded on SDS-polyacrylamide gels and Western blots were prepared as described previously [8]. Various rabbit anti-CLIP antibodies were diluted 1:2000 and anti-myosin VI antibodies 1:3000. After washing, blots were incubated with goat-anti-rabbit antibodies coupled to alkaline phosphatase (Sigma, 1:8000). Enzymatic detection of bound antibody was carried out using the Fast BCIP/NBT system (Sigma).

References

1. Tessier-Lavigne, M., and Goodman, C. S. (1996) The molecular biology of axon guidance. *Science* **274**(5290): 1123-33.
2. Roos, J., Hummel, T., Ng, N., Klambt, C., and Davis, G. W. (2000) Drosophila Futsch regulates synaptic microtubule organization and is necessary for synaptic growth. *Neuron* **26**(2): 371-82.

3. Kalil, K., Szebenyi, G., and Dent, E. W. (2000) Common mechanisms underlying growth cone guidance and axon branching. *J Neurobiol* **44**(2): 145-58.
4. Kneussel, M., and Betz, H. (2000) Clustering of inhibitory neurotransmitter receptors at developing postsynaptic sites: the membrane activation model. *Trends Neurosci* **23**(9): 429-35.
5. Hirokawa, N. (1998) Kinesin and dynein superfamily proteins and the mechanism of organelle transport. *Science* **279**(5350): 519-26.
6. Desai, A., and Mitchison, T. J. (1997) Microtubule polymerization dynamics. *Annu Rev Cell Dev Biol* **13**: 83-117
7. Perez, F., Diamantopoulos, G. S., Stalder, R., and Kreis, T. E. (1999) CLIP-170 highlights growing microtubule ends in vivo. *Cell* **96**(4): 517-27.
8. Hoogenraad, C. C., Akhmanova, A., Grosveld, F., De Zeeuw, C. I., and Galjart, N. (2000) Functional analysis of CLIP-115 and its binding to microtubules. *J Cell Sci* **113**(Pt 12): 2285-97.
9. Scheel, J., Pierre, P., Rickard, J. E., Diamantopoulos, G. S., Valetti, C., van der Goot, F. G., Haner, M., Aebi, U., and Kreis, T. E. (1999) Purification and analysis of authentic CLIP-170 and recombinant fragments. *J Biol Chem* **274**(36): 25883-91.
10. Brunner, D., and Nurse, P. (2000) CLIP170-like tip1p spatially organizes microtubular dynamics in fission yeast. *Cell* **102**(5): 695-704.
11. Akhmanova, A., Hoogenraad, C. C., Drabek, K., Stepanova, T., Dortland, B., Verkerk, T., Vermeulen, W., Burgering, B. M., De Zeeuw, C. I., Grosveld, F., and Galjart, N. (2001) Clasps are CLIP-115 and -170 associating proteins involved in the regional regulation of microtubule dynamics in motile fibroblasts. *Cell* **104**(6): 923-35.
12. Pierre, P., Scheel, J., Rickard, J. E., and Kreis, T. E. (1992) CLIP-170 links endocytic vesicles to microtubules. *Cell* **70**(6): 887-900.
13. Lantz, V. A., and Miller, K. G. (1998) A class VI unconventional myosin is associated with a homologue of a microtubule-binding protein, cytoplasmic linker protein-170, in neurons and at the posterior pole of Drosophila embryos. *J Cell Biol* **140**(4): 897-910.
14. Goode, B. L., Drubin, D. G., and Barnes, G. (2000) Functional cooperation between the microtubule and actin cytoskeletons. *Curr Opin Cell Biol* **12**(1): 63-71.
15. Wu, X., Jung, G., and Hammer, J. A., 3rd. (2000) Functions of unconventional myosins. *Curr Opin Cell Biol* **12**(1): 42-51.
16. Vaughan, K. T., Tynan, S. H., Faulkner, N. E., Echeverri, C. J., and Vallee, R. B. (1999) Colocalization of cytoplasmic dynein with dynactin and CLIP-170 at microtubule distal ends. *J Cell Sci* **112**(Pt 10): 1437-47.
17. Valetti, C., Wetzel, D. M., Schrader, M., Hasbani, M. J., Gill, S. R., Kreis, T. E., and Schroer, T. A. (1999) Role of dynactin in endocytic traffic: effects of dynamitin overexpression and colocalization with CLIP-170. *Mol Biol Cell* **10**(12): 4107-20.
18. Schroer, T. A. (2001) Microtubules don and doff their caps: dynamic attachments at plus and minus ends. *Curr Opin Cell Biol* **13**(1): 92-6.
19. Reiner, O., Carrozzo, R., Shen, Y., Wehnert, M., Faustinella, F., Dobyns, W. B., Caskey, C. T., and Ledbetter, D. H. (1993) Isolation of a Miller-Dieker lissencephaly gene containing G protein beta-subunit-like repeats. *Nature* **364**(6439): 717-21.
20. Liu, Z., Steward, R., and Luo, L. (2000) Drosophila Lis1 is required for neuroblast proliferation, dendritic elaboration and axonal transport. *Nat Cell Biol* **2**(11): 776-83.
21. Xiang, X., Osmani, A. H., Osmani, S. A., Xin, M., and Morris, N. R. (1995) NudF, a nuclear migration gene in Aspergillus nidulans, is similar to the human LIS-1 gene required for neuronal migration. *Mol Biol Cell* **6**(3): 297-310.
22. Willins, D. A., Liu, B., Xiang, X., and Morris, N. R. (1997) Mutations in the heavy chain of cytoplasmic dynein suppress the nudF nuclear migration mutation of Aspergillus nidulans. *Mol Gen Genet* **255**(2): 194-200.
23. Swan, A., Nguyen, T., and Suter, B. (1999) Drosophila Lissencephaly-1 functions with Bic-D and dynein in oocyte determination and nuclear positioning. *Nat Cell Biol* **1**(7): 444-9.
24. Smith, D. S., Niethammer, M., Ayala, R., Zhou, Y., Gambello, M. J., Wynshaw-Boris, A., and Tsai, L. H. (2000) Regulation of cytoplasmic dynein behaviour and microtubule organization by mammalian Lis1. *Nat Cell Biol* **2**(11): 767-75.
25. Faulkner, N. E., Dujardin, D. L., Tai, C. Y., Vaughan, K. T., O'Connell, C. B., Wang, Y., and Vallee, R. B. (2000) A role for the lissencephaly gene LIS1 in mitosis and cytoplasmic dynein function. *Nat Cell Biol* **2**(11): 784-91.
26. Sasaki, S., Shionoya, A., Ishida, M., Gambello, M. J., Yingling, J., Wynshaw-Boris, A., and Hirotsune, S. (2000) A LIS1/NUDEL/cytoplasmic dynein heavy chain complex in the developing and adult nervous system. *Neuron* **28**(3): 681-96.

27. Vallee, R. B., Tai, C., and Faulkner, N. E. (2001) LIS1: cellular function of a disease-causing gene. *Trends Cell Biol* **11**(4): 155-60.
28. Han, G., Liu, B., Zhang, J., Zuo, W., Morris, N. R., and Xiang, X. (2001) The Aspergillus cytoplasmic dynein heavy chain and NUDF localize to microtubule ends and affect microtubule dynamics. *Curr Biol* **11**(9): 719-24.
29. De Zeeuw, C. I., Hoogenraad, C. C., Goedknegt, E., Hertzberg, E., Neubauer, A., Grosveld, F., and Galjart, N. (1997) CLIP-115, a novel brain-specific cytoplasmic linker protein, mediates the localization of dendritic lamellar bodies. *Neuron* **19**(6): 1187-99.
30. Venter, J. C., Adams, M. D., Myers, E. W., Li, P. W., Mural, R. J., Sutton, G. G., Smith, H. O., Yandell, M., and al., e. (2001) The sequence of the human genome. *Science* **291**(5507): 1304-51.
31. Pierre, P., Pepperkok, R., and Kreis, T. E. (1994) Molecular characterization of two functional domains of CLIP-170 in vivo. *J Cell Sci* **107**(Pt 7): 1909-20.
32. Friederich, E., Vancompernolle, K., Huet, C., Goethals, M., Finidori, J., Vandekerckhove, J., and Louvard, D. (1992) An actin-binding site containing a conserved motif of charged amino acid residues is essential for the morphogenic effect of villin. *Cell* **70**(1): 81-92.
33. Friederich, E., Vancompernolle, K., Louvard, D., and Vandekerckhove, J. (1999) Villin function in the organization of the actin cytoskeleton. Correlation of in vivo effects to its biochemical activities in vitro. *J Biol Chem* **274**(38): 26751-60.
34. Waterman-Storer, C. M., Karki, S., and Holzbaur, E. L. (1995) The p150Glued component of the dynactin complex binds to both microtubules and the actin-related protein centractin (Arp-1). *Proc Natl Acad Sci U S A* **92**(5): 1634-8.
35. Griparic, L., and Keller, T. C. (1998) Identification and expression of two novel CLIP-170/Restin isoforms expressed predominantly in muscle. *Biochim Biophys Acta* **1405**(1-3): 35-46.
36. Griparic, L., Volosky, J. M., and Keller, T. C., 3rd. (1998) Cloning and expression of chicken CLIP-170 and restin isoforms. *Gene* **206**(2): 195-208.
37. Griparic, L., and Keller, T. C., 3rd. (1999) Differential usage of two 5' splice sites in a complex exon generates additional protein sequence complexity in chicken CLIP-170 isoforms. *Biochim Biophys Acta* **1449**(2): 119-24.
38. Hasson, T., Gillespie, P. G., Garcia, J. A., MacDonald, R. B., Zhao, Y., Yee, A. G., Mooseker, M. S., and Corey, D. P. (1997) Unconventional myosins in inner-ear sensory epithelia. *J Cell Biol* **137**(6): 1287-307.
39. Hasson, T., and Mooseker, M. S. (1994) Porcine myosin-VI: characterization of a new mammalian unconventional myosin. *J Cell Biol* **127**(2): 425-40.
40. Morris, S. M., Albrecht, U., Reiner, O., Eichele, G., and Yu-Lee, L. Y. (1998) The lissencephaly gene product Lis1, a protein involved in neuronal migration, interacts with a nuclear movement protein, NudC. *Curr Biol* **8**(10): 603-6.
41. Pollard, T. D. (2001) Genomics, the cytoskeleton and motility. *Nature* **409**(6822): 842-3.
42. Geiser, J. R., Kahana, J. A., Silver, P., and Hoyt, M. A. (1999) Establishing the role of *S.cerevisiae* Bik1p and Pac1p within the cytoplasmic dynein complex. *Mol Biol Cell* **10**(1482 suppl): 248a
43. Sapir, T., Elbaum, M., and Reiner, O. (1997) Reduction of microtubule catastrophe events by LIS1, platelet- activating factor acetylhydrolase subunit. *Embo J* **16**(23): 6977-84.
44. Schuyler, S. C., and Pellman, D. (2001) Microtubule "plus-end-tracking proteins". the end is just the beginning. *Cell* **105**(4): 421-4.
45. Niethammer, M., Smith, D. S., Ayala, R., Peng, J., Ko, J., Lee, M. S., Morabito, M., and Tsai, L. H. (2000) NUDEL is a novel Cdk5 substrate that associates with LIS1 and cytoplasmic dynein. *Neuron* **28**(3): 697-711.
46. Kitagawa, M., Umezu, M., Aoki, J., Koizumi, H., Arai, H., and Inoue, K. (2000) Direct association of LIS1, the lissencephaly gene product, with a mammalian homologue of a fungal nuclear distribution protein, rNUDE. *FEBS Lett* **479**(1-2): 57-62.
47. Feng, Y., Olson, E. C., Stukenberg, P. T., Flanagan, L. A., Kirschner, M. W., and Walsh, C. A. (2000) LIS1 regulates CNS lamination by interacting with mNudE, a central component of the centrosome. *Neuron* **28**(3): 665-79.
48. Reinsch, S., and Gonczy, P. (1998) Mechanisms of nuclear positioning. *J Cell Sci* **111**(Pt 16): 2283-95.
49. Morris, N. R. (2000) Nuclear migration. From fungi to the mammalian brain. *J Cell Biol* **148**(6): 1097-101.
50. Ishikawa, K., Nagase, T., Suyama, M., Miyajima, N., Tanaka, A., Kotani, H., Nomura, N., and Ohara, O. (1998) Prediction of the coding sequences of unidentified human genes. X. The complete sequences of 100 new cDNA clones from brain which can code for large proteins in vitro. *DNA Res* **5**(3): 169-76.
51. Ausubel, F. M., Brent, R., Kingston, R. E., Moore, D. D., Seidman, J. G., Smith, J. A., and Struhl, K. (1997) Current protocols in molecular biology, John Wiley & Sons, Inc., New York

Chapter 7

MAMMALIAN GOLGI-ASSOCIATED BICAUDAL-D2 FUNCTIONS IN THE DYNEIN/DYNACTIN PATHWAY BY INTERACTING WITH THESE COMPLEXES

Casper C. Hoogenraad[1,2*], Anna Akhmanova[1*], Steven A. Howell[3], Bjorn R. Dortland[1], Chris I. De Zeeuw[2], Rob Willemsen[1], Pim Visser[1], Frank Grosveld[1] and Niels Galjart[1]

MGC Departments of [1]Cell Biology and Genetics and of [2]Anatomy, Erasmus University, P.O. Box 1738, 3000 DR Rotterdam, The Netherlands. [3]Laboratory of Protein Structure, National Institute for Medical Research, The Ridgeway, London NW7 1AA, UK. *These authors contributed equally to the results described in this paper.

Mammalian Golgi-associated Bicaudal-D2 functions in the dynein–dynactin pathway by interacting with these complexes

Casper C.Hoogenraad[1,2], Anna Akhmanova[1], Steven A.Howell[3], Bjorn R.Dortland[1], Chris I.De Zeeuw[2], Rob Willemsen[1], Pim Visser[1], Frank Grosveld[1] and Niels Galjart[1,4]

[1]MGC Departments of Cell Biology and Genetics and [2]Department of Anatomy, Erasmus University, PO Box 1738, 3000 DR Rotterdam, The Netherlands and [3]Laboratory of Protein Structure, National Institute for Medical Research, The Ridgeway, London NW7 1AA, UK

[4]Corresponding author
e-mail: galjart@ch1.fgg.eur.nl

C.C.Hoogenraad and A.Akhmanova contributed equally to this work

Genetic analysis in *Drosophila* suggests that Bicaudal-D functions in an essential microtubule-based transport pathway, together with cytoplasmic dynein and dynactin. However, the molecular mechanism underlying interactions of these proteins has remained elusive. We show here that a mammalian homologue of Bicaudal-D, BICD2, binds to the dynamitin subunit of dynactin. This interaction is confirmed by mass spectrometry, immunoprecipitation studies and *in vitro* binding assays. In interphase cells, BICD2 mainly localizes to the Golgi complex and has properties of a peripheral coat protein, yet it also co-localizes with dynactin at microtubule plus ends. Overexpression studies using green fluorescent protein-tagged forms of BICD2 verify its intracellular distribution and co-localization with dynactin, and indicate that the C-terminus of BICD2 is responsible for Golgi targeting. Overexpression of the N-terminal domain of BICD2 disrupts minus-end-directed organelle distribution and this portion of BICD2 co-precipitates with cytoplasmic dynein. Nocodazole treatment of cells results in an extensive BICD2–dynactin–dynein co-localization. Taken together, these data suggest that mammalian BICD2 plays a role in the dynein–dynactin interaction on the surface of membranous organelles, by associating with these complexes.

Keywords: Bicaudal-D/dynactin/dynein/Golgi/vesicular transport

Introduction

The product of the *Drosophila melanogaster Bicaudal-D* gene, Bic-D, is a cytoplasmic, α-helical coiled-coil protein (Suter *et al.*, 1989; Wharton and Struhl, 1989), which is highly conserved from *Caenorhabditis elegans* to man and has two homologues in mammals, BICD1 (Baens and Marynen, 1997) and BICD2 (KIAA0699). In *D.melanogaster*, *Bic-D* is essential for the establishment of oocyte identity, as well as for the determination of the oocyte anterior–posterior axis and its dorsal–ventral polarity (Suter *et al.*, 1989; Wharton and Struhl, 1989; Suter and Steward, 1991; Swan and Suter, 1996). Mutations in *Bic-D* disrupt the proper accumulation and distribution of factors important for oocyte differentiation and patterning, and affect the organization and polarization of the microtubule network during oogenesis (Suter *et al.*, 1989; Theurkauf *et al.*, 1993; Mach and Lehmann, 1997). Based on genetic data and the localization of Bic-D protein, it has been suggested that it constitutes a part of the microtubule-dependent mRNA transport or anchoring mechanism (Swan and Suter, 1996; Mach and Lehmann, 1997; Swan *et al.*, 1999).

One of the major components of the intracellular transport machinery is cytoplasmic dynein, a minus-end-directed, microtubule-based motor. It is a large protein complex, which requires the activity of another multisubunit complex, dynactin, for most of its known cellular functions (for review see Karki and Holzbaur, 1999). Dynactin consists of two structural domains: an actin-like backbone, thought to be responsible for cargo attachment, and a projecting shoulder–sidearm that interacts with cytoplasmic dynein as well as with microtubules. The shoulder–sidearm complex contains $p150^{Glued}$, dynamitin (p50) and p24 subunits, while the actin-like backbone contains Arp1, CapZ, p62, Arp11, p27 and p25 (Eckley *et al.*, 1999). Genetic analysis in *D.melanogaster* suggests that Bic-D functions in a transport pathway that involves cytoplasmic dynein and dynactin (Swan *et al.*, 1999). This is in line with the fact that the distribution of Bic-D at different stages of oogenesis resembles the localization of the minus ends of microtubules (Mach and Lehmann, 1997) and of cytoplasmic dynein and dynactin (Li *et al.*, 1994; McGrail *et al.*, 1995). Bic-D has been shown to interact with the *Egalitarian* gene product (Mach and Lehmann, 1997). In addition, yeast two-hybrid analysis has suggested an association of Bic-D with lamin Dm0 (Stuurman *et al.*, 1999). How these interactions relate to the proposed role of Bic-D and how Bic-D acts in the dynein–dynactin pathway are currently unclear.

Recently, we isolated mouse BICD2 in a yeast two-hybrid screen, using the microtubule binding protein CLIP-115 as bait (C.Hoogenraad, A.Akhmanova, F.Grosveld and N.Galjart, in preparation). These data suggest that, similar to *D.melanogaster* Bic-D, BICD2 could also be involved in microtubule-dependent transport. Here we demonstrate an interaction between mammalian BICD2 and the dynein–dynactin complexes, and we show that BICD2 associates with membranous organelles. We propose that BICD proteins play a direct role in dynein-mediated transport and that this function is conserved from *D.melanogaster* to mammals.

Results

Association of BICD2 with dynein and dynactin

Mammalian BICD2 is a coiled-coil protein, which, like *D.melanogaster* Bic-D (Stuurman *et al.*, 1999), contains three segments with multiple heptad repeats (Figure 1A). The C-terminal segment 3 shows the highest degree of evolutionary conservation (Figure 1A). In order to characterize BICD2, we generated polyclonal antibodies against the N-terminal part of BICD2 [glutathione *S*-transferase (GST)–NBICD2; antiserum #2293], as well as antibodies against the C-terminal coiled-coil segment of the protein (GST–CBICD2; antiserum #2298; see Figure 1A). In COS-1 cell lysates, both antisera specifically recognize proteins of ~98 kDa, which correlates with the expected size of BICD2 (Figure 1B). In BICD2-transfected cells, the intensity of the signal at the 98 kDa position increases, confirming that it represents BICD2, while antibodies, pre-incubated with their corresponding antigens, display no reaction on western blots (Figure 1B). Thus, the #2293 and #2298 antibodies specifically recognize BICD2 in COS-1 cells.

Fractionation of COS-1 cell lysates by high-speed centrifugation suggests that BICD2 is associated with membranous organelles, as part of the endogenous BICD2 protein is present in the pellet in the absence of detergent, while in the presence of 1% Triton X-100 all BICD2 immunoreactivity is recovered in the supernatant (Figure 1C). In the presence of detergent, both antisera are able to immunoprecipitate BICD2 from total extracts of COS-1 and HeLa cells (Figure 1D and E and data not shown). Coomassie Blue staining of a large scale immunoprecipitation from HeLa cells with antiserum #2298 revealed that these antibodies precipitate two major proteins with an apparent molecular mass of 97–100 kDa, in addition to several other proteins, ranging in size from >200 to 130 kDa (Figure 1D). Mass spectrometry on excised gel slices identified the 97–100 kDa bands as BICD2 isoforms, while other proteins, co-precipitating with the #2298 antiserum, were shown to be dynein heavy chain, non-muscle myosin IIA, p150^{Glued} and leucine-rich protein (Figure 1D, Table I; proteins smaller than ~80 kDa could not be identified because of IgG contamination). Here we focus on the interaction between BICD2 and dynein–dynactin.

To verify the results of mass spectrometry, immunoprecipitates obtained with anti-BICD2 antibodies #2298 and #2293 were analysed by western blotting. This revealed that both antisera bring down cytoplasmic dynein, as detected with an anti-dynein intermediate chain (DIC) antibody, and dynactin, as detected with anti-p150^{Glued} and anti-Arp1 antibodies (Figure 1E). These co-precipitations are specific, as #2293 pre-immune serum does not bring down dynein–dynactin or BICD2, and as none of the antisera co-precipitate CLIP-170, a cytosolic, microtubule-associated protein (Figure 1E). Furthermore, in a reciprocal experiment, antibodies against DIC, p150^{Glued} and Arp1 co-precipitate BICD2 (Figure 1F). Thus, dynein and dynactin can be co-immunoprecipitated with BICD2 antisera and vice versa. As a substantial co-immunoprecipitation of dynein and dynactin, using specific antisera against components of these complexes, has not been observed (Gill *et al.*, 1991), it seems unlikely that the interaction of BICD2 with dynein occurs through dynactin, or vice versa.

Yeast two-hybrid interactions of BICD2

Structural studies have shown that *D.melanogaster* Bic-D forms dimers, which might fold up further via an intramolecular interaction of coiled-coil segments 2 and 3 (Stuurman *et al.*, 1999). To test whether mammalian BICD2 interacts with itself and with components of the dynactin complex, we set up a yeast two-hybrid assay, using each of the three coiled-coil segments of BICD2 as separate fusion proteins, either linked to the DNA binding domain (BD), or to the activation domain (AD) of GAL4 (Figure 2A). As fusions of coiled-coil segments 1 and 3 to the GAL4 DNA-BD already strongly activated transcription of the reporter gene in the absence of GAL4 AD fusions, these clones were not used further. The GAL4 DNA-BD fusions of segment 2 and of the C-terminal part of segment 3 (amino acids 706–810) did not activate transcription by themselves and could be used to test a putative self-association of BICD2 (Figure 2B). This analysis shows that segment 2 (BICD2B) interacts with itself, but not with other segments, while the C-terminal part of segment 3 (BICD2D) interacts with itself, with the complete segment 3 (BICD2C) and with segment 1 (BICD2A; Figure 2B). The lack of interaction between BICD2B and -D is somewhat unexpected, given the proposal that Bic-D dimers fold up via segments 2 and 3 (Stuurman *et al.*, 1999). Instead, we find that BICD2A and -D do associate; indicating that segments 1 and 3 might interact. However, it is possible that, *in vivo*, both associations (segment 1 with 3 and segment 2 with 3) occur. Such associations may serve as a mechanism for multimerization of BICD proteins and/or the regulation of interactions with other proteins.

We next examined the interaction of BICD2 fragments with all coiled-coil containing components of the dynactin complex, including p24, dynamitin and three adjacent p150^{Glued} fragments, as well as with the dynactin subunit Arp1 (Figure 2C). BICD2 does not associate with p150^{Glued}, p24, Arp1 or the control tropomyosin. Interestingly, coiled-coil segment 3 of BICD2 does interact with dynamitin, the C-terminal portion of this fragment (residues 706–810) being sufficient for the association. The other BICD2 fragments do not interact with dynamitin, suggesting that the association of the C-terminal domain is specific (Figure 2C). The direct nature of the BICD2–dynamitin interaction was confirmed by pull-down experiments, in which *in vitro* transcribed and translated BICD2 is retained by bacterially produced dynamitin (GST–p50), while myc- and green fluorescent protein (GFP)-tagged dynamitin (myc–GFP–p50) is retained by GST–CBICD2 (Figure 3A and B).

To demonstrate that BICD2 associates with dynamitin in transfected cells, we performed immunoprecipitations from extracts of COS-1 cells, overexpressing BICD2 (or GFP–BICD2$^{706–810}$) and myc–GFP–p50. We found that dynamitin co-precipitates with BICD2 from co-transfected cells (Figure 3C and D), whereas, in a similar experiment, no significant co-precipitation was detected between overexpressed BICD2 (or GFP–BICD2$^{706–810}$) and p150^{Glued} (Figure 3E). These results together support the yeast two-hybrid and pull-down analyses, and point to a

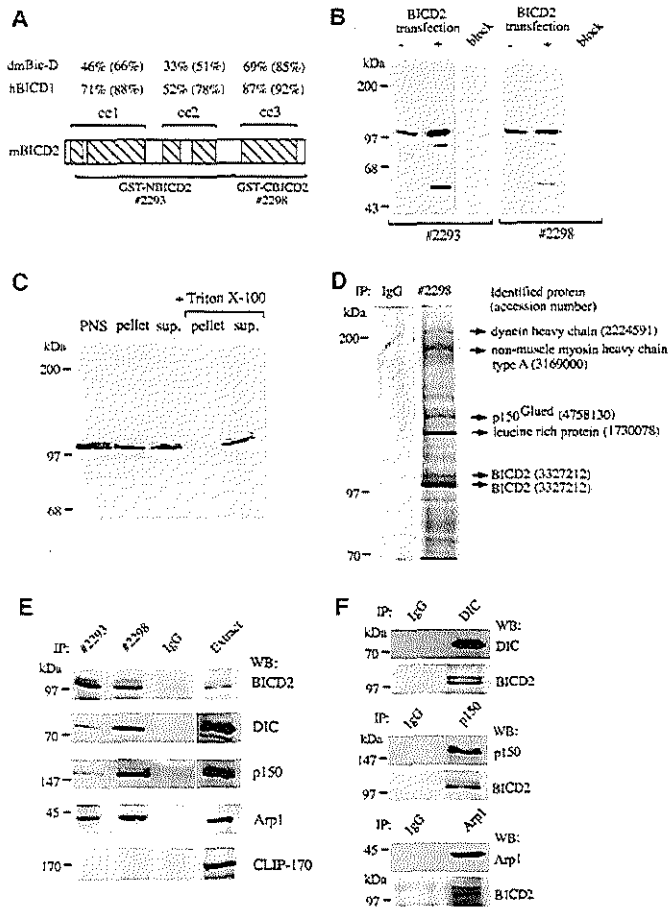

Fig. 1. Characterization of BICD2-specific antibodies. (A) Schematic representation of the domain structure of BICD2, which is characterized by five coiled-coil domains (hatched boxes) embedded in three segments (indicated above the diagram). The percentage of identity and (in parentheses) similarity between mouse BICD2 segments and those of human BICD1 (Baens and Marynen, 1997) or *D.melanogaster* Bic-D (accession No. P16568) is indicated. Antisera were directed against the N-terminal two segments of BICD2 (GST–NBICD2, antiserum #2293, amino acids 77–637) or the C-terminal segment (GST–CBICD2, antiserum #2298, amino acids 631–821). (B) Specificity of the BICD2 antibodies. Protein extracts, prepared from mock (–) or BICD2 (+) transfected COS-1 cells, were analysed by western blotting, using #2293 or #2298 antibodies, or antibodies pre-incubated with their corresponding antigens (lanes, marked 'block'). Approximately 5-fold less protein extract was loaded in the case of the BICD2 transfections, so that the signal in the transfected lanes was not too intense compared with the non-transfected samples. (C) Equal protein amounts of post-nuclear extracts (PNS), high-speed supernatant (sup.) and pellet fractions of COS-1 cells, incubated with or without 1% Triton X-100, were analysed by western blotting with antiserum #2293. (D) Coomassie Blue-stained 8% SDS–polyacrylamide gel of immunoprecipitates from HeLa cells, using anti-BICD2 antibody #2298 or pre-immune serum #2298 (IgG). The major protein bands were excised from the gel and subjected to mass spectrometry. Identified proteins, with their accession numbers, are shown on the right. Molecular weight markers are indicated. (E) Co-immunoprecipitation of cytoplasmic dynein and dynactin with BICD2 antisera. Lysates of HeLa cells were used for immunoprecipitation (IP) with anti-BICD2 antibodies #2293 and #2298, or pre-immune serum of #2293 (IgG). The precipitated proteins were resolved by SDS–PAGE and analysed by western blotting (WB) with antibodies against BICD2 (#2298), DIC, p150^{Glued} (p150), Arp1 and CLIP-170. Five per cent of the total extract used for immunoprecipitation was loaded as a control (BICD2 detection in the extract compared with the immunoprecipitate required five times longer exposure of the western blot; in all other cases, exposure times for immunoprecipitate and extract were the same). (F) Co-immunoprecipitation of BICD2 with cytoplasmic dynein and dynactin antibodies. Lysates of HeLa cells were used for immunoprecipitation (IP) with anti-DIC, anti-p150^{Glued} (p150) and anti-Arp1 antibodies, or with the #2293 pre-immune serum (IgG). Immunoprecipitates were analysed by western blotting (WB) with antibodies against BICD2 (#2298), DIC, p150^{Glued} (p150) and Arp1.

Table 1. Mass spectrometry identification of BICD2-co-precipitating proteins

Protein	Number of matching peptides by MALDI and MS-FIT rank	Percent sequence coverage	Confirmation by nanospray (crosses indicate number of different MS^2 spectra obtained)
BICD2 lower band	12 (1)	17	not attempted
BICD2 upper band	40 (1)	43	++
Leucine-rich protein	32 (1)	34	+++
p150^{Glued}	17 (1)	14	+++
Non-muscle myosin heavy chain type A	39 (1)	24	not attempted
Dynein heavy chain	28 (1)	15	+++

direct and specific binding of BICD2 to dynamitin via the C-terminal part of BICD2.

BICD2 localizes to the Golgi complex and has properties of a peripheral coat protein

To analyse the subcellular localization of BICD2, we performed immunofluorescence experiments on cultured cells. Both with affinity-purified (Figure 4A) and full (Figure 4D1) antiserum #2293, a bright perinuclear and punctate cytoplasmic distribution of BICD2 is observed, which appears to concentrate around the microtubule organizing centre (MTOC). Labelling is abolished by pre-incubation of the antiserum with its antigen GST–NBICD2 (Figure 4B), but not with the GST–CBICD2 fusion (data not shown). Antiserum #2298 produces a very similar labelling pattern to #2293, but the punctate cytoplasmic staining is more prominent with this antiserum (Figure 4C). Labelling by the #2298 antibodies is inhibited by pre-incubation with GST–CBICD2, but not by GST–NBICD2 (data not shown). These data suggest that the #2293 and #2298 antisera specifically recognize BICD2 in immunofluorescence studies.

The high-speed fractionation results (Figure 1C) indicated that BICD2 is associated with membranous organelles. Combined with the immunofluorescence data, this suggests that, in interphase cells, BICD2 is localized either to the Golgi apparatus, the endoplasmic reticulum (ER)-to-Golgi intermediate compartment (ERGIC), or to recycling endosomes, which show an MTOC-dependent distribution (Burkhardt *et al.*, 1997). To distinguish between these possibilities we carried out double-labelling experiments with specific markers of the different compartments. Both epifluorescence and confocal microscopy reveal that the BICD2-positive structures show little overlap with endosomes labelled with antibodies against the transferrin receptor (Figure 4D1–3 and H1–3), or with other endosomal markers such as EEA1 and Rab5 (data not shown). BICD2 distribution is also distinct from that of p115, which labels the ERGIC (Figure 4E1–3). In cells incubated at 15°C, proteins that recycle between the ER and Golgi, such as p115, redistribute partially to peripheral clusters (Nelson *et al.*, 1998). These p115-containing structures are clearly not labelled with anti-BICD2 antiserum (Figure 4F1–3), further suggesting that BICD2 is not associated with the ERGIC.

BICD2 distribution in COS-1 cells does largely overlap with that of γ-adaptin (Figure 4G1–3), a marker for clathrin-coated vesicles at the *trans*-Golgi network (TGN) (Robinson and Kreis, 1992). This conclusion is confirmed by confocal microscopy in HeLa cells, which shows substantial overlap (but not a complete co-localization) of

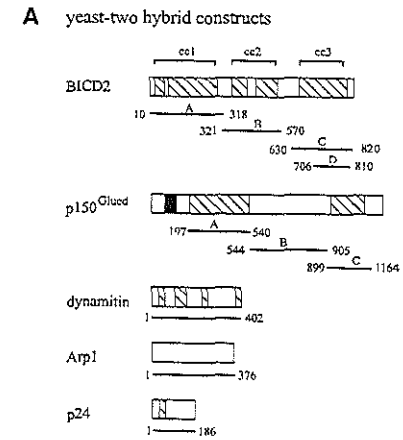

B

GAL4 DNA-BD fusion	GAL4 AD BICD2 A	B	C	D	tropomyosin
BICD2 B	–	++	–	–	–
BICD2 D	+	–	+	+	–

C

GAL4 DNA-BD fusion	GAL4 AD BICD2 A	B	C	D	tropomyosin
p150^{Glued}A	–	–	–	–	–
p150^{Glued}B	–	–	–	–	–
p150^{Glued}C	–	–	–	–	–
dynamitin	–	–	++	+	–
Arp1	–	–	–	–	–
p24	–	–	–	–	–

Fig. 2. Yeast two-hybrid interactions of BICD2. (A) Structure of the yeast two-hybrid constructs. The domain structure of BICD2, p150^{Glued}, dynamitin, Arp1 and p24, including coiled-coil regions (hatched boxes) and microtubule-binding motif (black box), are shown. The position of the protein fragments used in the yeast two-hybrid assay is indicated with horizontal lines below the respective diagrams. (B and C) Yeast two-hybrid analysis. Different segments of BICD2 were tested for BICD2 self-association (B), or for interaction with components of the dynactin complex (C). Protein segments were either fused to AD or DNA-BD of GAL4. The β-galactosidase activity in the yeast lysate is a measure of reporter gene activation. Enzymatic activity is expressed as (++), which indicates high activity (50–100 U); (+), which indicates moderate activity (5–50 U); and (–), which indicates low or no activity (0–5 U).

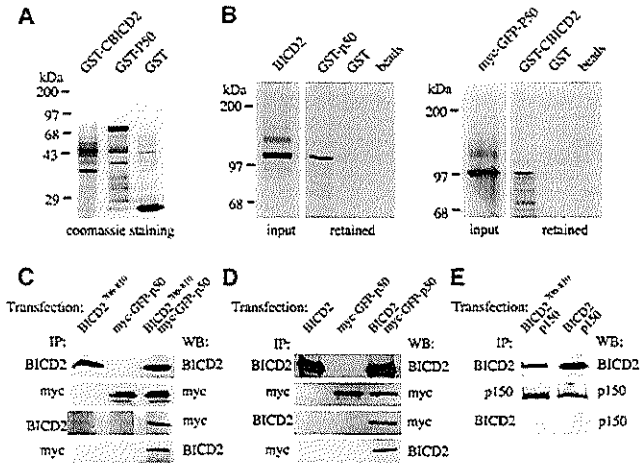

Fig. 3. Co-precipitation of dynamitin with BICD2. (A) Coomassie Blue-stained gel of purified bacterial fusion proteins (GST–CBICD2, GST–p50 and GST). Markers are indicated to the left. (B) *In vitro* interaction between BICD2 and p50 dynamitin. Radioactively labelled, *in vitro* transcribed and translated BICD2 (left panel, input lane) and myc- and GFP-tagged dynamitin (myc–GFP–p50, right panel, input lane) were incubated with the indicated, purified GST fusion proteins, or with glutathione beads only. Proteins, retained on the beads, were detected using SDS–PAGE and X-ray film exposure of dried gels. (C) Coiled-coil segment 3 of BICD2 co-precipitates with dynamitin. COS-1 cells were transfected with constructs expressing GFP–BICD2$^{706–810}$, myc–GFP–p50 or both proteins. Immunoprecipitations (IP) were performed using anti-BICD2 antibodies (#2298) or anti-myc antibodies. Western blots (WB) of the precipitated material were incubated with antibodies against myc, to detect dynamitin, or against BICD2 (#2298). (D) Full-length BICD2 co-precipitates with dynamitin. COS-1 cells were transfected with constructs expressing BICD2, myc–GFP–p50 or both proteins. IP were performed using anti-BICD2 antibodies (#2298) or anti-myc antibodies. WB of the precipitated material were incubated with antibodies against myc, to detect dynamitin, or against BICD2 (#2298). (E) BICD2 does not co-precipitate with p150^{Glued}. COS-1 cells were co-transfected with BICD2 (or GFP–BICD2$^{706–810}$) and p150^{Glued}, and protein homogenates were IP with anti-BICD2 (#2298) or anti-p150^{Glued} (p150) antibodies. WB of the IP material were incubated with anti-BICD2 antibodies (#2298) or with anti-p150^{Glued} (p150) antibodies. In (C–E), interactions between endogenous proteins are not detectable because ~8-fold less protein extract was used compared with (E) and (F) of Figure 1.

BICD2 and γ-adaptin (Figure 4I1–3). Incubation of cells at 20°C blocks vesicular transport from the TGN (Saraste and Kuismanen, 1984) and under these conditions the punctate cytoplasmic staining of BICD2 is no longer detectable (Figure 4J1). Instead, the protein accumulates in a region of the Golgi complex in close proximity to γ-adaptin (Figure 4J1–J3). These results suggest that the BICD2-labelled punctate structures, observed under normal growth conditions, could represent vesicles en route to (or from) the TGN.

Brefeldin A (BFA) is a fungal metabolite that interferes with ADP ribosylation factor-dependent vesicle budding in the secretory pathway (for review see Chardin and McCormick, 1999). After BFA treatment, p115 remains membrane bound (Nelson *et al.*, 1998) (Figure 4K2), while peripheral coat proteins, such as β-COP and γ-adaptin, are released into the cytosol. A similar loss of BICD2 signal from Golgi membranes is observed within minutes after BFA treatment of COS-1 cells (Figure 4K1–3), indicating that BICD2 has properties of a cytosolic peripheral coat protein.

Immunoelectron microscopy was used to investigate further the subcellular distribution of BICD2. Ultrathin cryosections of COS-1 cells were incubated with rabbit antibodies #2293 against BICD2 and mouse antibodies against γ-adaptin, followed by incubation with secondary anti-rabbit and anti-mouse antibodies, conjugated with 6 and 10 nm colloidal gold, respectively (Figure 5). In all sections, a sparse but specific BICD2 labelling is observed, which is mainly located in the vicinity of the TGN, as identified by the γ-adaptin labelling (Figure 5A). In line with the high-speed fractionation results (Figure 1C), BICD2 appears to associate with membranes, as labelling is detected on tubular extensions (Figure 5C), at or near membrane stacks (Figure 5A and data not shown), as well as on budding and/or small cytoplasmic vesicles (Figure 5). Interestingly, the gold particles are often clustered (Figure 5A, B and D), suggesting that multiple BICD2 molecules might be present in a complex at the membrane.

Deletion analysis of BICD2 reveals Golgi targeting and dispersion domains

To determine how BICD2 is targeted to the Golgi, we fused full-length and truncated forms of BICD2 to GFP and studied their intracellular behaviour in transfection studies (Figures 6 and 7). At low expression levels, both full-length GFP–BICD2 and fusion proteins, containing the C-terminal coiled-coil part (GFP–BICD2$^{630–820}$ and GFP–BICD2$^{706–810}$), display a perinuclear accumulation, similar to endogenous BICD2. A strong overlap of GFP and anti-γ-adaptin antibody signal is detected (Figure 6A1–3 and C1–3), while little co-localization with the transferrin receptor is seen (Figure 6B1–3 and D1–3). Interestingly, in cells that overexpress GFP–BICD2$^{706–810}$, almost no endogenous BICD2 is detected in the Golgi apparatus (Figure 6E1–3, labelling

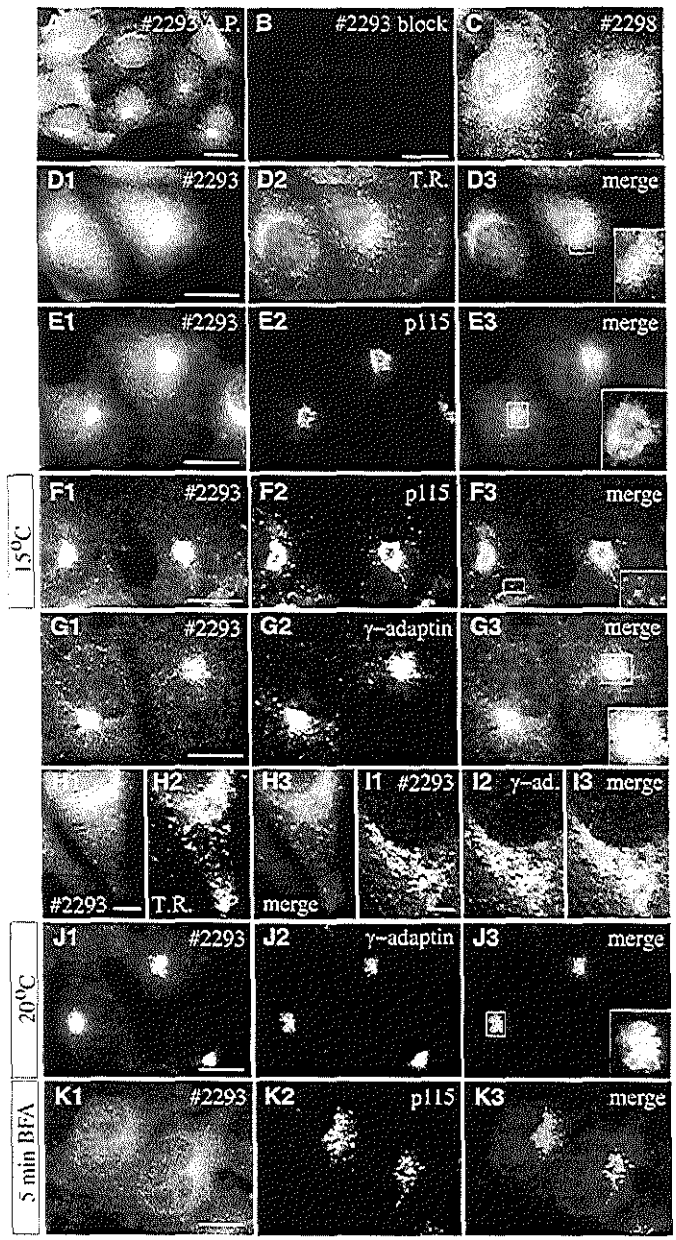
A #2293 A.P.
B #2293 block
C #2298
D1 #2293
D2 T.R.
D3 merge
E1 #2293
E2 p115
E3 merge
F1 #2293
F2 p115
F3 merge
15°C
G1 #2293
G2 γ-adaptin
G3 merge
H2
#2293
T.R.
H3
merge
I1 #2293
I2 γ-ad.
I3 merge
J1 #2293
J2 γ-adaptin
J3 merge
20°C
K1 #2293
K2 p115
K3 merge
5 min BFA

with antiserum #2293 against the N-terminus of BICD2). Nevertheless the Golgi remains in place and other resident proteins are detectable (Figure 6C2 and E3). These data indicate that the third coiled-coil segment of BICD2 contains a Golgi-targeting signal and that this fragment can compete with endogenous BICD2 for binding sites at the Golgi complex.

In contrast to the behaviour of the C-terminal BICD2 fusions, GFP proteins containing only the N-terminal or the middle part of BICD2 display a diffuse cytoplasmic staining (Figure 7A, B1 and C1). Surprisingly, overexpression of these proteins profoundly affects the organization of the Golgi apparatus (Figure 7B2). Deletion analysis reveals that fragmentation of the Golgi is dependent on amino acid residues 1–271 of BICD2, in which segment 1 is embedded (Figure 7A). As cells overexpressing full-length BICD2 (with or without a GFP tag, see Figures 6 and 8, respectively) show no apparent Golgi abnormalities, these data suggest that amino acids 1–271 perturb Golgi organization only when uncoupled from the remainder of BICD2.

Fragmentation of the Golgi apparatus is a characteristic feature of cells in which cytoplasmic dynein function is inhibited. Both overexpression of dynamitin (or other subunits of dynactin) and knock out of the cytoplasmic dynein heavy chain cause inhibition of dynein function (Burkhardt *et al.*, 1997; Harada *et al.*, 1998; Quintyne *et al.*, 1999). In such cells, the distribution of endosomes and lysosomes is also altered. We therefore analysed whether overexpression of the N-terminal BICD2 segment causes a redistribution of transferrin receptor-positive endosomes, and found this to be the case (Figure 7C2). These data suggest that the N-terminal segment of BICD2 perturbs dynein-based motile events. To test whether the BICD2 N-terminus and dynein interact, we investigated co-precipitation of the DIC with selected GFP–BICD2 mutants in lysates of transfected COS-1 cells (Figure 7D). The results of these experiments indicate that every

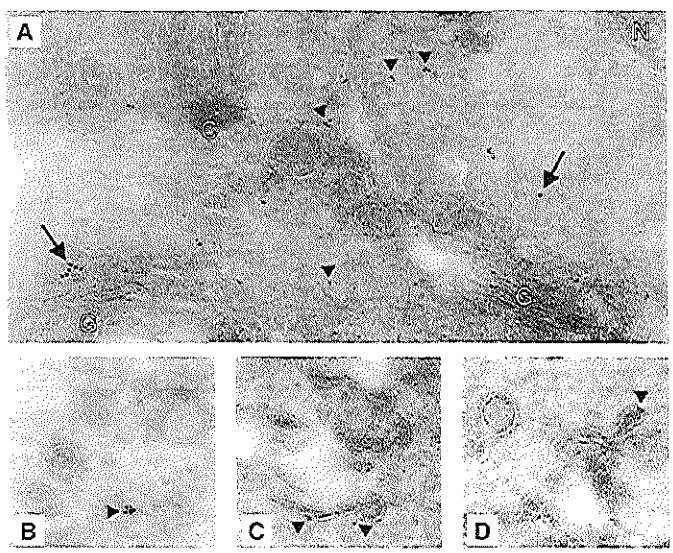

Fig. 5. Ultrastructural distribution of BICD2. (**A** and **B**) Ultrathin cryosections of COS-1 cells were immunolabelled with rabbit antiserum #2293 and mouse anti-γ-adaptin antibodies, followed by anti-rabbit and anti-mouse secondary antibodies, conjugated with 6 and 10 nm gold particles, respectively. Examples of BICD2 (arrowheads) and γ-adaptin (arrows) labelling are indicated. G, Golgi cisternae; C, centriole; N, nucleus. (**C** and **D**) Ultrathin cryosections were incubated with the #2293 antiserum only, followed by anti-rabbit secondary antibodies, conjugated with 6 nm gold. In (B, C and D), BICD2 labelling (arrowheads) of tubules and smooth vesicles in the proximity of the TGN is shown.

Fig. 4. Endogenous BICD2 distribution in COS-1 and HeLa cells. (A–C) COS-1 cells were fixed and processed for indirect immunofluorescence, using affinity purified (A.P.) #2293 anti-BICD2 antibodies (A), #2293 antibodies pre-incubated with GST–NBICD2 fusion protein (**B**) or #2298 anti-BICD2 antibodies (**C**). (D–K) Co-localization of BICD2 with different markers for membrane organelles. Each of the right-hand panels displays the merged signal of the left and middle images. The BICD2-specific (#2293) signal is shown in green and the corresponding marker in red. In some cases, a magnified view of the Golgi area is shown. Images were taken with an epifluorescence microscope, with the exception of H1-3 and I1-3, which were obtained with a confocal microscope. (**D** and **H**) HeLa cells, stained for BICD2 (D1, H1) and transferrin receptor (D2, H2). (**E**, **F** and **K**) COS-1 cells, stained for BICD2 (E1, F1, K1) and p115 (E2, F2, K2). Cells shown in F1-3 were cultured for 3 h at 15°C prior to fixation. Cells shown in K1-3 were incubated for 5 min in the presence of 5 μg/ml BFA. (G and J) COS-1 cells, stained for BICD2 (G1, J1) and γ-adaptin (G2, J2). Cells shown in J1-3 were incubated at 20°C for 3 h to block transport from the TGN. (**I**) HeLa cells stained for BICD2 (I1) and γ-adaptin (I2). Bars: 10 μm in (A–G), (J) and (K) and 5 μm in (H) and (I).

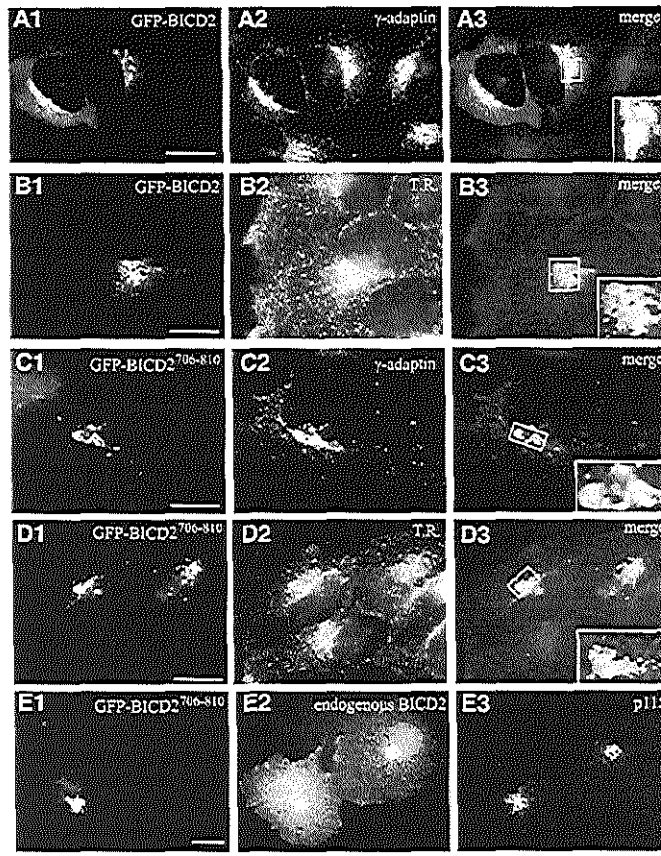

Fig. 6. C-terminal domain of BICD2 is responsible for Golgi localization. (A–D) HeLa cells were transfected with GFP–BICD2 (A and B) or GFP–BICD2$^{706-810}$ (C and D) and stained with antibodies against γ-adaptin (A2, C2) or transferrin receptor (B2, D2). Merged signal from GFP (green) and the organelle marker (shown in red) is shown on the right; a magnified view of the Golgi area is shown in the corner. (E) COS-1 cells were transfected with GFP–BICD2$^{706-810}$ and stained for endogenous BICD2 (#2293; E2) and p115 (E3). In the transfected cell, BICD2-specific staining in the Golgi area is strongly reduced compared with the neighbouring untransfected cell. Bars: 10 μm.

GFP–BICD2 construct, which includes amino acids 1–271, brings down the dynein complex, in line with an association between the N-teminus of BICD2 and dynein.

Co-localization of BICD2 and dynactin

As BICD2 interacts with dynamitin, we next investigated to what extent the intracellular distributions of these proteins overlap and how overexpression of these proteins affects their respective localization. In cells, expressing low levels of co-transfected myc–GFP–dynamitin and BICD2, prominent staining of the microtubule plus ends by GFP is detected (Figure 8A1 and B1). Accumulation of overexpressed BICD2 at the distal ends of microtubules is seen (Figure 8A2 and B2), which is enhanced compared with cells expressing low levels of BICD2 only (data not shown). Thus, overexpressed dynamitin and BICD2 co-localize to some extent. To investigate whether BICD2 co-localizes with dynactin in untransfected cells, Swiss 3T3 fibroblasts (Figure 8C–F) and COS-1 cells (data not shown) were stained with BICD2- and p150^{Glued}-specific antibodies. In these cells, some of the BICD2-positive, vesicle-like structures appear to assemble at those distal ends of microtubules which are also stained with anti-dynactin antibodies (Figure 8C and D). We next examined BICD2 distribution after a brief shift to room temperature, as this manipulation results in a significant co-localization of cytoplasmic dynein with dynactin, an association which is normally not observed (Vaughan *et al.*, 1999). Room temperature incubation leads to an increase in BICD2 and dynactin staining intensity at the microtubule plus ends, consistent with a direct association between BICD2 and dynactin (Figure 8E and F).

Co-localization of BICD2, dynactin and dynein in nocodazole-treated cells

Cultured cells treated with the tubulin sequestering compound nocodazole undergo microtubule depolymerization, resulting in inhibition of dynein-based motility and Golgi dispersal (Cole *et al.*, 1996). We noted that in such cells both GFP–BICD2 (Figure 9A1) and endogenous BICD2 (Figure 9B1 and C1) are mainly present in cytoplasmic vesicular and/or aggregate-like structures. These do not co-localize significantly with any of the Golgi or endosomal markers described above (data not shown), but instead contain a considerable proportion of the cytoplasmic pool of p150^{Glued} and dynamitin (Figure 9A and B), as well as DIC (Figure 9C). Thus, nocodazole treatment of cultured cells surprisingly induces the coalescence of BICD2, dynactin and cytoplasmic dynein into structures of unknown composition. Interestingly, overexpression of the N-terminal part of BICD2 or dynamitin, which have similar disruptive effects on dynein-based organelle distribution in normal cultured cells, prevents the formation of these nocodazole-induced, cytoplasmic aggregates (Figure 9D and E), whereas the C-terminal portion of BICD2 (GFP–BICD2$^{706-810}$) co-localizes with endogenous BICD2 in the structures at low expression levels and inhibits their formation at high expression levels (data not shown). These data support the interaction between BICD2, dynactin and dynein, and suggest that the formation of complexes of these proteins in nocodazole-treated cells might be based on the same protein–protein interactions that are important for dynein-mediated motility.

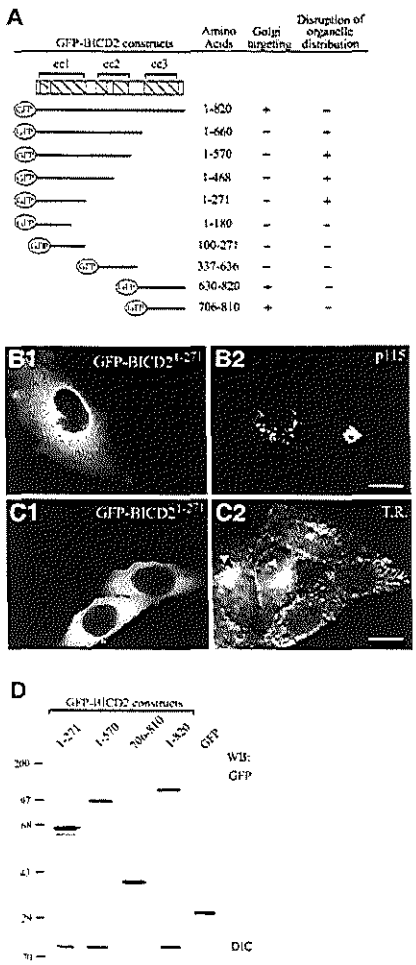

Fig. 7. N-terminal domain of BICD2 co-precipitates with dynein and disrupts microtubule minus-end-directed organelle distribution. (A) Overview of GFP–BICD2 deletion constructs. COS-1 or HeLa cells were transfected with the indicated GFP–BICD2 fusion constructs, fixed and stained with Golgi- or endosome-specific antibodies, to analyse whether the transfected construct was targeted to the Golgi (+ indicates Golgi accumulation of the GFP fusion construct and – indicates absence of such accumulation) and whether organelle distribution was affected by the transfection (+ indicates a disrupted Golgi and endosome distribution, and – indicates a normal Golgi and endosome organization). (**B** and **C**) Organelle disruption by GFP–BICD2$^{1-271}$ overexpression. In (B), fragmentation of the Golgi complex is scored, as detected with anti-p115 antibodies (B2). In (C), a redistribution of endosomes to the periphery of the cell is scored, as detected by staining with antibodies against the transferrin receptor (C2). Organelle disruption is a robust phenotype; when present it occurs in all transfected cells, while neighbouring, non-transfected cells show a normal, compact perinuclear Golgi staining (B2) and prominent juxtanuclear accumulation of endosomes (indicated by arrowheads in C2). Bars: 10 μm. (**D**) Lysates of COS-1 cells, transfected with the indicated GFP proteins, were immunoprecipitated with monoclonal anti-GFP antibodies, and precipitated proteins were analysed by western blotting with polyclonal anti-GFP antibodies or with anti-DIC antibodies.

Discussion

The molecular mechanisms regulating cytoplasmic dynein-mediated motility are not completely understood, but it is becoming increasingly clear that they involve multiple protein–protein interactions and post-translational modifications. The dynactin complex, which can be linked to dynein through the interaction of its p150^{Glued} subunit with DIC (Vaughan and Vallee, 1995), might play a role in dynein–cargo binding, e.g. by associating with spectrin (Muresan *et al.*, 2001), and might regulate the processivity of the dynein motor (King and Schroer, 2000). However, dynein itself can also bind to (and transport) various cargoes through its light and light intermediate chains (Tai *et al.*, 1999; Young *et al.*, 2000). We envisage a function for mammalian BICD2 in dynein-based transport that involves direct binding of BICD2 to the dynamitin subunit of dynactin and association with cytoplasmic dynein. These observations provide a molecular basis for the genetic evidence in *D.melanogaster*, which implicates Bic-D, dynein and dynactin functioning in a common pathway (Swan *et al.*, 1999). Our findings suggest that the

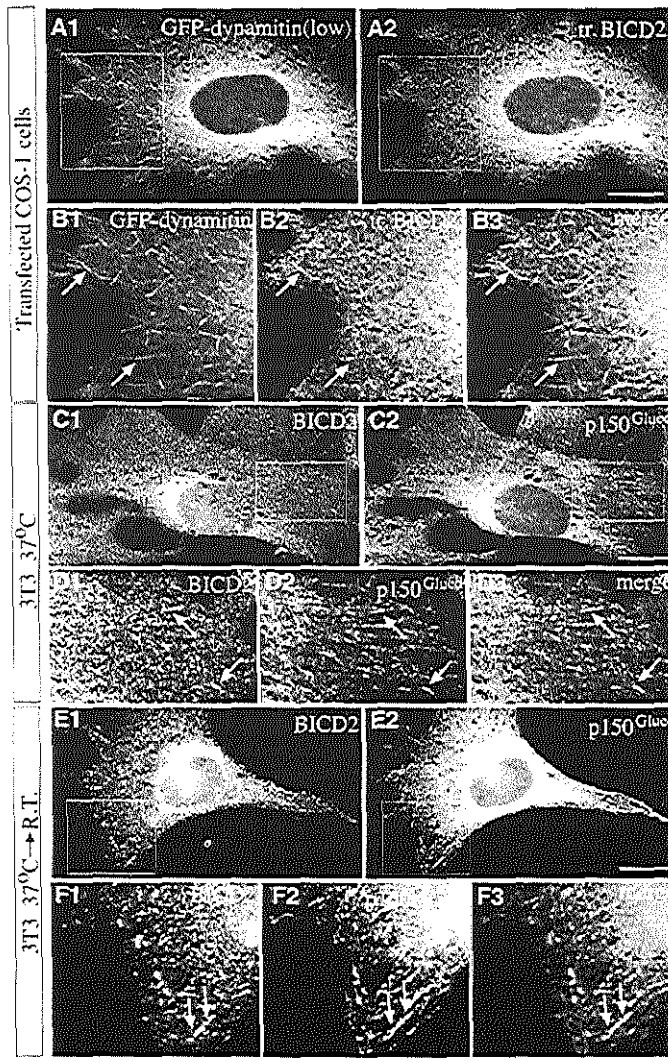

Fig. 8. Co-localization of BICD2 and dynactin components at microtubule distal ends. (A and B) COS-1 cells were co-transfected with myc–GFP–dynamitin and BICD2, and processed for immunofluorescence using anti-BICD2 antibodies #2293. GFP signal is shown in A1 and B1, while in A2 and B2 BICD2 is visualized. (B) A higher magnification view of the square, indicated in (A). B3 represents the merged image of B1 (green, GFP–dynamitin) and B2 (red, BICD2). Arrows indicate clear examples of co-localization of GFP–dynamitin and BICD2 at the distal ends of two microtubules. Bar: 10 μm. (C–F) Swiss 3T3 cells were stained with antibodies against BICD2 (C1, D1, E1, F1) and anti-p150^{Glued} (C2, D2, E2, F2). In D3 and F3, BICD2 (green) and p150^{Glued} (red) signals are merged. (D and F) Higher magnification views of the indicated parts in (C) and (E), respectively. Examples of co-localization of BICD2 and dynactin are indicated by arrows. In (E) and (F), cells were incubated at room temperature for 10 min prior to fixation. Bars: 10 μm.

BICD2 protein is a conserved component of the dynein–dynactin transport machinery.

BICD2 is a Golgi-associated protein, which could be part of the peripheral coat of particular membranes. Both the Golgi targeting of BICD2 and its binding to the dynamitin subunit of dynactin depend on coiled-coil segment 3. The relevance of these interactions is underscored by the fact that this is the most evolutionarily

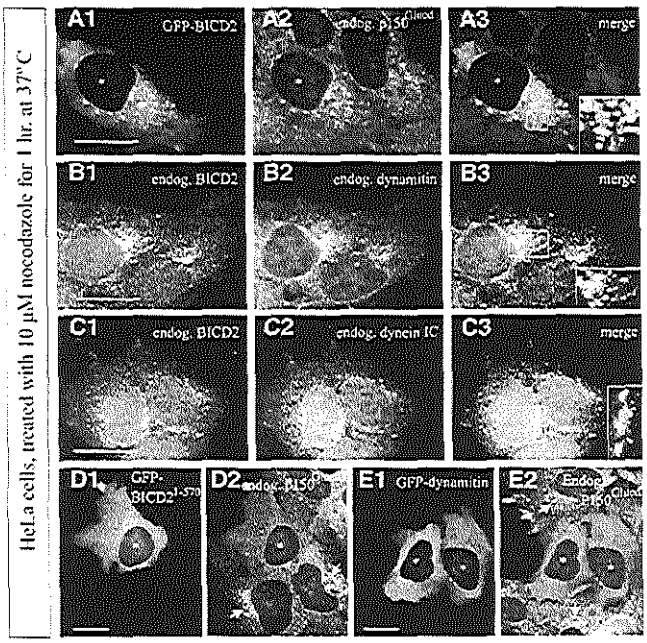

Fig. 9. Co-localization of BICD2 with dynactin and dynein components in nocodazole-treated cells. (A–E) HeLa cells, transfected with GFP–BICD2 (A), GFP–BICD2$^{1-570}$ (D), myc–GFP–dynamitin (E), or not transfected (B, C), were treated with 10 μM nocodazole for 1 h at 37°C prior to fixation, and processed for immunofluorescence with the indicated antibodies (endogenous signals). Asterisks mark the nuclei of transfected cells, and nocodazole-induced, dynactin-positive structures in untransfected cells are indicated by arrows. (A3–C3) are merged images (A1–C1 are in green; A2–C2 are in red). Higher magnification views of indicated areas are shown in the corner. Bars: 10 μm.

conserved part of the protein and the only *D.melanogaster* Bic-D segment indispensable for viability and proper localization during oogenesis (Oh *et al.*, 2000; Oh and Steward, 2001). On the other hand, truncated BICD2 forms, which lack the third, but contain the first coiled-coil segment, can co-precipitate cytoplasmic dynein, suggesting that segment 1 can interact with a component of the dynein complex. Finally, overexpression of the N-terminal portion of BICD2 causes dispersion of cytoplasmic organelles and prevents the formation of nocodazole-induced, dynactin-positive aggregates, while overexpression of full-length BICD2 has none of these effects. To explain all these observations, we propose that soluble (excess, free) BICD2 folds up, for example, as a result of interaction of segments 1 and 3 (as observed in our yeast two-hybrid assay), or of segments 2 and 3 [as proposed in the structural analysis (Stuurman *et al.*, 1999)]. Only when segment 3 engages in an interaction with one of its partners (dynamitin or a membrane-associated protein) do the other segments become available for interaction with other proteins (such as dynein components).

We hypothesize that when BICD2 is bound to a particular cargo through its C-terminus, it can stimulate the association of this cargo with dynein–dynactin through its N-terminus. If dynactin is the C-terminal cargo, then BICD2 might serve as a regulatory linker between dynein and dynactin. The role of BICD2 as such a linker is supported by the extensive co-localization of these protein complexes under conditions when dynein transport is inhibited by nocodazole treatment. Switching of BICD2 between different modes of interaction could regulate the affinity of the dynein–dynactin complex for (vesicular) cargo, or exercise a regulatory effect on dynein motor activity. A schematic representation of the putative conformations of BICD2 is shown in Figure 10.

In agreement with our hypothesis, we find co-localization of BICD2-positive, vesicular structures and dynactin at the distal ends of microtubules. The accumulation of dynactin and cytoplasmic dynein on microtubule plus ends was suggested to represent an early, cargo-loading stage of minus-end-directed organelle transport (Vaughan *et al.*, 1999). In this view, BICD2-containing vesicles might be loaded on dynactin-carrying microtubule distal ends, in order to be transported along microtubules. One possibility is that BICD2 interacts with dynactin and the peripheral coat of membrane organelles simultaneously. This could be a result of multimerization of BICD2 proteins on the membrane surface or through unfolding of the last coiled-coil segment within one BICD2 dimer. Whatever the actual mechanism, all models predict that overexpression of the C-terminal segment of BICD2 by itself should have a dominant-negative effect on BICD2 function.

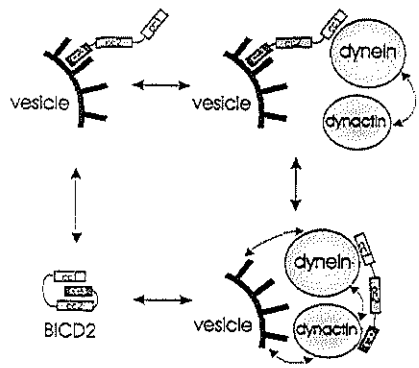

Fig. 10. Schematic representation of the possible conformations and interactions of BICD2. The BICD2 homodimer is represented by three boxes, corresponding to the three coiled-coil segments (cc1,cc2 and cc3), which are connected by lines (corresponding to putative flexible linker regions). Vesicular surface (with its coat proteins) is shown in black, and dynein and dynactin complexes as grey spheres (microtubule-BDs and microtubules are omitted for simplicity). Notice that the interaction of BICD2 with dynactin is direct, while that with dynein could be indirect. Stippled arrows indicate putative interactions of dynein and dynactin with each other and with the membrane coat; these interactions are not directly dependent on BICD2, but can be influenced by its presence in the complex.

Elucidation of the exact nature of the BICD2-associated cargoes would be necessary to test this prediction.

Studies in *Drosophila* oogenesis have shown that the genetic pathway involving Bic-D and cytoplasmic dynein–dynactin also includes Lis1 (Swan *et al.*, 1999). Lis1 is a highly conserved protein, which was shown to have a function in dynein-mediated nuclear migration in filamentous fungi and to be essential for neuronal migration during brain development (for review see Vallee *et al.*, 2001). Similar to BICD2, mammalian Lis1 co-precipitates both with the dynein and dynactin complexes, is partially localized to microtubule plus ends and is suggested to play a role in dynein function. We examined whether murine Lis1 interacts with BICD2 or the components of the dynactin complex described above using the yeast two-hybrid assay, but failed to show a positive reaction (data not shown). In addition, we could not show co-precipitation between BICD2 and GFP–Lis1 in overexpressing COS-1 cells (data not shown), indicating that BICD2 and Lis1 do not interact directly. Therefore, the respective roles of these proteins in dynein function await further analysis.

The membrane association of BICD2, described in this study, is a novel finding. It is supported by the high-speed fractionation and immunocytochemistry results (light microscopy and electron microscopy). The BFA studies suggest that BICD2 could be part of the peripheral coat of membranes. These data could be pertinent to the possible involvement of *D.melanogaster* Bic-D in microtubule-dependent mRNA transport (for discussion see Mach and Lehmann, 1997). Intracellular structures involved in mRNA localization, such as the *D.melanogaster* 'sponge body' and *Xenopus* mitochondrial cloud, contain abundant membranous components (Wilsch-Brauninger *et al.*, 1997). An attractive possibility is that mRNA transport in early development and vesicular trafficking in cultured cells represent different aspects of essentially similar molecular mechanisms.

Materials and methods

Mammalian expression constructs

Full-length mouse BICD2 cDNA (ATCC 1364234) was sequenced on both strands (DDBJ/EMBL/GenBank accession No. AJ250106). The mammalian expression vectors pEGFP-C1 and -C2 (Clontech) were used to construct plasmids for the expression of full-length and truncated forms of mouse BICD2. Constructs for expressing GFP- and myc-tagged dynamitin and p150^{Glued} were a kind gift from Dr T.Schroer.

GST–BICD2 constructs and antibodies

For BICD2 antibody production, GST fusion proteins were made, purified and injected as described (Hoogenraad *et al.*, 2000). Affinity purification of the antibodies was performed using standard methods (Spector *et al.*, 1998). Monoclonal anti-Arp1 antiserum 45A (a kind gift from Dr T.Schroer) has been described (Schafer *et al.*, 1994). Other antibodies, e.g. polyclonal anti-GFP antiserum (Clontech), monoclonal anti-γ-adaptin antibodies (Sigma), monoclonal anti-p115 and anti-p150^{Glued} antibodies (Transduction Laboratories), monoclonal anti-transferrin receptor and anti-myc antibodies (Boehringer) and monoclonal anti-intermediate chain dynein antibodies (IC74; Chemicon), were commercially acquired.

DNA transfections and immunofluorescence

COS-1 cells were transfected by the DEAE–dextran method as described (Hoogenraad *et al.*, 2000), and HeLa cells were transfected with Superfect (Qiagen). BFA was purchased from Molecular Probes and nocodazole from Sigma. For immunofluorescence experiments, transfected cells were grown in Lab-Tek chambers slides (Nunc) for 18 or 40 h after transfection. Cells were fixed with 2% paraformaldehyde for 20 min at 20°C or with 100% methanol/1 mM EGTA for 10 min at –20°C, followed directly by a 2% paraformaldehyde fixation for 20 min at 20°C. Subsequent incubation steps were performed as described earlier (Hoogenraad *et al.*, 2000). Polyclonal anti-BICD2 antibodies were used in a dilution of 1:300 and various monoclonal antibodies in a dilution of 1:100. Secondary antibodies used were fluorescein isothiocyanate (FITC)-conjugated goat anti-rabbit antibodies (Nordic Laboratories; 1:100), rhodamine-labelled sheep anti-mouse antibodies (Boehringer Mannheim; 1:25), Alexa 594-conjugated goat anti-rabbit antibodies (Molecular Probes; 1:500) and Alexa 350-conjugated sheep anti-mouse antibodies (Molecular Probes; 1:250). Slides were analysed with a Leica DMRBE microscope, equipped with a Hamamatsu CCD camera (C4880), or with a Zeiss confocal laser scanning microscope (LSM510). In the latter case, optical sections of 0.7–0.9 μm were taken.

Immunoelectron microscopy

The subcellular distribution of BICD2 was analysed by immunoelectron microscopy on ultrathin frozen sections, as plastic embedding was found to abolish antigen recognition by #2293 and #2298 antisera. COS cells were fixed with 3% paraformaldehyde for 1 h and scraped from the dish. Cell pellets were embedded in 10% gelatin and post-fixed in 3% paraformaldehyde for 24 h. Sectioning, immunolabelling and staining were performed as described before (Willemsen *et al.*, 1987). Sections were examined in a Philips CM100 electron microscope at 80 kV.

Immunoprecipitations and western blot analysis

Immunoprecipitations were carried out using total protein extracts, prepared from HeLa cells or (transfected) COS-1 cells. Cells were lysed in buffer containing 25 mM Tris–HCl pH 8.0, 50 mM NaCl, 0.5% Triton X-100 and protease inhibitors (Boehringer), and incubated at 4°C for 30 min to depolymerize microtubules. All subsequent steps were performed as described (Hoogenraad *et al.*, 2000). Anti-BICD2 antibodies were diluted 1:200 for immunoprecipitation and 1:2000 for western blotting, polyclonal anti-GFP and anti-CLIP-170 antibodies (Hoogenraad *et al.*, 2000) were diluted 1:1000 for western blotting, and various monoclonal antibodies were diluted 1:100 for immunoprecipitation and 1:500 for western blotting.

For the immunodetection of BICD2 by western blotting, total protein extract was prepared from mock-transfected or BICD2-transfected COS-1 cells by homogenization in phosphate-buffered saline (PBS)/1% Triton X-100, in the presence of protease inhibitors. For fractionation experiments, COS-1 cells were homogenized in a sucrose buffer (10 mM HEPES pH 7.4, 0.25 M sucrose, 1 mM EDTA) using a glass homogenizer. A post-nuclear supernatant was recovered after centrifugation at 1000 *g*. Samples were subsequently centrifuged at 100 000 *g*, and pellet and high-speed supernatant were collected.

In-gel digestion of proteins

For the mass spectrometry identification of proteins co-precipitating with BICD2 antiserum, one flask (150 cm^2) of confluent HeLa cells was harvested and incubated with antibodies, as described above. Proteins were visualized with Coomassie Blue after SDS–PAGE (see Figure 1D) and the major bands were cut out. Excised, diced protein gel bands were washed, reduced and *S*-alkylated essentially as described (Wilm *et al.*, 1996). A sufficient volume of 2 ng/μl trypsin (modified sequencing grade; Promega, Madison, WI) in 5 mM NH_4HCO_3 was added to cover the gel pieces and digestion performed overnight at 32°C in an incubator. The digests were then acidified by the addition of a 1/10 vol. of 2% trifluoroacetic acid prior to MALDI analysis.

Peptide mass mapping by MALDI

A Reflex III MALDI time-of-flight mass spectrometer (Bruker Daltonik GmbH, Bremen, Germany), equipped with a nitrogen laser and a Scout-384 probe, was used to obtain positive ion mass spectra of digested protein with pulsed ion extraction in reflectron mode. An accelerating voltage of 26 kV was used with detector bias gating set to 2 kV and a mass cut-off of 650 *m/z*. Thin-layer matrix surfaces of α-cyano-4-hydroxycinnamic acid mixed with nitrocellulose were prepared as described (Shevchenko *et al.*, 1996). An aliquot (0.4 μl) of acidified digestion supernatant was deposited onto the thin layer and allowed to dry prior to rinsing with water.

Peptide mass fingerprints thus obtained were searched against the non-redundant protein database placed in the public domain by the National Centre for Biotechnology Information (NCBI) using the program MS-FIT (Regents of the University of California).

Nanospray tandem mass spectrometry

Remaining digestion supernatant was loaded onto a 2 × 0.8 mm C18 microcolumn (LC Packings, Amsterdam, The Netherlands), washed and step eluted with 60% methanol, 0.1% formic acid directly into an Econo12 nanospray needle (New Objective Inc., Cambridge, MA). Nanospray mass spectra were acquired on an LCQ 'classic' quadrupole ion trap mass spectrometer (ThermoQuest Corporation, Austin, TX) equipped with a nanospray source (Protana, Odense, Denmark) operated at a spray voltage of 800 V and a capillary temperature of 150°C. Tandem (MS^2) mass spectra were acquired at a collision energy of 30% and a parent ion isolation width of 3 Da. Proteins were identified using the program SEQUEST (ThermoQuest Corporation, Austin, TX) to search tandem mass spectra against the NCBI non-redundant protein database.

Yeast two-hybrid analysis

The yeast two-hybrid analysis was performed as described previously (Wolthuis *et al.*, 1996). Different mouse BICD2 fragments were linked to the GAL4 DNA-BD in the pPC97 yeast two-hybrid vector and to the GAL4 AD in the pPC86 yeast two-hybrid vector. Dynamitin and $p150^{Glued}$ cDNA fragments were generated by PCR, using the corresponding full-length cDNAs as templates. Arp1 and p24 cDNAs were generated by PCR, using total mouse brain cDNA as a template. Fragments were subcloned into pPC97. Production of the yeast fusion proteins of correct size was verified by western blotting, using antibodies against GAL4 DNA-BD and GAL4 AD and according to the protocol of the manufacturer (Clontech). β-galactosidase activity measurements (expressed in arbitrary units) were performed in triplicate from two independent experiments, as described previously (Ausubel *et al.*, 1997).

Acknowledgements

We would like to thank Dr T.Schroer for the p50 and $p150^{Glued}$-encoding plasmids and the anti-Arp1 antibodies, Yvonne Krom and Arjan Theil for technical assistance, and Ruud Koppenol for photography. This research was supported by grants from the NWO (GB-MW 903-68-361) and SLW (805.33.310). N.G. was supported by the Royal Dutch Academy of Sciences (KNAW).

References

Ausubel,F.M., Brent,R., Kingston,R.E., Moore,D.D., Seidman,J.G., Smith,J.A. and Struhl,K. (1997) *Current Protocols in Molecular Biology*. John Wiley & Sons, Inc., New York, NY.

Baens,M. and Marynen,P. (1997) A human homologue (BICD1) of the *Drosophila* bicaudal-D gene. *Genomics*, **45**, 601–606.

Burkhardt,J.K., Echeverri,C.J., Nilsson,T. and Vallee,R.B. (1997) Overexpression of the dynamitin (p50) subunit of the dynactin complex disrupts dynein-dependent maintenance of membrane organelle distribution. *J. Cell Biol.*, **139**, 469–484.

Chardin,P. and McCormick,F. (1999) Brefeldin A: the advantage of being uncompetitive. *Cell*, **97**, 153–155.

Cole,N.B., Sciaky,N., Marotta,A., Song,J. and Lippincott-Schwartz,J. (1996) Golgi dispersal during microtubule disruption: regeneration of Golgi stacks at peripheral endoplasmic reticulum exit sites. *Mol. Biol. Cell*, **7**, 631–650.

Eckley,D.M., Gill,S.R., Melkonian,K.A., Bingham,J.B., Goodson,H.V., Heuser,J.E. and Schroer,T.A. (1999) Analysis of dynactin subcomplexes reveals a novel actin-related protein associated with the arp1 minifilament pointed end. *J. Cell Biol.*, **147**, 307–320.

Gill,S.R., Schroer,T.A., Szilak,I., Steuer,E.R., Sheetz,M.P. and Cleveland,D.W. (1991) Dynactin, a conserved, ubiquitously expressed component of an activator of vesicle motility mediated by cytoplasmic dynein. *J. Cell Biol.*, **115**, 1639–1650.

Harada,A., Takei,Y., Kanai,Y., Tanaka,Y., Nonaka,S. and Hirokawa,N. (1998) Golgi vesiculation and lysosome dispersion in cells lacking cytoplasmic dynein. *J. Cell Biol.*, **141**, 51–59.

Hoogenraad,C.C., Akhmanova,A., Grosveld,F., De Zeeuw,C.I. and Galjart,N. (2000) Functional analysis of CLIP-115 and its binding to microtubules. *J. Cell Sci.*, **113**, 2285–2297.

Karki,S. and Holzbaur,E.L. (1999) Cytoplasmic dynein and dynactin in cell division and intracellular transport. *Curr. Opin. Cell Biol.*, **11**, 45–53.

King,S.J. and Schroer,T.A. (2000) Dynactin increases the processivity of the cytoplasmic dynein motor. *Nature Cell Biol.*, **2**, 20–24.

Li,M., McGrail,M., Serr,M. and Hays,T.S. (1994) *Drosophila* cytoplasmic dynein, a microtubule motor that is asymmetrically localized in the oocyte. *J. Cell Biol.*, **126**, 1475–1494.

Mach,J.M. and Lehmann,R. (1997) An Egalitarian–Bicaudal-D complex is essential for oocyte specification and axis determination in *Drosophila*. *Genes Dev.*, **11**, 423–435.

McGrail,M., Gepner,J., Silvanovich,A., Ludmann,S., Serr,M. and Hays,T.S. (1995) Regulation of cytoplasmic dynein function *in vivo* by the *Drosophila* Glued complex. *J. Cell Biol.*, **131**, 411–425.

Muresan,V., Stankewich,M.C., Steffen,W., Morrow,J.S., Holzbaur,E.L. and Schnapp,B.J. (2001) Dynactin-dependent, dynein-driven vesicle transport in the absence of membrane proteins: a role for spectrin and acidic phospholipids. *Mol. Cell*, **7**, 173–183.

Nelson,D.S., Alvarez,C., Gao,Y.S., Garcia-Mata,R., Fialkowski,E. and Sztul,E. (1998) The membrane transport factor TAP/p115 cycles between the Golgi and earlier secretory compartments and contains distinct domains required for its localization and function. *J. Cell Biol.*, **143**, 319–331.

Oh,J. and Steward,R. (2001) Bicaudal-D is essential for egg chamber formation and cytoskeletal organization in *Drosophila* oogenesis. *Dev. Biol.*, **232**, 91–104.

Oh,J., Baksa,K. and Steward,R. (2000) Functional domains of the *Drosophila* Bicaudal-D protein. *Genetics*, **154**, 713–724.

Quintyne,N.J., Gill,S.R., Eckley,D.M., Crego,C.L., Compton,D.A. and Schroer,T.A. (1999) Dynactin is required for microtubule anchoring at centrosomes. *J. Cell Biol.*, **147**, 321–334.

Robinson,M.S. and Kreis,T.E. (1992) Recruitment of coat proteins onto Golgi membranes in intact and permeabilized cells: effects of brefeldin A and G protein activators. *Cell*, **69**, 129–138.

Saraste,J. and Kuismanen,E. (1984) Pre- and post-Golgi vacuoles operate in the transport of Semliki Forest virus membrane glycoproteins to the cell surface. *Cell*, **38**, 535–549.

Schafer,D.A., Gill,S.R., Cooper,J.A., Heuser,J.E. and Schroer,T.A. (1994) Ultrastructural analysis of the dynactin complex: an actin-related protein is a component of a filament that resembles F-actin. *J. Cell Biol.*, **126**, 403–412.

Shevchenko,A., Jensen,O.N., Podtelejnikov,A.V., Sagliocco,F., Wilm,M., Vorm,O., Mortensen,P., Boucherie,H. and Mann,M. (1996) Linking genome and proteome by mass spectrometry: large-

scale identification of yeast proteins from two dimensional gels. *Proc. Natl Acad. Sci. USA*, **93**, 14440–14445.
Spector,D.L., Goldman,R.D. and Leinwand,L.A. (1998) *Cells: A Laboratory Manual*. Cold Spring Harbor Laboratory Press, Cold Spring Harbor, NY.
Stuurman,N., Heins,M., Sasse,B., Hubner,W., Suter,B. and Aebi,U. (1999) Interactions between coiled-coil proteins: *Drosophila* lamin Dm0 binds to the Bicaudal-D protein. *Eur. J. Cell Biol.*, **78**, 278–287.
Suter,B. and Steward,R. (1991) Requirement for phosphorylation and localization of the Bicaudal-D protein in Drosophila oocyte differentiation. *Cell*, **67**, 917–926.
Suter,B., Romberg,L.M. and Steward,R. (1989) *Bicaudal-D*, a *Drosophila* gene involved in developmental asymmetry: localized transcript accumulation in ovaries and sequence similarity to myosin heavy chain tail domains. *Genes Dev.*, **3**, 1957–1968.
Swan,A. and Suter,B. (1996) Role of Bicaudal-D in patterning the Drosophila egg chamber in mid-oogenesis. *Development*, **122**, 3577–3586.
Swan,A., Nguyen,T. and Suter,B. (1999) *Drosophila* Lissencephaly-1 functions with Bic-D and dynein in oocyte determination and nuclear positioning. *Nature Cell Biol.*, **1**, 444–449.
Tai,A.W., Chuang,J.Z., Bode,C., Wolfrum,U. and Sung,C.H. (1999) Rhodopsin's carboxy-terminal cytoplasmic tail acts as a membrane receptor for cytoplasmic dynein by binding to the dynein light chain Tctex-1. *Cell*, **97**, 877–887.
Theurkauf,W.E., Alberts,B.M., Jan,Y.N. and Jongens,T.A. (1993) A central role for microtubules in the differentiation of *Drosophila* oocytes. *Development*, **118**, 1169–1180.
Vallee,R.B., Tai,C. and Faulkner,N.E. (2001) LIS1: cellular function of a disease-causing gene. *Trends Cell Biol.*, **11**, 155–160.
Vaughan,K.T. and Vallee,R.B. (1995) Cytoplasmic dynein binds dynactin through a direct interaction between the intermediate chains and p150Glued. *J. Cell Biol.*, **131**, 1507–1516.
Vaughan,K.T., Tynan,S.H., Faulkner,N.E., Echeverri,C.J. and Vallee,R.B. (1999) Colocalization of cytoplasmic dynein with dynactin and CLIP-170 at microtubule distal ends. *J. Cell Sci.*, **112**, 1437–1447.
Wharton,R.P. and Struhl,G. (1989) Structure of the *Drosophila* Bicaudal-D protein and its role in localizing the posterior determinant nanos. *Cell*, **59**, 881–892.
Willemsen,R., van Dongen,J.M., Ginns,E.I., Sips,H.J., Schram,A.W., Tager,J.M., Barranger,J.A. and Reuser,A.J. (1987) Ultrastructural localization of glucocerebrosidase in cultured Gaucher's disease fibroblasts by immunocytochemistry. *J. Neurol.*, **234**, 44–51.
Wilm,M., Shevchenko,A., Houthaeve,T., Breit,S., Schweigerer,L., Fotsis,T. and Mann,M. (1996) Femtomole sequencing of proteins from polyacrylamide gels by nano-electrospray mass spectrometry. *Nature*, **379**, 466–469.
Wilsch-Brauninger,M., Schwarz,H. and Nusslein-Volhard,C. (1997) A sponge-like structure involved in the association and transport of maternal products during *Drosophila* oogenesis. *J. Cell Biol.*, **139**, 817–829.
Wolthuis,R.M., Bauer,B., van't Veer,L.J., de Vries-Smits,A.M., Cool,R.H., Spaargaren,M., Wittinghofer,A., Burgering,B.M. and Bos,J.L. (1996) RalGDS-like factor (Rlf) is a novel Ras and Rap 1A-associating protein. *Oncogene*, **13**, 353–362.
Young,A., Dictenberg,J.B., Purohit,A., Tuft,R. and Doxsey,S.J. (2000) Cytoplasmic dynein-mediated assembly of pericentrin and γ tubulin onto centrosomes. *Mol. Biol. Cell*, **11**, 2047–2056.

Received January 4, 2001; revised May 31, 2001; accepted June 11, 2001

Chapter 8

THE MICROTUBULE PLUS END BINDING PROTEIN CLIP-115 INTERACTS WITH BOTH MAMMALIAN HOMOLOGUES OF *DROSOPHILA* BICAUDAL-D

Casper C. Hoogenraad[1,2*], Anna Akhmanova[1*], Bjorn R. Dortland[1], Chris I. De Zeeuw[2], Frank Grosveld[1] and Niels Galjart[1]

MGC Departments of [1]Cell Biology and Genetics, [2]Anatomy, Erasmus Univerisity, P.O. Box 1738, 3000 DR Rotterdam, The Netherlands. *These authors contributed equally to the results described in this paper.

Abstract

Cytoplasmic linker proteins (CLIPs) have been proposed to link organelles to distal ends of microtubules, in order to facilitate translocation by motor proteins. However, the mechanism of CLIP-mediated organelle transport has not yet been resolved. Here we demonstrate that CLIP-115 interacts with both mammalian homologues of the *Drosophila* Bicaudal-D protein, BICD1 and BICD2 in a yeast two hybrid assay. The direct nature of the interaction is further supported by GST-pull down experiments, co-immunoprecipitations from transfected COS-1 cells and brain extracts. The CLIP-115 homologue, CLIP-170, is not able to bind to BICD proteins. Northern blot analyses reveals that BICD2 displays a broad tissue distribution while BICD1 is found highly expressed in the brain. Since BICD proteins have been shown to associate with cytoplasmic vesicles and the trans-Golgi network, the results described here suggest that BICD may act as a membrane adapter for CLIP-115 in neuronal transport.

Introduction

The Golgi apparatus is a polarized structure of cisternal stacks, bounded on each side by extensive tubulo-vesicular networks and vacuoles of variable size. In many interphase cells, the Golgi occupies a juxta-nuclear position and is organized around the microtubule organizing center (MTOC). The Golgi complex serves as a major way station for the specific sorting of proteins and lipids in the secretory pathways. Selective vesicular transport becomes particularly evident at the *trans*-Golgi network (TGN), where, for example, lysosomal enzymes are packaged into clathrin-coated vesicles, whereas proteins destined for the plasma membrane are not.

Both the maintenance of Golgi structure and vesicular trafficking are controlled by the microtubule network and two motor proteins families: the dyneins and the kinesins [1,2]. The dyneins drive movement to the microtubule minus ends, while most members of the kinesin superfamily (KIFs) move organelles towards the plus ends, which are the growing, dynamic ends of the microtubules. Accessory proteins are required to regulate and specify organelle-microtubule interactions. For example, cargo binding and activation of cytoplasmic dynein requires a multisubunit complex called dynactin [3]. Cytoplasmic linker proteins (CLIPs) are another class of accessory proteins, which have been proposed to mediate the transient interaction between specific membranous organelles and microtubules and facilitate subsequent translocation by motor proteins [4]. Until now two mammalian CLIPs have been identified, CLIP-170 [5] and CLIP-115 [6]. Both proteins are homodimeric molecules in which a basic N-terminal domain is connected to a C-terminal tail through a long coiled-coil region. The N-terminal domain of the CLIPs is characterized by two microtubule binding motifs, which are also found as a single domain in other proteins [5]. Both CLIP-170 [7] and CLIP-115 [8] localize preferentially to the distal, growing ends of microtubules in transfected fibroblasts, suggesting that these proteins are required for the regulation of microtubule growth or for organelle binding to dynamic

microtubules. Recently, indirect evidence has been presented, that suggests that CLIP-170 may interact with the dynactin complex [9-11], perhaps acting as capture device to establish initial contact between a particle and microtubules. This raises the possibility that CLIPs capture or transfer cargo to motor proteins at the microtubule distal end. However, while CLIP-170 is ubiquitously expressed [12], CLIP-115 is detected almost exclusively in the brain [6], indicating that although the CLIPs have a similar structure and overlapping activities, each protein has a distinct intracellular role.

In search of proteins that interact directly with CLIP-115, we performed a yeast two-hybrid screen, using CLIP-115 as a bait and isolated CLASP (chapter 5) [13] and the mammalian homologue of the *Drosophila* Bicaudal-D (Bic-D) protein, BICD2. *Drosophila* Bic-D is a cytoplasmic coiled-coil protein, which is most intensively studied for its role in oogenesis. BicD is required for specification of the oocyte cell fate as well as establishment and maintenance of a polarized microtubule network during oogenesis. Genetic analysis in *Drosophila* suggests that Bic-D participates in the same transport pathway as cytoplasmic dynein and dynactin. Recently, we have shown that mammalian BICD2 interacts with the dynamitin subunit of the dynactin complex and we propose a conserved function for BICD in dynein-mediated transport [14]. Furthermore, immunofluorescence and electron microscopy studies revealed that BICD2 is localized to the trans-Golgi network and membranous vesicle within the cytoplasm [14]. In mammals two Bicaudal-D homologues are present, i.e. BICD1 and BICD2. In this report we show that both BICD proteins interact, in vitro and in vivo, with CLIP-115 and not with CLIP-170. These results suggest that BICD may acts as a membrane adapter for CLIP-115 in neuronal vesicular transport.

Results

Mammalian BICD2 is isolated in a yeast two-hybrid screen with CLIP-115

In order to isolate proteins that interact with CLIP-115, we performed a yeast two-hybrid screen, using the GAL4 DNA binding domain, linked to CLIP-115$^{287\text{-}591}$, as a bait (Fig. 2) (chapter 5) [13]. In this construct, the microtubule binding motifs of CLIP-115 are not included, yet the first coiled-coil stretches are present. Screening of a mouse E14.5 day cDNA library with this bait yielded his+, lacZ+ clones. One of the clones encodes 114 amino acids of the C-terminus of a protein, homologous to the *Drosophila* Bicaudal-D protein [15]. Two human Bicaudal-D homologues, encoded by different genes, have been deposited in the databases, i.e. *BICD1* [16] and KIAA0699. The mouse yeast two-hybrid clone is more similar to KIAA0699 and hence we have named this cDNA *BICD2*, to distinguish it from *BICD1*. Since *Drosophila* BicD protein is suggested to play a role in the microtubule dependent transport mechanism in the oocyte [17] and CLIP-115 is a microtubule binding protein, the interaction between CLIP-115 and both mammalian BICD proteins was further investigated. In order to study the BICD-CLIP-115 interaction in more detail, we first cloned cDNAs containing full length BICD1 and BICD2.

Characterization of human BICD1 and rat BICD2 isoforms

We isolated *BICD2* cDNAs from a rat hippocampus library, using a *BICD2*-specific probe, to obtain specific information about the *BICD2* expression pattern, the configuration of its mRNA and the primary structure of the protein. Two types of cDNAs were isolated, representing splice variants of the *BICD2* gene (Fig. 1a). One of these clones (type I) contains an open reading frame of 2460 nt, encoding a protein of 820 amino acids, with a predicted molecular mass of 93.4 kDa. The ORF is preceded by an in-frame stop codon, suggesting the cDNA covers the complete coding region. The *BICD2* type I cDNA is 4.6 kb in length and is virtually identical in its coding region to a mouse *BICD2* EST cDNA clone (ATCC 1364234; data not shown). We have also isolated several, incomplete *BICD2* cDNA clones (type II), which contain an insertion of 1736 nt at the position of the last amino acid of BICD2 type I. This insertion, which is also present in the human cDNA clone KIAA0699, results in a frame-shift and thereby in the extension of the C-terminus of BICD2 type II with 30 amino acids. Taken together, the data indicate that two evolutionary conserved BICD2 isoforms exist, which are identical until the last amino acid of BICD2 type I. Each isoform is predicted to have 5 coiled-coil domains (Fig. 1a). The minimal region of BICD2, that still interacts with CLIP-115 in the yeast two-hybrid assay (amino acids 705-810), is contained within the last coiled-coil domain of BICD2 (Fig. 2) and is present in both BICD2 isoforms.

To analyze the expression profile of *BICD2*, northern blots with total RNA from various rat and human tissues were probed with a *BICD2*-specific probe (Fig. 1c). While a *BICD2* transcript of approximately 5 kb is present in all tissues examined, a longer mRNA of approximately 7 kb is predominantly found in brain and testis. In addition to the 5 and 7 kb mRNAs, a transcript of approximately 3.5 kb is detected in testis. Thus, *BICD2* is a widely expressed gene, which can be transcribed into at least 3 different messages.

Alignment of rat type I BICD2 with *Drosophila melanogaster* BicD (DmBicD), a putative *Caenorhabditis elegans* BICD (CeBicD; accession no. U70848) and human BICD1 (hBicD1), shows that most of the sequence conservation among the different proteins is within presumptive coiled-coil stretches (data not shown). The alignment further shows that the C-terminal region in BICD2, that is necessary for the interaction with CLIP-115 is highly conserved in BICD1. Therefore, the major splice form of BICD1 [16] was cloned from human brain RNA using RT-PCR (Fig. 1b). The composite BICD1 sequence has an ORF of 2505 bp that encodes a protein of 835 amino acids. BICD1 has been shown to consist of exist as several isoforms, all differing in their C-terminal region [16].

Northern blots analysis of total RNA from various mouse tissues using a *BICD1*-specific fragment as a probe showed a large transcript of >9 kb, which is predominately expressed in the brain (Fig. 1d). This is in agreement with published data [16]. In the adult brain BICD1 is detected in the hippocampus, piriform cortex and

cerebellum. Thus, while *BICD2* is ubiquitously expressed, *BICD1* is mainly present in the brain.

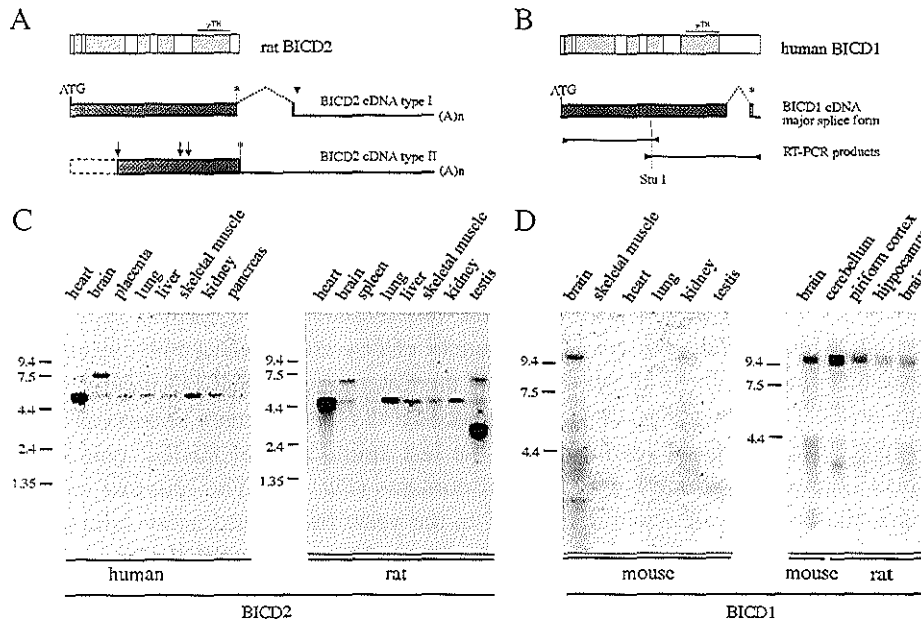

Figure 1. Characterization of human BICD1 and rat BICD2 isoforms
A) Cloning of rat BICD2 cDNAs. BICD2 is contains 5 coiled-coil domains (hatched boxes). The minimal domain of BICD2, that still interacts with CLIP-115 in the yeast two hybrid assay (y-TH) is shown. Screening of a rat hippocampus cDNA library for BICD2 clones yielded 2 types of cDNA, indicated underneath the BICD2 structure. Type I BICD2 encodes a full length BICD2 isoform (ATG and stopcodons (*) are indicated) and is virtually identical in the coding region (cross-hatched box) to the mouse clone ATCC 1364234 (the 3'UTR of the mouse clone is very short; its 3'end is marked by an arrowhead). Of type II BICD2 cDNA 3 clones were isolated, the longest is shown, the starts are indicated by vertical arrows. Each cDNA contains an insertion of approximately 1.7 kb, located directly upstream of the stopcodon in type I BICD2 cDNA. **B**) Cloning of major splice form of human BICD1 cDNA. Indicated is the proposed domain structure for BICD1, which has 5 coiled-coil domains (hatched boxes). The minimal domain of BICD1, that still interacts with CLIP-115 in the yeast two hybrid assay (y-TH) is shown. BICD1 cDNA was cloned from human brain mRNA using a RT-PCR strategy. PCR products were ligated using the unique Stu I restriction site, to obtain the full length BICD1 cDNA. **C**) Northern blot analysis of BICD2 expression in human and rat tissues. Size markers (in kb) are indicated. **D**) Northern blot analysis of BICD1 expression in mouse tissue and different brain areas from rat. Size markers (in kb) are indicated.

BICD1 and BICD2 interact with CLIP-115 but not with CLIP-170

We further investigated the interaction between BICD2 and CLIP-115 in a the yeast two hybrid assay. Four criteria indicate that the yeast two-hybrid interaction between CLIP-115$^{287\text{-}591}$ (bait) and BICD2$^{706\text{-}810}$ (fish) is specific. First, when fish and bait domains are swapped, the interaction still occurs (data not shown). Second, BICD2$^{706\text{-}810}$ does not interact with other part of the CLIP-115 coiled-coil region or a tropomyosin control bait, which contains a long coiled coil structure (Fig 2 and data not shown); third, the CLIP-115$^{287\text{-}591}$ does not interact with other BICD2 regions or

with the tropomyosin control bait (Fig 2 and data not shown); fourth, the region of CLIP-170 (amino acids 277-588), that is very similar to the positive CLIP-115 bait, does not associate with BICD2 (Fig. 2). To localize the binding site for BICD2 on CLIP-115, CLIP-115$^{287\text{-}591}$ was divided in three overlapping clones (Fig. 2), which were each tested for their ability to interact with BICD2 in the yeast two-hybrid system. The results of these experiments show that binding of CLIP-115 to BICD2 is dependent on the presence of residues 353-591 (Fig. 2), i.e. to the initial coiled-coil segments of CLIP-115.

BICD1 and BICD2 are highly conserved, especially the C-terminal regions. Since this region of BICD2 is the CLIP-115 interacting domain, we tested whether CLIP-115 is also able to interact with this region of BICD1. These experiments show that, BICD1 interacts with CLIP-115 in a yeast two hybrid assay (Fig 2). No interactions of BICD1$^{707\text{-}820}$ with other parts of CLIP-115 or the homologous region of CLIP-170 were detected. Together these data indicate that both BICD1 and BICD2 interact with CLIP-115 and not with CLIP-170.

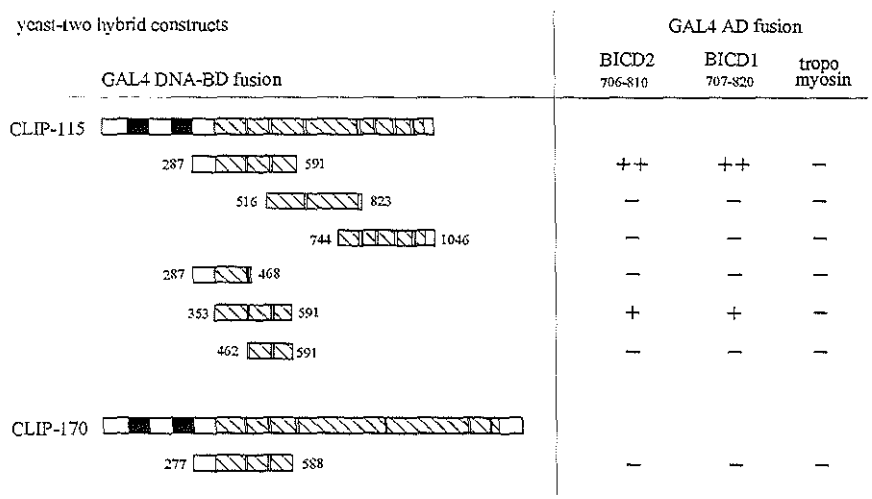

Figure 2. Yeast two hybrid interaction of BICD1 and BICD2 with CLIP-115
Interaction between CLIP-115 and BICD1 and BICD2. The domain structure of CLIP-115 and CLIP-170, including the two microtubule binding motifs (black bars) and coiled coil regions (hatched bars; the regions are interrupted by small stretches of coil-breaking residues) are shown. Below these are the fragments of CLIP-115 and CLIP-170, that are fused to DNA-binding domain (DNA-BD) used in the yeast two-hybrid experiments. Fragment 287-591 of CLIP-115 was used to screen an E14.5 day mouse cDNA library. From this screen the BICD2 cDNA was isolated, that encodes amino acids 706-820 from murine BICD2. This fragment was truncated (residue 706-810) and tested in direct yeast two hybrid assays with the other CLIP-115 and -170 encoding domains. Next, the homologous region of BICD1 (707-820) and tropomyosin were fused to activation domain (AD) and used in the same experiment. Results of β-galactosidase activity, measured in yeast lysate, are expressed as (++), which indicates high activation (50-100 units); (+), which indicates moderate activity (5-50 units); and (–), which indicates low or no activity (0-5 units).

BICD interacts with CLIP-115 in vitro and in vivo

The direct nature of the interactions between CLIP-115 and BICD2 was confirmed by in vitro binding assays. Equal amounts of various glutathione S-transferase (GST) fusion proteins, purified on glutathione beads, were added to in vitro transcribed and translated CLIP-115. After washing of the beads, radioactive proteins were detected using SDS-PAGE and autoradiography. In Fig. 3a-b, a schematic representation of the fusion proteins is shown, as well as their size and purity. Radioactively labeled CLIP-115 is indicated. The results show that CLIP-115 binds to

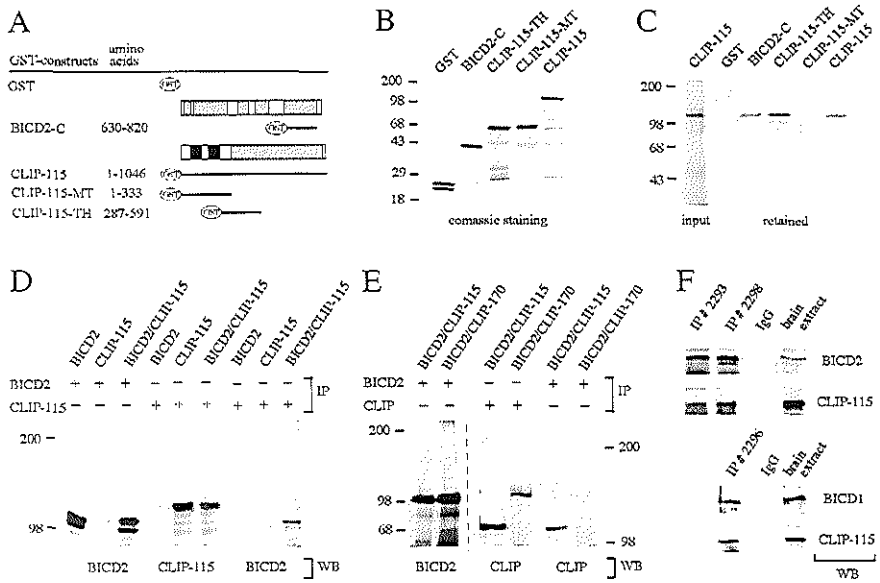

Figure 3. Binding and coprecipitation of BICD and CLIP-115

A) Structure of GST fusion proteins. The portions of the CLIP-115 and BICD2 proteins, that were cloned in frame with GST, are indicated. **B**) Analysis of the purified fusion proteins by SDS-polyacrylamide gel. The coomassie stained gel shows all purified proteins have the expected size. Molecular weight markers are indicated. **C**) In vitro binding of CLIP-115 to bacterial fusion proteins. ^{35}S-labeled CLIP-115 (marked "input") was incubated with the different GST fusion proteins shown. Purified radioactive proteins were analyzed by X-ray film exposure of dried SDS-gels (marked "retained"). Molecular weight markers are indicated. **D**) Co-immunoprecipitation of BICD2 with CLIP-115. COS-1 cells were transfected with BICD2, CLIP-115 or a combination of these proteins. Immunoprecipitated (IP) were performed using an anti-BICD2 antibody (#2298), or anti-CLIP-115 antibody (#2238). Western blots (WB) of the precipitated material were incubated with anti-BICD2 antibodies #2298), or with anti-CLIP-115 antibodies (#2238). Molecular weight markers are indicated. **E**) Co-immunoprecipitation of CLIP-115 with BICD2. COS-1 cells were transfected with BICD2 and CLIP-115, or with BICD2 and CLIP-170. Precipitation and detection of BICD2 was as in D). Precipitation and detection of CLIP-115 and CLIP-170 was done using an antibody, that recognizes both proteins (CLIP). While BICD2 was detected on an 8 % gel, the CLIPs were detected on 6 % gels, since they are larger proteins. A stippled line distinguishes the different gels. **F**) Co-immunoprecipitations from mouse brain extracts. All three BICD antibodies (#2293, #2298 and #2296) were able to coprecipitate CLIP-115. Molecular weight markers are indicated.

GST-BICD2 but not to GST (Fig 3c). These data support the conclusion that CLIP-115 and BICD2 interact directly. Our results also indicate that CLIP-115 binds to GST-CLIP-115$^{287-591}$ and GST-CLIP-115$^{1-1046}$ (Fig. 3c), corroborating our previous experiments that CLIP-115 dimerize via its coiled-coil region chapter 4 [8].

The association of BICD2 with CLIP-115 was further examined in co-immunoprecipitation studies from transfected COS-1 cells. One set of transfections was done with full length BICD2 and/or CLIP-115 (see Fig. 3d). The second set of transfections was with full length BICD2 and CLIP-115 or, as a negative control, BICD2 and CLIP-170 (Fig. 3e). Immunoprecipitations were carried out with an antiserum against BICD2 (#2293), CLIP-115 (#2338,) or an antiserum that recognizes both CLIPs (#2221) [8]. Western blots of the immunoprecipitated proteins were incubated with BICD2, CLIP-115 or CLIP-115/170 (CLIP) antibodies. As shown in Figure 3d, BICD2 coprecipitates with CLIP-115. The reciprocal immunnoprecipitation shows that anti-BICD2 antiserum was able to coprecipitate CLIP-115 (Fig. 3e), as shown by the western blot detection with the anti-CLIP antiserum. The anti-BICD2 antibodies do not, however, coprecipitate CLIP-170 (Fig. 3e), despite the fact that these proteins are expressed at the same level as CLIP-115 (Fig. 3e). Taken together, these results support a specific and direct interaction between BICD2 and CLIP-115.

CLIP-115 binds directly to BICD1 and BICD2 in vitro. To obtain in vivo evidence for these interactions, we performed coimmunoprecipitation experiments from mouse brain extracts, using anti-BICD1 antibody (#2296) and two anti-BICD2 antibodies (#2293, #2298). In addition to BICD itself, all three BICD antisera were able to coprecipitate CLIP-115 (Fig 3f). Non of these proteins were immunoprecipitated by non-specific control rabbit antiserum (Fig 3f). These results indicate that both BICD1 and BICD2 can bind to CLIP-115 in vivo.

Discussion

In this report we demonstrate that the microtubule binding protein, CLIP-115, which is predominantely present in the brain, interacts with BICD1 and BICD2, two mammalian homologues of the *Drosophila* Bicaudal-D gene product. Four lines of evidence support the direct nature of this interaction: 1) the yeast two-hybrid assay, 2) the GST-pull down experiments 3) the co-immunoprecipitations from transfected COS-1 cells, 4) co-immunoprecipitations from brain extracts. Further evidence, such as colocalization of CLIP-115, BICD1 and BICD2 in cultured hippocampal neurons and brain sections is necessary to prove the physiological relevance for this interaction. The CLIP-115 interaction with both BICD proteins appears highly specific, since the closest relative of CLIP-115, CLIP-170, does not interact with BICD although CLIP-115 and –170 are very similar in the region that was shown to be essential for the interaction of CLIP-115 with BICD interaction.

In *Drosophila*, the only well characterized partner for BicD is the *egalitarian* gene product [18]. Since, egalitarian (egl) has no apparent mammalian counterpart, it indicates that the function of the egl-Bic-D protein complex is not conserved. Genetic

studies in *Drosophila* suggest that BicD is involved in the cytoplasmic dynein pathway, since the *BicD* displays a genetic interaction with dynactin and with the *Drosophila* homologue of the *Lissencephaly* gene, an important component of the dynein-based nuclear migration mechanism in fungi [19]. Recently, we showed that the C-terminal coiled coil segment 3 of mammalian BICD2 directly interacts with the dynactin complex via dynamitin and that the N-terminal segment 1 of BICD2 possibly binds to one of the subunits of cytoplasmic dynein [14]. Since CLIP-115 has been preferentially localized to the growing ends of microtubules and dynein transports cargo towards microtubule minus ends, CLIP-115 is likely to capture BICD containing vesicles at the plus ends and subsequently hand over the cargo to cytoplasmic dynein. This model for 'cooperation' between CLIPs and a motor protein resembles the one described by Rickard and Kreis (1996) [4]. Recently, it was shown that CLIP-170 and the dynactin complex colocalize at the microtubule distal ends and that overexpression of CLIP-170 results in relocalization of dynactin [9-11]. These data suggest that CLIP-170 associates with this complex. Here we show that CLIP-170 is not able to bind to BICD, so the suggested interaction between CLIP-170 and dynactin does not occur via BICD.

The immunoelectron microscopy data have shown that multiple BICD2 molecules cluster on a single membranous vesicle (chapter 7) [14]. These data suggest that CLIP-115 and dynactin could bind to the same vesicle via the BICD2 multimeric coat complex at the surface. One possibility is that CLIP-115 and dynactin act simultaneously, i.e. CLIP-115 anchors BICD2-positive membranes to microtubule plus ends, while dynactin interacts with other BICD2 molecules on the same membrane and subsequently activates cytoplasmic dynein. Dynein may take off to power minus end movement, thereby generating tubulo-vesicular extensions along microtubules. Alternatively, since both dynactin and CLIP-115 bind to the C-terminal coiled-coil of BICD, CLIP-115 and dynactin may compete for the same BICD molecule. In this way, CLIP-115 may act as a simple equivalent of the dynactin complex. CLIP-115, by itself, could recruit BICD to microtubule plus ends. Subsequently, BICD, free or bound to a vesicles, may stimulate the interaction of cytoplasmic dynein and regulate motility. This suggests that vesicles can be loaded to microtubule plus ends, via a mechanism independent of CLIP-170/dynactin.

Since CLIP-115 is only found in mammals, and BICD proteins are, like dynactin and cytoplasmic dynein, highly conserved from *C. elegans* to humans and present in multiple tissues, an intriguing question to address is why mammalian neurons have evolved an additional pathway for minus-end directed transport that involves CLIP-115. Immunocytochemistry studies have revealed that CLIP-115 is mainly detected in dendrites of neurons (chapter 3 and 6) [6]. One possibility is that cytoplasmic dynein transport of BICD-positive membranes is more complex in dendrites, since the microtubule organization is non-uniform [20]. In this view, BICD containing vesicles that are transported along one microtubule can be handed over to CLIP-115, located on the plus end of a neighboring microtubule.

Materials and methods

Yeast two-hybrid screen

A mouse E14.5 day embryonic cDNA library was screened using the yeast two-hybrid approach [21], with a fragment of rat CLIP-115 cDNA (amino acids 287-591, see Fig. 2), fused to the GAL4 DNA-binding domain (DNA-BD) into the pPC97 yeast two-hybrid vector [22]. Other fragments of CLIP-115 and CLIP-170 were cloned into the same vector. BICD2 interaction with CLIP-115 was verified by exchanging the inserts of bait and fish vectors. The positive BICD2-clone (amino acids 706-820 of BICD2) was trimmed at its C-terminus by 10 amino acids, so that only the conserved part of the C-terminus of BICD was contained within the construct. This small protein was shown to interact with CLIP-115 in the yeast two-hybrid approach. The C-terminal region of human BICD1 (residue 707-820) and the tropomyosin control was fused to the GAL4 activation domain (AD) in the pPC86 vector.

cDNA and RNA analysis

A rat hippocampal library was plated and screened with BICD2 specific probes as described previously [6]. Clones were sequenced on both strands, except for the type II BICD2 cDNAs, which were sequenced on one strand in the parts that were identical to the type I clones. The BICD1 cDNA was obtained by RT-PCR. EMBL database accession numbers are; rat BICD2 type I (AJ250312); rat BICD2 type II (AJ250313). Human and rat multiple tissue northern blots (Clontech, CA) and home-made northern blots of multiple mouse tissues and different rat brain regions were hybridized according to standard procedures [23].

GST fusion constructs and antisera

Glutathione S-transferase (GST) fusion proteins were made in BL21 *E. coli* cells as described in [8], using plasmids pGEX-2T and pGEX-3X (Pharmacia). For in vitro binding studies the following proteins were purified: GST; GST-BICD2 (amino acids 706-812), GST-CLIP-115-TH (amino acids 287-591), GST-CLIP-115-MT (amino acids 1-333), GST-CLIP-115 (amino acids 1-1046), GST-CLIP-115 (amino acids 755-899/1026-1046). Antiserum against BICD2 (#2293), CLIP-115 (#2238) and antiserum #2221, which recognizes the N-termini of both CLIP-115 and CLIP-170, are described elsewhere [8,14]

Protein analysis

CLIP-115 was transcribed and translated using the TnT coupled transcription-translation system (Promega) and ^{35}S-methionine (Trans35S label, ICN, >1000 Ci/mmol). Aliquots of radiolabelled proteins were incubated with different GST fusion proteins in NETT buffer (100 mM NaCl, 50 mM Tris (pH 7.5), 5 mM EDTA, 0.5 % Triton X-100), for 2 hr at room temperature. Afterwards, samples were washed 5 times in NETT buffer. Proteins were eluted by boiling in sample buffer and analyzed by SDS-PAGE. Dried gels were exposed to film [13,14].

In the co-immunoprecipitation experiments, extracts of mouse brain or COS-1 cells transfected by the DEAE dextran method [8] were prepared in buffer containing 30 mM HEPES (pH 7.4), 100 mM KCl, 1 % NP40, supplemented with protease inhibitors (Boehringer) and incubated at 4^{0}C for 30 min, to depolymerize microtubules. All subsequent steps were also carried out at 4^{0}C. Cell lysates were centrifuged at 13,000 rpm for 10 min, and the supernatant was precleared with protein A beads for 30 min, after which beads were removed by low speed centrifugation. Precleared supernatants were incubated with the different antibodies for 2 hr, in the presence of protein A beads. Immunoprecipitated material was collected on the beads, washed extensively and purified proteins were eluted in sample buffer. Precipitated proteins were analyzed on western blot as described before [8].

References

1. Hirokawa, N. (1998) Kinesin and dynein superfamily proteins and the mechanism of organelle transport. *Science* **279**(5350): 519-26.
2. Vallee, R. B., and Sheetz, M. P. (1996) Targeting of motor proteins. *Science* **271**(5255): 1539-44.
3. Allan, V. J., and Schroer, T. A. (1999) Membrane motors. *Curr Opin Cell Biol* **11**(4): 476-82.
4. Rickard, J. E., and Kreis, T. E. (1996) CLIPs for organelle-microtubule interactions. *Trends Cell Biol* **6**: 178-182
5. Pierre, P., Scheel, J., Rickard, J. E., and Kreis, T. E. (1992) CLIP-170 links endocytic vesicles to microtubules. *Cell* **70**(6): 887-900.
6. De Zeeuw, C. I., Hoogenraad, C. C., Goedknegt, E., Hertzberg, E., Neubauer, A., Grosveld, F., and Galjart, N. (1997) CLIP-115, a novel brain-specific cytoplasmic linker protein, mediates the localization of dendritic lamellar bodies. *Neuron* **19**(6): 1187-99.

7. Perez, F., Diamantopoulos, G. S., Stalder, R., and Kreis, T. E. (1999) CLIP-170 highlights growing microtubule ends in vivo. *Cell* **96**(4): 517-27.
8. Hoogenraad, C. C., Akhmanova, A., Grosveld, F., De Zeeuw, C. I., and Galjart, N. (2000) Functional analysis of CLIP-115 and its binding to microtubules. *J Cell Sci* **113**(Pt 12): 2285-97.
9. Dujardin, D., Wacker, U. I., Moreau, A., Schroer, T. A., Rickard, J. E., and De Mey, J. R. (1998) Evidence for a role of CLIP-170 in the establishment of metaphase chromosome alignment. *J Cell Biol* **141**(4): 849-62.
10. Valetti, C., Wetzel, D. M., Schrader, M., Hasbani, M. J., Gill, S. R., Kreis, T. E., and Schroer, T. A. (1999) Role of dynactin in endocytic traffic: effects of dynamitin overexpression and colocalization with CLIP-170. *Mol Biol Cell* **10**(12): 4107-20.
11. Vaughan, K. T., Tynan, S. H., Faulkner, N. E., Echeverri, C. J., and Vallee, R. B. (1999) Colocalization of cytoplasmic dynein with dynactin and CLIP-170 at microtubule distal ends. *J Cell Sci* **112**(Pt 10): 1437-47.
12. Griparic, L., Volosky, J. M., and Keller, T. C., 3rd. (1998) Cloning and expression of chicken CLIP-170 and restin isoforms. *Gene* **206**(2): 195-208.
13. Akhmanova, A., Hoogenraad, C. C., Drabek, K., Stepanova, T., Dortland, B., Verkerk, T., Vermeulen, W., Burgering, B. M., De Zeeuw, C. I., Grosveld, F., and Galjart, N. (2001) Clasps are CLIP-115 and -170 associating proteins involved in the regional regulation of microtubule dynamics in motile fibroblasts. *Cell* **104**(6): 923-35.
14. Hoogenraad, C. C., Akhmanova, A., Howell, S. A., Dortland, B. R., De Zeeuw, C. I., Willemsen, R., Visser, P., Grosveld, F., and Galjart, N. (2001) Mammalian Golgi-associated Bicaudal-D2 functions in the dynein/dynactin pathway by interacting with these complexes. *Embo J* (In Press):
15. Suter, B., Romberg, L. M., and Steward, R. (1989) Bicaudal-D, a Drosophila gene involved in developmental asymmetry: localized transcript accumulation in ovaries and sequence similarity to myosin heavy chain tail domains. *Genes Dev* 3(12A): 1957-68
16. Baens, M., and Marynen, P. (1997) A human homologue (BICD1) of the Drosophila bicaudal-D gene. *Genomics* **45**(3): 601-6
17. Theurkauf, W. E., Alberts, B. M., Jan, Y. N., and Jongens, T. A. (1993) A central role for microtubules in the differentiation of Drosophila oocytes. *Development* **118**(4): 1169-80
18. Mach, J. M., and Lehmann, R. (1997) An Egalitarian-BicaudalD complex is essential for oocyte specification and axis determination in Drosophila. *Genes Dev* **11**(4): 423-35
19. Swan, A., Nguyen, T., and Suter, B. (1999) Drosophila Lissencephaly-1 functions with Bic-D and dynein in oocyte determination and nuclear positioning. *Nat Cell Biol* **1**(7): 444-449
20. Baas, P. W., Deitch, J. S., Black, M. M., and Banker, G. A. (1988) Polarity orientation of microtubules in hippocampal neurons: uniformity in the axon and nonuniformity in the dendrite. *Proc Natl Acad Sci U S A* **85**(21): 8335-9.
21. Chevray, P. M., and Nathans, D. (1992) Protein interaction cloning in yeast: identification of mammalian proteins that react with the leucine zipper of Jun. *Proc Natl Acad Sci U S A* **89**(13): 5789-93
22. Wolthuis, R. M., Bauer, B., van't Veer, L. J., de Vries-Smits, A. M., Cool, R. H., Spaargaren, M., Wittinghofer, A., Burgering, B. M., and Bos, J. L. (1996) RalGDS-like factor (Rlf) is a novel Ras and Rap 1A-associating protein. *Oncogene* **13**(2): 353-62
23. Sambrook, J., Fritsch, E. F., and Maniatis, T. (1989) Molecular cloning: a laboratory manual, 2 Edition, Cold Spring Harbor Laboratory Press, New York

Chapter 9

THE MURINE CYLN2 GENE: GENOMIC ORGANIZATION, CHROMOSOME LOCALIZATION, AND COMPARISON TO THE HUMAN GENE THAT IS LOCATED WITHIN THE 7q11.23 WILLIAMS SYNDROME CRITICAL REGION

Casper C. Hoogenraad[1,2], Bert H.J. Eussen[3], An Langeveld[1], Rien van Haperen[1], Suzanne Winterberg[1,2], Cokkie H. Wouters[3], Frank Grosveld[1], Chris I. De Zeeuw[2], Niels Galjart[1].

MGC Departments of [1]Cell Biology and Genetics, [2]Anatomy, [3]Clinical Genetics, Erasmus Univerisity, P.O. Box 1738, 3000 DR Rotterdam, The Netherlands.

The Murine *CYLN2* Gene: Genomic Organization, Chromosome Localization, and Comparison to the Human Gene That Is Located within the 7q11.23 Williams Syndrome Critical Region

Casper C. Hoogenraad,*,† Bert H. J. Eussen,‡ An Langeveld,* Rien van Haperen,* Suzanne Winterberg,*,† Cokkie H. Wouters,‡ Frank Grosveld,* Chris I. De Zeeuw,†,[1] and Niels Galjart*,[1]

MGC Department of Cell Biology and Genetics, ‡MGC Department of Clinical Genetics, and †Department of Anatomy, Erasmus University, P.O. Box 1738, 3000 DR Rotterdam, The Netherlands

Received May 12, 1998; accepted August 7, 1998

Cytoplasmic linker proteins (CLIPs) have been proposed to mediate the interaction between specific membranous organelles and microtubules. We have recently characterized a novel member of this family, called CLIP-115. This protein is most abundantly expressed in the brain and was found to associate both with microtubules and with an organelle called the dendritic lamellar body. CLIP-115 is highly homologous to CLIP-170, or restin, which is a protein involved in the binding of endosomes to microtubules. Using the rat cDNA as a probe we have isolated overlapping cosmids containing the complete murine and part of the human *CYLN2* (cytoplasmic linker-2) genes, which encode CLIP-115. The murine gene spans 60 kb and consists of 17 exons, and its promoter is embedded in a CpG island. Murine *CYLN2* maps to the telomeric end of mouse chromosome 5. The human *CYLN2* gene is localized to a syntenic region on chromosome 7q11.23, which is commonly deleted in Williams syndrome. It spans at least 140 kb at the 3′ end of the deletion. Human *CYLN2* is very likely identical to the previously characterized, incomplete *WSCR4* and *WSCR3* transcription units.

INTRODUCTION

The transport and localization of membranous organelles are guided by microtubules. There is a large protein machinery that enables membranes to attach to, move along, and disassemble from the cytoskeleton (for reviews see Vallee and Sheetz, 1996; Lippincott-Schwartz, 1998). Among these components are the family of cytoplasmic linker proteins (CLIPs), which have been proposed to mediate the interaction of membranes and microtubules (Pierre *et al.*, 1992; Rickard and Kreis, 1996). Its prototype member is CLIP-170, a protein that is involved in the attachment of endosomes to microtubules (Pierre *et al.*, 1992). CLIP-170 is characterized by two N-terminally located microtubule binding domains, a long coiled-coil region, and a cysteine-rich tail. CLIP-170 is identical to restin, which was originally thought to be an intermediate filament-associated protein and which is highly expressed in the Reed–Sternberg cells of Hodgkin disease (Bilbe *et al.*, 1992). We have recently cloned a rat cDNA encoding CLIP-115 (cytoplasmic linker protein of 115 kDa), which is quite similar to CLIP-170 but which lacks the C-terminal cysteine-rich structure (De Zeeuw *et al.*, 1997). *CLIP-115* is most abundantly expressed in the brain, and it is exclusively present in neurons, with the exception of Bergmann glia cells of the cerebellum. Immunoelectron microscopy demonstrates that CLIP-115 decorates microtubules as well as a very specialized type of membrane structure called the dendritic lamellar body (DLB). The DLB is enriched in areas of the brain in which dendrodendritic gap junctions are prominent, and it is found in bulbous dendritic appendages from which dendritic spines arise that are linked by gap junctions (De Zeeuw *et al.*, 1995). Since Bergmann glia also contain extensive gap junction plaques, the hypothesis that CLIP-115 may be involved in the formation and/or turnover of gap junction channels has evolved (De Zeeuw *et al.*, 1997). This is in line with the idea that specific CLIPs exist for coupling specific membranes to microtubules (Rickard and Kreis, 1996).

The approved symbol for the gene encoding CLIP-115 is *CYLN2* (for cytoplasmic linker-2 gene, the gene encoding CLIP170/restin being *CYLN1*). *CYLN2* is very likely identical to the incomplete *WSCR4* transcription unit (Osborne *et al.*, 1996), since a database comparison shows that the partial protein product encoded by this gene is almost identical to CLIP-115.

Sequence data from this article have been deposited with the EMBL/GenBank Data Libraries under Accession Nos. AJ228863–AJ228880.

[1] To whom correspondence should be addressed. Telephone: (+31)-10-4087166 or (+31)-10-4087299. Fax: (+31)-10-4360225. E-mail: galjart@ch1.fgg.eur.nl or dezeeuw@anat.fgg.eur.nl.

WSCR4 has previously been localized on human chromosome 7q11.23, within the Williams Syndrome critical region (Osborne *et al.*, 1996). Williams(–Beuren) syndrome (WBS or WS; MIM No. 194050) is a developmental disorder including multiple system manifestations such as cardiovascular disease, connective tissue abnormalities, short stature, infantile hypercalcemia, a characteristic "elfin-like" facial appearance, and several behavioral and neurological deficits (Morris *et al.*, 1988; Jones, 1990). The behavioral profile of WS patients is unique in that it is characterized by mental retardation (average IQ of 50), impaired visuospatial cognitive abilities, and attention-deficit and hyperactivity disorder (ADHD), while the language abilities are relatively well preserved (Bellugi *et al.*, 1990). The neurological defects are most prominently reflected in sensory integration dysfunction and multiple developmental motor disabilities affecting balance, strength, coordination, and motor planning. Although these latter symptoms suggest a dysfunction of the cerebellum, quantitative MRI measurements of WS patients show a clear microcephaly with a relatively normal cerebellar volume (Bellugi *et al.*, 1990; Jernigan and Bellugi, 1990).

In virtually all WS patients a hemizygous deletion of more than 500 kb at chromosome band 7q11.23 can be detected (Osborne *et al.*, 1996, 1997). The deletion includes the *elastin* (*ELN*) and *LIM-kinase 1* (*LIMK1*) genes, which have been reported to be largely responsible for supravalvular aortic stenosis and specific visuospatial cognitive defects, respectively (Ewart *et al.*, 1993, 1994; Olson *et al.*, 1995; Frangiskakis *et al.*, 1996). In addition, the *GTF2I, FZD3, syntaxin 1A, RFC2,* and *WSCR1–4* transcription units have been reported to be located within the WS critical region (Osborne *et al.*, 1996, 1997; Peoples *et al.*, 1996; Wang *et al.*, 1997; Perez-Jurado *et al.*, 1998), and like *CYLN2*, some of these genes are specifically expressed in the brain. Therefore, it may well be possible that hemizygous deletion of these genes, including human *CYLN2*, is responsible for some of the neurological dysfunctions in Williams syndrome.

To design constructs for targeted inactivation of the murine *CYLN2* gene and to understand further the function of the *CYLN2* gene and its involvement in WS, we characterized the gene in mouse and human. Here we report on the complete genomic organization and chromosomal localization of the murine *CYLN2* gene. It spans 60 kb and is covered by four overlapping cosmids. The gene consists of 17 exons, and its presumptive promoter is located in a CpG island. We also show that the human *CYLN2* gene is much larger than its mouse homologue; it is identical to the *WSCR4* locus, and the *CYLN2* 5′ end presumably overlaps with the *WSCR3* transcription unit. FISH analysis with labeled cosmid DNA as the probe localizes murine *CYLN2* to chromosome 5, near the telomeric tip. This region is syntenic to human chromosome 7q11.23, where human *CYLN2* is localized.

MATERIALS AND METHODS

Isolation and characterization of cosmid clones. The mouse cosmid library, prepared from AB-1 embryonic stem cell DNA, has been previously described (Mazarakis *et al.*, 1996). The human cosmid library was made in an identical fashion, using normal human blood DNA. Rat *CLIP-115* cDNA (De Zeeuw *et al.*, 1997) probes were labeled to high specific activity (Feinberg and Vogelstein, 1983) and used to screen both libraries. To obtain the 5′ end of the mouse *CYLN2* gene, the murine cosmid library was rescreened with a 5′ end 166-bp rat probe, generated by PCR (Saiki *et al.*, 1988). The integrity of the cosmid clones was verified by comparison to mouse and human genomic DNA using conventional Southern blot analysis (Sambrook *et al.*, 1989). Mapping was done with overlapping cosmids 2.1, 2.6, 3.7, and 4.2 (mouse *CYLN2*) and 47, 63, and 67 (human *CYLN2*). The 12 human chromosome 7-specific cosmid clones from the LL07NC01'Y' library (Lawrence Livermore National Laboratories, library constructed by Jennifer S. McNinch), covering a large part of the Williams syndrome critical region, were ordered from the German RessourcenZentrum/PrimärDatenbank (number of the library, 130; prefix, LLNLc).

Murine *CYLN2* exon–intron boundaries were determined by sequencing with *CLIP-115*-specific primers. All coding exons were sequenced on both strands. From the alignment of the exons a putative mouse *CLIP-115* cDNA sequence was derived. Sequences were deposited at the EMBL database under Accession Nos. AJ228863 (for the composite mouse *CLIP-115* cDNA), AJ228864 (for the murine *CYLN2* promoter–exon 1–intron 1 sequence), and AJ228865–AJ228880 (for exons 2–17, including small adjacent intronic sequences). Murine genomic sequences were compared to rat *CLIP-115* and human *WSCR4* (Accession Nos. AF041055–AF041059) and KIAA0291 (Accession No. AB006629) nucleotide and amino acid sequences. Human cosmid sequences, upstream of or covering the *CYLN2* gene, were retrieved from http://darwin.ceh.uvic.ca/Martindale/Chromosome7.html (Osborne *et al.*, 1996).

Localization of the murine and human CYLN2 genes. FISH was performed on metaphase spreads of mouse cultured bone marrow cells or human lymphocytes (Mulder *et al.*, 1995), using biotin- or digoxygenin-labeled cosmids 4.2 and 2.6 as probes for the mouse *CYLN2* gene and cosmids 47, 63, and 67 as probes for the human *CYLN2* gene. DNA was labeled with biotin- or digoxigenin-11-UTP by nick-translation (Boehringer Mannheim). The *ELN* cosmids, including the 7q36 probe, were already digoxigenin labeled (Oncor). For detection of hybridization, slides were incubated with two alternating layers of avidin–FITC (Vector) or a single layer of anti-digoxigenin–rhodamine (Boehringer). The α satellite probe for the centromere of chromosome 7 (pa7t1; Waye *et al.*, 1987) was directly labeled with tetramethyl-rhodamine-6-dUTP (Boehringer Mannheim). Mouse chromosomes were counterstained with propidium iodide and DAPI, while human chromosomes were counterstained with DAPI.

Northern blot analysis. A human multiple-tissue Northern blot was purchased (Clontech) and hybridized with rat *CLIP-115* cDNA probes according to the protocol of the supplier.

RESULTS

Chromosomal Localization of the Single-Copy Murine and Human CYLN2 Genes

Previously we have shown that under stringent hybridization conditions 5-kb rat and mouse *CLIP-115* mRNAs can be detected using rat *CLIP-115* cDNA as a probe (De Zeeuw *et al.*, 1997). These data indicated that mouse and rat *CYLN2* genes are highly homologous. To analyze whether this also applies to human *CYLN2* and to investigate whether one or more homologous genes exist in these species we hybridized Southern blots containing different digests of total genomic rat, mouse, and

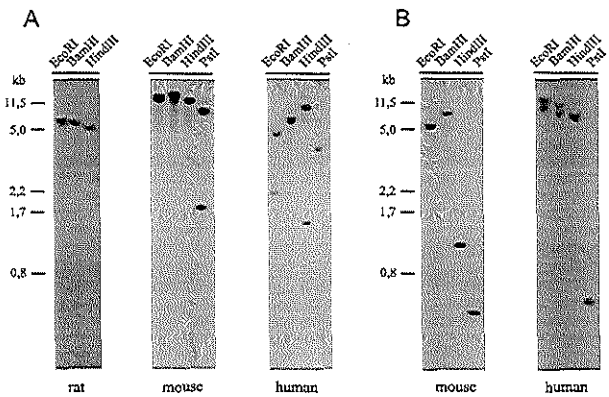

FIG. 1. Southern blot analysis of rat, mouse, and human *CYLN2* genes. Southern blots of digested rat, mouse, and human genomic DNA were hybridized with a 0.36-kb *Eco*RI–*Eag*I probe (**A**) or with a 0.48-kb *Pst*I probe (**B**) derived from the rat *CLIP-115* cDNA. Blots were exposed to PhosphorImager screens (Molecular Dynamics). Molecular size markers are indicated on the left.

human DNA with *CLIP-115*-specific probes. Under stringent hybridization and washing conditions, single fragments are detected in all three species with a 0.36-kb *Eco*RI–*Eag*I rat probe (Fig. 1A) that encodes the second microtubule binding domain and a serine-rich region. Unique fragments are also detected under stringent conditions in mouse and human DNA using a 0.48-kb *Pst*I fragment derived from the middle, unique part of the rat *CLIP-115* cDNA (Fig. 1B). However, while *Pst*I and *Hin*dIII digests give rise to single bands, *Eco*RI and *Bam*HI digests yield a doublet in human (Fig. 1B, right). This doublet appears after low- and high-stringency washing of the blot (data not shown). Subsequently, we tested 73 genomic DNA samples derived from different control subjects for the presence of these *Eco*RI and *Bam*HI doublets (data not shown). In 35 samples (48%) a doublet like that in Fig. 1B was visualized, while 14 samples (19%) contained the upper band and 24 samples (33%) the lower. These data indicate that a polymorphism (a deletion or insertion) that is picked up with the 0.48-kb *Pst*I probe is present in the human *CYLN2* gene. Together these results strongly suggest that a single functional *CYLN2* gene is present in rat, mouse, and human.

The 0.36-kb *Eco*RI–*Eag*I and 0.48-kb *Pst*I probes were next used to screen homemade mouse and human genomic cosmid libraries to isolate the murine and human genes encoding CLIP-115. Initially 29 mouse and 18 human cosmid clones were identified. To obtain the 5′ end of the murine *CYLN2* gene, the mouse cosmid library was rescreened with a 5′-end PCR probe, which yielded two positives, one of which (2.1) was further used. Thus, four mouse (2.1, 2.6, 3.7, and 4.2) and three human (47, 63, and 67) cosmids were selected for further analysis.

Murine cosmids 4.2 and 2.6 and human cosmids 47, 63, and 67 were labeled with biotin or digoxygenin and hybridized to denatured metaphase spreads of mouse cultured bone marrow cells or human lymphocytes. All cosmids gave a clear fluorescent signal on both chromatids at the telomeric end of chromosome 5 in the mouse (band 5G) and band 7q11.23 in human. Only human cosmid 67 gave an additional signal near the centromere of chromosome 10 (data not shown), which could be due to repetitive sequences present in the cosmid. Examples of these hybridizations are shown in Fig. 2 (A, mouse, cosmid 4.2; B and D, human, cosmid 47). Interestingly, the position of the *CYLN2* locus in mouse is syntenic to that in human.

Since *CYLN2* could be identical to *WSCR4* and the latter was reported to be located within the 7q11.23 Williams syndrome critical region, telomeric to the *ELN* gene (Osborne *et al.*, 1996), we verified the localization of the human *CYLN2* gene with 7q36- and *ELN*-specific cosmids. On normal chromosomes double signals for *CYLN2* (green) and *ELN* (red) are present on the same chromosome, close to each other (Fig. 2B), indicating that the *CYLN2* gene is close to the *ELN* locus and suggesting it is identical to the *WSCR4* gene. Since it has been shown that *ELN* is commonly deleted in WS, we investigated whether this holds true for *CYLN2*. Eight patients, who met the WS criteria (Preus, 1984), were tested for hemizygous deletion of *CYLN2* and *ELN* by FISH. In all eight patients examined, the *ELN* cosmids hybridized to only one chromosome 7 homologue in metaphase cells (Fig. 2C). The chromosome 7-specific cosmid at 7q36 hybridized with both chromosomes 7 in these patients. In the same patients, signals specific for *CYLN2* were also only present on one chromosome 7, consistent with a deletion of the locus on the other chromosome 7 homologue (Fig. 2D). As a control, a probe for the centromere of chromosome 7 hybridized to both chromosome 7 homologues in metaphase cells from affected individuals (Fig. 2D). These results demonstrate that the *CYLN2* gene is hemizygously deleted in WS.

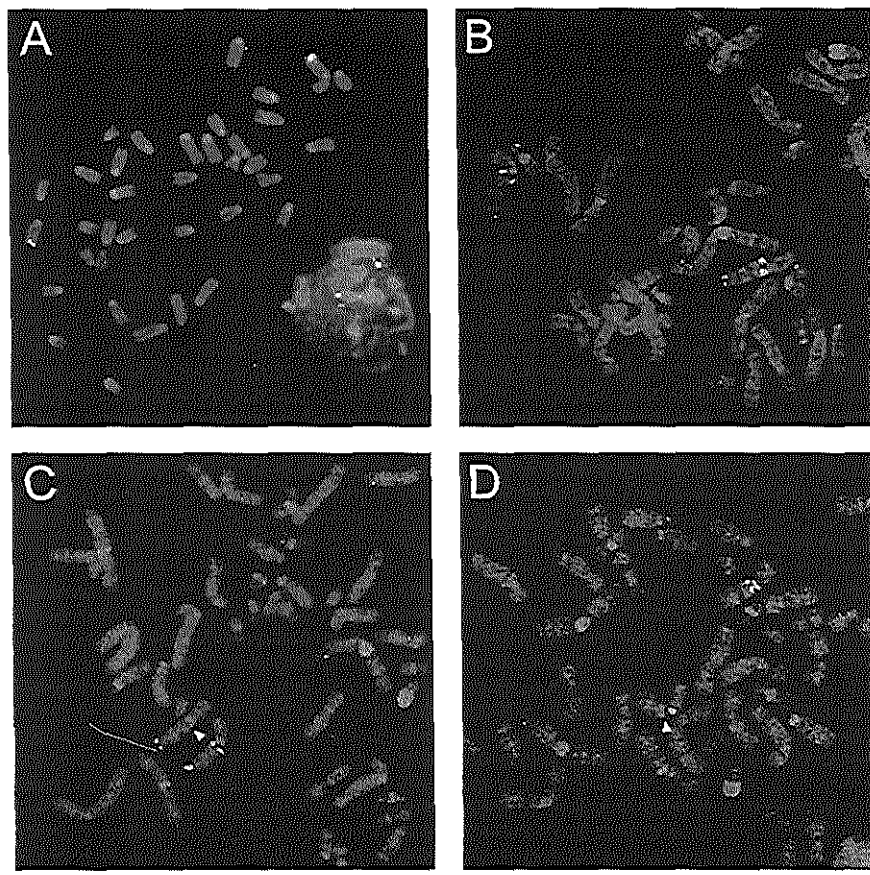

FIG. 2. Cytogenetic analysis of murine and human *CYLN2* genes. (A) Murine *CYLN2* cosmid 4.2 (green), hybridized to metaphase spreads from cultured mouse bone marrow cells. Chromosomes were counterstained with propidium iodide and DAPI. Signals are present near the telomeric tip of mouse chromosome 5 (band 5G). (B) Human *CYLN2* cosmid 47 (green), hybridized together with *ELN* and 7q36-specific cosmid signals (red). Two clear *CYLN2* signals (green) are detected on chromosome 7, adjacent to the *ELN* locus (red) on 7q11.23. (C) WS patients show hybridization signals for the *ELN* cosmid (red) on one chromosome 7 homologue but not on the other (arrowhead). Both chromosomes 7 do show specific signals for the chromosome 7q36-specific cosmid (red). (D) WS-affected individuals show hybridization signals for the *CYLN2* gene (green) on one chromosome 7 homologue, but not on the other (arrowhead). Both chromosomes 7 show signals for the chromosome 7-specific centromere probe (red).

Genomic Organization of the Murine CYLN2 Gene and Comparison to Its Human Homologue

Using conventional restriction enzyme mapping and Southern blot analysis with different *CLIP-115* probes, mouse cosmids 2.1, 2.6, 3.7, and 4.2 were aligned to one another (Fig. 3). Comparison of the rat cDNA to sequenced mouse genomic DNA revealed that the murine *CYLN2* gene consists of 17 exons (Fig. 3, see Table 1 for exact exon–intron boundaries). The sizes of the *CYLN2* introns range from 0.5 to 13 kb, the introns located between exons 1–2 and 2–3 both having a length of 13 kb (Fig. 3). All introns have splice donor and acceptor sites that conform to the general GT–AG consensus motif (Table 1). In addition all presumptive splice acceptor sites are preceded by a stretch of pyrimidines, suggesting that they can function as true acceptors. The sizes of the exons vary from 58 bp (exon 11) to 1398 bp (exon 17). The putative CLIP-115 translation initiation codon is located on exon 2, while the stop codon is on exon 17. Interestingly, the latter exon is the largest.

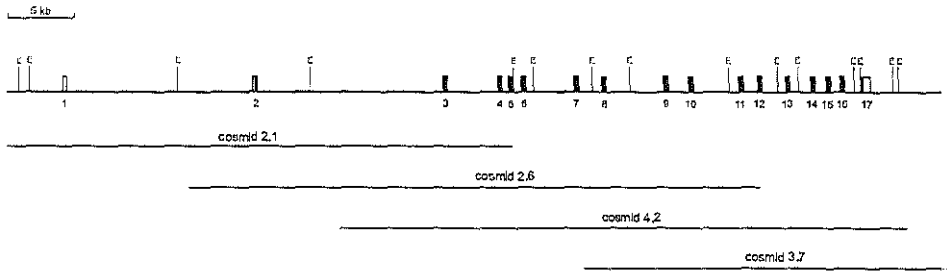

FIG. 3. Genomic structure of the murine *CYLN2* gene. Four overlapping cosmids, whose inserts are shown as lines beneath the murine *CYLN2* locus, were mapped using *Eco*RI (E) and a variety of other enzymes (not shown). Exons (not to scale) are indicated by boxes, their numbers correspond to the exon numbering in Table 1. Open bars, noncoding 5′ and 3′ ends; solid bars, coding sequences.

but it only contains the last 3 amino acids from the CLIP-115 coding sequence. Exon 17 does contain the complete 3′UTR, including a single consensus polyadenylation signal at the same position as one of the two polyadenylation signals in the rat *CLIP-115* cDNA (Table 1).

Murine exon 1 (216 nt) is very GC rich, and it is embedded in a CpG island, which is indicative of a promoter area. Comparison of mouse exon 1 to rat *CLIP-115* cDNA reveals a high degree of conservation in this part of the 5′UTRs of the two messages (85% identity; see also Fig. 4). Rat and mouse *CLIP-115* mRNAs are both ~5 kb; the rat cDNA that was cloned is 4.8 kb, and it was proposed to be full length (De Zeeuw *et al.*, 1997). Taken together, these data suggest that we have cloned the promoter of the *CYLN2* gene in

TABLE 1

Exon–Intron Organization of the Mouse *CYLN2* Gene and Comparison to Its Human Homologue

Exon	Exon size[a] (bp)	Species	3′ splice site[a,b]	5′ splice site[a,b]	Accession No.
1	216	M	CGCCTCGGGG	GA-GCTCCAAGgtaggcgccg	AJ228864
		H[c]	G---G-----	--A-GA-G---.....g..t.	
2	191	M	ctgcccgcagGTGACCGAGG	TCCAAAGAAGgtacgtaaag	AJ228865
		H[c]	.....----GT--A-	-----G-----.....ggca	
3	557	M	ttatccacagGGTCTCCCCT	CCGTGTGCTGgtaagttggg	AJ228866
		H[d]	..c..tg...-C--C--A--	---C------..g...gc..	
4	125	M	gtgccaacagGTTGGTGGGA	CAGGAACCAGgtacaagagg	AJ228867
		H[d]	.....g.....-----C----	-G--C------...tggtg..	
5	214	M	cgctcccagGTACTTCCAG	CAGTGGCCTGgtaaggtcag	AJ228868
		H[d]	gct...a..----------	----------..ga..gtg.	
6	198	M	ctctctgcagCTCACAGAGA	GCATGAGCAGgtgggtggct	AJ228869
		H[d]	..tc.....-----G----	----------...a.....a	
7	104	M	tctgggtcagTATGTTGCAG	AGGAGAGGAGgtacgtggcc	AJ228870
		H[d]	ggg..cc...----------	---------.....ctg	
8	61	M	ttcctgtagGAAGGTGCAG	AGACTTGCAGgtaacggtga	AJ228871
		H[d]	.c.....c.----------	----C------....a..c.	
9	105	M	ggtggagcagACCCAGACCC	GGATAACAGGgtaaataaac	AJ228872
10	933	M	ctcctgctagCTGACCACAG	GCACAGCCATgtaggctgca	AJ228873
11	58	M	gttctttcagGTGATCGAAT	ACTGTAGAGGgtgagtagcc	AJ228874
12	84	M	tctctcctagGCCTGCAGCA	CAAGTAAGTGgtaagtctcc	AJ228875
13	157	M	gatccactagTTCTAGAAAA	GGAAAGAGAGgtgagcgccc	AJ228876
14	160	M	cccactccagGAGTCTGAAC	GACCGGGCTGgtatgtgcag	AJ228877
15	186	M	cacctttccagGACAAGGACA	CAGGACTCAGgtgagcacac	AJ228878
16	63	M	cccctcacagACCATCAGCA	CAAACAGGAGgtaagtgcgc	AJ228879
17	1398	M	ttctctctagGACAAACACT	AATAAAGCTTGTGATTGAGGT[e]	AJ228880

Note. M, mouse; H, human.

[a] Exon sizes were calculated by comparison to the rat *CLIP-115* cDNA sequence reported by de Zeeuw *et al.* (1997).

[b] Exon sequences are in uppercase letters and intron sequences are in lowercase letters. Residues in human exons that are identical to the nucleotide sequence in mouse *CYLN2* are indicated by a dash; identical residues in human introns are indicated by a dot.

[c] Data obtained by comparison to manually retrieved sequences from cosmid 237h1.

[d] Data obtained by comparison with *WSCR4* sequences from the database.

[e] The mouse *CLIP-115* polyadenylation signal is underlined.

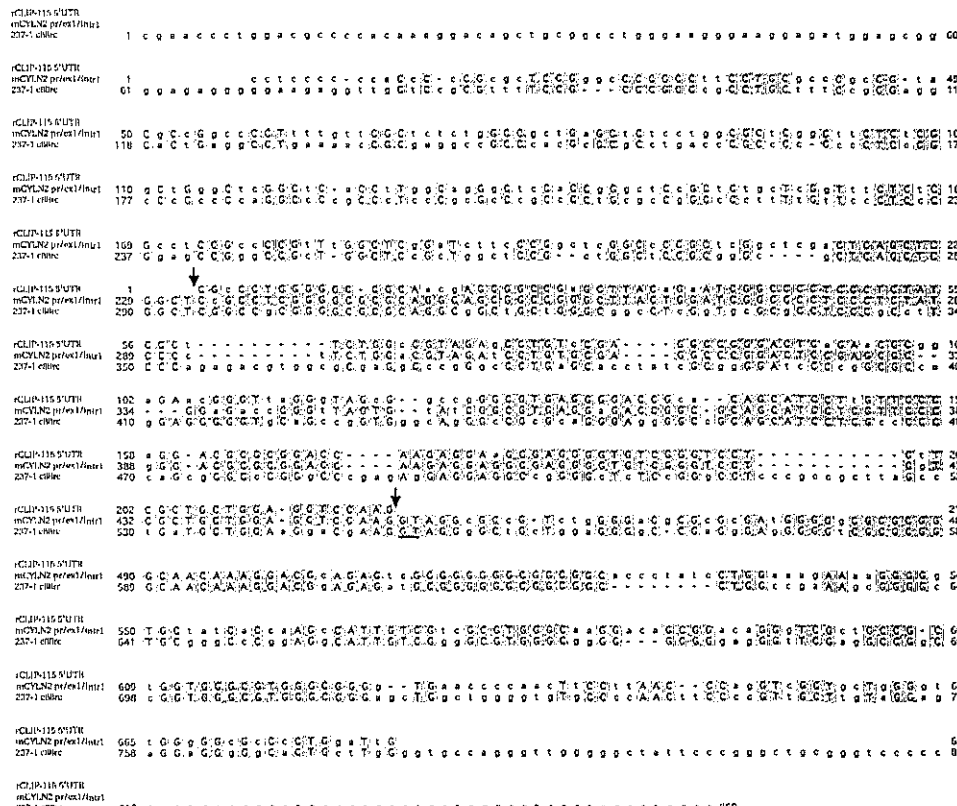

FIG. 4. *CYLN2* exon 1 sequence comparisons. Alignment of rat *CLIP-115* 5'UTR (bp 1–219), murine *CYLN2* 5' end (containing exon 1 and upstream and downstream sequences (681 nt)), and contig 88 from LLNL cosmid 237h1 (860 nt, reverse and complementary sequence (rc)). Nucleotide numbering is on the side. Mismatches are indicated in lowercase letters. The start and end of the rat *CLIP-115* cDNA are indicated by arrows. Note the high GC content in the presumptive *CYLN2* promoter regions. Similarity among the three sequences becomes highly significant 13 bp upstream of the rat *CLIP-115* cDNA start. Blocks of human and mouse sequences remain conserved downstream of the 5' splice donor site (GT residues are underlined) of intron 1.

the mouse. However, the exact transcription initiation site(s) of the murine *CYLN2* gene needs to be determined by S1 nuclease analysis and other methods.

We compared the *CYLN2* exon–intron map to the incomplete *WSCR4* transcription unit submitted to the public databases and found that exons 3–8 have been conserved between mouse and human (Table 1). These data confirm that *WSCR4* is part of the *CYLN2* gene. To determine where the human *CYLN2* 5' end might be located, the sequences of LLNL cosmids 135f3, 157f3, 237h1, and 63f7, which together cover a region largely upstream of the human *WSCR4* gene (Osborne *et al.*, 1996), were compared to rat *CLIP-115* cDNA and mouse *CYLN2* genomic 5'-end sequences. This revealed two areas of homology among the three sequences, one encompassing exon 2 (Table 1) and the most 5' end similarity covering exon 1 (Fig. 4). While the similarity between mouse and human genomic sequences upstream of the 5' end of the *CLIP-115* cDNA is due to a high GC content in both sequences, it becomes highly significant 13 nt 5' of the *CLIP-115* cDNA start (Fig. 4). Mouse and rat noncoding sequences are more similar than mouse and human 5'UTRs; however, those sequences surrounding the exon–intron boundary at the 3' end of exon 1 of murine *CYLN2* have been completely conserved in human. In addition, there are stretches of complete conservation in mouse and human, downstream of exon 1 (Fig. 4). Together,

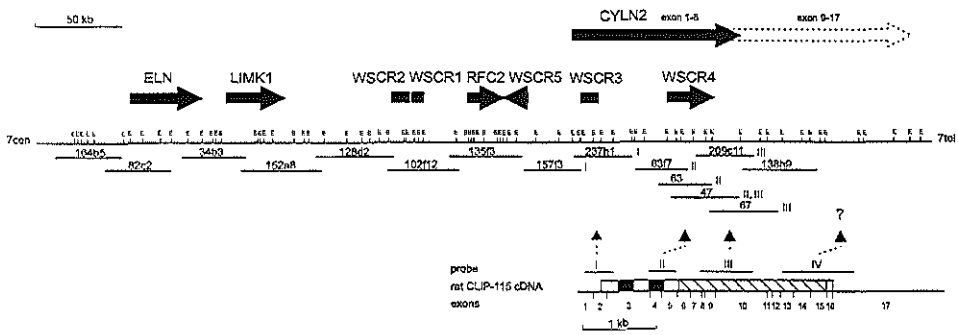

FIG. 5. Map of a 500-kb region commonly deleted in Williams Syndrome. The map of the WS critical region drawn here is based on the one presented by Osborne *et al.* (1996). Genes, including the *WSCR1–4* transcription units, are represented by solid thick lines or arrows. Locations of the LLNL and human *CYLN2* cosmids 63, 47, and 67 are indicated by thin lines. A schematic drawing of the *CLIP-115* cDNA is given underneath the 500 kb map. Noncoding 5′ and 3′ ends are represented by lines, solid bars indicate the two microtubule binding domains, and the hatched bar represents the coiled-coil region. Exon–intron boundaries (vertical lines), exon numbers, and the positions of the various probes are indicated below and above the schematic drawing. Thin dashed arrows show to which cosmids these probes hybridize (also indicated behind the cosmids). The position of part of the human *CYLN2* gene is indicated (thick arrow). The solid black part of this arrow represents the region of exons 1–8, the dashed part of the arrow represents the unidentified remainder of the human *CYLN2* gene. The distance from the overlap of the 157f3 and 237h1 cosmids to the end of cosmid 138h9 (which does not hybridize to the *CLIP-115* probes) is approximately 140 kb.

these results strongly indicate that we have mapped the 5′ regions of both mouse and human *CYLN2* genes.

Interestingly, sequence homology between murine *CYLN2* exon 1 and human cosmid contigs is found in a subclone derived from cosmid 157f3 as well as in a contig from cosmid 237h1 (data not shown). Thus, exon 1 of the human *CYLN2* gene must be located in the region of overlap between cosmids 157f3 and 237h1 (Fig. 5). This area, in turn, forms the border of the incomplete *WSCR3* transcription unit (Osborne *et al.*, 1996), suggesting that both *WSCR3* and *WSCR4* transcription units actually are part of the *CYLN2* gene. Based on the YAC/PAC/cosmid map for the WS critical region (Osborne *et al.*, 1996), 12 overlapping, human chromosome 7-specific cosmids (including 135f3, 157f3, 237h1, and 63f7) that together cover a large part of this region were ordered. Southern blot analysis was next used to align human cosmids 47, 63, and 67 with respect to each other and to the chromosome 7-specific cosmids (Fig. 5). Hybridization to *Eco*RI-digested cosmids with 5′ (I), middle (II and III), and 3′ end (IV) *CLIP-115* probes revealed that cosmid 157f3 hybridizes weakly to probe I, while in 237h1 one strongly and one weakly hybridizing fragment to this probe are present (Fig. 5). These data are consistent with the sequence comparison results presented in Table 1 and Fig. 4, i.e., exon 1 is represented by the weakly hybridizing fragment on cosmids 157f3 and 237h1, and exon 2 is represented by the strongly hybridizing band present only on 237h1. Cosmids 63f7, 63, and 47 hybridize strongly to probe II (middle) and cosmids 209c11 and 67 to probe III (middle), while none of the cosmids hybridizes to probe IV (3′ end). Taken together, the sequence comparison and hybridization data strongly suggest that the human *CYLN2* gene runs from the overlap between cosmid 157f3 and 237h1 toward the telomere and extends beyond cosmid 138h9 (see large arrow in Fig. 5). Thus the human *CYLN2* gene encompasses the incomplete *WSCR3* and *WSCR4* transcription units; it spans at least 140 kb, and thus far it is the largest gene detected in the WS critical region.

The Human CYLN2 Gene Is Expressed in Adult Brain

Although *CLIP-115* is expressed in rat and mouse brain (De Zeeuw *et al.*, 1997), neither *WSCR3* nor *WSCR4* mRNAs could be detected in any human tissue by PCR analysis (Osborne *et al.*, 1996). Therefore, the expression of the human *CYLN2* gene was investigated on a multiple-tissue Northern blot containing ~2 μg of poly(A)$^+$ mRNA. A message of ~5.5 kb is detected in the adult human brain sample, after hybridization of the blot with rat *CLIP-115* cDNA, while a weakly hybridizing, larger transcript is visible in heart and skeletal muscle (Fig. 6). The size of the human brain transcript corresponds well to the *CLIP-115* mRNA size detected in mouse and rat brains. These results demonstrate that *CLIP-115* is expressed in human brain, albeit at a low level.

Comparison of CLIP-115 Amino Acid Sequences from Rat, Mouse, and Human

Assembly of mouse *CYLN2* exons 1–17 into a presumptive mRNA and translation of this transcript yield a putative murine CLIP-115 amino acid se-

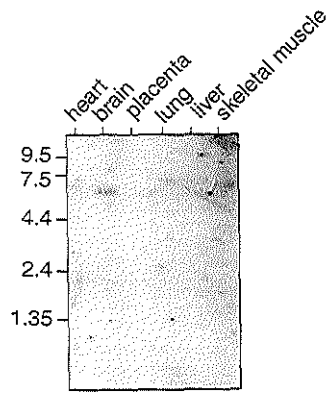

FIG. 6. *CLIP-115* expression in human. A human multiple-tissue Northern blot was hybridized with rat *CLIP-115* cDNA. After stringent washing an ~5.5-kb mRNA is detected in the brain and weakly hybridizing transcripts of larger size in heart and skeletal muscle. Molecular weight standards are indicated on the left.

quence. By aligning the recently submitted partial human *CLIP-115* cDNA KIAA0291 to *WSCR4* and the sequence from human cosmid 237h1, which is homologous to mouse exon 2, a composite human *CLIP-115* cDNA is obtained from which human CLIP-115 can be translated. Alignment of rat, mouse, and human CLIP-115 at the amino acid sequence level (Fig. 7) shows that the three proteins are very similar (97% overall identity between rat and mouse, 91% identity between mouse and human), and they are of equal length. Thus, like rat CLIP-115, murine and human proteins are characterized by an N-terminal globular region in which two microtubule binding domains are located, followed by a long region with a potential to form α-helical coiled-coils (Lupas, 1996). In only two small stretches, located in the N-terminal region upstream of the microtubule binding domains and in a presumptive coiled-coil stretch (amino acids 32–36 and 712–716 in human CLIP-115, respectively; see Fig. 7), do mouse and rat CLIP-115 deviate from the human protein. To investigate whether any of the mouse *CYLN2* exons encodes a specific protein domain, exon boundaries were plotted onto the protein sequences (Fig. 7). The boundaries of *CYLN2* exons 9–10 and 10–11 correspond to ends of potential coiled-coil domains (data not shown); however, the other exons do not define specific protein regions. In particular, the two microtubule binding domains present in CLIP-115 (De Zeeuw *et al.*, 1997) are not enclosed within single exons (Fig. 7).

Previously two *CLIP-115* cDNA clones were isolated from a rat hippocampus library; they have a deletion of 378 bp in the 3′ end of the *CLIP-115* ORF compared to other cDNAs (De Zeeuw *et al.*, 1997). Deletion of this internal fragment results in the removal of 126 amino acids from the C-terminus of CLIP-115, without altering the remainder of the reading frame. Based on these observations we hypothesized that alternative splicing takes place in rat *CLIP-115* mRNA (De Zeeuw *et al.*, 1997). However, such a splicing event cannot take place in the mouse. Deletion of exons 14 and 15 would yield a transcript that is very similar in size and sequence to the alternatively spliced rat product (Fig. 6), but if this deletion takes place the reading frame in mouse *CLIP-115* is not maintained. Therefore, the rat *CYLN2* genomic structure needs to be determined to address whether different alternative splicing events can occur in rat and mouse.

DISCUSSION

In the present study we report on the isolation and characterization of four overlapping murine and three overlapping human cosmids containing the complete mouse and part of the human *CYLN2* genes, respectively. Using these cosmids we have localized murine *CYLN2* to mouse chromosome 5 (band 5G) and human *CYLN2* to human chromosome 7 (band 7q11.23). These two regions are syntenic, for example, the murine *eln*, *limk1*, and *gtf2i* genes have been localized to mouse chromosome band 5G, while in human these genes (of which *GTF2I* was found to be duplicated (Perez-Jurado *et al.*, 1998)) have been mapped to the Williams syndrome critical region on human chromosome 7q11.23 (Wang *et al.*, 1998). Indeed, we have established that the *CYLN2* gene is hemizygously deleted in eight WS patients tested, demonstrating that it is within the WS critical region. Recently, it was published that a gene homologous to *CLIP-170/restin* (*WSCR4*) is located in the WS critical region (Osborne *et al.*, 1996). The data presented here demonstrate that *WSCR4* is part of the *CYLN2* locus.

Although the human *CYLN2* gene has not yet been completely mapped, the data show that it is much larger than its murine counterpart, i.e., exons 1–8 span 140 kb, and the complete gene might extend considerably toward the telomeric end of the WS critical region. Thus far the *CYLN2* gene is the largest gene mapped in this region. Our data actually suggest that the human *CYLN2* 5′ end overlaps with the boundary of the incomplete *WSCR3* transcription unit. This result raises the possibility that, like *WSCR4*, *WSCR3* is part of the human *CYLN2* gene.

The murine *CYLN2* gene consists of 17 exons that are spread over an area of 60 kb. The coding region of the *CYLN2* gene starts in exon 2 and ends in exon 17. Thus exon 1 and part of exon 2 constitute the 5′UTR. Human cosmid 157f3 hybridizes weakly to a 5′-end *CLIP-115* probe that spans exons 1 and 2, while 237h1 gives one strong and one weakly hybridizing band, suggesting that 157f3 contains only exon 1 and 237h1 contains exons 1 and 2. Moreover, when murine exon 1 is compared to the overlapping human LLNL cosmids 135f3, 157f3, 237h1, and 63f7, a region of high similarity is found in the overlap between cosmids 157f3 and

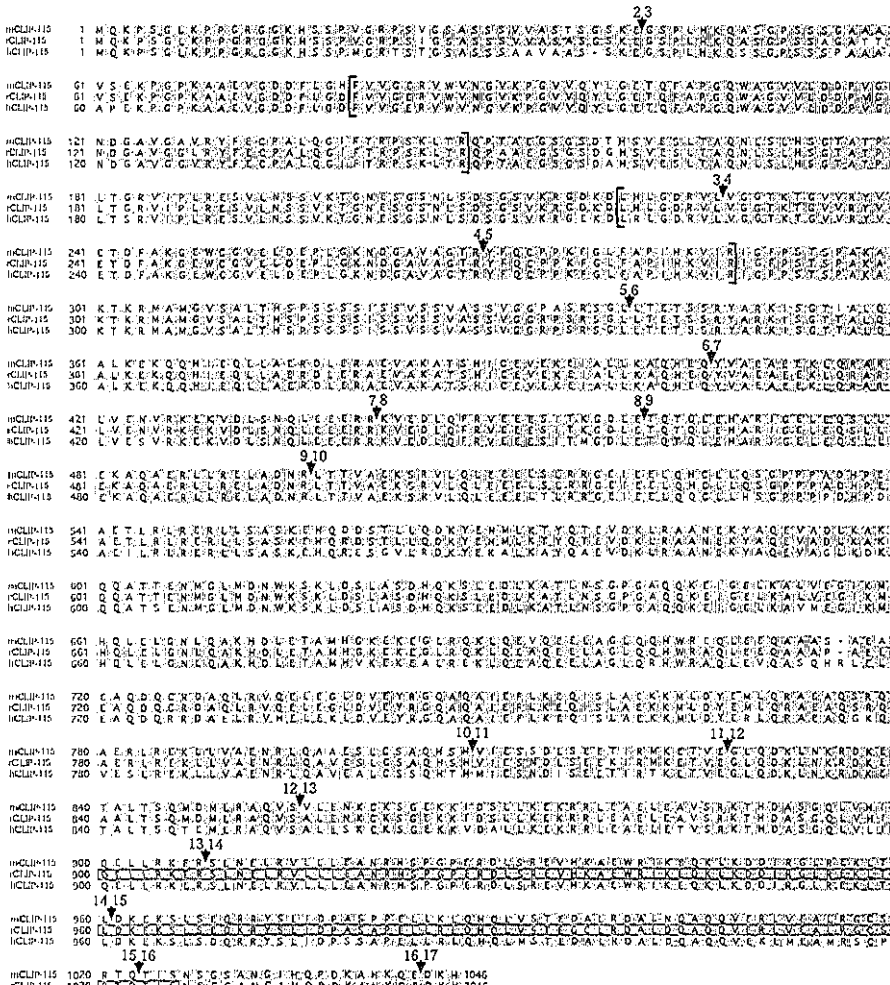

FIG. 7. Alignment of murine, rat, and human CLIP-115 at the amino acid level. Composite mouse and human CLIP-115 were aligned to the rat protein. Identical residues are shaded. Amino acid numbering is given on the side. Murine *CYLN2* exons are indicated on top of the amino acid sequence. The microtubule binding domains are between brackets. The proposed alternatively spliced rat *CLIP-115* sequence is boxed.

237h1. Together these data indicate that we have mapped the human *CYLN2* 5′ end. Both murine and human *CYLN2* exon 1 are embedded in a CpG island, and in the presumptive promoter area of the genes no TATA box is detected. Interestingly, we have found sequences downstream of *CYLN2* exon 1, i.e., in intron 1, that are highly conserved between mouse and human, indicating that they might be important for the control of *CYLN2* expression. Tissue-specific control elements have also been found in intron 1 of the *Thy-1* gene (Vidal *et al.*, 1990). Footprint experiments should reveal whether such elements exist in the *CYLN2* gene at the conserved sequence sites.

CLIP-115 is a recently characterized member of a

family of membrane–microtubule interacting proteins (De Zeeuw *et al.*, 1997) that is highly enriched in the DLB, a membranous organelle found exclusively in the dendritic bulbous appendages of neurons connected by dendrodendritic gap junctions (De Zeeuw *et al.*, 1995). This organelle is present in neurons in areas such as the hippocampus, piriform cortex, olfactory bulb, and inferior olive, which are the same brain areas in which CLIP-115 is detected. In addition, CLIP-115 is ubiquitously distributed in the Bergmann glia fibers in the cerebellar cortex. These cells are required for the geometrical organization of cerebellar constituents, and they strongly interact with Purkinje cells during important processes such as the induction and maintenance of long-term depression (Shibuki *et al.*, 1996). Interestingly, Bergmann glia cells are also coupled by extensive gap junction plaques (Palay and Chan-Palay, 1974), which has led to the suggestion that CLIP-115 might be involved in the turnover of gap junctions (De Zeeuw *et al.*, 1997). The fact that only one *CYLN2* gene is found in mouse, rat, and human and that this gene gives rise to a highly conserved protein that is expressed in the brain of the three species, suggests a conserved function for the *CYLN2* gene. We therefore speculate that, apart from putative neurodevelopmental defects, haploinsuffiency at the human *CYLN2* locus could contribute to the WS phenotype by affecting both the level of electrotonic coupling in neurons with DLBs and Bergmann glia cells and metabolic interactions between Bergmann glia fibers and Purkinje cells. As a consequence these deficits might disturb the synchronous and oscillatory activity of neurons in various brain regions (Llinás and Sasaki, 1989), and they may compromise mechanisms of memory formation. These abnormalities, in turn, may lead to the neuropsychological and neurological disorders observed in WS patients (Bellugi *et al.*, 1990).

As mentioned above, other genes present in the WS critical region have also been shown to be expressed in the brain. Analogous to our reasoning here, it has been suggested that hemizygous deletion of the *syntaxin 1A* gene, which encodes a protein involved in synaptic neurotransmitter release, is in part responsible for ADHD (Osborne *et al.*, 1997). In addition, haploinsufficiency of the *FZD3* gene, which encodes a putative homologue of the wingless receptor, might account for some of the neurodevelopmental phenotypes and systemic symptoms in WS, such as hypercalcemia (Wang *et al.*, 1997). Finally small deletions including the *LIMK1* gene have been shown to account for specific visuospatial cognitive defects (Frangiskakis *et al.*, 1996). With the characterization of the murine *CYLN2* gene it is now possible to generate *CYLN2* knockout mice to look at the effect of a lack of one or both copies of this gene on mouse development and (brain) function.

ACKNOWLEDGMENTS

We thank Dr. L. Govaerts for selection of WS patients, B. Smit and A. van der Heide for their expert technical assistance in the FISH experiments, and Dr. D. Halley for providing the genomic DNA samples. This research was supported by grants from the Netherlands Organization for Scientific Research (NWO; GB-MW 903-68-361), the Life Sciences Foundation (SLW; 805.33.310), and the Royal Dutch Academy of Sciences (KNAW).

REFERENCES

Bellugi, U., Bihrle, A., Jernigan, T., Trauner, D., and Doherty, S. (1990). Neuropsychological, neurological, and neuroanatomical profile of Williams syndrome. *Am. J. Med. Genet. Suppl.* **6:** 115–125.

Bilbe, G., Delable, J., Bruggen, J., Richener, H., Asselbergs, F. A., Cerletti, N., Sorg, C., Odink, K., Tarcsay, L., Wiesendanger, W., *et al.* (1992). Restin: A novel intermediate filament-associated protein highly expressed in the Reed–Sternberg cells of Hodgkin's disease. *EMBO J.* **11:** 2103–2113.

De Zeeuw, C. I., Hertzberg, E. L., and Mugnaini, E. (1995). The dendritic lamellar body: A new neuronal organelle putatively associated with dendrodendritic gap junctions. *J. Neurosci.* **15:** 1587–1604.

De Zeeuw, C. I., Hoogenraad, C. C., Goedknegt, E., Hertzberg, E., Neubauer, A., Grosveld, F., and Galjart, N. (1997). CLIP-115, a novel brain-specific cytoplasmic linker protein, mediates the localization of dendritic lamellar bodies. *Neuron* **19:** 1187–1199.

Ewart, A. K., Jin, W., Atkinson, D., Morris, C. A., and Keating, M. T. (1994). Supravalvular aortic stenosis associated with a deletion disrupting the elastin gene. *J. Clin. Invest.* **93:** 1071–1077.

Ewart, A. K., Morris, C. A., Atkinson, D., Jin, W., Sternes, K., Spallone, P., Stock, A. D., Leppert, M., and Keating, M. T. (1993). Hemizygosity at the elastin locus in a developmental disorder, Williams syndrome. *Nat. Genet.* **5:** 11–16.

Feinberg, A. P., and Vogelstein, B. (1983). A technique for radiolabeling DNA restriction endonuclease fragments to high specific activity. *Anal. Biochem.* **132:** 6–13.

Frangiskakis, J. M., Ewart, A. K., Morris, C. A., Mervis, C. B., Bertrand, J., Robinson, B. F., Klein, B. P., Ensing, G. J., Everett, L. A., Green, E. D., Proschel, C., Gutowski, N. J., Noble, M., Atkinson, D. L., Odelberg, S. J., and Keating, M. T. (1996). LIM-kinase1 hemizygosity implicated in impaired visuospatial constructive cognition. *Cell* **86:** 59–69.

Jernigan, T. L., and Bellugi, U. (1990). Anomalous brain morphology on magnetic resonance images in Williams syndrome and Down syndrome. *Arch. Neurol.* **47:** 529–533.

Jones, K. L. (1990). Williams syndrome: An historical perspective of its evolution, natural history, and etiology. *Am. J. Med. Genet. Suppl.* **6:** 89–96.

Lippincott-Schwartz, J. (1998). Cytoskeletal proteins and Golgi dynamics. *Curr. Opin. Cell Biol.* **10:** 52–59.

Llinás, R., and Sasaki, K. (1989). The functional organisation of the olivo-cerebellar system as examined by multiple Purkinje cell recordings. *Eur. J. Neurosci.* **1:** 587–602.

Lupas, A. (1996). Prediction and analysis of coiled-coil structures. *Methods Enzymol.* **266:** 513–525.

Mazarakis, N., Michalovich, D., Karis, A., Grosveld, F., and Galjart, N. (1996). Zfp-37 is a member of the KRAB zinc finger gene family and is expressed in neurons of the developing and adult CNS. *Genomics* **33:** 247–257.

Morris, C. A., Demsey, S. A., Leonard, C. O., Dilts, C., and Blackburn, B. L. (1988). Natural history of Williams syndrome: Physical characteristics. *J. Pediatr.* **113:** 318–326.

Mulder, M. P., Wilke, M., Langeveld, A., Wilming, L. G., Hagemeijer, A., van Drunen, E., Zwarthoff, E. C., Riegman, P. H., Deelen,

W. H., van den Ouweland, A. M. W., Halley, D. J. J., and Meijers, C. (1995). Positional mapping of loci in the DiGeorge critical region at chromosome 22q11 using a new marker (D22S183). *Hum. Genet.* **96:** 133–141.

Olson, T. M., Michels, V. V., Urban, Z., Csiszar, K., Christiano, A. M., Driscoll, D. J., Feldt, R. H., Boyd, C. D., and Thibodeau, S. N. (1995). A 30 kb deletion within the elastin gene results in familial supravalvular aortic stenosis. *Hum. Mol. Genet.* **4:** 1677–1679.

Osborne, L. R., Herbrick, J. A., Greavette, T., Heng, H. H., Tsui, L. C., and Scherer, S. W. (1997). PMS2-related genes flank the rearrangement breakpoints associated with Williams syndrome and other diseases on human chromosome 7. *Genomics* **45:** 402–406.

Osborne, L. R., Martindale, D., Scherer, S. W., Shi, X. M., Hulzenga, J., Heng, H. H. Q., Costa, T., Pober, B., Lew, L., Brinkman, J., Rommens, J., Koop, B., and Tsui, L. C. (1996). Identification of genes from a 500-kb region at 7q11.23 that is commonly deleted in Williams syndrome patients. *Genomics* **36:** 328–336.

Palay, S. L., and Chan-Palay, V. (1974). "Cerebellar Cortex: Cytology and Organisation," Springer-Verlag, New York.

Peoples, R., Perez-Jurado, L., Wang, Y. K., Kaplan, P., and Francke, U. (1996). The gene for replication factor C subunit 2 (RFC2) is within the 7q11.23 Williams syndrome deletion. *Am. J. Hum. Genet.* **58:** 1370–1373.

Perez-Jurado, L. A., Wang, Y. K., Peoples, R., Coloma, A., Cruces, J., and Francke, U. (1998). A duplicated gene in the breakpoint regions of the 7q11.23 Williams–Beuren syndrome deletion encodes the initiator binding protein TFII-I and BAP-135, a phosphorylation target of BTK. *Hum. Mol. Genet.* **7:** 325–334.

Pierre, P., Scheel, J., Rickard, J. E., and Kreis, T. E. (1992). CLIP-170 links endocytic vesicles to microtubules. *Cell* **70:** 887–900.

Preus, M. (1984). The Williams syndrome: Objective definition and diagnosis. *Clin. Genet.* **25:** 422–428.

Rickard, J. E., and Kreis, T. E. (1996). CLIPs for organelle–microtubule interactions. *Trends Cell Biol.* **6:** 178–183.

Saiki, R. K., Gelfand, D. H., Stoffel, S., Scharf, S. J., Higuchi, R., Horn, G. T., Mullis, K. B., and Erlich, H. A. (1988). Primer-directed enzymatic amplification of DNA with a thermostable DNA polymerase. *Science* **239:** 487–91.

Sambrook, J., Fritsch, E. F., and Maniatis, T. (1989). "Molecular Cloning: A Laboratory Manual," 2nd ed., Cold Spring Harbor Laboratory Press, Cold Spring Harbor, NY.

Shibuki, K., Gomi, H., Chen, L., Bao, S., Kim, J. J., Wakatsuki, H., Fujisaki, T., Fujimoto, K., Katoh, A., Ikeda, T., Chen, C., Thompson, R. F., and Itohara, S. (1996). Deficient cerebellar long-term depression, impaired eyeblink conditioning, and normal motor coordination in GFAP mutant mice. *Neuron* **16:** 587–599.

Vallee, R. B., and Sheetz, M. P. (1996). Targeting of motor proteins. *Science* **271:** 1539–1544.

Vidal, M., Morris, R., Grosveld, F., and Spanopoulou, E. (1990). Tissue-specific control elements of the Thy-1 gene. *EMBO J.* **9:** 833–840.

Wang, Y. K., Perez-Jurado, L. A., and Francke, U. (1998). A mouse single-copy gene, Gtf2i, the homolog of human GTF2I, that is duplicated in the Williams–Beuren syndrome deletion region. *Genomics* **48:** 163–170.

Wang, Y. K., Samos, C. H., Peoples, R., Perez-Jurado, L. A., Nusse, R., and Francke, U. (1997). A novel human homologue of the *Drosophila* frizzled wnt receptor gene binds wingless protein and is in the Williams syndrome deletion at 7q11.23. *Hum. Mol. Genet.* **6:** 465–472.

Waye, J. S., England, S. B., and Willard, H. F. (1987). Genomic organisation of alpha satellite DNA on human chromosome 7: Evidence for two distinct alphoid domains on a single chromosome. *Mol. Cell. Biol.* **7:** 349–356.

Chapter 10

CYLN2 GENE TARGETING LINKS CLIP-115 HAPLOINSUFFICIENCY TO NEURODEVELOPMENTAL FEATURES OF WILLIAMS SYNDROME

Casper C. Hoogenraad[1,2], Bjorn Dortland[1], Bas Koekkoek[2], Anna Akhmanova[1], Mandy Rutteman[1,2], Werner Kistler[2], Martine Jaegle[1], Manousos Koutsourakis[1], Annemie van der Linden[3], Nadja Van Camp[3], Harm Krugers[4], Frank Grosveld[1], Chris. I De Zeeuw[2], Niels Galjart[1].

MGC Departments of [1]Cell Biology and Genetics and of [2]Neurosciences, Erasmus University, P.O. Box 1738, 3000 DR Rotterdam, The Netherlands. [3]Bio-Imaging Lab, University of Antwerp (RUCA), Groenenborgerlaan 171, 2020 Antwerp, Belgium. [4]Swammerdam Instituut for Life Sciences, University of Amsterdam, Kruislaan 320 1098 SM, Amsterdam, The Netherlands.

Summary
Williams Syndrome (WS) is a neurodevelopmental disorder, caused by hemizygous deletion of a region on chromosome 7q11.23, which spans the genes encoding elastin (*ELN*), the microtubule binding protein CLIP-115 (*CYLN2*) and several others. Haploinsufficiency of the *ELN* gene has been firmly linked to cardiovascular abnormalities in WS. Here, we describe the inducible knock out of the *CYLN2* gene in mice. We show that lower levels of CLIP-115 results in a mild growth deficiency, enlarged ventricle size in the brain and leads to specific behavioral deficits. This phenotype mimics features of WS, establishing a link between deficiency of the *CYLN2* gene and neurologic alterations in this disorder.

Introduction

Williams(-Beuren) Syndrome (WBS or WS; OMIM 194050) is a neurodevelopmental disorder, which is characterized by cardiovascular abnormalities, transient juvenile hypercalcemia, short stature and very typical facial and neurological features [1]. Most prominent among the cardiovascular problems is supravalvular aortic stenosis (SVAS). However, the main reason why WS attracts so much attention is that these patients generally have a unique neurological and behavioral profile [2-4]. For example, WS patients have a poor coordination and abnormal sensitivity to certain classes of sounds and their IQ is in the mild-to-moderate range of mental retardation. They are weak in spatial cognition, but they have remarkably preserved language and musical abilities and are relatively strong in face processing. Other characteristic behaviors include a friendly, outgoing personality, which involves an apparent lack of fear.

WS is a rare disorder, with an incidence of 1:20,000. It is caused by the hemizygous, submicroscopic deletion of a region of approximately 1.6 Mb on chromosome band 7q11.23, which contains 16-17 genes and is called the WS critical region [5,6]. Genes that fall within this domain include those encoding syntaxin 1A (STX1A), elastin (ELN), LIM kinase 1 (LIMK1) and CLIP-115 (CYLN2), as well as a homologue of the Drosophila frizzled gene (FZD9) [7-9]. The WS critical region is bounded by repeats, which has lead to the hypothesis that WS is caused by illegitimate, homologous recombination at the repeats, leading to the *de novo* deletion of the intervening sequence at very early stages of embryonic development. However, patients have been discovered which carry minor deletions that span only part of the WS critical region [7-9]. Study of these patients and of those with point mutations have firmly established that haploinsufficiency for the *ELN* gene is linked to cardiovascular abnormalities in WS, in particular SVAS [10,11]. Another report suggested that insufficiency of LIM kinase 1 results in visuo-spatial cognition problems [12]. More recent studies have, however, not verified this hypothesis [13]. Therefore, although deficiency of the *LIMK1* gene may contribute to part of the cognitive problems in WS, it is now thought that other genes are responsible for the majority of the behavioral abnormalities. Patient data actually indicate that these genes

might be located in a region telomeric to the *LIMK1* gene and centromeric to *GTF2I* [8,9,13,14].

In an effort to characterize proteins that are part of the dendritic lamellar body, a Golgi-like element found in the dendritic appendages of a restricted number of neuronal nuclei in the brain, we have recently cloned the cDNA encoding the cytoplasmic linker protein of 115 kDa, CLIP-115 [15]. In mice, this protein is most abundantly expressed in dendrites and cell bodies of many neurons in the brain [15,16]. The gene encoding CLIP-115 is named *CYLN2* and both our group [17] and others [18] have shown that this gene is located in the WS critical region. Because of this and the fact that CLIP-115 is most predominately expressed in the brain, we have hypothesized that insufficient levels of this protein might underlie the development of neurological and/or behavioral aspects of WS [17].

In the mouse the *CYLN2* gene is located on the telomeric end of chromosome 5 [17], in an area that is syntenic to human chromosome 7q11.23 [5]. In both cases the *CYLN2* gene is located in between the *LIMK1* and *GTF2I* loci [5,6]. Based on data obtained from WS patients with small deletions, the *CYLN2* gene is therefore a prime candidate to be involved in the neurodevelopmental problems observed in WS. To test this hypothesis we have generated an inducible *CYLN2* knock out allele in ES cells (CLIP-T allele), which was further modified with Cre recombinase to generate the *CYLN2* knock out gene (CLIP-L allele). Mice were generated carrying either the CLIP-T or the CLIP-L allele. Only in the CLIP-L strain, we observe mild growth deficiency and enlarged ventricle sizes in the brain and specific behavioral deficits. Since these alterations mimic part of the WS phenotype and are observed already at the heterozygous level in CLIP-L mice, these data strongly suggest that deletion of the *CYLN2* gene is responsible for at least part of the neurodevelopmental profile of WS patients.

Results

An inducible CYLN2 knock out gene

The murine *CYLN2* gene consists of 17 exons, of which the second contains the translation initiation codon and the last the 3'UTR [17]. The *CYLN2* gene covers approximately 60 kb; the introns between exons 1 and 2 and exons 2 and 3 being the largest ones. To completely inactivate the gene we therefore decided to introduce a neomycin resistance gene, surrounded by loxP sequences in a 5' position and a puromycin selection marker, surrounded by LoxP sequences and followed by a modified lacZ reporter gene, downstream of the *CYLN2* gene (Fig. 1a). We placed the 5' neo cassette in intron 2, so that insertion of this cassette would have a low chance of affecting endogenous *CYLN2* enhancer elements. Resistance markers were introduced into the same *CYLN2* allele by two sequential rounds of homologous recombination in 129-derived ES cells (first round, neomycin cassette introduction: 12 % of picked clones targeted; second round, puromycin cassette, 15 % targeted). Homologous recombination was confirmed by a combination of Southern blot, PCR and FISH

analyses, using external and internal probes and specific PCR primer pairs (Fig. 1b and data not shown). The doubly targeted *CYLN2* allele was called *CLIP-T* (Fig. 1a). Subsequently, Cre-mediated excision of the region between the outermost loxP sites in the *CLIP-T* allele was achieved by transfecting ES cell clones with a Cre-recombinase plasmid. Excision of the region was monitored by Southern blot and PCR analyses (Fig. 1b) and the knocked out *CYLN2* allele was called *CLIP-L* (Fig. 1a). In the *CLIP-L* allele, the lacZ reporter gene is in close proximity to exon 2 of the *CYLN2* gene. Since a splice acceptor site is present at the 5'end of the reporter cassette, it will be spliced on to *CYLN2* exon 2 sequences, generating a hybrid *CYLN2-lacZ* transcript.

ES cells with the *CLIP-T* and *CLIP-L* alleles were injected into recipient C57Bl6 blastocysts and chimeric offspring was bred to wild type mice to pass on the modified *CYLN2* to the germline. Germline transmission was obtained in both cases and the newly derived CLIP-T and CLIP-L mice were crossed back to C57Bl6 mice for another two generations, after which homozygous and heterozygous CLIP-T and CLIP-L mice were generated. To determine whether CLIP-115 is expressed in the CLIP-T or -L mouse strains, northern and western blot experiments were performed on brain-derived total RNA and protein, respectively. The northern blot data demonstrate that *CLIP-115* mRNA is not expressed from the *CLIP-L* allele but *lacZ* is, whereas from the *CLIP-T* allele *CLIP-115* is normally expressed (Fig. 1d). We tested whether other genes, surrounding the *CYLN2* locus, are affected by the targeting, but did not find any evidence for altered expression of *EIF4H (WBSCR1), RFC2* and *GTF2IRD1 (WBSCR11)* (data not shown). In line with the northern blot data, the western blots demonstrate that no CLIP-115 is produced in homozygous *CYLN2* knock out mice, whereas reduced levels are detected in heterozygous mice and normal levels of the protein appear to be present in the CLIP-T mice as compared to wild type controls (Fig. 1e). Reduction in the levels of CLIP-115 in the CLIP-L mice does not to lead to a significant upregulation of the levels of CLIP-170 (Fig. 1e), the closed mammalian CLIP-115 homologue, indicating that there is no compensation for the lack of CLIP-115 by CLIP-170.

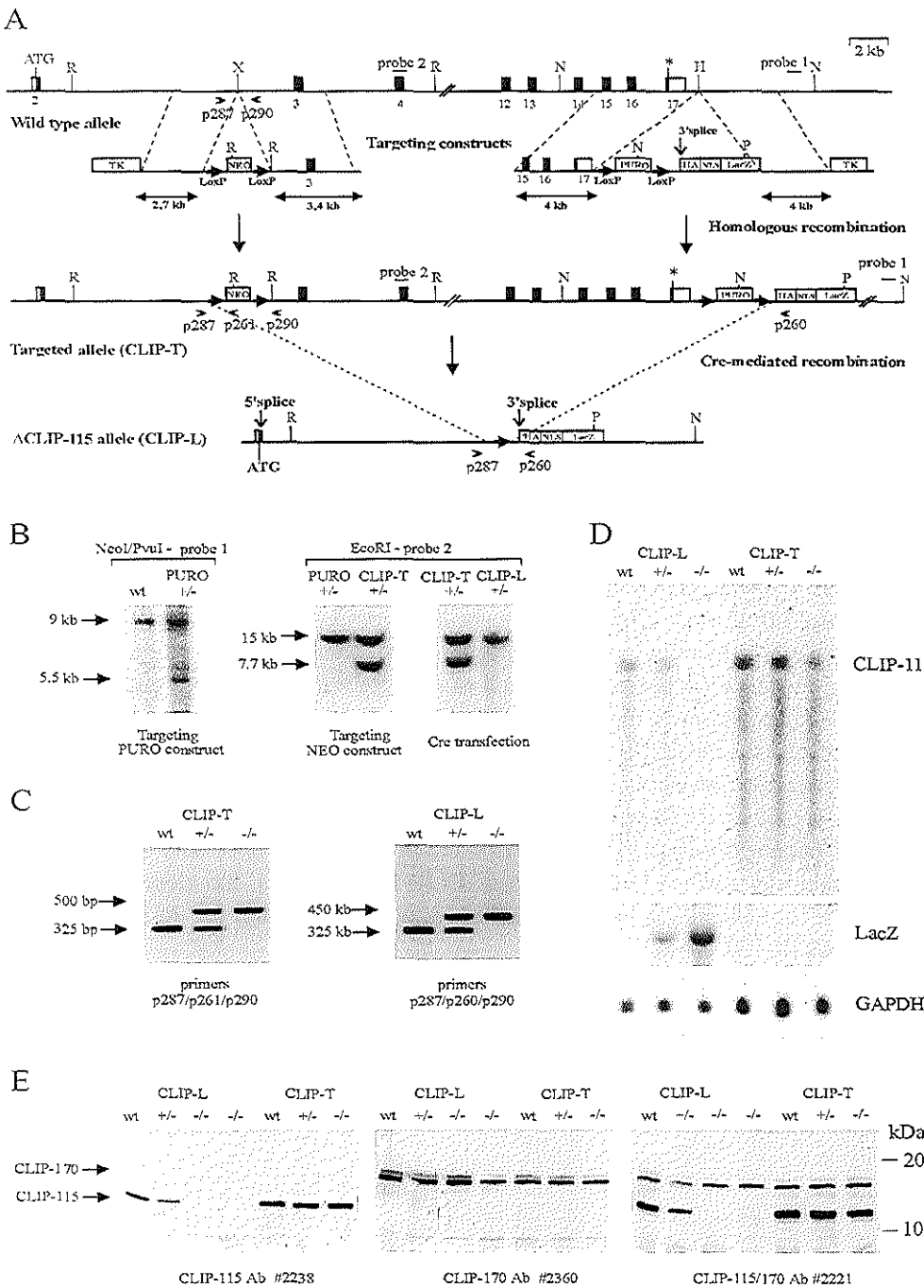
A
ATG
R
X
probe 2
N
H
probe 1
2 kb
Wild type allele
p287
p290
Targeting constructs
3'splice
TK
NEO
PURO
LoxP
2,7 kb
3,4 kb
4 kb
Homologous recombination
p261
p260
Targeted allele (CLIP-T)
Cre-mediated recombination
5'splice
ΔCLIP-115 allele (CLIP-L)
ATG
B
NcoI/PvuI - probe 1
EcoRI - probe 2
PURO
CLIP-T
CLIP-L
wt
+/-
9 kb
5.5 kb
15 kb
7.7 kb
Targeting PURO construct
Targeting NEO construct
Cre transfection
C
500 bp
325 bp
450 kb
primers p287/p261/p290
primers p287/p260/p290
D
CLIP-115
LacZ
GAPDH
E
CLIP-170
CLIP-115
kDa
200
100
CLIP-115 Ab #2238
CLIP-170 Ab #2360
CLIP-115/170 Ab #2221

Figure 1. Construction and characterization of CLIP-115 mutant mice CLIP-T and –L
A Structure of the genomic murine *CYLN2* locus and gene targeting constructs. The top line represents the approximately 60 kb *CYLN2* genomic locus. Exons are indicated by solid boxes. Open boxes are noncoding 5' end 3' ends. Exon 2 contains the start codon (ATG) and exon 17 the stop codon (asterisk). The lines above exon 4 and upstream of exon 17 indicate the position of the probes used to screen for the targeted allele. Primers used for PCR analyses (p287, p260, p261 and p290) are indicated as arrow heads. Shown are the locations of selected restriction sites; R = EcoRI, X = XbaI, N = NcoI, P = PvuI. The next two lines represent the targeting constructs and shows the position of the selectable marker genes neomycin (NEO) flanked by LoxP sequences in intron 2, puromycin (PURO) flanked by LoxP sequences upstream of exon 17, thymidine kinase (TK) at one end of the constructs and the HA-tagged NLS-β-galactosidase (LacZ) sequence containing a 3' splice acceptor site. The third line represents the double targeted *CYLN2* allele, CLIP-T(argeted). The disrupted *CYLN2* gene locus is represented at the bottom line, CLIP-L(oxed). The splice acceptor site present at the 5'end of the reporter LacZ cassette, will be spliced on to *CYLN2* exon 2 sequences, generating a hybrid *CYLN2-lacZ* transcript. **B** Southern blot analyses of wild type and mutant CLIP-T and -L ES cells. ES cells were first electroporated with the 3' PURO targeting construct. From individual clones ES cell DNA was isolated, digested with EcoRI to test for homologous recombination of the PURO targeting construct, blotted and hybridized with external probe 1 (wt : 9 kb and PURO targeting: 9kb / 5.5 kb). A clone with the correct karyotype was electroporated with the second 5' NEO targeting construct. Correct replacement events were identified by Southern blot analyses of EcoRI digested genomic DNA probed with external probe 2 (PURO targeting: 15 kb and NEO targeting = CLIP-T: 15 kb /7.7 kb). FISH analyses was used to determine the localization of both constructs. One of the cell lines (with the correct karyotype and where both constructs targeted to the same allele) is named the CLIP-T line. This cell line was injected into C57Bl/6 mice, to generate CLIP-T mice and electroporated with the Cre-recombinase construct with a hygromycin cassette to obtain the floxed *CYLN2* locus. Cre-mediated recombination events were identified by Southern blot analyses of EcoRI digested genomic DNA probed with external probe 2 (CLIP-T: 15 kb / 7.7 kb and CLIP-L 15 kb). A cell line heterozygously deleted for the *CYLN2* gene is named the CLIP-L line and was injected into C57Bl/6 mice. **C** PCR analyses on genomic tail DNA of wild type, CLIP-T and -L mice. Genotyping of mutant mice was mainly done by PCR analyses with a three primer set. Wt and CLIP-T and -L genomic DNA is amplified by primer combination p287-p290 (wt: 325 bp), p287-p261 (CLIP-T: 500 bp) and p287-p260 (CLIP-L: 450 bp). **D** Northern blot analyses RNA from wild type, CLIP-T and -L mice. Total RNA was extracted from brains of wild type and heterozygous and homozygous CLIP-T and –L mice and hybridized with CLIP-115 (top), β-galactosidase (LacZ) (middle) and GAPDH (bottom) probes. GAPDH levels indicate the amount of RNA loaded in each lane. **E** Western blot of brain extracts of wild type, CLIP-T and -L mice with anti-CLIP antibodies. Protein extracts of wild type, heterozygous and homozygous CLIP-T and –L mice were separated on a 6% SDS-PAGE gel, transferred to blot and hybridized with anti-CLIP-115 antibody (#2238), anti-CLIP-170 (#2360) and anti-CLIP-115/170 (#2221) antibodies. The size of the protein marker is indicated on the right. The arrows indicate the position of CLIP-115 and CLIP-170 proteins. Wt, wild type, +/- heterozygous and -/- homozygous.

Although it has been established that CLIP-115 is mainly expressed in the brain [15,16], relatively little is known about regional variations in expression level of the protein in this organ. To investigate this in more detail, we used the lacZ marker in the CLIP-L mice as an indicator of *CYLN2* gene activity, either on whole brain mounts or on 40 μm sections of the brain. These results indicate that lacZ (and by implication CLIP-115) is most abundantly expressed in CA pyramidal neurons, but not in dentate gyrus neurons of the hippocampus, in the amygdala and in Purkinje cells of the cerebellum (data not shown). In the latter brain area an obviously striped pattern of lacZ activity is observed, that resembles the functional sagittal division of the cerebellum (data not shown). Longer periods of lacZ staining reveal that many neurons

of the brain express this marker, albeit much less intense than the areas mentioned above (data not shown). Notable regions, that remain weakly labeled by lacZ, despite prolonged incubations, are the dentate gyrus and inferior olive (data not shown). The lacZ staining data correlate well with antibody staining data using antisera against bacterially expressed CLIP-115 [16]), but deviate somewhat from the original results with the low affinity anti-peptide CLIP-115 antibodies [15].

Growth deficits and brain abnormalities in CYLN2 knock out mice

Both the CLIP-L and CLIP-T strains of mice are viable and fertile, whether they are heterozygous or homozygous for the modified *CYLN2* allele. Offspring derived from of heterozygous CLIP-L x CLIP-L and CLIP-T x CLIP-T crosses are born in a normal Mendelian fashion (data not shown), suggesting that CLIP-115 is not essential for life. However, adult homozygous CLIP-L mice are lighter than their wild type littermates, or than CLIP-T controls (Fig. 2a). The difference in weight is more pronounced in female than in male CLIP-L mice. In the case of adult female mice the decrease in body weight between homozygote and wild types (and CLIP-T) is statistically significant, while in the adult males it is not (Fig. 2a). Weights of heterozygous animals are in between wild types and homozygous. These weight differences correlate well with a decrease in body and bone length in the adult female CLIP-L mice (Fig. 2d), strongly suggesting that these mice have a general growth deficit. Already, during postnatal development a growth retardation is present. From 2 weeks of age onward, the weight difference between wild type and homozygous knock out littermates for both male and female mice are statistically significant (Fig. 2c, d). Depending on their age, homozygous females and males between 3 and 10 weeks old were on average 10-22% and 4-16% lighter, respectively, than their wild type littermates and the CLIP-T mice. Again, weights of heterozygous animals are in between wild types and homozygotes. Similar to WS patients, the growth deficit in CLIP-115 mutant mice is already apparent at a young age and persists into adulthood. Sectioning of the brains of CLIP-L and -T mice and staining with hematoxylin/eosin did not reveal any gross abnormalities in brain morphology in either type of mouse strain (data not shown). In addition, total brain weight of newborn and adult CLIP-L and -T mice are comparable to those of wild type controls (data not shown). To investigate whether subtle macroscopic abnormalities can be detected in these mice we performed a MRI analysis. While the volume of the cerebellum, cerebrum, hippocampus and amygdala do not differ among knock outs and wild types, the size of the ventricle of CLIP-L knock-out mice is significantly enlarged as compared to that of wild type littermates (Fig. 3a,b and data not shown). The average size of the ventricle heterozygous animals is in between that of wild types and knock outs. These data indicate that a reduction in normal CLIP-115 levels in the mouse causes mild growth and brain abnormalities.

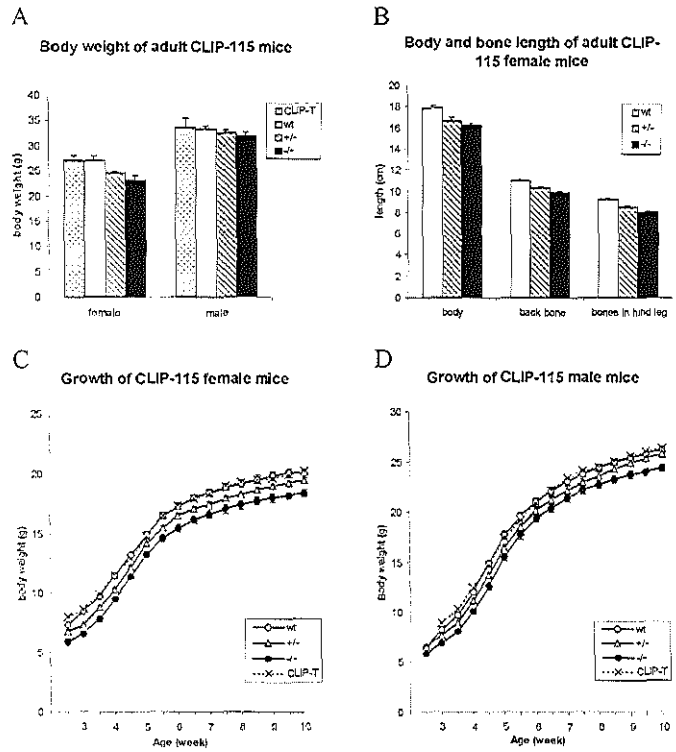

Figure 2. Body weight and growth curves of CLIP-115 mutant mice

A Body weight of female and male wild type and CLIP-T and -L mice. Wt (n = 7), CLIP-T (n = 11), and heterozygous (n = 34) and homozygous (n = 5) CLIP-L female mice and wt (n = 7), CLIP-T (n= 7), and heterozygous (n =17) and homozygous (n = 7) CLIP-L male mice at 6.5 months of age were monitored for their body weight (mean (±SEM)). Both heterozygous and homozygous female CLIP-L mice had a significant lower weight 9% and 15%, respectively, than their wild type littermates and the CLIP-T (T) mice. Statistics was performed with a two-tailed unpaired Student's t-test. P values are from comparison between +/- and wt ($P<0.05$), -/- and wt ($P<0.005$), +/- and CLIP-T ($P<0.05$), and -/- and CLIP-T ($P<0.005$). The body weight of heterozygous and homozygous male CLIP-L mice are not significantly different from those of wild type littermates and CLIP-T mice, but male mutant mice also show a trend towards reduced body weight. P values are from comparison between +/- and wt ($P = 0.5$), -/- and wt ($P = 0.2$), +/- and CLIP-T ($P = 0.5$), and -/- and CLIP-T ($P = 0.7$). **B** Body and bone length of wild type (n = 5), heterozygous (n = 5) and homozygous CLIP-L (n = 5) female mice. The body and bone length of 6 months old female mice were determined by X-ray analyses. Measurements of the total body length, the back bone and length of the bones in left hind leg showed on average a 11% decrease in body and bone length in homozygous CLIP-L mice and a 7% decrease in heterozygous CLIP-L mice. P values are from comparison between homozygous CLIP-L and wt mice for body length ($P<0.001$), back bone ($P<0.001$) and bones in hind leg ($P<0.001$) and heterozygous CLIP-L and wt mice for body length ($P<0.05$), back bone ($P<0.005$) and bones in hind leg ($P<0.005$). **C** Growth curve of wild type (n = 15), CLIP-T (n = 24), heterozygous (n = 40) and homozygous (n = 12) CLIP-L female mice. Body weight of grouped mice were measured twice a week from two weeks of age onward. Depending on their age, heterozygous and homozygous CLIP-L female mice were on average 5-14% and 10-22%, respectively, lighter then their wild type littermates and the CLIP-T mice. The P value of every data point is not shown, in contrast, the average P values (from week 2 to 10) are compared between +/- and wt ($P<0.05$), -/- and wt ($P<0.001$), +/- and CLIP-T ($P<0.05$), and -/- and CLIP-T ($P<0.005$). **D** Growth curve of wild type (n = 20), CLIP-T (n = 17), heterozygous (n = 31) and homozygous (n = 23) CLIP-L male mice. Body weight of grouped mice were measured twice a week from two weeks of age onward. Depending on their age, heterozygous and homozygous CLIP-L male mice were on average 2-8% and 7-17%, respectively, lighter than their wild type littermates and the CLIP-T mice. Only homozygous knock-out male mice are significantly different. The average P values (from week 2 to 10) are compared between +/- and wt ($P = 0.2$), -/- and wt ($P<0.005$), +/- and CLIP-T ($P = 0.2$), and -/- and CLIP-T ($P<0.01$).

Behavioral analysis of CLIP-L and -T mouse strains

The increased levels of lacZ in the hippocampus, amygdala and cerebellum of CLIP-L mice suggest that neuronal functioning, pertaining to these brain areas might be affected in these mice, due to the absence of CLIP-115. We therefore set up a number of behavioral assays to investigate performance of the different brain areas. In all experiments both the CLIP-T strain (which carries exactly the same, 129 ES cell derived DNA sequences, surrounding the CYLN2 locus, as the CLIP-L strain) as well as wild type littermates of the CLIP-L mice, served as controls for the assays, to circumvent potential strain background problems. Interestingly, there are a number of gross motor function tests in which the CLIP-L mice behave like the control strains, i.e. in open field activity (Fig. 4a), in the hanging wire (Fig. 4b), horizontal (Fig. 4c) and vertical (data not shown) beam walk tests and in circadian rhythm experiments (data not shown). These data indicate that general strength and circadian activity are not affected in the CLIP-L mice. Moreover, in spite of the pronounced, striped expression of CLIP-115 in Purkinje cells of the cerebellum, compensatory eye movements are not affected in CLIP-L mice as compared to CLIP-T and wild type controls. Measurement of the compensatory eye movements is a robust and highly accurate test for performance of the olivo-cerebellar system [19].

In contrast to the aforementioned tests, CLIP-L mice perform very poor in the accelerating rotorod set up (Fig. 4d), which is a measure of more complicated motor behaviors [20,21]. The rotorod test measures the ability of an animal to maintain balance by coordinating the movement of all four feet and making the necessary adjustments. The heterozygous and homozygous CLIP-L mice perform comparably bad in this experiment, but both types of mice are capable of learning to stay on the rotorod for longer periods of time over the 5 day training period. Since, the CLIP-L mice improve at approximately the same rate as wild type mice during rotorod performance, the motor learning appears not to be severely affected in CLIP-L mice. Similar to the rotorod studies, when CLIP-L mice are monitored in a running wheel, they initially demonstrate a very poor coordination (Fig. 4e), resulting in highly erratic motions and occasional ejection from the running wheel (see supplement data). However, in the course of a few days CLIP-L mice learn to tread the running wheel normally and their circadian activity patterns (which are measured through running wheel turns) are like wild types. Together these data are highly suggestive of a motor coordination problem in CLIP-L mice, which reveals itself already at the heterozygous level.

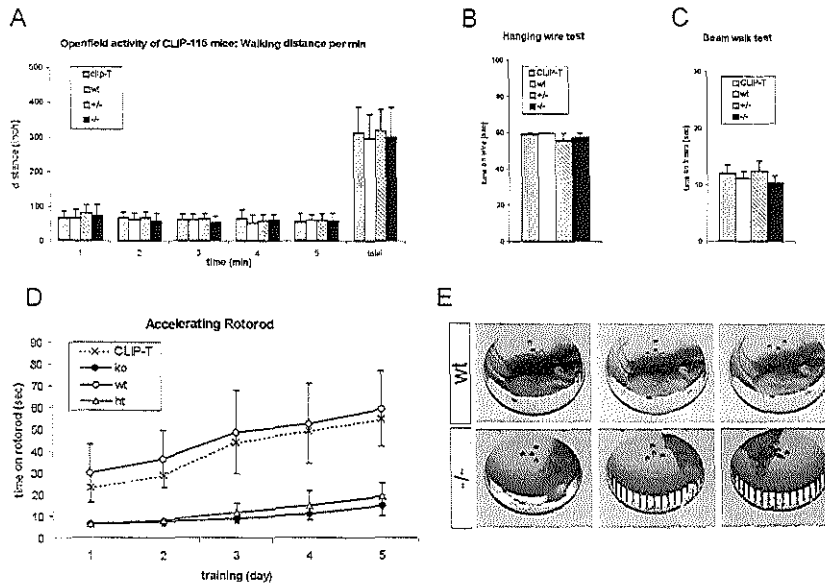

Figure 4. Motor coordination in CLIP-115 mutant mice

A Spontaneous locomotion in a openfield. Wild type (n = 11), CLIP-T (n = 13) and heterozygous (n = 24) and homozygous (n = 13) CLIP-L mice were tested for spontaneous locomotor activity by monitoring their movement per 1 minute intervals (mean ± SEM). No significant difference among the mice were observed. **B** Hanging wire test. To measure the balance and grip strength of wild type (n = 7), CLIP-T (n = 7) and heterozygous (n = 10) and homozygous (n = 8) CLIP-L mice a hanging wire test was performed. The latency to fall was recorded with a 60 seconds cut off time. That results obtained are comparable between the mice. **C** Beam walk test. Wild type (n = 7), CLIP-T (n = 7) and heterozygous (n = 10) and homozygous (n = 8) CLIP-L mice were tested for their basic motor coordination and balance. The beam walk test measures the ability of the mice to cross a wooden beam. The time required to cross the beam was indistinguishable between the groups of mice. **D** Accelerating rotorod test. To measure more complicated motor behaviors and a form of motor learning, wild type (n = 7), CLIP-T (n = 7) and heterozygous (n = 10) and homozygous (n = 8) CLIP-L mice, the rotorod test was assessed. Mice were placed on the rotorod at a constant velocity, after 10 seconds the rotational speed is gradually increased up to 2 minutes. Mice were tested over five days and the latency to fall off is measured. Both the heterozygous and homozygous CLIP-L mice have a significant performance deficit that is already evident from day one. The P values, compared between +/- and wt, -/- and wt, +/- and CLIP-T, and -/- and CLIP-T at every training day is $P<0.05$. Note that there is an improvement of the heterozygous and homozygous CLIP-L mice across days of training. **E** The circadian running wheel test. Wild type (n = 4), heterozygous (n = 4) and homozygous (n = 4) CLIP-L mice were tested for their 24 hour home cage activity. The running wheel activity was measured for one week. No significant difference in circadian activity patterns between the mice was observed. However, when CLIP-L mice are monitored in a running wheel, they show a very poor coordination. Films were recorded for wild type (wt), heterozygous (data not shown) and homozygous (-/-) CLIP-L mice. While wild type mice run in the wheel with a constant rate, both +/- and -/- mice have highly variable motions. The homozygous CLIP-L knock out mice perform poorer than the heterozygous mice and are occasional ejected from the running wheel. Both CLIP-L mice improve throughout the week. Pictures shown here are taken at day 3.

Since lacZ activity in the hippocampus and amygdala of CLIP-L mice is quite striking, we next investigated whether the performance of these brain areas are affected in CLIP-L mice, using both contextual (Fig. 5a) and cued (Fig. 5b) fear conditioning experiments [22,23]. Both cued and contextual conditionings are sensitive to lesions in the amygdala [24], whereas contextual fear conditioning is though to be more sensitive to lesions in the hippocampus [24-26]. In the contextual fear conditioning experiment mice are put into a cage and their normal freezing behavior measured (in terms of percentage of time spent in the cage). After several minutes the mice receive a foot shock, after which they are removed from the cage to be put back 24 hours later. If they remember the context, the percentage freezing time should be significantly increased. As shown in Fig. 5a this is the case for wild type and CLIP-T mice, but not for the CLIP-L mice, whether heterozygous or homozygous for the *CYLN2* deletion. In contrast, all mice behave similar in the cued fear conditioning test (Fig. 5b), in which mice are put in a cage and receive a tone (the conditioning stimulus or CS) prior to the foot shock (the unconditioned stimulus or US). After 24 hr the mice are put back in a different cage and percentage freezing time is measured after applying the CS. Together these experiments suggests that reduction in the levels of CLIP-115 in the CLIP-L mice affects hippocampal behavior more than the amygdala.

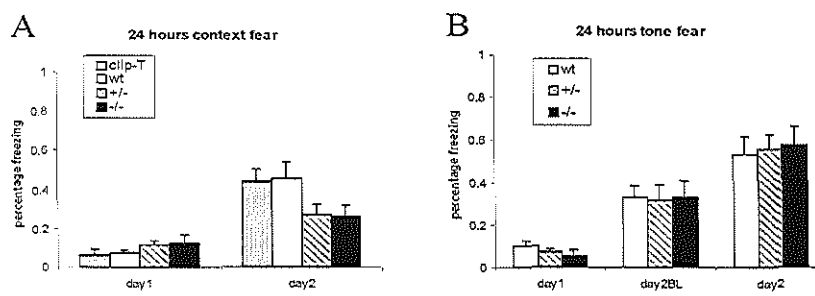

Figure 5. Fear conditioning in CLIP-115 mutant mice.
A Twenty four hour context fear test in CLIP-T (n = 10), wild type (n = 12), CLIP-L +/- (n = 14), CLIP-L -/- (n = 10) mice. Mean percentage of freezing (±SEM) of the 2 minutes context test is shown for wild type and CLIP-T and -L mice. At day 1, mice were placed in the conditioning chamber, assessed for 2 minutes (baseline activity), given a single foot shock and returned to their home cage. There is no significant effect during the baseline period (all P>0.15). 24 hours later (day 2), the mice were tested in the same conditioning chamber for a 2 minute period. Both heterozygous and homozygous CLIP-L mice exhibit a significant deficit in freezing relative to wild type and CLIP-T mice after 24 hours (all P<0.05). **B** Twenty four hour cued fear test in wild type (n = 7), CLIP-L +/- (n = 11), CLIP-L -/- (n = 11) mice. Mean percentage of freezing (±SEM) of the 2 minutes context test is shown for wild type and CLIP-L mice at day 1, day 2 baseline (BL) and day 2. At day 1, mice were placed in the conditioning chamber, assessed for 2 minutes, given a tone-foot shock pairing and returned to there home cage. 24 hours later, after the mice were placed in an other chamber for a 2 minute period (day 2BL), the training tone was played for 2 minutes (day 2). There is no significant difference in the levels of freezing between CLIP-L and wild type mice during the baseline period at day 1 (P=0.2), day 2 (P=0.6) and the tone test (P=0.3).

Discussion

Although the common deletion region in WS has been characterized in great detail [8,9] and a firm linkage between mutations in the ELN gene and cardiovascular abnormalities has been established some time ago [10,11,27,28], those genes that, when mutated, contribute to neurodevelopmental aspects of WS have thus far remained elusive. Because the neurological symptoms and behavioral profile in WS patients are so reproducible, finding these genes is of considerable interest to neuroscience, since they might reveal molecular mechanisms underlying basic neuronal functioning. An initial report, which suggests that the visuo-spatial cognitive defects in WS result from hemizygosity of the LIMK1 gene [12] has not been confirmed by recent investigations [13]. Here we provide strong evidence that reduced levels of CLIP-115 result in a mild growth deficit in mice, as well as in enlarged ventricle size in the brains of these mice and in specific behavioral deficits. These phenotypes mimic part of the neurodevelopmental problems present in WS patients, in particular the growth deficiency and the typical motor coordination defects. Together with the fact that these phenotypes exert themselves already at the heterozygous level in CLIP-L mice, these data strongly suggest that haploinsufficiency for the *CYLN2* gene in man underlies part of the developmental, neurologic and behavioral abnormalities observed in WS. This conclusion is further underscored by the studies in rare patients with small deletions in the WS critical region [8,9,13,14].

Differences in genetic background in strains of mice are known to cause behavioral differences [29-31]. In knock out strategies the genetic background surrounding the knock out allele is (mostly) of the 129-derived mouse background, while C57Bl6 is often used as recipient strain. When comparing the behavior of homozygous, heterozygous and wild type littermates, behavioral differences might be induced by the 129-derived background surrounding the knock out gene. Even when knock out strains of mice are crossed back for several generations into the C57Bl6 background, the genetic difference between wild type animals and knock out mice at the knock out locus can not be compensated for. This is why we have used CLIP-T mice as another control for the CLIP-L mice, since both types of have exactly the same 129-derived genetic background at the *CYLN2* locus and differ only in the fact that an intervening sequence, containing a large part of the *CYLN2* gene, has been removed in the CLIP-L mice. This strongly indicates that the behavioral differences reported here are due to lack of CLIP-115 and not to strain background differences.

Growth deficiency and motor coordination problems occur in WS patients, as they do in CLIP-L mice. The growth deficiency points to a need for CLIP-115 during development. Hence, although this protein is not essential for life, it is required for correct development of mice and man. The motor coordination abnormalities are actually strikingly similar between CLIP-L mice and WS patients. The contextual fear conditioning abnormalities have not been documented in WS patients, for obvious reasons. However the fact that these patients score poorly on spatial cognition and recognition of danger, suggests some kind of correlation between the deficits observed

in CLIP-L mice and those observed in WS patients. Furthermore, enlarged ventrical volumes in CLIP-L mice are also reported for WS patients [32]. Although, in WS patients the total brain volume is decreased [2,33], a phenomenon we do not observe in our CLIP-L mice, the cerebrospinal fluid (CSF) volume in WS is significantly increased with age [32]. These observations all deserve further detailed study. Since we have made an inducible knock out of the *CYLN2* gene, it will be possible in the future, by crossing the CLIP-T mice to specific Cre-expressing lines, to dissect the spatio-temporal contribution of CLIP-115 to growth, brain development and behavior.

We have previously suggested that CLIP-115 is associated with dendritic lamellar bodies [15]. This hypothesis was largely based on the observation that immuno-EM studies with anti-peptide antibodies localized CLIP-115 to Golgi-like structures in dendrites of the inferior olive. We also reported that expression of CLIP-115 is abundant in dendrites of many types of neurons in the brain [15,16]. In recent studies we were not able to clearly label dendritic lamellar bodies in the inferior olive, using monospecific antibodies against bacterially produced CLIP-115 (#2238) [16], suggesting that the previously used anti-peptide antisera against CLIP-115 (#2131 and #2133) are of low affinity and are not completely monospecific. Thus, the role of CLIP-115 in the formation and functioning of dendritic lamellar bodies remained enigmatic. The lacZ expression data obtained here actually indicate that CLIP-115 is neither expressed in the inferior olive (data not shown) and EM studies reveal that dendritic lamellar bodies are normally present in CLIP-L mice, which lack CLIP-115 (data not shown). Together with the fact that CLIP-L mice have completely normal compensatory eye movements, these data suggest that CLIP-115 does not have a prominent role in the olivo-cerebellar system. The labeling pattern observed with the new CLIP-115 antibodies in wild type brain sections [16] is completely abolished in brain sections from homozygous *CYLN2* knock-out mice, indicating that the new antibodies are specific for CLIP-115. From these data we conclude that anti-CLIP antibody #2238 reflects the CLIP-115 distribution in the brain.

CLIP-115 is similar in sequence and structure to CLIP-170, a microtubule binding protein originally proposed to be involved in the linking of endocytic vesicles to microtubules [34]. However, more recent data suggest that both CLIP-170 [35] and CLIP-115 [36] specifically associate with the growing ends of microtubules and may have a role in regulating the dynamics of this cytoskeletal network. This is corroborated by two recent findings. First, the homologue of CLIP-170 in fission yeast, tip1p, is involved in preventing catastrophes at specific areas of the cell [37]. Second, both CLIP-115 and –170 interact with CLASPs, which are evolutionary conserved proteins involved in the regulation of microtubule dynamics in specialized areas of the cell, such as the leading edge of motile fibroblasts [38]. Thus a deficit in CLIP-115 levels in neurons may cause alterations in microtubule dynamics and affect important processes, for example growth cone motility and synaptic plasticity, both of which are known to be dependent on microtubule dynamics [39-42].

Materials and Methods

Generation of CLIP-T and –L mutant mice

CLIP-115 cDNA was used to screen a cosmid library made from a 129/sv mouse strain as described [36]. Four overlapping cosmids were isolated, genomic fragments were subcloned, sequenced and restriction site mapping was performed. An approximately 6.1 kb XbaI-SalI fragment encompassing exon 3 with a XbaI site in intron 2 (5' fragment) and a 8 kb NcoI-BamHI fragment containing exons 15, 16 and 17 with a HindIII site downstream of the last exon (3' fragment) was used. Two targeting vectors were made. The 5' NEO construct was made by inserting a neomycin resistance gene (NEO), which is driven by a TK promotor, flanked by LoxP sequences in the unique XbaI site. The 3' PURO construct was made by inserting a PGK puromycin cassette (PURO) flanked by LoxP sequences together with a HA-tagged NLS-LacZ sequence containing a 3' splice acceptor site in the HindIII site. In both constructs, a negative selection marker gene thymidine kinase (TK) was inserted in the polylinker of the vector. E14 ES cells were electroporated with the 3' targeting construct and cultured in BRL cell conditioned medium in the presence of Leukemia inhibitory factor (LIF) as described [Jaegle, 1996 #442]. After selection with puromycin (0.7 μg/ml), colonies were isolated and expanded. Isolated genomic DNA from individual ES cell lines was digested with NcoI/PvuI and analyzed by DNA blotting using an external 3' probe (probe 1). A number of puromycin resistant ES cell lines were karyotyped and a line with the correct number of chromosomes was electroporated with the second (5') targeting construct. After selection with G418 (200 μg/ml), correct replacement events were identified by Southern blot analyses of EcoRI digested genomic DNA probed with an external 3' probe (probe 2). FISH analyses was performed using the NEO and PURO-LacZ cassettes as probes, to determine the localization of both constructs on chromosome 5. A cell line with correct karyotype were both constructs targeted to the same allele, the CLIP-T cell line, was injected into C57Bl/6 mice. Male chimeric mice were mated with female C57Bl/6 mice to transmit the CLIP-T allele to the germline.

Furthermore, the ES cells of the CLIP-T line were electroporated with a Cre-recombinase gene driven by a TK promotor in a vector with a PGK hygromycin cassette. After selection with hygromycin B (100 μg/ml), deletion of the *CYLN2* region between the outer most LoxP sites was detected on Southern blot of EcoRI digested DNA with probe 2. A cell line, which carries the disrupted *CYLN2* and the correct karyotype, the CLIP-L cell line, was injected into C57Bl/6 mice. Male chimeric mice were mated with female C57Bl/6 mice to transmit the CLIP-L allele to the germline. All CLIP-T and -L mice were backcrossed in C57Bl/6. The mice used in behavioral studies were at the F3 and F4 generation. As a control, wild type littermates and CLIP-T mice are used. If no genotype is indicated for CLIP-T mice, both heterozygous and homozygous CLIP-T mice are used in the experiment. Genotyping of the CLIP-T and -L mice was done with the flanking probes 1 and 2 or with PCR analyses with a three primer set p287 (5'ATGTAGCCCAGGCTGGCTCTAG3') (or p288 (CTTTGAGACAGGTTCTTATGTAGC)) /p290 (5'GTAACACACTGGCCAGGCTTTC3') /p261 (CGGCATCAGAGCAGCCGATTG) to amplifiy the CLIP-T or wt allele and p287 (or p288) / p290 / p260 (TGGTCACTAATCTCCACCTCACAG) to amplify the CLIP-L or wt allele.

RNA and protein analyses

Total RNA and protein from mouse brain was isolated as described [15,36]. Northern and Western blot analyses were done as using standard protocols [43]. The CLIP-115, LacZ, GAPDH, EIF4H, RFC2 and GTF2IRD1 probes hybridized on Northern blot were labeled by PCR or random priming. The EIF4H, RFC2 and GTF2IRD1 probes used here were obtained from ESTs sequences (IMAGE clone 1276725, 1396169, 555547). The anti-CLIP-115 (#2238), anti-CLIP-170 (#2360) and anti-CLIP-115/170 (#2221) antibodies used for Western blotting are described [16,36].

Histology and Electron microscopy

Immunohistochemistry and electron microscopy were performed as described [15]. Brain sections and total brains from adult mice were processes for X-gal staining. Dissected brains were fixed for 30 minutes at RT in 2% paraformaldehyde, 0.2% glutaraldehyde, 2 mM $MgCl_2$, 5 mM EGTA pH 8.0, 0.02% NP-40 in PBS. Subsequently, brains were washed 3 times for 10 minutes at RT in 0.02% NP-40 in PBS. Staining of whole mount brains and sections was done for 2 hours or overnight at 37° in PBS containing 1 mg/ml X-gal, 5 mM $K3Fe(CN)_6$, 5 mM $K_4Fe(CN)_6$, 2 mM $MgCl_2$, 0.01% SDS and 0.02% NP40. Stained embryos were washed and post fixed in 2% paraformaldehyde.

Magnetic resonance imaging (MRI)

CYLN2 homozygous (4 animals) and heterozygous (4 animals) knock out mice and 4 control littermates (5 months old) were submitted to an MRI protocol. Animals were anaesthetized with 5% isoflurane induction and 1.5 to 1 % isoflurane maintenance. Isoflurane was administrated in a mixture of 30% oxygen and 70% NO_2. The head of the mouse was firmly fixed in a stereotactic device consisting of ear plugs and a tooth bar. During MRI, the temperature of the mouse was kept constant at (37.0 ± 0.5) °C. Using Visual Basic code, the temperature was monitored with a rectal probe (PT100) and fed back to a temperature-controlled electrical

heating pad (Uty Nelson). MRI imaging was performed at 300 MHz on an SMIS MR microscope (SMIS, Guildford, UK) with a 7T horizontal bore magnet and 8 cm aperture self-shielded gradients with a strength of 0.1 T/m (Oxford Instruments). The stereotactical apparatus was positioned in the centre of a 30 mm wide RF bird cage coil - used for both transmitting and receiving. Scouting gradient echo images in the 3 orthogonal directions were acquired to guide the reproducible positioning of the 3D slab of the mouse head. High resolution coronal slices of the mouse brain were obtained using a 3D Fast Spin Echo [44-46] sequence with an echo train length of four, reducing the imaging time by a factor of 4.

MR signals of a 3D volume of (20 x 20 x 20) mm^3 were acquired within a (256 x 128 x 64) matrix. The images were taken with a repetition time (TR) of 2500 ms and a first echo time (TE) of 35 ms with an inter echo delay of 25 ms (echo times=35,60,85,110 ms). The central line of the k-space was sampled at the first echo. These parameters were chosen to obtain 3D images of the brain with optimal contrast between the ventricles and the surrounding brain tissue, within an acceptable time. The imaging procedure took about 85 minutes and allowed a short anaesthesia period. The MR data was reconstructed to an image matrix of (256 x 256 x 256) containing 256 coronal slices of 78 µm with spatial resolution of (78 x 78) $µm^2$. Volumes from different brain structures were estimated to find differences between wild type, CLIP-L +/- and CLIP-L -/- mice. Brain and ventricular structures were defined on coronal MR images, according to the Mouse Brain atlas. Their positions were defined as antero-posterior distance to the interaural line (IA) in accordance to the Mouse brain atlas.

All image processing was performed on a PC workstation. To extract quantitative volume of the total brain, the cerebellum (started from IA –2.00 mm) from a set of in vivo obtained images of the mouse, a semi-automatic 3D segmentation technique [47] was applied on the 3D MR images data set using visual C routines and Interactive Data Language (IDL, Research Systems). The volumes of the hippocampus (located from IA 2.86 mm to IA 0.72 mm), amygdala (located from IA 2.86 to 1.26 mm) and ventricular system were segmented using Surfdriver software. MRI parameters were chosen such that an apparent intensity distinction existed between the ventricles and its surroundings which allowed segmentation for these structures: cerebrospinal fluid in the ventricular system was white on the T_2-weighted gradient echo images. The entire ventricular system, when visible on the coronal images, was segmented. Later on the entire ventricular system was divided into the fourth ventricle, the aquaduct of Sylvius, the third ventricle and the lateral ventricles according to the stereotactic atlas of Paxinos. Values are indicated as means ± SEM, and statistical analyses were performed with a two-tailed Student's t-test.

Behavioral testing

Wild type and mutant mice were analyzed for motor coordination as described [20,21]. All behavioral experiments were carried out double blind. Openfield behavior were performed to asses the spontaneous motor activity in a open field (50x50 cm^2). Mice always started from the same corner of the arena and were recorded for 5 minutes using a computerized video tracking system to measure the walking distance, moving episodes and moving time at the horizontal plane, moving episodes and moving time at the vertical plane and entries of the mice in different imaginary parts of the field. Motor coordination and balance of mice were assessed by measuring the ability of the mice to cross a wooden beam of 1 cm wide and 30 cm long, placed horizontal above the bench surface. During training the mice were allowed to explore the beam for 5 minutes. During the test the mice were placed on one end of the beam and the time to walk across the beam was recorded up to a maximum of 60 seconds. Four trails were carried out four each mice. If a mouse fell off the beam, the trail was scored as 60 seconds. In the hanging wire test (to measure balance and grip strength) a wire cage lid is used that is taped around the edge of the lid. The mice are place on top of the lid 30 cm above the cage. The lid is shacked three times and turned upside down. The latency to fall was recorded with a 60 seconds cut off time. The accelerating rotorod test determines more complicated motor behaviors and motor learning. The rotorod consists of a smooth plastic roller (8 cm diameter; 14 cm long) flanked by two large round plates (30 cm) to prevent animals from escaping. Mice were placed on the roller for 10 seconds at a constant velocity (2 rpm). The rotational speed is gradually increased up to 2 minutes (12 rpm). Mice were trained at day one (on a stationary rotorod) and tested over the next five days. Three trails were carried out for each mice every day. The latency to fall off is measured. The circadian running wheel test measures the 24 hour home cage activity. Mice were placed in cages with running wheels for one week and the running wheel activity during 24 hours was analyses as described by [48]. Statistics was performed with a two-tailed unpaired Student's t-test

Computer-assisted Pavlovian Fear conditioning

Computer-assisted 24 hours contextual fear and cued (tone) conditioning was performed as described by Anagnostaras et al. (2000) [22], with slight modifications. 24 hours contextual fear: Mice (5-6 months old littermates) were placed into the conditioning chamber and after a 2 minute baseline period, received a 2 seconds, 1.0 mA foot shock. One day later, the mice were placed back into the same conditioning chamber for a 2 minute contextual freezing test. 24 hours tone fear: A separate group of mice was subjected to tone conditioning. On the first day, the mice were placed into the conditioning chamber and after 2 minutes received a 10 seconds, 75 dB, 2.8-kHz tone coterminated with a 2 seconds, 1.0 mA foot shock. On the next day the were brought into a novel chamber and after a 2 minute baseline, the original training tone was played for 2 minutes.

The freezing was scored by computerized technics using a creative webcam at 5Hz and customary written software (Matlab) to score freezing and activity on a frame to frame basis similarly as described by [22]. Values were means of percentage of freezing ± SEM, and statistical analyses were performed with a two-tailed Student's t-test.

References

1. Morris, C. A., Demsey, S. A., Leonard, C. O., Dilts, C., and Blackburn, B. L. (1988) Natural history of Williams syndrome: physical characteristics. *J Pediatr* **113**(2): 318-26.
2. Bellugi, U., Lichtenberger, L., Mills, D., Galaburda, A., and Korenberg, J. R. (1999) Bridging cognition, the brain and molecular genetics: evidence from Williams syndrome. *Trends Neurosci* **22**(5): 197-207.
3. Bellugi, U., Lichtenberger, L., Jones, W., Lai, Z., and St George, M. (2000) I. The neurocognitive profile of Williams Syndrome: a complex pattern of strengths and weaknesses. *J Cogn Neurosci* **12**(Suppl 1): 7-29.
4. Jones, W., Bellugi, U., Lai, Z., Chiles, M., Reilly, J., Lincoln, A., and Adolphs, R. (2000) II. Hypersociability in Williams Syndrome. *J Cogn Neurosci* **12**(Suppl 1): 30-46.
5. Valero, M. C., de Luis, O., Cruces, J., and Perez Jurado, L. A. (2000) Fine-scale comparative mapping of the human 7q11.23 region and the orthologous region on mouse chromosome 5G: the low-copy repeats that flank the Williams-Beuren syndrome deletion arose at breakpoint sites of an evolutionary inversion(s). *Genomics* **69**(1): 1-13.
6. Peoples, R., Franke, Y., Wang, Y. K., Perez-Jurado, L., Paperna, T., Cisco, M., and Francke, U. (2000) A physical map, including a BAC/PAC clone contig, of the Williams- Beuren syndrome--deletion region at 7q11.23. *Am J Hum Genet* **66**(1): 47-68.
7. Korenberg, J. R., Chen, X. N., Hirota, H., Lai, Z., Bellugi, U., Burian, D., Roe, B., and Matsuoka, R. (2000) VI. Genome structure and cognitive map of Williams syndrome. *J Cogn Neurosci* **12**(Suppl 1): 89-107.
8. Osborne, L. R. (1999) Williams-Beuren syndrome: unraveling the mysteries of a microdeletion disorder. *Mol Genet Metab* **67**(1): 1-10.
9. Francke, U. (1999) Williams-Beuren syndrome: genes and mechanisms. *Hum Mol Genet* **8**(10): 1947-54
10. Tassabehji, M., Metcalfe, K., Donnai, D., Hurst, J., Reardon, W., Burch, M., and Read, A. P. (1997) Elastin: genomic structure and point mutations in patients with supravalvular aortic stenosis. *Hum Mol Genet* **6**(7): 1029-36.
11. Olson, T. M., Michels, V. V., Urban, Z., Csiszar, K., Christiano, A. M., Driscoll, D. J., Feldt, R. H., Boyd, C. D., and Thibodeau, S. N. (1995) A 30 kb deletion within the elastin gene results in familial supravalvular aortic stenosis. *Hum Mol Genet* **4**(9): 1677-9.
12. Frangiskakis, J. M., Ewart, A. K., Morris, C. A., Mervis, C. B., Bertrand, J., Robinson, B. F., Klein, B. P., Ensing, G. J., Everett, L. A., Green, E. D., Proschel, C., Gutowski, N. J., Noble, M., Atkinson, D. L., Odelberg, S. J., and Keating, M. T. (1996) LIM-kinase1 hemizygosity implicated in impaired visuospatial constructive cognition. *Cell* **86**(1): 59-69.
13. Tassabehji, M., Metcalfe, K., Karmiloff-Smith, A., Carette, M. J., Grant, J., Dennis, N., Reardon, W., Splitt, M., Read, A. P., and Donnai, D. (1999) Williams syndrome: use of chromosomal microdeletions as a tool to dissect cognitive and physical phenotypes. *Am J Hum Genet* **64**(1): 118-25.
14. Botta, A., Novelli, G., Mari, A., Novelli, A., Sabani, M., Korenberg, J., Osborne, L. R., Digilio, M. C., Giannotti, A., and Dallapiccola, B. (1999) Detection of an atypical 7q11.23 deletion in Williams syndrome patients which does not include the STX1A and FZD3 genes. *J Med Genet* **36**(6): 478-80.
15. De Zeeuw, C. I., Hoogenraad, C. C., Goedknegt, E., Hertzberg, E., Neubauer, A., Grosveld, F., and Galjart, N. (1997) CLIP-115, a novel brain-specific cytoplasmic linker protein, mediates the localization of dendritic lamellar bodies. *Neuron* **19**(6): 1187-99.
16. Hoogenraad, C. C., Akhmanova, A., Krom, Y., Dortland, B. R., De Zeeuw, C. I., Hasson, T., Grosveld, F., and Galjart, N. Comparative analysis of CLIP-115 and CLIP-170: expression patterns and binding partners in the brain. (submitted for publication):
17. Hoogenraad, C. C., Eussen, B. H., Langeveld, A., van Haperen, R., Winterberg, S., Wouters, C. H., Grosveld, F., De Zeeuw, C. I., and Galjart, N. (1998) The murine CYLN2 gene: genomic organization, chromosome localization, and comparison to the human gene that is located within the 7q11.23 Williams syndrome critical region. *Genomics* **53**(3): 348-58.
18. Osborne, L. R., Martindale, D., Scherer, S. W., Shi, X. M., Huizenga, J., Heng, H. H., Costa, T., Pober, B., Lew, L., Brinkman, J., Rommens, J., Koop, B., and Tsui, L. C. (1996) Identification of genes from a 500-kb region at 7q11.23 that is commonly deleted in Williams syndrome patients. *Genomics* **36**(2): 328-36.

19. Koekkoek, S. K., v Alphen, A. M., vd Burg, J., Grosveld, F., Galjart, N., and De Zeeuw, C. I. (1997) Gain adaptation and phase dynamics of compensatory eye movements in mice. *Genes Funct* **1**(3): 175-90.
20. De Zeeuw, C. I., Hansel, C., Bian, F., Koekkoek, S. K., van Alphen, A. M., Linden, D. J., and Oberdick, J. (1998) Expression of a protein kinase C inhibitor in Purkinje cells blocks cerebellar LTD and adaptation of the vestibulo-ocular reflex. *Neuron* **20**(3): 495-508.
21. Storm, D. R., Hansel, C., Hacker, B., Parent, A., and Linden, D. J. (1998) Impaired cerebellar long-term potentiation in type I adenylyl cyclase mutant mice. *Neuron* **20**(6): 1199-210.
22. Anagnostaras, S. G., Josselyn, S. A., Frankland, P. W., and Silva, A. J. (2000) Computer-assisted behavioral assessment of Pavlovian fear conditioning in mice. *Learn Mem* **7**(1): 58-72.
23. Ferguson, G. D., Anagnostaras, S. G., Silva, A. J., and Herschman, H. R. (2000) Deficits in memory and motor performance in synaptotagmin IV mutant mice. *Proc Natl Acad Sci U S A* **97**(10): 5598-603.
24. Phillips, R. G., and LeDoux, J. E. (1992) Differential contribution of amygdala and hippocampus to cued and contextual fear conditioning. *Behav Neurosci* **106**(2): 274-85.
25. Bourtchuladze, R., Frenguelli, B., Blendy, J., Cioffi, D., Schutz, G., and Silva, A. J. (1994) Deficient long-term memory in mice with a targeted mutation of the cAMP- responsive element-binding protein. *Cell* **79**(1): 59-68.
26. Kim, J. J., and Fanselow, M. S. (1992) Modality-specific retrograde amnesia of fear. *Science* **256**(5057): 675-7.
27. Li, D. Y., Brooke, B., Davis, E. C., Mecham, R. P., Sorensen, L. K., Boak, B. B., Eichwald, E., and Keating, M. T. (1998) Elastin is an essential determinant of arterial morphogenesis. *Nature* **393**(6682): 276-80.
28. Li, D. Y., Faury, G., Taylor, D. G., Davis, E. C., Boyle, W. A., Mecham, R. P., Stenzel, P., Boak, B., and Keating, M. T. (1998) Novel arterial pathology in mice and humans hemizygous for elastin. *J Clin Invest* **102**(10): 1783-7.
29. Silva, a. j., and et al. (1997) Mutant mice and neuroscience: recommendations concerning genetic background. Banbury Conference on genetic background in mice. *Neuron* **19**(4): 755-9.
30. Logue, S. F., Paylor, R., and Wehner, J. M. (1997) Hippocampal lesions cause learning deficits in inbred mice in the Morris water maze and conditioned-fear task. *Behav Neurosci* **111**(1): 104-13.
31. Tarantino, L. M., Gould, T. J., Druhan, J. P., and Bucan, M. (2000) Behavior and mutagenesis screens: the importance of baseline analysis of inbred strains. *Mamm Genome* **11**(7): 555-64.
32. Reiss, A. L., Eliez, S., Schmitt, J. E., Straus, E., Lai, Z., Jones, W., and Bellugi, U. (2000) IV. Neuroanatomy of Williams syndrome: a high-resolution MRI study. *J Cogn Neurosci* **12**(Suppl 1): 65-73.
33. Bellugi, U., Bihrle, A., Jernigan, T., Trauner, D., and Doherty, S. (1990) Neuropsychological, neurological, and neuroanatomical profile of Williams syndrome. *Am J Med Genet Suppl* **6**: 115-25
34. Pierre, P., Scheel, J., Rickard, J. E., and Kreis, T. E. (1992) CLIP-170 links endocytic vesicles to microtubules. *Cell* **70**(6): 887-900.
35. Perez, F., Diamantopoulos, G. S., Stalder, R., and Kreis, T. E. (1999) CLIP-170 highlights growing microtubule ends in vivo. *Cell* **96**(4): 517-27.
36. Hoogenraad, C. C., Akhmanova, A., Grosveld, F., De Zeeuw, C. I., and Galjart, N. (2000) Functional analysis of CLIP-115 and its binding to microtubules. *J Cell Sci* **113**(Pt 12): 2285-97.
37. Brunner, D., and Nurse, P. (2000) CLIP170-like tip1p spatially organizes microtubular dynamics in fission yeast. *Cell* **102**(5): 695-704.
38. Akhmanova, A., Hoogenraad, C. C., Drabek, K., Stepanova, T., Dortland, B., Verkerk, T., Vermeulen, W., Burgering, B. M., De Zeeuw, C. I., Grosveld, F., and Galjart, N. (2001) Clasps are CLIP-115 and -170 associating proteins involved in the regional regulation of microtubule dynamics in motile fibroblasts. *Cell* **104**(6): 923-35.
39. Kneussel, M., and Betz, H. (2000) Clustering of inhibitory neurotransmitter receptors at developing postsynaptic sites: the membrane activation model. *Trends Neurosci* **23**(9): 429-35.
40. Kalil, K., Szebenyi, G., and Dent, E. W. (2000) Common mechanisms underlying growth cone guidance and axon branching. *J Neurobiol* **44**(2): 145-58.
41. Roos, J., Hummel, T., Ng, N., Klambt, C., and Davis, G. W. (2000) Drosophila Futsch regulates synaptic microtubule organization and is necessary for synaptic growth. *Neuron* **26**(2): 371-82.
42. van Rossum, D., and Hanisch, U. K. (1999) Cytoskeletal dynamics in dendritic spines: direct modulation by glutamate receptors? *Trends Neurosci* **22**(7): 290-5.
43. Sambrook, J., Fritsch, E. F., and Maniatis, T. (1989) Molecular cloning: a laboratory manual, 2 Edition, Cold Spring Harbor Laboratory Press, New York

44. Kooy, R. F., Reyniers, E., Verhoye, M., Sijbers, J., Bakker, C. E., Oostra, B. A., Willems, P. J., and Van Der Linden, A. (1999) Neuroanatomy of the fragile X knockout mouse brain studied using in vivo high resolution magnetic resonance imaging. *Eur J Hum Genet* **7**(5): 526-32.
45. Fransen, E., D'Hooge, R., Van Camp, G., Verhoye, M., Sijbers, J., Reyniers, E., Soriano, P., Kamiguchi, H., Willemsen, R., Koekkoek, S. K., De Zeeuw, C. I., De Deyn, P. P., Van der Linden, A., Lemmon, V., Kooy, R. F., and Willems, P. J. (1998) L1 knockout mice show dilated ventricles, vermis hypoplasia and impaired exploration patterns. *Hum Mol Genet* **7**(6): 999-1009.
46. Yuan, C., Schmiedl, U. P., Weinberger, E., Krueck, W. R., and Rand, S. D. (1993) Three-dimensional fast spin-echo imaging: pulse sequence and in vivo image evaluation. *J Magn Reson Imaging* **3**(6): 894-9.
47. Sijbers, J., Scheunders, P., Verhoye, M., van der Linden, A., van Dyck, D., and Raman, E. (1997) Watershed-based segmentation of 3D MR data for volume quantization. *Magn Reson Imaging* **15**(6): 679-88
48. van der Horst, G. T., Muijtjens, M., Kobayashi, K., Takano, R., Kanno, S., Takao, M., de Wit, J., Verkerk, A., Eker, A. P., van Leenen, D., Buijs, R., Bootsma, D., Hoeijmakers, J. H., and Yasui, A. (1999) Mammalian Cry1 and Cry2 are essential for maintenance of circadian rhythms. *Nature* **398**(6728): 627-30.

Chapter 11

GENERAL DISCUSSION AND FUTURE DIRECTIONS

Over the past few years, insight into the role of microtubule associated proteins has increased enormously. The work has been greatly facilitated by the use of green fluorescent protein (GFP) as a tag, which has allowed microtubule associated proteins to be visualized in real time. Several groups have reported on the identification of proteins, which specifically concentrate at the tips of microtubules. For example, EB1, APC, CLIP and CLASP family proteins have recently been observed to be present at growing ends of microtubules. These microtubule plus end binding proteins could serve a number of purposes, such as to initiate the interaction of microtubules with the cell cortex, to prepare local sites on microtubules for specific organelle binding, or to regulate microtubule dynamics. In addition to their role in interphase, microtubule plus end binding proteins have been shown to be very important during mitosis [5-8]. Several experiments suggest that, indeed, microtubule plus end binding proteins play an important role in these processes. For example, in yeast, the EB1 homologue, Bim1p, and the CLIP-170 homologue, tip1p, affect microtubule dynamics and are key regulators of the interaction between microtubules and the cortex [1-3]. CLASPs are responsible for local effects on microtubule dynamics and some CLASP isoforms bind directly to membrane compartments in the cell [4]. Furthermore, CLIP-170 has been implicated in the binding of endosomes and is able to relocalize the dynactin complex to microtubule plus ends. Several models have been proposed to describe the role of microtubule plus end binding proteins in microtubule dynamics and microtubule-membrane interactions [8-11]. However, many fundamental issues are still unresolved. Some of these issues directly related to the experimental work presented in this thesis, will be addressed in this chapter

11.1 CLIPs, CLASPs and microtubule dynamics

As mentioned earlier (section 2.5.1), experiments suggest that some CLIP family proteins are involved in the regulation of microtubule dynamics. For example, disruption of tip1p and Bik1p in yeast, results in aberrant microtubule dynamics [3,12]. With the identification of the CLIP associated proteins (CLASPs) in chapter 5 we provide further evidence that CLIPs, in association with other proteins, are important in microtubule turnover [4]. Overexpression and antibody injection experiments suggest that CLASPs are involved in the stabilization of microtubules.

Although these studies provide some clues about the roles of CLIPs and CLASPs in microtubule dynamics, the biochemical details of the interaction of these proteins with the microtubule tip are not yet known. For example, it is not clear which mechanisms are responsible for binding to microtubule plus ends. We and others have shown that the complete N-terminal domain of CLIPs, containing two microtubule binding CAP-Gly motifs surrounded by basic serine-rich regions, is sufficient for microtubule plus end binding [13,14]. We further have demonstrated that one CAP-Gly motif, together with one basic serine-rich region, binds microtubules along their length. However, whether this minimal domain is sufficient for efficient binding to

microtubule plus ends needs to be investigated. In this respect it is noteworthy that not all CLIP family proteins have a basic serine-rich region next to their CAP-GLY motif. For example, both tubulin folding factors (class II CLIP family proteins) lack such a region. These proteins are not associated with microtubules but bind free α-tubulin [15]. Therefore, it could be that CLIP family proteins which do have a basic region adjacent to their microtubule binding domain, possess a higher affinity for the microtubule polymer than for monomeric tubulin. Alternatively, some minor amino acid modifications of the conserved CAP-Gly may have conferred the ability to discriminate between monomeric and polymerized tubulins in the cell. Detailed domain analysis or domain swapping experiments between different classes of CLIP proteins will be required for further clarification of the role of the CAP-Gly domain and basic serine-rich regions in tubulin and microtubule binding. CLASP family proteins do not have a microtubule binding CAP-Gly motif but do contain a basic domain, which shares only limited homology with other microtubule binding proteins [4,6,7]. Since CLASPs bind microtubule plus ends independently of the CLIPs it will be interesting to determine which amino acids of CLASPs are involved in the dynamic localization of these proteins to the microtubule tip. Identification of the plus end microtubule binding domain of CLASPs would allow DNA/protein database searches to define other putative plus end binding proteins. Like for most CLIPs, it is unclear whether CLASP family proteins have a preference for binding to α- or β-tubulin. Competition of purified CLASPs and CLIPs for microtubule binding, or of CLASP and other MAPs (with known tubulin binding sites, such as classical MAPs or kinesin motor proteins) may resolve this question. On the other hand interaction studies between CLASPs and mutated α- or β-tubulin molecules would define a more detailed map of the binding site for CLASP on the tubulin dimer.

It is currently not clear how CLIP and CLASP family members assemble on growing microtubule plus ends. The simplest assumption is that CLIPs and CLASPs either bind to a unique structure at the microtubule plus end (tubulin sheets) or to a specific nucleotide bound state of tubulin (GTP-cap) (chapter 2, Fig. 3). However, it has been shown by *in vitro* microtubule polymerization experiments that CLIP-170 does not have a preference for a specific conformation change of the microtubule [13]. Instead, CLIP-170 has been shown to bind to tubulin oligomers and may associate with growing microtubules by copolymerization with tubulin [13]. Although this mechanism is currently favored in the literature, it remains possible that the *in vitro* microtubule experiments with CLIP-170 do not exactly mimic the correct microtubule conformational change *in vivo*. Cryoelectron microscopy or atomic force microscopy of microtubules incubated with purified CLIPs and/or CLASPs, may provide further insight into the structure of the protein complexes at the microtubule plus ends. Crystal structures of CLIP- and CLASP-tubulin complexes may give a more detailed description of their specific microtubule interactions.

It is currently also unknown what is the mechanism which releases CLIPs and CLASPs from the microtubule plus ends. Other MAPs, such as tau and XMAP-215

[16,17] also bind microtubules by copolymerization at the growing end. These proteins are subsequently not released from the microtubule and therefore localized along its entire length. Since the CLIP and CLASP binding to microtubules is inhibited by phosphorylation [4,14,18], the dissociation of these proteins from microtubules could be regulated by associated kinases. For CLASP it has been shown that a constitutively active form of GSK3β inhibits the plus end microtubule binding of CLASP. Whether GSK3β directly phosphorylates CLASP needs to be further investigated. For CLIPs it is unknown which kinase is involved in the release of the protein from the microtubule ends. Since the microtubule binding of CLIP-115 and CLIP-170 is sensitive to the serine phosphatase inhibitor okadaic acid, it is likely that the basic serine-rich regions are involved the regulation of microtubule binding. This is in line with the evidence presented in chapter 4. Interestingly, in budding yeast the TOR (target of rapamycin) serine kinase, is associated with the CLIP-170 homologue Bik1p [19]. Inhibition of TOR affects microtubule dynamics. Thus, in yeast TOR might regulate the selective release of CLIPs from the microtubule plus ends and thereby influence microtubule dynamics.

Although several models could be proposed to explain the role of CLIPs and CLASPs in the regulation of microtubule dynamics at the microtubule tip, two mechanisms can be considered that are based on the function of only CLIP and CLASP (Fig. 1). In these models, CLIPs may stimulate the loading of CLASPs onto the microtubule plus ends and/or vice versa. In the first model, CLASPs act as catastrophe-inhibiting factors. CLIPs may be involved in attracting the catastrophe-inhibiting factor CLASP to the microtubule plus ends, which results in a more stable microtubule (Fig. 1a). In the second model, CLIP themselves are anti-catastrophe factors, which may rescue the pausing of CLASP-positive microtubules and induce them into a growing state (Fig. 1b). This also results in the formation of stabilized microtubules. The last model is in line with the anti-catastrophe role of tip1p in fission yeast [3].

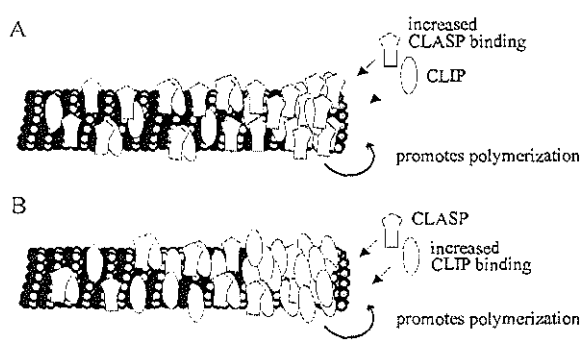

Figure 1. The CLIP-CLASP interaction at the microtubule tip affects microtubule dynamics.
Both CLIPs and CLASPs bind to microtubule plus ends. The affinity of CLIPs and CLASPs for microtubule plus ends is not dependent on the interaction with each other. However, CLIPs and CLASPs may change the binding capacity of each other for microtubule plus ends. **A** CLIPs may stimulate the loading of CLASPs onto the microtubule plus ends. CLASPs may act as catastrophe-inhibiting factors and could be attracted by the CLIP positive microtubule tip. **B** CLASPs may stimulate the loading of CLIPs onto to the microtubule plus end. CLIPs may act as anti-catastrophe factors and could be attracted by a CLASP positive microtubule tip. Both models promote the polymerization (or rescue) of microtubules, which may result in a more stable microtubule network.

One interesting line of experiments will be to examine how CLIPs and CLASPs affect microtubule dynamics. A standard *in vitro* approach is to measure microtubule dynamics in centrosomal extracts prepared from Xenopus eggs. Purified CLIP and CLASP can be added alone or together to these extracts and the microtubule (de)polymerization rate and catastrophe and rescue frequencies could be defined. An alternative approach is to use single or double inducible knock-out cells of CLIPs and CLASPs and measure microtubule growth and shrinkage *in vivo*. Although very laborious and time-consuming, this approach would provide the most compelling evidence for the role of CLIPs and CLASPs in microtubule dynamics.

Future progress on the regulation of microtubule dynamics will also come from studying the interaction between CLIPs and/or CLASPs with EB and APC family proteins. Since EB-related proteins exhibit the same treadmilling behavior on growing microtubules and are present on the same microtubule plus ends as CLIP and CLASP, these proteins may function cooperatively in a 'plus end complex'. Alternatively, competition between the CLIP/CLASP and EB/APC protein families may also occur. Interestingly, Bim1p (EB1) in yeast has been suggested to bind to Bik1p (CLIP-170) in a yeast two hybrid system [20]. All proteins found to associate with CLIP-115 and/or CLIP-170 homologues are shown in figure 2a.

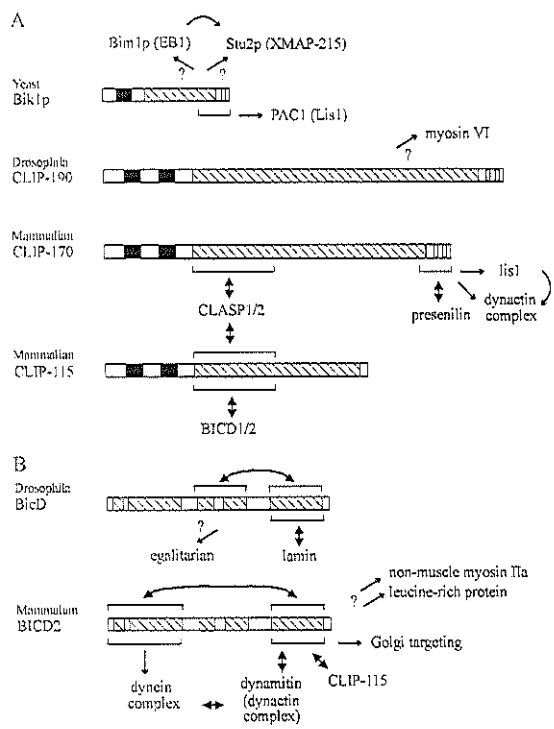

Figure 2. Overview of CLIP and BICD associated proteins.
A Putative binding partners of CLIP-115 and CLIP-170 homologues from yeast (Bik1p), fly (CLIP-190) and mammals (CLIP-170). Bim1p and Stu2p may interact with Bik1p (unpublished results [20,21]). Myosin VI has been shown to associate with CLIP-190 [22]. CLIP-170 has a functional interaction with dynactin and LIS1 and binds directly to presenilin [23-25]. Both CLIP-115 and CLIP-170 bind directly to CLASP [4]. CLIP-115 interacts with BICD1/2 (chapter 8). **B** Putative binding partners of *Drosophila* and mammalian BICD. BICD from fly interacts with egalitarian [26], with itself (middle with C-terminal part) and with lamin [27]. Mammalian BICD2 is associated with CLIP-115 (chapter 8), with itself (N-terminus with C-terminal part), with the dynamitin subunit of the dynactin complex and with cytoplasmic dynein, myosin IIa, leucine-rich protein and a factor present on the Golgi membrane (chapter 7). Arrow with two heads indicates a direct interaction. Arrow with one head indicates that it is unknown whether the interaction is direct or indirect. Question mark indicates that the binding site on CLIP or BICD is unknown.

11. 2 CLIPs and membrane traffic

As described in the introduction in section 2.5.1, several studies suggest that in addition to their role in microtubule dynamics, CLIPs might also link membranes to microtubule plus ends. For example, CLIPs may represent the endpoint of plus-end directed membrane transport, or specify local microtubule binding sites for organelles to direct minus-end driven motor protein transport. Alternatively, CLIPs may be involved in a search and capture mechanism by promoting the interaction with the plasma membrane. Although we believe that CLIPs (indirectly) associate with membranes, we raise considerable questions concerning the validity of the claims made in some of the initial CLIP papers [22,28,29]

First, CLIP-170 was reported as a linker between endocytotic vesicles and microtubules by Pierre et al. (1992) [28]. This theory was based on two lines of evidence: CLIP-170 antibodies inhibited the binding of endosomes to microtubules *in vitro* and CLIP-170 partially colocalized with early endosomes in cultured cells. However, no further evidence has been presented that CLIP-170 is directly and/or stably associated with endosomes. Furthermore, there is no data that shows that CLIP-170 binds to membranes in general or that this protein is enriched in the endosomal fraction and no electron microscopy study has shown that CLIP-170 localizes to endosomes or other membrane organelles. Finally, there is no *in vivo* evidence for an interaction between CLIP-170 and endosomes. Since the role of CLIP-170 during endocytosis remains controversial, we stained for endosomal markers in CLIP-170 overexpressing COS-1 cells and in cells where CLIP-170 is removed from the microtubule plus ends. Both treatments had no effect on the localization of endosomes (Akhmanova A, Hoogenraad CC and Galjart N, unpublished results). Although, these experiments also have their limitations, they suggests that CLIP-170 is not essential for the proper distribution of endosomes. A conclusive answer will come from experiments in CLIP-170 knock-out cells.

Lantz and Miller, (1998) [22] have shown that *Drosophila* CLIP-190 associates with the vesicle motor myosin VI. Based on this, it has been speculated that CLIPs may act to coordinate actin- and microtubule based organelle movements or to target microtubules to cortical actin [30,31]. In chapter 6, we investigated whether there is an interaction between CLIP-170 and the myosin VI homologue in vertebrates. Results of our cotransfection and coimmunoprecipitation experiments provide no evidence for a direct association between myosin VI and CLIP-170. In addition, no colocalization is detected in cultured cells or in chicken cochlea, where myosin VI is highly expressed. These findings could be explained by the fact that the binding between myosin VI and CLIP-170 is not conserved in mammals. However, since the interaction between *Drosophila* myosin VI and CLIP-190 has only been shown by coimmunoprecipitation experiments, its direct nature has not been established. Additional proteins could link actin filaments to microtubules and may cause the association of myosin VI and CLIP-190 in *Drosophila*.

We have previously suggested that CLIP-115 is associated with dendritic lamellar bodies (DLBs) [29]. This hypothesis was based on the isolation of CLIP-115 cDNA from an expression library, screened with an antiserum against DLBs, and on immuno-electron microscopy experiments, using newly raised anti-peptide CLIP-115 antibodies. Recently, we made new antibodies against bacterially produced CLIP-115 and showed that they specifically recognize CLIP-115 on Western blot. Immunohistochemistry studies on brain sections with the new antibodies only reveal partial overlap in staining pattern, compared to the peptide antibodies (chapter 6) [25]. Most notably DLBs in the inferior olive and Bergmann glia cells in the cerebellum are not stained using the new CLIP-115 antibodies. These data suggest that CLIP-115 is not present in DLBs and that the proposed direct role for CLIP-115 in mediating the structure and localization of this organelle is unlikely. This conclusion is consistent with the observation that in CLIP-115 knock-out mice DLBs are normally present (chapter 10). Since CLIP-115 therefore appears not to be the protein constituent of DLBs, it remains interesting to determine which protein is recognized by the original α12B/18 antibody [29] and what is the DLB. A proteomic approach is well suited to answer this question. Purification of membranous organelles with the use of sucrose gradients or immunoisolation of DLBs with the α12B/18 antibody and subsequent analysis of the isolated proteins by mass spectrometry may identify the molecules associated with the DLBs.

Although the claims made in these initial CLIP reports seem to be unconvincing for a role of CLIP-115 and CLIP-170 in membrane transport, compelling evidence comes from some recent observations. First, CLIP-115 and CLIP-170 associate with a membrane bound form of CLASP, CLASP2β, which is palmitoylated [4]. Furthermore, CLASPs are observed at the Golgi apparatus and the cell cortex, suggesting that CLIP-CLASP interactions might regulate vesicle transport or initiate the interaction between microtubules and the plasma membrane. Moreover, CLIP-170 directly interacts with presenilin [32], which is a transmembrane protein localized to the Golgi apparatus, endoplasmic reticulum and cytoplasmic vesicles and which is involved in amyloid precursor protein metabolism and the activation of Notch [23]. Mutations in presenilin are linked to familial Alzheimer's disease. The interaction of presenilin with CLIP-170 may therefore allow attachment of presenilin containing vesicles to microtubule plus ends. In this way presenilin might act as a membrane receptor for CLIP-170. Interestingly, Ca^{2+} is required for the binding of presenilin to CLIP-170, suggesting that changes in Ca^{2+} concentrations in the cell could modulate this interaction. However, since all these data are based on *in vitro* experiments further studies are required. Finally, CLIP-170 associates with both dynactin and LIS1 (chapter 6 [25] and [24,33]). CLIP-170 colocalizes with the minus end directed motor protein dynein and its regulator dynactin at microtubule plus ends and overexpression of CLIP-170 relocalizes dynactin to CLIP-170 positive structures. It has been proposed that CLIP-170 is involved in vesicle docking at microtubule plus ends and the initiation of motor protein based motility (Fig. 3) [24,33]. CLIP-170 may initially load

dynactin and vesicles to the microtubule tip and mediate the recruitment of dynein to power transport of the vesicles. How CLIP-170 associates with dynactin and how these proteins recruit membranous vesicles is unknown. Since both dynactin and dynein are able to bind to vesicles, both complexes are candidates to recruit membranes to the microtubule plus end. Thus, CLIP-170 may only function as a scaffold to load dynactin/dynein/vesicles to the microtubule plus end. In addition, we suggested that LIS1 has a function in the CLIP-170/dynactin/dynein pathway at the microtubule plus end (chapter 6) [25]. Similar to the effect on dynactin, overexpression of CLIP-170 relocalizes LIS1 to the microtubules plus ends. Since LIS1 binds to dynactin and dynein and its overexpression abolishes the dynactin localization at microtubule plus ends [34,35], LIS1 may act together with CLIP-170/dynactin/dynein to regulate motor protein transport. Alternatively, since LIS1 has been shown to affect microtubule dynamics [36], the putative CLIP-170-LIS1 interaction may modulate the microtubule network.

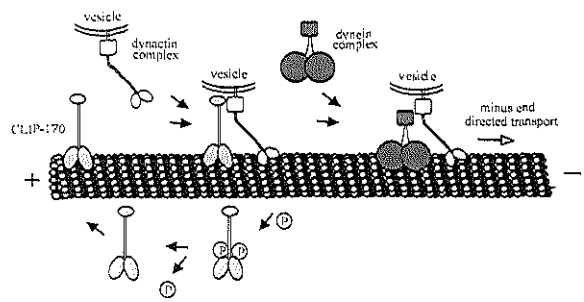

Figure 3. Model for CLIP-170/dynactin dependent vesicle docking at microtubule plus ends and the initiation of motor protein based motility. The model is based on the interaction between CLIP-170 and dynactin at microtubule plus ends [24,33]. Since CLIP-170 and dynactin colocalize at microtubule plus ends and dynactin binding is CLIP-170 dependent, CLIP-170 may load dynactin to the microtubule tip. Subsequently dynactin may provide a dynein binding site at microtubule plus ends. Phosphorylation of CLIP-170 releases their microtubule binding and minus end directed transport could occur. In this model, loading of vesicles to the microtubule tip occurs by the association of vesicles with the dynactin complex. Since, dynein has been shown to bind membranes [37] and CLIP-170 might associate with a receptor on the endosomal membrane [38], other models are possible as well. In addition, function of the CLIP-170-LIS1 interaction at microtubule plus ends remains unclear.

A role for CLIP-115 in membrane-microtubule interactions is suggested through its direct interaction with both mammalian Bicaudal-D proteins. In chapter 7, we have shown that mammalian BICD2 is associated with the dynactin and dynein complexes and is localized to the trans-Golgi network and cytoplasmic vesicles. The dynamitin subunit of dynactin interacts with the C-terminal part of BICD2, while dynein associates with the N-terminal part. On the basis of these observations, we hypothesized that BICD might regulate the interaction between dynactin, dynein and (membranous) cargo (chapter 7 and Fig. 4a-c). The role of the CLIP-115/BICD association remains unclear but it is tempting to speculate that it may be an alternative mechanism to the CLIP-170/dynactin model (Fig. 3), to recruit vesicles to microtubules (Fig. 4d). While CLIP-115 may be specific for loading BICD coated vesicles to microtubules in neurons, CLIP-170/dynactin may be a more ubiquitous cargo loading mechanism. A central assumption in the CLIP-115/BICD model is that

dimeric BICD must be able to unfold its C-terminal domain in order to interact with both the vesicle surface and CLIP-115. Since dynactin also binds to the C-terminal part of BICD, a key question is, whether CLIP-115 works together with dynactin to activate dynein or that the action of CLIP-115 alone is sufficient to drive dynein mediated membrane transport. In figure 4d a model is shown where dynactin is involved in CLIP-115/BICD dependent vesicle docking. Here, dynactin may compete with CLIP-115 for the same BICD molecule or CLIP-115 and dynactin may interact with different BICDs on the same membranous surface. Since many aspects of the CLIP-115/BICD/dynactin/dynein/vesicle interaction remain to be resolved, all models concerning the CLIP-BICD and BICD/dynactin/dynein association are highly speculative. In addition, BICD has been shown to interact with other factors. All proteins known to associate with *Drosophila* and mammalian BICD are summarized in figure 2b. These interactions may also be relevant to the BICD-CLIP-vesicle pathway.

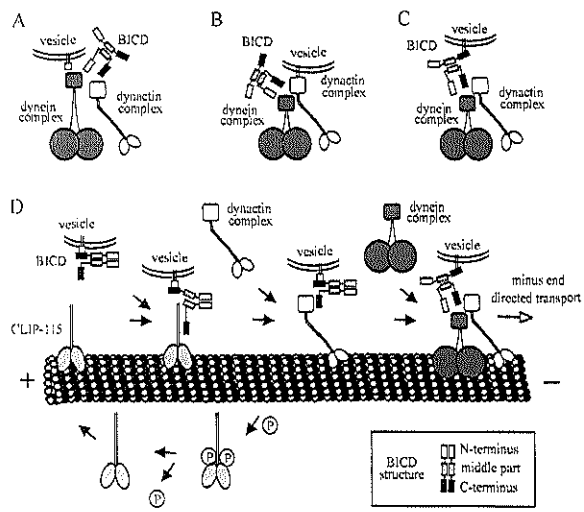

Figure 4. Model for CLIP-115/BICD dependent vesicle docking at microtubule plus ends and the initiation of motor protein based motility. **A-C** Model for the BICD interaction with dynactin, dynein and vesicles. Since BICD binds to dynactin and dynein, and BICD, dynactin and dynein are able to associate with membranes, different mechanisms could account for the binding of all proteins to the vesicle surface. For example, dynein (A) or dynactin (B) might bind to membranes and BICD regulates the interaction between dynein and dynactin (chapter 7). Alternatively, BICD binds to membranes and might link dynein and dynactin to the same vesicles (C). In these models dimeric BICD is unfolded. However multimerization may also account for the interaction of BICD on one vesicle with both dynein and dynactin. **D** Model for CLIP-115 in loading BICD positive vesicles to microtubule plus ends in neurons. The model is based on the direct interaction between CLIP-115 and BICD. The C-terminal tail of BICD also interacts with dynactin. Dynactin may compete with CLIP-115 for the same BICD molecule. Alternatively, CLIP-115 and dynactin may interact with different BICDs on the same vesicle (not shown). When dynactin is bound to the microtubule, it may provide a dynein loading site and stimulate minus end directed transport. Phosphorylation of CLIP-115 removes the protein from the microtubules. In theory, CLIP-115 could also load dynein (A) or dynactin (B) coated vesicles via an interaction with BICD.

One way to address these questions, is to use an *in vitro* motility system. By adding purified dynactin, CLIP-115 and/or isolated BICD vesicles to this in vitro system, the effect on minus end directed mobility could be tested. Alternatively, homozygous

CLIP-115 (CLIP-L) knock-out mice, may provide an excellent tool to study BICD associated vesicle transport in neurons. Another interesting line of experiments will be to examine what is transported by BICD coated vesicles and in which transport pathway BICD is involved. Identification of constituent proteins of the BICD positive vesicles will provide clues to the role of BICD in membrane transport.

11.3 CLIP-115 and Williams syndrome

The *CYLN2* gene, encoding CLIP-115, is one of the 16 genes shown to be hemizygously deleted in patients with Williams Syndrome (WS) (chapter 9 [39] and [40]). WS is a developmental disorder involving vascular, connective tissue and central nervous system abnormalities. The complex neurological features of this disorder include mental retardation, visuospatial cognitive deficits, relatively preserved language development, yet poor motor coordination and balance [41]. In chapter 10, we demonstrate, through targeted deletion of the *CYLN2* gene in mice, that the lack of CLIP-115 is likely responsible for some of the neurological aspects of WS. Both heterozygous and homozygous *CYLN2* knock out mice show a mild growth deficiency, enlarged ventricular system in the brain, motor coordination deficits and are disrupted in a hippocampus-dependent learning task. In addition, electrophysiological measurements in hippocampal slices from homozygous and heterozygous *CYLN2* knock out and wild type (and CLIP-T) control mice clearly suggest that LTP is affected in mice deleted for CLIP-115 (Krugers H, Hoogenraad CC, Galjart N, unpublished results).

The mechanism by which reduced levels of CLIP-115 might contribute to the neurological phenotype of WS is not clear. Since CLIPs are implicated in microtubule-membrane interactions, a deficit in CLIP-115 levels in neurons may cause altered vesicle transport. Alternatively, it is plausible that CLIP-115 is required to regulate microtubule dynamics. In neurons, dynamic microtubules may participate in important neuronal processes, such as growth cone motility and synaptic plasticity. Recent studies indicate that sprouting of new dendritic spines may be correlated with long-term synaptic plasticity [42,43]. It has been suggested that microtubule dynamics could contribute to some of the morphological adaptations of dendritic spines [44]. CLIP-115 may regulate local microtubule assembly and stabilization within the spines either directly or through its CLASP interaction. In *CYLN2* knockout mice and WS patients, the structural remodeling of synapses and the formation of new synaptic contacts might be altered. On the other hand, microtubules (and associated) proteins are believed to generate a scaffold for certain isoforms of GABA and glycine receptors at postsynaptic membranes [45]. Reduced levels of CLIP-115 might lead to a aberrant targeting and clustering of these receptors. Both hypotheses correlate well with the observed electrophysiological abnormalities in the hippocampus and specific behavioral deficits in *CYLN2* knock out mice. Electron microscopy studies to analyze the morphology of synapses and a more detailed cell physiological investigation of

CYLN2 knock out mice may give a conclusive answer about the (cell biological) effect of a CLIP-115 deletion. In addition, measurements on microtubule dynamics in cultured hippocampal neurons of CLIP-115 deleted mice could lead to a deeper understanding of the role of CLIP-115 in WS.

References

1. Korinek, W. S., Copeland, M. J., Chaudhuri, A., and Chant, J. (2000) Molecular linkage underlying microtubule orientation toward cortical sites in yeast. *Science* **287**(5461): 2257-9.
2. Lee, L., Tirnauer, J. S., Li, J., Schuyler, S. C., Liu, J. Y., and Pellman, D. (2000) Positioning of the mitotic spindle by a cortical-microtubule capture mechanism. *Science* **287**(5461): 2260-2.
3. Brunner, D., and Nurse, P. (2000) CLIP170-like tip1p spatially organizes microtubular dynamics in fission yeast. *Cell* **102**(5): 695-704.
4. Akhmanova, A., Hoogenraad, C. C., Drabek, K., Stepanova, T., Dortland, B., Verkerk, T., Vermeulen, W., Burgering, B. M., De Zeeuw, C. I., Grosveld, F., and Galjart, N. (2001) Clasps are CLIP-115 and -170 associating proteins involved in the regional regulation of microtubule dynamics in motile fibroblasts. *Cell* **104**(6): 923-35.
5. Dujardin, D., Wacker, U. I., Moreau, A., Schroer, T. A., Rickard, J. E., and De Mey, J. R. (1998) Evidence for a role of CLIP-170 in the establishment of metaphase chromosome alignment. *J Cell Biol* **141**(4): 849-62.
6. Lemos, C. L., Sampaio, P., Maiato, H., Costa, M., Omel'yanchuk, L. V., Liberal, V., and Sunkel, C. E. (2000) Mast, a conserved microtubule-associated protein required for bipolar mitotic spindle organization. *Embo J* **19**(14): 3668-82.
7. Inoue, Y. H., do Carmo Avides, M., Shiraki, M., Deak, P., Yamaguchi, M., Nishimoto, Y., Matsukage, A., and Glover, D. M. (2000) Orbit, a novel microtubule-associated protein essential for mitosis in Drosophila melanogaster. *J Cell Biol* **149**(1): 153-66.
8. Tirnauer, J. S., and Bierer, B. E. (2000) EB1 proteins regulate microtubule dynamics, cell polarity, and chromosome stability. *J Cell Biol* **149**(4): 761-6.
9. Sawin, K. E. (2000) Microtubule dynamics: the view from the tip. *Curr Biol* **10**(23): R860-2.
10. Schroer, T. A. (2001) Microtubules don and doff their caps: dynamic attachments at plus and minus ends. *Curr Opin Cell Biol* **13**(1): 92-6.
11. Schuyler, S. C., and Pellman, D. (2001) Microtubule "plus-end-tracking proteins", the end is just the beginning. *Cell* **105**(4): 421-4.
12. Berlin, V., Styles, C. A., and Fink, G. R. (1990) BIK1, a protein required for microtubule function during mating and mitosis in Saccharomyces cerevisiae, colocalizes with tubulin. *J Cell Biol* **111**(6 Pt 1): 2573-86.
13. Diamantopoulos, G. S., Perez, F., Goodson, H. V., Batelier, G., Melki, R., Kreis, T. E., and Rickard, J. E. (1999) Dynamic localization of CLIP-170 to microtubule plus ends is coupled to microtubule assembly. *J Cell Biol* **144**(1): 99-112.
14. Hoogenraad, C. C., Akhmanova, A., Grosveld, F., De Zeeuw, C. I., and Galjart, N. (2000) Functional analysis of CLIP-115 and its binding to microtubules. *J Cell Sci* **113**(Pt 12): 2285-97.
15. Feierbach, B., Nogales, E., Downing, K. H., and Stearns, T. (1999) Alf1p, a CLIP-170 domain-containing protein, is functionally and physically associated with alpha-tubulin. *J Cell Biol* **144**(1): 113-24.
16. Drechsel, D. N., Hyman, A. A., Cobb, M. H., and Kirschner, M. W. (1992) Modulation of the dynamic instability of tubulin assembly by the microtubule-associated protein tau. *Mol Biol Cell* **3**(10): 1141-54.
17. Vasquez, R. J., Gard, D. L., and Cassimeris, L. (1994) XMAP from Xenopus eggs promotes rapid plus end assembly of microtubules and rapid microtubule polymer turnover. *J Cell Biol* **127**(4): 985-93.
18. Rickard, J. E., and Kreis, T. E. (1991) Binding of pp170 to microtubules is regulated by phosphorylation. *J Biol Chem* **266**(26): 17597-605.
19. Choi, J. H., Adames, N. R., Chan, T. F., Zeng, C., Cooper, J. A., and Zheng, X. F. (2000) TOR signaling regulates microtubule structure and function. *Curr Biol* **10**(14): 861-4.
20. Kosco, K. A., Adams, I. R., and Huffaker, T. (1999) Stu2 interacts with Bik1 and Bim1 to modulate microtubule assembly in *S.cerevisiae*. *Mol Biol Cell* **10**(1482 suppl): 256a
21. Geiser, J. R., Kahana, J. A., Silver, P., and Hoyt, M. A. (1999) Establishing the role of *S.cerevisiae* Bik1p and Pac1p within the cytoplasmic dynein complex. *Mol Biol Cell* **10**(1436 suppl): 248a

22. Lantz, V. A., and Miller, K. G. (1998) A class VI unconventional myosin is associated with a homologue of a microtubule-binding protein, cytoplasmic linker protein-170, in neurons and at the posterior pole of Drosophila embryos. *J Cell Biol* **140**(4): 897-910.
23. Struhl, G., and Adachi, A. (2000) Requirements for presenilin-dependent cleavage of notch and other transmembrane proteins. *Mol Cell* **6**(3): 625-36.
24. Valetti, C., Wetzel, D. M., Schrader, M., Hasbani, M. J., Gill, S. R., Kreis, T. E., and Schroer, T. A. (1999) Role of dynactin in endocytic traffic: effects of dynamitin overexpression and colocalization with CLIP-170. *Mol Biol Cell* **10**(12): 4107-20.
25. Hoogenraad, C. C., Akhmanova, A., Krom, Y., Dortland, B. R., De Zeeuw, C. I., Hasson, T., Grosveld, F., and Galjart, N. Comparative analysis of CLIP-115 and CLIP-170: expression patterns and binding partners in the brain. (submitted for publication):
26. Mach, J. M., and Lehmann, R. (1997) An Egalitarian-BicaudalD complex is essential for oocyte specification and axis determination in Drosophila. *Genes Dev* **11**(4): 423-35
27. Stuurman, N., Haner, M., Sasse, B., Hubner, W., Suter, B., and Aebi, U. (1999) Interactions between coiled-coil proteins: Drosophila lamin Dm0 binds to the bicaudal-D protein. *Eur J Cell Biol* **78**(4): 278-87
28. Pierre, P., Scheel, J., Rickard, J. E., and Kreis, T. E. (1992) CLIP-170 links endocytic vesicles to microtubules. *Cell* **70**(6): 887-900.
29. De Zeeuw, C. I., Hoogenraad, C. C., Goedknegt, E., Hertzberg, E., Neubauer, A., Grosveld, F., and Galjart, N. (1997) CLIP-115, a novel brain-specific cytoplasmic linker protein, mediates the localization of dendritic lamellar bodies. *Neuron* **19**(6): 1187-99.
30. Wu, X., Jung, G., and Hammer, J. A., 3rd. (2000) Functions of unconventional myosins. *Curr Opin Cell Biol* **12**(1): 42-51.
31. Goode, B. L., Drubin, D. G., and Barnes, G. (2000) Functional cooperation between the microtubule and actin cytoskeletons. *Curr Opin Cell Biol* **12**(1): 63-71.
32. Johnsingh, A. A., Johnston, J. M., Merz, G., Xu, J., Kotula, L., Jacobsen, J. S., and Tezapsidis, N. (2000) Altered binding of mutated presenilin with cytoskeleton-interacting proteins. *FEBS Lett* **465**(1): 53-8.
33. Vaughan, K. T., Tynan, S. H., Faulkner, N. E., Echeverri, C. J., and Vallee, R. B. (1999) Colocalization of cytoplasmic dynein with dynactin and CLIP-170 at microtubule distal ends. *J Cell Sci* **112**(Pt 10): 1437-47.
34. Vallee, R. B., and Sheetz, M. P. (1996) Targeting of motor proteins. *Science* **271**(5255): 1539-44.
35. Faulkner, N. E., Dujardin, D. L., Tai, C. Y., Vaughan, K. T., O'Connell, C. B., Wang, Y., and Vallee, R. B. (2000) A role for the lissencephaly gene LIS1 in mitosis and cytoplasmic dynein function. *Nat Cell Biol* **2**(11): 784-91.
36. Sapir, T., Elbaum, M., and Reiner, O. (1997) Reduction of microtubule catastrophe events by LIS1, platelet- activating factor acetylhydrolase subunit. *Embo J* **16**(23): 6977-84.
37. Lacey, M. L., and Haimo, L. T. (1994) Cytoplasmic dynein binds to phospholipid vesicles. *Cell Motil Cytoskeleton* **28**(3): 205-12
38. Rickard, J. E., and Kreis, T. E. (1996) CLIPs for organelle-microtubule interactions. *Trends Cell Biol* **6**: 178-182
39. Hoogenraad, C. C., Eussen, B. H., Langeveld, A., van Haperen, R., Winterberg, S., Wouters, C. H., Grosveld, F., De Zeeuw, C. I., and Galjart, N. (1998) The murine CYLN2 gene: genomic organization, chromosome localization, and comparison to the human gene that is located within the 7q11.23 Williams syndrome critical region. *Genomics* **53**(3): 348-58.
40. Francke, U. (1999) Williams-Beuren syndrome: genes and mechanisms. *Hum Mol Genet* **8**(10): 1947-54
41. Bellugi, U., Lichtenberger, L., Mills, D., Galaburda, A., and Korenberg, J. R. (1999) Bridging cognition, the brain and molecular genetics: evidence from Williams syndrome. *Trends Neurosci* **22**(5): 197-207.
42. Toni, N., Buchs, P. A., Nikonenko, I., Bron, C. R., and Muller, D. (1999) LTP promotes formation of multiple spine synapses between a single axon terminal and a dendrite. *Nature* **402**(6760): 421-5.
43. Engert, F., and Bonhoeffer, T. (1999) Dendritic spine changes associated with hippocampal long-term synaptic plasticity. *Nature* **399**(6731): 66-70.
44. van Rossum, D., and Hanisch, U. K. (1999) Cytoskeletal dynamics in dendritic spines: direct modulation by glutamate receptors? *Trends Neurosci* **22**(7): 290-5.
45. Kneussel, M., and Betz, H. (2000) Clustering of inhibitory neurotransmitter receptors at developing postsynaptic sites: the membrane activation model. *Trends Neurosci* **23**(9): 429-35.

LIST OF ABBREVIATIONS

aa	amino acid
Ab	antibody
Ac-tubulin	acetylated tubulin
ALS	amyothropic lateral sclerosis
APC	adenomatous polyposis coli protein
Arp	actin-related protein
ATP	adenosine triphosphate
bp	base pair
BICD	Bicaudal-D
Bim1p	binding to microtubules 1 protein
C. elegans	Caenorhabditis elegans
C-terminus	carboxy-terminus
CAP-Gly	cytoskeletal associated protein glycine conserved domain
CLASP	CLIP associated protein
CLIP	cytoplasmic linker protein
cDNA	complementary deoxyribonucleic acid
CYLN2	cytoplasmic linker protein 2 gene
DLB	Dendritic Lamellar Body
DNA	deoxyribonucleic acid
FISH	fluorescense in situ hybridization
GFP	green fluorescent protein
Glu-tubulin	glutamylated (detyrosinated) tubulin
GSK-3β	glycogen synthase kinase 3β
GTP	guanosine triphosphate
γ-TuRC	γ-tubulin ring complex
kb	kilo base pairs
kDa	kilo Dalton
KIF	kinesin superfamily
LacZ	β-galactosidase
LIS	lissencephaly
LPA	lipid lysophosphatidic acid
MAP	microtubule associated protein
mRNA	messenger ribonucleic acid
MT	microtubule
MTB	microtubule binding
MTOC	microtubule organizing center
NF	neurofilament
N-terminus	amino-terminus
S. cerevisiae	Saccharomyces cerevisiae
S. pombe	Schizosaccharomyces pombe
+Tips	plus end-tracking proteins
TAC	tip attachment complex
WS	Williams Syndrome
XMAP	Xenopus microtubule associated protein

SUMMARY

Microtubules are polar structures composed of α/β-tubulin heterodimers and are found in all eukaryotic cells. In interphase cells, microtubules form a dynamic network and play a major role in intracellular movement and positioning of organelles. The polarity of microtubules is relevant for the transport properties of microtubule motor proteins. Some organelles are transported preferentially toward the plus end of the microtubule while others are preferentially transported toward the minus end. When the cell enters mitosis, the interphase network disappears and microtubules start to assemble the mitotic spindle, which segregates the chromosomes between the two daughter cells. Therefore, one of the most important functions of microtubules, in interphase as well as in mitosis, is to guide and orient intracellular movements. Microtubules are also identified as the most prominent component of flagella and cilia. Flagella provide the means for locomotion of single eukaryotic cells, like flagellated protozoa. In mammals, many epithelial cells are ciliated in order to move material across the tissue surface. Microtubules are also involved in the migration of cells which do not have flagella or cilia, like fibroblasts and macrophages. In this way, microtubules are crucial for many migration dependent processes, such as embryonic development, inflammatory immune response, wound repair, growth cone pathfinding and tumor metastasis.

Microtubules are dynamic polymers with a slow growing minus end and fast growing plus end. There are three distinct steps in the life of dynamic microtubules, namely nucleation, assembly (polymerization) and disassembly (depolymerization). The dynamic microtubule array usually originates at the centrosome. The centrosome anchors microtubules at their minus ends and organizes the microtubule network by initiating microtubule assembly. During polymerization, free α/β-tubulin heterodimers are added to the microtubule plus-ends. Subsequently the microtubules grow from the centrosome and extend distally to the periphery of the cell. Disassembly of the microtubule occurs by loss of α/β-tubulin heterodimers at the plus ends. The dynamic behavior of microtubules is regulated by GTP hydrolysis and is essential for their biological function. Since microtubules grow randomly to the periphery of the cell, they are able to explore the intracellular space while they polymerize. This enables microtubules to capture specific targets within the cell. As the growing microtubule contacts the target site, the microtubule does not depolymerize but is stabilized. Several studies have shown that a selective capture (and stabilization) of individual microtubules in specific regions in the cell promotes the establishment of cellular asymmetry. Since the tip of growing microtubules will be the first to contact the capture region, microtubule plus ends are one of the primary sites for regulating microtubule-target interactions and microtubule dynamic behavior. Various plus end binding proteins have been implicated in these phenomena. In this thesis, experiments are described that study the role of microtubule plus end binding proteins, especially cytoplasmic linker proteins (CLIPs) in microtubule dynamics and membrane transport.

Generally, three main experimental approaches have been taken to investigate the role of CLIP-115 in the cell; 1) isolation and characterization of CLIP-115 and functional analyses of GFP tagged CLIP-115, 2) identification of proteins that interact with CLIP-115 by a yeast two hybrid screen and 3) the generation of CLIP-115 knock-out mice by homologous recombination.

In these studies, we isolated and characterized a new member of the CLIP-family, CLIP-115. CLIP-115 is predominantly expressed in the brain and abundantly present in the dendritic compartments of neurons. Video microscopy of GFP-CLIP-115 in living cells showed that it is dynamically localized to the tip of growing microtubules. The CLIP-115 protein structure consists of an N-terminal domain, with two microtubule binding domains and basic serine-rich regions, followed by a long coiled-coil region. Truncation of the CLIP-115 protein revealed that the microtubule binding domains together with the serine rich regions are involved in efficient microtubule binding. A yeast two hybrid screen has identified proteins that interact with CLIP-115. Among these, the CLIP associated proteins (CLASPs), bind to both CLIP-115 and CLIP-170 and associate with microtubule plus ends. CLASPs are asymmetrically distributed in motile fibroblasts and have a microtubule stabilizing effect. In contrast to CLIPs, CLASPs localize asymmetrically to the leading edge of fibroblasts. The other proteins isolated from the yeast two hybrid screen are the mammalian homologues of Bicaudal-D, a well studied protein in *Drosophila*. Mutations in *Drosophila* Bicaudal-D show a developmental defect, which results in symmetric fly embryos containing two tails (bicaudal). In mammals there are two Bicaudal-D genes, Bicaudal-D1 and 2. Bicaudal-D2 is associated with the Golgi apparatus and cytoplasmic vesicles. In addition, we show that Bicaudal-D2 binds to both the dynein and dynactin complexes and might be involved in the microtubule minus end directed dynein motor protein pathway. Since Bicaudal-D is associated with vesicles and is identified as a CLIP-115 binding protein, we suggest that Bicaudal-D and CLIP-115 act together in a microtubule transport pathway in neurons. The third approach was to determine the biological effect of deleting the CLIP-115 gene. We generated CLIP-115 inducible knock-out mice by using homologous recombination and the Cre-Lox system in embryonic stem cells. CLIP-115 knock-out mice are born in a normal Mendelian fashion, they are apparently healthy and fertile and do not show any macroscopic abnormalities. These data indicate that CLIP-115 is not essential for life. The gene for CLIP-115, named CYLN2, is located on human chromosome 7q11.23 and is one of the sixteen genes that are hemizygously deleted in Williams Syndrome patients. Since these patients have both physiological and neurological defects, we tried to identify the corresponding symptoms in our knock out mice. Both heterozygous and homozygous CLIP-115 knock-out mice show growth deficiency and neurological deficits, including problems with motor coordination and memory. These phenotypes are comparable to some of the symptoms observed in Williams Syndrome patients. The results show that CLIP-115 is one of the proteins that, when deleted, contributes to the neurological abnormalities in Williams Syndrome patients.

POPULAIRE SAMENVATTING

Gewervelde dieren, zoals de mens, zijn opgebouwd uit een hiërarchie van structuren. De kleinste structuren zijn de cellen. Cellen zijn de basale bouwstenen van het organisme en bevatten het genetische materiaal in de vorm van DNA. Er zijn ongeveer twee honderd verschillende soorten cellen aanwezig in het menselijk lichaam, zoals zenuwcellen, spiercellen en bloedcellen. Uiteenlopende cel types samen vormen een hogere orde structuur, de weefsels en organen. Deze weefsels en organen zijn gespecialiseerd in het uitvoeren van een bepaalde taak. De maag, darmen en galblaas hebben bijvoorbeeld elk een eigen functie bij de spijsvertering. Naast verschillende weefsels en organen hebben gewervelde dieren een skelet, ook wel geraamte genoemd, gemaakt van botten en kraakbeen. De functie van het skelet is om stevigheid en vorm te bieden aan het lichaam. Ook beschermt het skelet de vitale organen tegen invloeden van buiten af. De schedel beschermt, bijvoorbeeld, de hersenen en de ribben vormen een soort kooi om het hart en de longen. Van groot belang is ook de interactie tussen het skelet en de spieren. Het skelet geeft de spieren een stevige aanhechting en afzet mogelijkheid waardoor gewervelde dieren zich kunnen bewegen.

Elke cel in het lichaam heeft ook een intern geraamte, het zogeheten celskelet. Dit celskelet is opgebouwd uit een fijnmazig vlechtwerk van eiwitdraden en bepaalt, net als het beenderskelet van het menselijk lichaam, de vorm en stevigheid van de cel. Ook zorgt het celskelet er voor dat alle onderdelen binnen in een cel op hun plaats blijven zitten. Het celskelet doet echter nog veel meer. Ten eerste is het celskelet heel dynamisch, het wisselt voortdurend van opbouw en samenstelling. De vorm van de cel kan hierdoor heel snel ingrijpend veranderen, bijvoorbeeld bij celdeling of celspecialisatie. Als een neuronale stamcel zich gaat differentieren tot een zenuwcel, legt het celskelet de basis voor de karakteristieke vertakkingen die vervolgens de zenuwuitlopers, het axon en de dendrieten vormen. Ook bepaalt het celskelet de dikte en lengte van de zenuwuitlopers. In de tweede plaats zijn sommige van de 'botten' van het celskelet tegelijkertijd 'spieren'. Dit stelt de cel in staat om zich te bewegen. Dankzij het celskelet kunnen immunologische afweercellen zich verplaatsen naar de plek van infectie in het lichaam en kunnen zenuwcellen de juiste contacten vinden. Ten derde zorgt het celskelet voor het transport van verschillende bestanddelen in de cel. Het is bijvoorbeeld betrokken bij het verplaatsen van de chromosomen gedurende de celdeling en het transport van cel materiaal van de ene kant van de cel naar de andere kant.

Steeds meer ziekten blijken (mede) veroorzaakt te worden door veranderingen in het celskelet. Fouten in het celskelet kunnen leiden tot karakteristieke spierziekten, huidaandoeningen en neurologische afwijkingen. De ziekte van Alzheimer wordt bijvoorbeeld gekenmerkt door ophoping van het celskelet bindend eiwit 'tau'. Specifieke veranderingen in het celskelet kunnen zelfs bijdragen in de diagnose van sommige ziekte beelden. De identiteit van bepaalde uitgezaaide tumoren kan bijvoorbeeld worden bepaald aan de hand van specifieke celskelet markers.

Het celskelet is opgebouwd is uit drie verschillende soorten eiwitdraden: de intermediaire filamenten, de actine filamenten en de microtubuli. Alle drie de soorten zijn lange aaneengeregen ketens van duizenden afzonderlijke eiwitten. Elke van de onderdelen van het celskelet heeft zo zijn eigen specifieke functie. De intermediaire filamenten zorgen vaak voor de stevigheid en stabiliteit in de cel en benaderen daarmee het dichtst de structuur die bij de eigenschappen van een skelet horen. Naast elkaar liggende epitheelcellen in de huid bezitten veel intermediaire filamenten die met elkaar contact maken. Hierdoor ontstaat een stabiele en goed gehechte cellaag die zorgt voor de stevigheid van de huid. Veranderingen in intermediaire filament eiwitten leiden soms tot ernstige erfelijke huidaandoeningen. Het tweede type celskelet, de actine filamenten vormen de spierbundels van het cel. Ze komen vaak voor net onder de celmembraan en zorgen voor de beweging van de cel. Het voortbewegen van bijvoorbeeld primitieve eencellige organismen, zoals amoeben, wordt geheel verzorgd door het actine celskelet. Het derde, zeer belangrijke, bestanddeel van het celskelet is het netwerk van microtubuli. Microtubuli zijn buisvormige structuren met een doorsnede van 25 nm en zijn opgebouwd uit twee type eiwitten. Deze eiwitten worden α en β tubuline genoemd. Dankzij de oriëntatie waarmee de α en β tubuline worden ingebouwd bezitten microtubuli een polariteit, met een min en plus kant. De min kant van de microtubuli is verankerd in een centraal punt bij de celkern. Dit punt wordt het microtubuli organisatie centrum of centrosoom genoemd. Doordat de min kant stevig vast zit, kan de microtubulus aan het plus einde nieuwe tubuline moleculen inbouwen. Dankzij deze eigenschap kunnen microtubuli vanuit het midden van de cel naar de buitenkant (de celmembraan) groeien.

Alle eukaryoten organismen, zoals gisten, vliegen, wormen, planten en dieren gebruiken microtubuli voor het sorteren en verdelen van de chromosomen tijdens de celdeling. Als tijdens de deling de microtubuli functie verstoord wordt kan de cel zich niet meer vermenigvuldigen. Dit heeft tot gevolg dat het organisme zich niet meer kan ontwikkelen en voortplanten. Microtubuli zijn dus essentieel in het leven van zowel eencellige als meercellige organismen. De meeste cellen in het menselijk lichaam zijn niet bezig met delen maar bevinden zich in een rust fase. Microtubuli hebben ook dan belangrijke functies. Microtubuli kunnen heel stabiel zijn en gebruikt worden als een soort transportrails. Langs deze rails vervoeren motor eiwitten diverse materialen (bijvoorbeeld celorganellen of eiwit moleculen) binnen in de cel. Kinesine motor eiwitten vervoeren materiaal van het microtubuli min einde (het centrosoom) naar het plus einde (de celmembraan). Dyneine motor eiwitten doen dit juist andersom en transporteren materiaal van de plus naar de min kant. Motor eiwitten zijn ook betrokken bij het transport van celmateriaal in zenuwcellen. Aangezien zenuwcellen wel een meter lang kunnen worden, is er een zeer ontwikkeld regulatie mechanisme nodig om de motor eiwitten, letterlijk, in goede banen te leiden.

Zoals hierboven al is beschreven zit de min kant van de microtubuli verankerd in het centrosoom en is het plus einde vrij om nieuwe tubuline eiwitten in te bouwen. Op deze manier groeien de microtubuli vanuit het midden van de cel naar de

celmembraan. Als microtubuli tegen de celmembraan aan groeien of op een andere manier lang genoeg zijn, krimpen ze weer. Het voortdurend groeien en afbreken van microtubuli wordt dynamische instabiliteit genoemd. Dankzij deze eigenschappen kunnen microtubuli de drie dimensionale ruimte van de cel 'doorzoeken' en interacties aangaan met verschillende bindingsplaatsen. Als de microtubuli eenmaal een bindingsplaats gevonden hebben krimpen ze niet meer en zijn ze tijdelijk stabiel. Met andere woorden, de microtubuli die 'gevangen' zijn genomen door de bepaalde bindingsplaatsen zijn in rust en pauzeren even. Het systeem van locale stabilisatie van microtubuli wordt dan ook wel het 'zoek en vang' mechanisme genoemd. Dynamische instabiliteit en het 'zoek en vang' mechanisme zijn verantwoordelijk voor de opbouw van een asymmetrisch microtubuli netwerk in de cel. De asymmetrische oriëntatie van microtubuli in de richting van de membraan is cruciaal voor vorm en structuur van de cel. Een cel kan hierdoor bijvoorbeeld bepalen wat zijn 'voor' en 'achterkant' is. Op deze manier kunnen zenuwcellen uitgroeien in de gewenste richting, fibroblasten over een ondergrond lopen en macrofagen in het lichaam zich voortbewegen in de richting van de infectie. Een asymmetrisch netwerk van microtubuli wordt experimenteel zichtbaar door in het laboratorium uitgevoerde 'wond heling' experimenten. Hierbij wordt in een volle schaal met fibroblast cellen een dunne streep getrokken. Een aantal cellen wordt hierdoor van het schaaltje afgeschraapt en een zone zonder cellen, de 'wond' blijft achter. De cellen aan de rand van de wond gaan zich nu zo ontwikkelen dat hun 'voorkant' in de richting van de wond gaat wijzen. Hierdoor kunnen de fibroblasten zich in die richting bewegen. De meeste microtubuli in de fibroblast cellen zijn nu georiënteerd naar de kant van de wond toe en worden gestabiliseerd in die bewegingsrichting. Uit de 'wond heling' blijkt dat de dynamiek van de microtubuli en de interacties die de microtubuli aangaan met de bindingsplaatsen aan de 'voorkant' van de cel gereguleerd worden door verschillende factoren. Deze factoren bevinden zich zowel buiten de cel (zoals groeifactoren) als binnen de cel (zoals bijvoorbeeld membraan eiwitten en microtubuli bindende factoren).

Dit proefschrift tracht inzicht te verschaffen in de rol die de zogenaamde CLIP eiwitten spelen bij verschillende cellulaire processen. CLIP is de (Engelse) afkorting voor 'cytoplasmatisch linker eiwit'. Aangezien CLIPs zich specifiek bevinden aan het uiteinde van groeiende microtubuli, is het zeer aannemelijk dat ze betrokken zijn bij de regulatie van de groei van microtubuli. Ook is het mogelijk dat CLIPs het einde van de microtubuli definiëren. Ze hebben als het ware een signaalfunctie. Hierdoor kan de plus kant van de microtubulus, via de CLIP eiwitten, een interactie aangaan met membraanachtige celorganellen, of met specifieke delen van de celmembraan. De titel van dit proefschrift luid dan ook; De rol van cytoplasmatische linker eiwitten (CLIPs) bij microtubuli dynamiek en membraan verkeer.

In de eerste twee inleidende hoofdstukken wordt de huidige kennis omtrent het cytoskelet samengevat. In **hoofstuk 1** word voornamelijk de structuur van microtubuli en hun dynamiek beschreven. Vervolgens worden enkele voorbeelden genoemd van processen in de cel waarbij microtubuli betrokken zijn. In **hoofstuk 2** worden vier

verschillende soorten microtubuli bindende eiwitten behandeld; de klassieke microtubuli geassocieerde eiwitten, eiwitten die de microtubuli dynamiek reguleren, microtubuli motor eiwitten en microtubuli plus eind bindende eiwitten. Van deze laatste groep worden de CLIP en EB1 families gedetailleerd besproken. Er wordt duidelijk gemaakt dat de leden van deze families voorkomen in zowel lagere als hogere organismen. CLIP-115 en CLIP-170 zijn onderdeel van de CLIP familie die voorkomen bij zoogdieren.

De **hoofstukken 3 tot en met 10** vatten het praktische werk van dit promotieonderzoek samen. De vraag die centraal stond bij dit onderzoek was: wat is de functie van het CLIP-115 eiwit. Om een antwoord te krijgen op deze vraag zijn verschillende experimentele benaderingen gebruikt. Zo werd er bijvoorbeeld in gekweekte cellen gekeken naar de lokalisatie van CLIP-115 eiwitten die gekoppeld zijn aan een groene fluorescente stof, GFP genaamd. Omdat dit GFP-CLIP-115 fusie eiwit ook in levend materiaal zichtbaar is, kan de dynamiek van CLIP-115 onderzocht worden. Ook is er gebruik gemaakt een bepaalde techniek, de 'yeast two hybrid assay', die het mogelijk maakt om de eiwitten te identificeren die een interactie aangaan met CLIP-115. Daarnaast is met behulp van een andere techniek, homologe recombinatie, het CLIP-115 coderende gen verwijderd uit het DNA van alle cellen van de muis.

In **hoofdstuk 3** wordt beschreven op welke manier CLIP-115 is geïsoleerd en dat het eiwit voornamelijk in de hersenen blijkt voor te komen. Dit is in tegenstelling tot CLIP-170, wat in alle weefsels tot expressie komt. In **hoofdstuk 4** wordt CLIP-115 meer in detail bestudeerd. Hier wordt aangetoond dat het eiwit aan plus eindes van microtubuli bindt. Verder is in kaart gebracht welke aminozuren van CLIP-115 belangrijk zijn bij de binding aan microtubuli en laten we zien dat twee CLIP-115 monomeren met elkaar associëren en gestabiliseerd kunnen worden door cysteine bruggen. In **hoofdstuk 5** onderzoeken we waar CLIP-115 en CLIP-170 voorkomen in de hersenen. Ook laten we zien dat CLIP-170 een interactie heeft met de eiwitten dynactine en LIS1. Dynactine en LIS1 zijn beschreven als eiwitten die binden aan het motor eiwit dyneine. CLIP-170 speelt dus mogelijk een rol bij het dyneine afhankelijk membraan transport. In **hoofdstuk 6** wordt de isolatie en karakterisatie van CLASP, een nieuw microtubuli plus eind bindend eiwit beschreven. CLASP bind zowel aan CLIP-115 als aan CLIP-170 en in bewegende fibroblasten is het eiwit voornamelijk aanwezig aan de 'voorkant' van cel. CLASP is betrokken bij de stabilisatie van microtubuli aan de 'voorkant'. In **hoofdstuk 7** wordt het eiwit Bicaudal-D (BICD) geïntroduceerd. BICD is voornamelijk bekend van studies in het fruitvliegje, *Drosophila*. Mutaties in het BICD gen veroorzaken een defect in de ontwikkeling van het fruitvliegje: in plaats van vliegjes met een kop en staart hebben deze mutanten twee staarten (bicaudaal). In mensen zijn twee BICD eiwitten aanwezig, BICD1 en BICD2. Wij laten zien dat BICD2 is geassocieerd met Golgi membranen en cytoplasmatische blaasjes en dat het direct bindt aan een van de onderdelen van het dynactine complex. Overexpressie van een gedeelte van het BICD2 eiwit beïnvloed dyneine transport. In **hoofdstuk 8** bestuderen we de interactie tussen beide CLIP eiwitten en BICD. We

vinden dat terwijl CLIP-170 niet associeert met BICD1/2, CLIP-115 aan zowel BICD1 als BICD2 bindt. Dit suggereert dat CLIP-115 is betrokken bij membraan transport. In **hoofdstuk 9** wordt de genomische organisatie en de chromosoom positie van het muizen *CYLN2* gen beschreven. Het *CYLN2* gen codeert voor het CLIP-115 eiwit en ligt op chromosoom 7q11.23 van de mens. Een van de allelen van het *CYLN2* gen is afwezig bij Williams Syndroom patiënten. In **hoofdstuk 10** wordt beschreven hoe met een bepaalde techniek, homologe recombinatie, het CLIP-115 gen uit het DNA van alle cellen van de muis is verwijderd. Deze muizen kunnen geen CLIP-115 eiwit meer aanmaken. Uit ons onderzoek is gebleken dat deze muizen kleiner zijn en bepaalde gedragsafwijkingen vertonen. Muizen die geen CLIP-115 meer aanmaken hebben problemen met hun balans en coördinatie en hebben een minder goed geheugen in vergelijking met muizen die wel CLIP-115 eiwit aan kunnen maken. Deze afwijkingen zijn vergelijkbaar met sommige symptomen van Williams Syndroom patiënten. Deze resultaten duiden er op dat een reductie in het CLIP-115 eiwit (mede) verantwoordelijk is voor de afwijkingen in Williams Syndroom patiënten. In **hoofdstuk 11** worden de resultaten van het in dit proefschrift beschreven onderzoek besproken en bekijken we waar toekomstig onderzoek zich op zou kunnen richten.

LIST OF PUBLICATIONS

De Zeeuw CI[#], Hoogenraad CC[#], Goedknegt E, Hertzberg E, Neubauer A, Grosveld F, Galjart N. (1997) CLIP-115, a novel brain-specific cytoplasmic linker protein, mediates the localization of dendritic lamellar bodies. *Neuron* **19**(6): 1187-99.

De Zeeuw CI, Simpson JI, Hoogenraad CC, Galjart N, Koekkoek SK, Ruigrok TJ. (1998) Microcircuitry and function of the inferior olive. *Trends Neurosci* **21**(9): 391-400

Hoogenraad CC, Eussen BH, Langeveld A, van Haperen R, Winterberg S, Wouters CH, Grosveld F, De Zeeuw CI, Galjart N. (1998) The murine CYLN2 gene: genomic organization, chromosome localization, and comparison to the human gene that is located within the 7q11.23 Williams syndrome critical region. *Genomics* **53**(3): 348-58

Hoogenraad CC, Akhmanova A, Grosveld F, De Zeeuw CI, Galjart N. (2000) Functional analysis of CLIP-115 and its binding to microtubules. *J Cell Sci* **113**(12): 2285-97

Sun JC, van Alphen AM, Wagenaar M, Huygen P, Hoogenraad CC, Hasson T, Koekkoek SK, Bohne BA, De Zeeuw CI. (2001) Origin of vestibular dysfunction in usher syndrome type 1b. *Neurobiol Dis* **8**(1): 69-77

Akhmanova A[#], Hoogenraad CC[#], Drabek K, Stepanova T, Dortland B, Verkerk T, Vermeulen W, Burgering BM, De Zeeuw CI, Grosveld F, Galjart N. (2001) Clasps are CLIP-115 and -170 associating proteins involved in the regional regulation of microtubule dynamics in motile fibroblasts. *Cell* **104**(6): 923-35

Hoogenraad CC[#], Akhmanova A[#], Howell SA, Dortland BR, De Zeeuw CI, Willemsen R, Visser P, Grosveld F, Galjart N. (2001) Mammalian Golgi-associated Bicaudal-D2 functions in the dynein-dynactin pathway by binding to both complexes. *EMBO J* **20**(15):4041-4054

Hoogenraad CC[#], Akhmanova A[#], Krom Y, Dortland BR, De Zeeuw CI, Hasson T, Grosveld F, Galjart N. Comparison of CLIP-115 and CLIP-170: expression pattern and binding partners in the brain. *To be submitted*

Hoogenraad CC[#], Akhmanova A[#], Dortland BR, De Zeeuw CI, Grosveld F, Galjart N. The microtubule plus end binding protein CLIP-115 interacts with both mammalian homologues of *Drosophila* Bicaudal-D. *To be submitted*

Hoogenraad CC, Dortland BR, Koekkoek SK, Akhmanova A, Rutteman M, Kistler W, Jaegle M, Koutsourakis M, van der Linden A, van Camp N, Krugers H, Grosveld F, De Zeeuw C, Galjart N. *CYLN2* gene targeting links CLIP-115 haploinsufficiency to neurodevelopmental features of Williams Syndrome. *To be submitted*

[#] *These authors contributed equally to this work*

CURRICULUM VITAE

Name: Casper Cassander Hoogenraad
Born: 31 January 1973, Delft, The Netherlands

Sept. 1985 - June 1990:	HAVO at Rijksscholengemeenschap (RSG), Gouda
Aug. 1991 - May 1994:	Undergraduate student, Hoger Laboratorium Onderwijs (HLO), Biochemistry, Hogeschool Rotterdam en Omstreken, Delft
Sept. 1993 - May 1994:	Endocrine Oncology, Department of Medical Oncology, Dr. Daniel den Hoed Cancer Centre, Rotterdam (Dr. B. Han, Dr. J.A. Foekens)
June 1994 - Aug. 1994:	Technician, Laboratory of Experimental Patho-Oncology, Dr. Daniel den Hoed Cancer Centre, Rotterdam (Dr. L.H.J. Looijenga, Prof. Dr. J.W. Oosterhuis)
Sept. 1994 - Sept. 1996:	Undergraduate student, Faculty of Biology, Molecular Genetics, University of Utrecht
Sept. 1995 - May 1996:	Department of Cell Biology and Genetics, Medical faculty, Erasmus University, Rotterdam (Dr.ir. D. Meijer, Prof.dr. D. Bootsma)
Sept. 1996 – June 2001:	PhD. student, Department of Cell Biology and Genetics, Medical faculty, Erasmus University, Rotterdam (Promotor: Prof.dr. F. Grosveld, Prof.dr. C.I. de Zeeuw and co-promotor: Dr.ir. N. Galjart)
Dec. 1998:	Culturing hippocampal neurons, EMBL, Heidelberg, Germany (Dr. C. Dotti)
since June 2001:	Research scientist, Neuroscience Institute, Medical faculty, Erasmus University, Rotterdam

DANKWOORD

Dankzij bemoeienissen, suggesties, hulp, steun en gezelligheid van velen ben ik in staat geweest dit proefschrift te schrijven. Daarom wil ik iedereen bedanken die op één of andere manier een bijdrage heeft geleverd aan het tot stand komen van dit boekje. Enkele van hen wil ik hier graag noemen. Aan mijn promotoren, Frank Grosveld en Chris de Zeeuw de bijzondere eer om dit rijtje van mensen te openen. Frank, graag wil ik je bedanken voor het scheppen van een perfect wetenschappelijk klimaat op de afdeling. Vooral je kritische vragen en opmerkingen tijdens de werkbespreking hebben het onderzoek de goede kant opgestuurd. Is het trouwens echt zo vreselijk daar op de 12e? Chris, het is een eer de eerste promovendus te zijn waar je als promotor fungeert. Hoewel CLIP-115 niks te maken lijkt te hebben met DLBs, blijft het toch een interessant organel. Zullen we op een onbewaakt ogenblik nog een keer een 'boost-18' gokje wagen? Verder bedankt voor je vertrouwen en de mogelijkheid onderzoek te doen in de nieuwe neuroscience-tent.

Mijn grootste dank gaat uit naar mijn co-promotor Niels Galjart. Niels, ik ben je zeer dankbaar voor je inspirerende begeleiding en het overbrengen van je enthousiasme voor fundamenteel wetenschappelijk onderzoek. Ik waardeer het zeer dat je altijd weer tijd wist vrij te maken om over de nieuwste proeven te praten. We hebben wat afgewed de afgelopen jaren ('wat was ook al weer de inzet?'). Toch geinig wat zo'n microtubuli bindend eiwit te weeg kan brengen. Ik hoop dat ik je een beetje van je knock-out-zonder-fenotype-syndroom afgeholpen heb. Hoe zit het eigenlijk met zfp-37? Ook de gezelligheid tijdens de congressen mag niet onvermeld blijven; rood koffertje, Nederland-Belgie, hasjhonden, terugtrekken, cous cous en heb jij nog dorst? Om de afgelopen jaren in je eigen woorden samen te vatten: BEDANKT VOOR DE LES! En oh ja, vergeet je stropdas niet op de dag zelf.

Vervolgens wil ik de CLIPers en C(L)ASPers ontzettend bedanken voor hun bijdrage aan dit promotieonderzoek. Anna, jij en ik hebben samen een paar gave experimenten gedaan. Die ene yeast-two hybrid screen moeten we eigenlijk heilig verklaren. Hoe jij jezelf een 'nieuw' onderzoeksveld eigen maakt is ongekend: even een beetje lithium toevoegen en we hebben een signaal route. Samen naar het overdadige-voedsel-congres in Italië, om vervolgens totaal 'random' Rome te doorkruisen was een hele bijzondere ervaring. Veel plezier met je impuls en spasibo za vse! Bjorn, of jouw aanwezigheid in de groep dit proefschrift echt ten goede is gekomen is nog steeds niet duidelijk, het was in ieder geval een feest om met jou op een lab te zitten. Bedankt voor je hulp bij de muizen experimenten ('moet die dood?') en je altijd falende klonering ('platen in de stoof'), je algemene gekeuvel op de afdeling ('wie is er nu weer zwanger?') en je 'spontane' reactie op 'goedenavond' als je wel een keer voor 10 uur binnen bent. De inmiddels alom bekende donderdagavond sportavond ('ik voel me ijzersterk') zijn onmisbaar. Wanneer ga je weer eens een Big Mac-menu bestellen in een overvolle Burger King?

Lab710 bewoners, Filipe, Helen, Tatiana, Ksenija, Zjak en sinds kort Anita, ik wil jullie bedanken voor de gezellige tijd. Ik kom graag nog eens een stuk taart eten als er weer eens iets te vieren is. Het blijft een goed idee om ook op verjaardagen van de 'kids' te trakteren. Ook de studenten, Michael, Yvonne, Arjan en Marjolein, die de afgelopen jaren menig ep hebben opengeklikt, bedankt. Verder wil ik de oude lab710 mollen bedanken voor hun steun en interesse. Rini (le crom), het was toch wel knus zo met z'n drieën op een kamer. Rien, bedankt voor de haperbank. Ton, een eigen kantoor maar je hoort er nog steeds bij hoor (27 juni 2002 dan pakken we 'm). Phebe, rubbûr? Jij ook bedankt hoor Jansens. Dear neighbors, Edgar, Elena, Amy, Patrick, Albert, John, thanks for all the chitchats and constant (ab)use of your computer. John, thanks for organizing BNO (even when n=3) and kicking my ass with squash ('who's is paying tonight?'). Wouter, lekker hè als een stel wijven over de kleine monsters praten. Ook hulde voor je gouden telefoonactie (kip?). Het oude Dies/Sjaak-lab791, Dies, Fokke, Nynke, Peter, Sjaak, Ulrike, Ludo, Wim, bedankt voor jullie gezellige introductie op de Erasmus. Dies, gelukkig ben ik, ondanks het aandringen van Niels, toch niet alles vergeten wat ik bij je geleerd heb. Marieke, Rita, Jasperina, Rein, Melle, Jan Jos, Sjozef, de keuken, EDCers: bedankt voor het regelen van een hele boel dingen. Voor de rest iedereen van de 7e en 10e, succes, de groeten en bedankt voor de goede sfeer. Kom gerust eens op bezoek op lab1271.

Dan zijn er nog de peoples van de 12e. Elize, Erica en Mandy, bedankt voor jullie vele snij-, kleur- en plak-werk. Arjan en Bas, jullie hebben mij een beetje geïntroduceerd in het muizen veld. Proefschrift? Jongens, gewoon een nietje door al die papers, kafje erom en klaar. Edith, Margriet, Moshe, Eddy, Dick en Tom bedankt voor de vele zaken. Jullie krijgen vanaf nu alleen nog maar meer last van me. En niet te vergeten iedereen van de 'Williams groep' voor de altijd interessante werk besprekingen. Ook alle mensen waar we mee samenwerken om het fenotype van de CLIP-115 muis te achterhalen ben ik veel dank verschuldigd.

Dan rest mij nog om mijn vrienden en familie te bedanken. Jossie, veel dank voor de betere stap avonden, die elke keer vol zaten met bier, gelul en mooie ogen. Goed dat je mijn paranimf wil zijn. Bereid je een beetje voor, je weet nooit wat voor vragen er komen. Pascal, bedankt voor je oprechte interesse en het opleuken van de cover. Mijn ouders wil ik bedanken voor de steun die zij mij altijd geven, ook al gaan we een tijdje naar het buitenland. Frans en Trudy bedankt voor jullie belangstelling en gezelligheid. En natuurlijk, last but not least, Patricia. Jouw relativerend vermogen en heldere kijk op het leven, laten me elke keer weer inzien dat er veel meer is dan alleen proeven doen. Vooral nu er een kleine muppet is bijgekomen. Bedankt voor alles. Tenslotte hulde aan iedereen die de moeite heeft genomen om dit boekje open te slaan, het dankwoord op te zoeken en het ook daadwerkelijk te lezen. Doe eens gek en probeer hierna ook de Nederlandse samenvatting.